UNIVERSITY OF SOUTHAMPTON

STRATIGRAPHY, GEOCHEMISTRY AND ZIRCON GEOCHRONOLOGY OF THE MIDLANDS GREENSTONE BELT, ZIMBABWE.

by Matthew Simon Anthony Horstwood

Submitted in candidature for the degree of Doctor of Philosophy

Department of Geology

Faculty of Science

July 1998

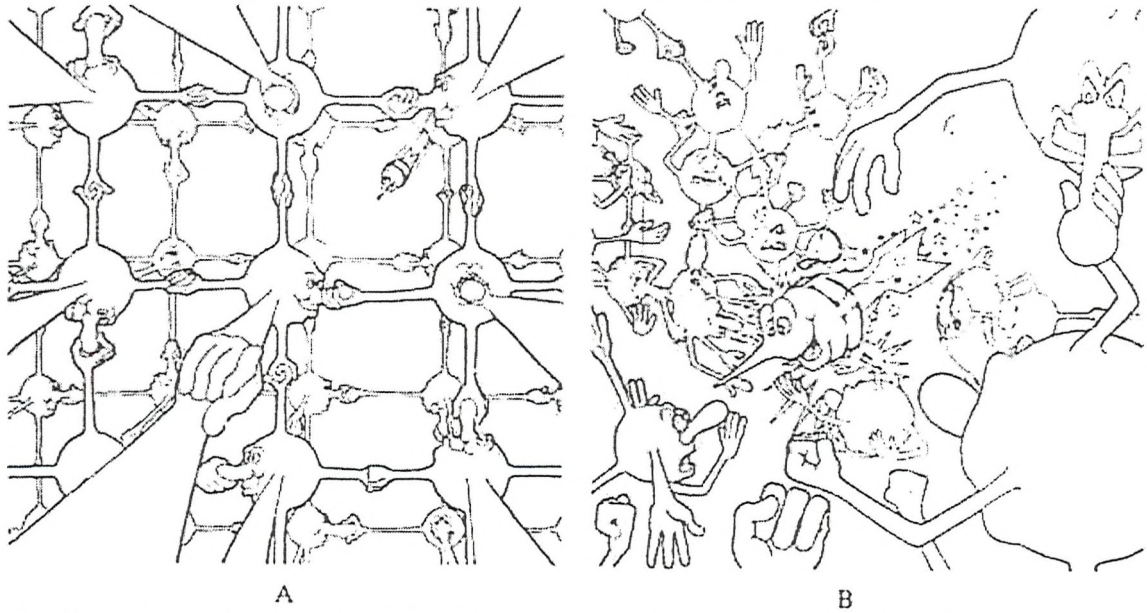

A B

Fig. 223. (a) An alpha particle formed from the spontaneous decay of U or Th approaches a stable portion of a mineral where atoms are bonded together. (b) The energetic alpha particle collides with atoms of the structure causing displacements and structural damage (after Mitchell, 1973, drawn by A. R. Cook for *The Minerals and Gemstones of Nebraska* by R. K. Pabian with permission from the Conservation and Survey Division of the University of Nebraska).

DECLARATION

The work displayed in this thesis is original work conducted by the author whilst under postgraduate candidature at the Department of Geology, University of Southampton.

This thesis was submitted for examination in July 1998. This copy has been supplied on the understanding that it is copyright material and that no quotation from the thesis may be published without proper acknowledgement.

UNIVERSITY OF SOUTHAMPTON

ABSTRACT

FACULTY OF SCIENCE
DEPARTMENT OF GEOLOGY

Doctor of Philosophy

STRATIGRAPHY, GEOCHEMISTRY AND ZIRCON GEOCHRONOLOGY OF THE MIDLANDS GREENSTONE BELT, ZIMBABWE.

by Matthew Simon Anthony Horstwood

Fieldwork, petrography, major, trace and rare-earth element geochemistry, Sm-Nd isotope geochemistry and single-grain zircon geochronology have been conducted on rocks from the Midlands Greenstone Belt, Zimbabwe and other regionally important rocks from around the craton.

A 2880 ± 8Ma volcanic sequence has been identified by single-grain zircon geochronology within what had formally been considered the 2.7Ga Upper Bulawayan stratigraphy of the Midlands Greenstone Belt. The Mafic Formation is therefore redefined as Lower Belingwean in age in accordance with the stratigraphic nomenclature of Wilson *et al.* (1995). The Maliyami and Felsic Formations are dated at 2739 ± 33Ma by Sm-Nd isochron determination, agreeing with the 2701 ± 6Ma zircon age of Wilson *et al.* (1995). The Mafic Formation is recognised as comprising bimodal volcanism with siliciclastic and chemical sedimentation deposited on an ancient granitoid basement. The Maliyami and Felsic Formations exhibit basalt-andesite-rhyodacite mingled volcanism reflecting increased volcanism, with decreased siliciclastic and chemical sedimentation, and an oolitic limestone indicating an increase in the oxygen content of the environment. The environment of deposition is therefore considered to reflect a shallow, continental marginal sea or basin.

Petrographic and geochemical data suggest that the volcanic lithologies can be divided into two distinct suites: basalt and andesite-rhyodacite. The basalts have fractionated clinopyroxene and plagioclase whilst the andesite-rhyodacite suite reflect ilmenite, amphibole and plagioclase fractionation. Continental crustal contamination is present in some samples but the variation of $\varepsilon_{Nd(t)}$ seen in most samples reflects a heterogeneous mantle source. The 2.9Ga and 2.7Ga basalts formed by melting of a 3.2-3.4Ga depleted sub-continental lithospheric mantle component, whilst the 2.7Ga andesite-rhyodacite suite reflects melting of an underlying 2.9Ga basaltic underplate emplaced during this earlier event. As such, a model of formation for the Midlands Greenstone Belt is envisioned through magmagenesis resulting from impingement of a thermal anomaly beneath the Zimbabwe Craton at 2.9Ga and 2.7Ga.

On a regional scale, single-grain zircon geochronology has provided direct evidence for an ancient proto-craton here named the Tokwe Proto-craton, confirming the hypothesis of Kusky (1998). The oldest rocks from the Zimbabwe Craton are dated by single-grain zircon geochronology in the Midlands Greenstone Belt as the 3565 ± 21Ma Sebakwe River Gneiss and the 3456 ± 6Ma Kwekwe Gneiss (part of the Rhodesdale Granitoid). An age of 3455 ± 2Ma is obtained for the Tokwe River Gneisses in the south of the craton, suggesting synchronous formation of these two basement areas. This supports the conclusion of a single, 3.2-3.6Ga proto-cratonic nucleus rather than separate smaller regional nuclei and in conjunction with other published and unpublished data indicates that the Tokwe Proto-craton underlies much of the Zimbabwe Craton as seen today.

CONTENTS

Chapter 5) - Zircon Geochronology - Methods and Application

LIST OF FIGURES, TABLES & PLATES

Figures

Tables

Page

Plates

Page

PREFACE

The geology of Zimbabwe provides a very interesting and stimulating challenge. Investigations into the events and lithologies that comprise the craton are numerous and have been occurring in earnest since the 1930's. In the past, geologists concentrated on the field relationships and spent years mapping vast tracts of the country. In more recent times, effort has been concentrated on analyses of the rocks collected and interpretation of the geochemical data with a view to determining the larger scale picture within and between individual greenstone belts, principally as an aid to gold exploration. Nowadays, with the advent of precise (and presumably accurate) dating techniques, the scale of investigations has taken on an even larger scope, attempting to construct a craton-wide description of the events from which it is shaped.

To a certain extent, this project attempts to do the same but within the confines imposed by the observations of grass-roots field geology. It is hoped that this project will achieve a rigorous petrologic investigation of the Midlands Greenstone Belt, with this part of the stratigraphy positioned in the time-frame of broader cratonic events by some precise and accurate radiometric dates. A coherent, reasonable and well-balanced model for the series of formation events is the aim. The challenge therefore, is to step back from, but consider, all that has gone before and attempt to arrive at such conclusions through fresh data and objective, impartial and fresh thinking, immune from the prejudices of previous workers. This is the challenge set in the face of the plethora of previous work. I hope I have been to some extent successful.

ACKNOWLEDGEMENTS

This project has been funded by the Natural Environment Research Council through NERC studentship GT 4/94/410/G and NERC Isotope Geoscience Laboratory (NIGL) grant no. IP/452/0995.

Many thanks go to my supervisor Bob Nesbitt for guiding me through this project and all that involves. The geology of Zimbabwe has provided great interest and even greater field trips!

In the Geology Department at Southampton much gratitude is owed to Rex Taylor and Andy Milton for help and advice with mass spectrometric techniques and for great coffee; Posy Boella for tuition and guidance in the geochem labs; Bob Jones and John Ford for help with anything and everything in preparation of my samples; Andy Barker for discussions on the finer points of metamorphic petrology; and all my fellow postgrads for help and endurance at all times. Thanks also to Bob Foster for suggesting the study and some inauguration into Zimbabwean culture.

At NIGL, my thanks to everyone for the help and welcome you gave me with particular thanks to Steve Noble, my tutor in the black art of zircon geochronology; Geoff Nowell, for floor space (and red wine) of infinite availability; Lorraine Williams (just for being 'Chicky'); Donna Kean; Jane Evans, Ian Millar and Adrian Wood.

In Zimbabwe, special thanks go to Jim Wilson for all the help and advice on Zimbabwean geology as well as field advice and general support. Thanks Jim! Thanks to everyone past and present at the Geology Department in Harare particularly Tom Blenkinsop, John Orpen, Kudzai Madziwa, Hielke Jelsma and Paul Dirks. Thanks also to Richard Wormald for numerous stays in Harare and introduction to the social culture there.

At Indarama Mine, many thanks to Pan Reef Mining; Terry and Molly Lahee, for their excellent braais and unending hospitality and generosity; Steve Watt for helping keep me sane during 5 months on the mine and taking me to explore the wildlife of Zimbabwe (in all its guises!); and to Enoch Bere, my ever-cheerful, ever-present field assistant, I wish you well my friend. Thanks also to everyone at the Kwekwe Golf Club for their goodwill and pool playing.

Many thanks to Ursula Edwards for everything from car hire to dances in Sandros, floor space, cheap rafting and game viewing trips. Thanks Urch!

Many thanks to the British Council without whom I would have struggled to attend the Harare '97 conference, and to Heather Stubbs my 'partner in crime' on that trip and the following 'expedition'.

Lots of love and thanks to all my family for help, support and belief throughout my time at university.

Last but probably furthest from least, huge thanks to Cathy McKeagney; for company on two field seasons, ringing round the whole of the Eastern Highlands to find me, and for taking almost as long as me to do your PhD. Thanks Cathy!

To anyone I may have forgotten here, my sincerest apologies and great thanks!

LIST OF ABBREVIATIONS

BIF	- Banded Iron Formation
BSE	- Back-scattered electron
CHUR	- Chondrite uniform reservoir
CL	- cathodoluminescence
DM	- depleted mantle
EMMA	- energy dispersive mini-probe multielement analyser
GD	- Great Dyke
HREE	- heavy rare earth elements
ICP-MS	- Inductively Coupled Plasma Mass Spectrometry
ID	- Isotope Dilution
KKG	- Kwekwe Gneiss
KUC	- Kwekwe Ultramafic Complex
LA	- Laser Ablation
LILE	- large ion lithophile elements
LOI	- loss on ignition
LREE	- light rare earth elements
MGB	- Midlands Greenstone Belt
MREE	- mid rare earth elements
MSWD	- mean square of weighted deviates
MSZ	- Munyati Shear Zone
MUS	- Mashaba Ultramafic Suite
NIGL	- NERC Isotope Geoscience Laboratory
REE	- Rare Earth Elements
SCLM	- sub-continental lithospheric mantle
SEM	- Scanning Electron Microscopy
SHRIMP	- Sensitive High Resolution Ion Micro-Probe
SRC	- Sebakwe River Conglomerate
SRG	- Sebakwe River Gneiss
SSZ	- Sherwood Shear Zone
TIMS	- Thermal Ionisation Mass Spectrometry
TMSZ	- Taba-Mali Shear Zone
TRG	- Tokwe River Gneiss
TTG	- Tonalite-Trondhjemite-Granodiorite
XRF	- X-ray Fluorescence

CHAPTER 1 -INTRODUCTION

1.1 PROJECT AIMS AND TECHNIQUES

The aims of this project are to petrologically characterise the volcanic lithologies in the stratigraphy of the Midlands Greenstone Belt, Zimbabwe, and to date some of these and other stratigraphically important lithologies from around the Zimbabwe Craton. To document the change in the nature and geochemistry of the lithologies with time, is a primary objective in order to better understand the generation and development of greenstone belt magmas and enhance the comprehension of cratonic petrogenesis as a whole. The techniques employed to achieve this aim include:

1) Field investigation and sample collection
2) Thin-section petrography
    - transmitted-light
3) X-Ray Fluorescence (XRF)
    - major, minor and trace element geochemistry
4) Inductively Coupled Plasma Mass Spectrometry (ICP-MS)
    - Rare Earth Element (REE) geochemistry
5) Isotope Dilution Thermal Ionisation Mass Spectrometry (ID-TIMS)
    - Nd-isotope geochemistry & geochronology
    - U-Pb zircon geochronology
6) Scanning Electron Microscopy (SEM)
    - back-scattered electron (BSE) imaging of zircons

Each technique has involved considerable amounts of time, either during preparation or data analysis and interpretation, but the most time consuming components by far have been the fieldwork (5 months), U-Pb zircon geochronology by ID-TIMS at the NERC Isotope Geoscience Laboratory (NIGL) in Keyworth (7 months), and the considerable amount of rock crushing and separation which has been done for all the above listed techniques.

This investigation has concentrated on the lithologies exposed in the bed of the Sebakwe river near Kwekwe, which provides a section across strike at the narrowest part of the greenstone belt. A detailed log has been drawn (see sleeve at the back of the thesis)

illustrating the changes of lithology and encompassing virtually all the lithologies represented in the greenstone belt. Samples were collected throughout this section as well as during other sampling forays conducted on porphyry stocks considered important to the study.

1.2 CONVENTIONS ADOPTED

1) Town names in Zimbabwe will be written as today with their pre-independance (1980) names following in brackets where it is thought that this will aid understanding.

2) Rb-Sr dates given in the text will cite the original author but will be recalculated for a ^{87}Rb decay constant of $1.42 \times 10^{-11} yr^{-1}$ where appropriate, and all errors for quoted ages will be two standard deviations from the mean (2σ) unless otherwise stated.

3) Throughout this report the nomenclature as defined by Wilson *et al.* (1995) will be adhered to with any variations being discussed in detail, in an attempt to aid clarity and understanding when discussing stratigraphically equivalent formations from different greenstone belts.

4) Reference to granites will be made on a strictly petrographic basis. Hence granites will be refered to *sensu stricto* whereas other granitoids (e.g. tonalites and granodiorites) will be refered to as such i.e. granites *sensu lato*.

1.3 STRUCTURE OF THE THESIS

The intention during the course of writing this thesis has been to guide the reader through the text, illustrating the logical progression of thought which has been the primary aim of this scientific study. In this way, the work to date will be collated followed by a description and interpretation of the field and petrographic evidence. Desciption and interpretation of the geochemistry will be followed by a chapter on zircon geochronology. Samples from both the Midlands Greenstone Belt and some of the stratigraphy-defining regional granitoids have been dated and provide the most comprehensive geochronological study conducted on the Midlands Greenstone Belt and indeed any greenstone belt in the Zimbabwe Craton after the study of the Harare Greenstone Belt by Jelsma (1993). The zircon chapter (Chapter 5) discusses the background theory behind zircon geochronology including

all the pitfalls of analysis and interpretation with respect to the various techniques employed both in this study and those used generally within the scientific community.

A discussion of all the data and interpretations will then be undertaken before consideration of major palaeotectonic models. In conclusion all the work will be summarised and the more salient points resulting from the study emphasised.

CHAPTER 2 - REGIONAL GEOLOGY AND STRATIGRAPHY OF THE ZIMBABWE CRATON - CURRENT CONSENSUS AND CONTROVERSIES

2.1) REGIONAL GEOLOGY

The Zimbabwe Craton (Fig.2.1) has a long and varied history extending from the Early Archaean to the Proterozoic with most of the activity concentrated in the Archaean between *c.*3.5-2.5Ga. The craton is almost completely surrounded by mobile belts of different ages thought to reflect a gradual process of cratonic accretion. These mobile belts are the Limpopo Belt to the SE (*c.*2.6 and 2.0Ga) - separating the Zimbabwe and Kaapvaal cratons; the Magondi Belt to the NW (*c.*1.9Ga); the Zambezi Belt to the N (*c.*0.9-0.5Ga) and the Mozambique Belt to the E (*c.*1.1-0.5Ga). To the SW, the craton extends into Botswana.

The craton is composed dominantly of granite-greenstone terrains. Several phases of magmatic activity can be recognised, each greenstone cycle being preceded, succeeded and often punctuated, by granitoid magmatism. The granitoids range in composition from granites *sensu stricto*, to tonalite-trondhjemite-granodiorite (TTG) suites, and may be homogeneous or gneissic.

In the south-central region of the craton is the oldest recorded portion of crust, known as the Tokwe Segment. At *c.*3.5Ga, this triangular area of crust with its apices roughly correlating to the townships of Zvishavane, Shurugwi and Masvingo, is thought to represent the core from which the rest of the craton grew in what is now roughly a NW direction (Wilson, 1979). In general, a decrease in the age of the rocks exposed is considered to occur on progression in a northerly direction from the Tokwe segment, with diachroneity of those equivalents exposed in both southern and northern regions.

The principal age of the volcanics now exposed is Upper Bulawayan (*c.*2.7Ga) but some Lower Bulawayan (*c.*2.8Ga) and Belingwean (*c.*2.9Ga) volcanism is also apparent. Indeed, in the Mberengwa (Belingwe) greenstone belt (see Fig.2.1) representatives of all three cycles are exposed and this greenstone belt has long been accepted as the type locality for this

Figure 2.1

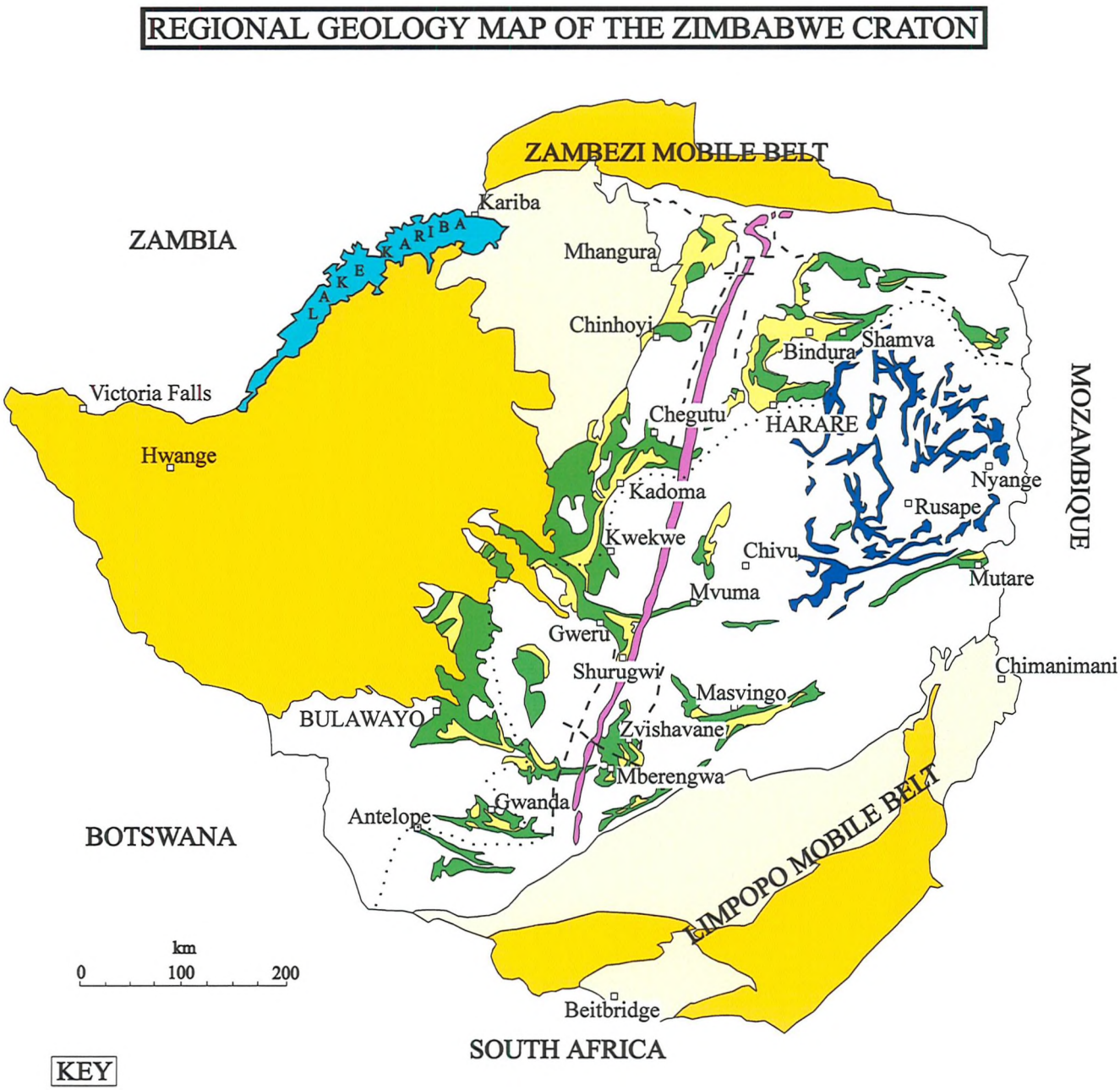
REGIONAL GEOLOGY MAP OF THE ZIMBABWE CRATON
ZAMBEZI MOBILE BELT
ZAMBIA
LAKE KARIBA
Kariba
Mhangura
Chinhoyi
Bindura
Shamva
Victoria Falls
Hwange
Chegutu
HARARE
MOZAMBIQUE
Nyange
Kadoma
Rusape
Kwekwe
Chivu
Mutare
Mvuma
Gweru
Shurugwi
Masvingo
Chimanimani
BULAWAYO
Zvishavane
Mberengwa
Gwanda
Antelope
BOTSWANA
LIMPOPO MOBILE BELT
km
0
100
200
Beitbridge
SOUTH AFRICA
KEY
Boundary between eastern and western succession of Upper Bulawayan
Fault
Edge of Craton
Mashonaland Dyke Suite
Phanerozoic Cover
Shamvaian Sediments
Granitoids of various ages
Proterozoic Cover
Greenstone Belt Volcanics
Great Dyke

part of the stratigraphy. To date most of the work on the Zimbabwe craton has focused on this belt (Martin, 1978; Martin *et al.*, 1993; Orpen, 1978; Orpen & Wilson, 1981; Nisbet *et al.*, 1987; Blenkinsop *et al.*, 1993; Wilson *et al.*, 1995). A craton-wide variation in the nature of the Upper-Bulawayan magmatism has been recognised with a change from predominantly mafic volcanism in the east, to a laterally-equivalent bimodal mafic-felsic succession in the west (Wilson *et al.*, 1978, Wilson, 1979) (Fig.2.1). This stratigraphic horizon is correlatable across the craton and validates a broad scale interpretation and comparison between greenstone belts.

Gold mineralisation is associated with the volcanic sequences but appears to be principally controlled by the structure of the region *and* the fluid composition at the time since not all structures are gold bearing and not all fluid-altered rocks are enriched in gold. The Midlands Greenstone Belt is one of the richest areas for gold mineralisation, with numerous mines of all sizes working the deposits (Campbell & Pitfield, 1994).

Sediments were also deposited during lulls in the volcanism but the principal period of sedimentation is represented by the Shamvaian Supergroup (*c.*2.65Ga) which rests unconformably on top of the volcanics (Fig.2.2).

Two major dyke suites exist; one in the south - the Mashaba-Chibi suite, and one which crops out across the craton but is predominantly exposed in the east - the Mashonaland suite. These provide excellent stratigraphic markers at *c.*2.7Ga and *c.*1.8Ga respectively (Wilson, 1990). The Great Dyke trends NNE-SSW across the craton for a distance of around 500km and at its maximum reaches only 11km in width. This huge north-south fracture is thought to result from previously determined structural weaknesses in the crust (Wilson, 1990) and to represent the last abortive attempts at greenstone belt formation (Wilson *et al.*, 1978). As such, it would indicate that the craton must have become stable by this time (2461 ± 16Ma, Rb-Sr, Hamilton, 1977; 2587 ± 8Ma, Mukasa *pers. commun.*, 1997). The dyke consists of four lopolithic (elongate funnel in cross-section), layered, mafic-ultramafic intrusions containing approximately 15% of the world's chromium reserves.

The north-west portion of the craton is obscured by late-Karoo (Triassic/Jurassic) sediments and basalts, and Recent (Kalahari) aeolian sands. These are the youngest lithified deposits present in Zimbabwe.

2.2) STRATIGRAPHIC FRAMEWORK OF THE CRATON - THE STORY SO FAR

2.2.1) Sebakwian Supergroup

Three principal ages of greenstone belt volcanism - Sebakwian, Belingwean and Bulawayan - have been recognised in the Zimbabwe Craton (see Fig.2.2). The oldest of these and the oldest rocks exposed in the craton, are the *c.*3.5Ga Sebakwian Group. These rocks crop out at the west end of the Masvingo greenstone belt at Mashava and in the Tokwe Segment as amphibolite, BIF, and mafic-ultramafic remnants of early greenstone belt volcanism. The majority of the Shurugwi greenstone belt was once thought to be Sebakwian but this has recently been revised (Tsomondo *et al.*, 1992) and it is now considered Belingwean (*c.*2.9) in age.

The Tokwe segment currently represents the oldest known portion of exposed sialic crust in Zimbabwe. It consists of tonalitic gneisses which enclose tightly infolded remnants of the Sebakwian Group. The Tokwe gneisses themselves have been dated at 3426 ± 400 Ma (Rb-Sr, Hawkesworth *et al.*, 1975) and 3475 ± 90 Ma (Pb-Pb WR, Taylor *et al.*, 1991), and are thought to be the source of the detrital xenocrystic zircons dated at 3.2-3.8Ga, extracted from the Buchwa Quartzite (L3?) and Wanderer Formation (U1) by Dodson *et al.*, (1988).

2.2.2) Belingwean Supergroup

The second cycle of volcanism is dated at *c.*2.9Ga (Rb-Sr, Hawkesworth *et al.*, 1979; 2904 ± 9Ma, U-Pb SHRIMP, Wilson *et al.*, 1995) and is best exposed in the south-west of the Mberengwa (Belingwe) greenstone belt. Previously known as the Lower Greenstones (Wilson, 1979; Foster *et al.*, 1986), this cycle has now been renamed the Belingwean (Wilson *et al.*, 1995) based on the nature of the volcanic units and the recognition of several incomplete cycles separated by major unconformities. One of these, the Bend unconformity, separates the Lower Belingwean Bvute (L1) and Hokonui (L2) Formations, from the Upper Belingwean Bend (L3) Formation (see Fig.2.2).

Figure 2.2

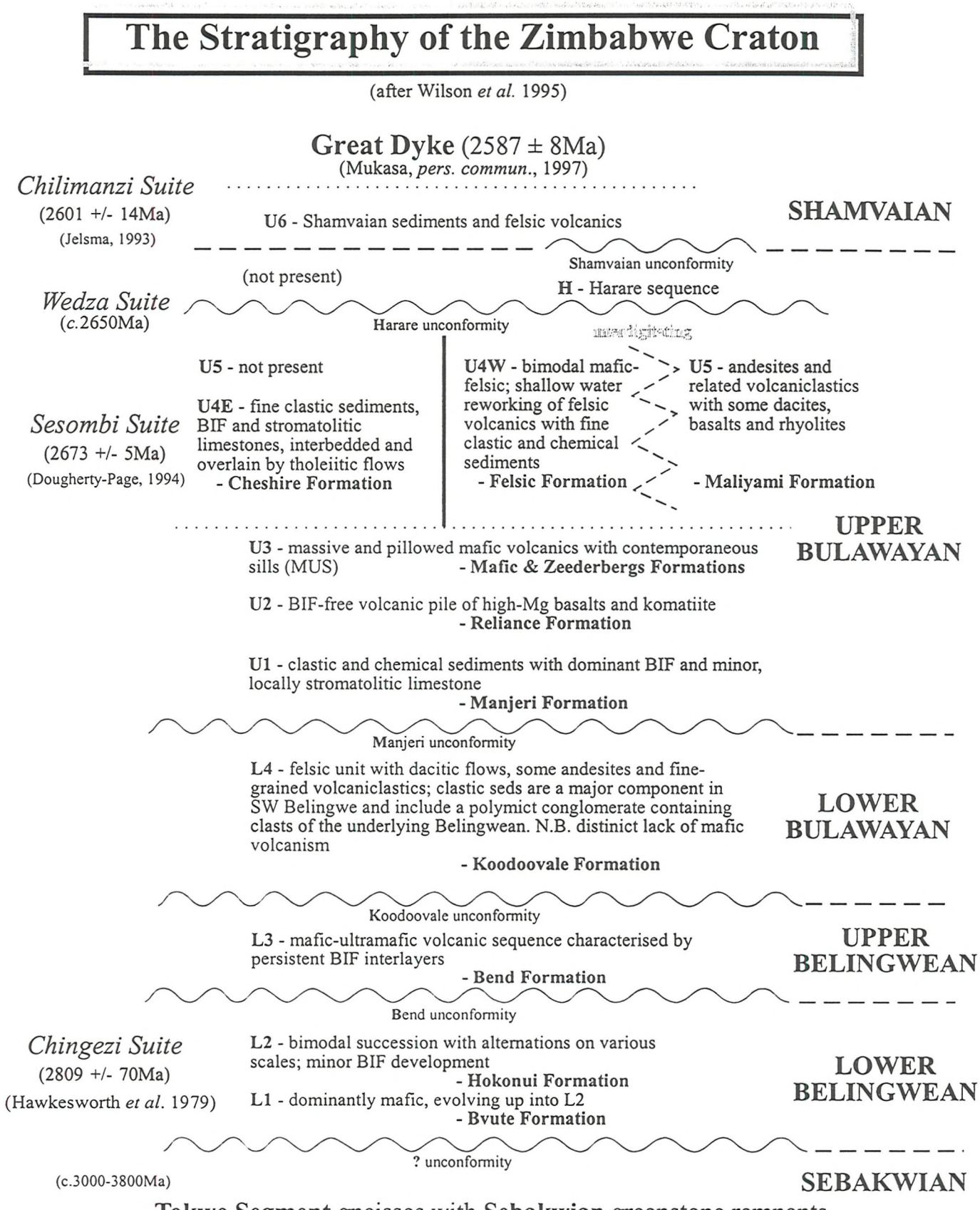
The Stratigraphy of the Zimbabwe Craton
(after Wilson et al. 1995)
Great Dyke (2587 ± 8Ma)
(Mukasa, pers. commun., 1997)
Chilimanzi Suite
(2601 +/- 14Ma)
(Jelsma, 1993)
U6 - Shamvaian sediments and felsic volcanics
SHAMVAIAN
Shamvaian unconformity
(not present)
H - Harare sequence
Wedza Suite
(c.2650Ma)
Harare unconformity
U5 - not present
U4E - fine clastic sediments, BIF and stromatolitic limestones, interbedded and overlain by tholeiitic flows
- Cheshire Formation
Sesombi Suite
(2673 +/- 5Ma)
(Dougherty-Page, 1994)
U4W - bimodal mafic-felsic; shallow water reworking of felsic volcanics with fine clastic and chemical sediments
- Felsic Formation
U5 - andesites and related volcaniclastics with some dacites, basalts and rhyolites
- Maliyami Formation
UPPER BULAWAYAN
U3 - massive and pillowed mafic volcanics with contemporaneous sills (MUS)
- Mafic & Zeederbergs Formations
U2 - BIF-free volcanic pile of high-Mg basalts and komatiite
- Reliance Formation
U1 - clastic and chemical sediments with dominant BIF and minor, locally stromatolitic limestone
- Manjeri Formation
Manjeri unconformity
L4 - felsic unit with dacitic flows, some andesites and fine-grained volcaniclastics; clastic seds are a major component in SW Belingwe and include a polymict conglomerate containing clasts of the underlying Belingwean. N.B. distinict lack of mafic volcanism
- Koodoovale Formation
LOWER BULAWAYAN
Koodoovale unconformity
L3 - mafic-ultramafic volcanic sequence characterised by persistent BIF interlayers
- Bend Formation
UPPER BELINGWEAN
Bend unconformity
Chingezi Suite
(2809 +/- 70Ma)
(Hawkesworth et al. 1979)
L2 - bimodal succession with alternations on various scales; minor BIF development
- Hokonui Formation
L1 - dominantly mafic, evolving up into L2
- Bvute Formation
LOWER BELINGWEAN
? unconformity
(c.3000-3800Ma)
SEBAKWIAN
Tokwe Segment gneisses with Sebakwian greenstone remnants

Probably of intrusive equivalence to the Lower Belingwean Hokonui (L2) Formation, but with the actual relationship unsure (Martin *et al.*, 1993), the Chingezi gneiss is dated at 2809 ± 70Ma by Hawkesworth *et al.* (1979) (Rb-Sr). However, the authors of this date do not distinguish between the Chingezi gneiss and the Chingezi tonalites which intrude them. Taylor *et al.* (1991) show Pb-Pb WR ages for the tonalites from 2874 ± 32Ma to 2686 ± 94Ma. The upper of these two ages is generally favoured since good stratigraphic control is present in the form of the Mashaba-Chibi dykes, thought to be the feeders to the Upper Bulawayan volcanic succession, and thus *c.*2.7Ga in age.

These L1-L3 subdivisions are recognised in the west of the Mberengwa (Belingwe) greenstone belt. However, in the east the stratigraphy differs and a separate formation, the Brooklands Formation, is thought to be equivalent to the Bend Formation (Martin *et al.*, 1993). However, significant differences are apparent and the Brooklands Formation as described, may include rocks which should actually be part of the Sebakwian Group (Wilson *et al.*, 1995: Fig.1 caption).

2.2.3 Bulawayan Supergroup

The history of the stratigraphic nomenclature of the unit now termed the Bulawayan, is complex and Table 2.1 is an attempt to summarise the literature on this matter. Principally however, the Bulawayan is now defined as a Supergroup which is split into the Upper and Lower Bulawayan groups. The Bulawayan Supergroup has recently seen a plethora of work and dates published on it (Baldock & Evans, 1988; Taylor *et al.*, 1991; Blenkinsop *et al.*, 1993; Wilson *et al.*, 1995). Under the Wilson *et al.* (1995) stratigraphy, the Koodoovale Formation is considered Lower Bulawayan (L4) and hence separates the Bulawayan Supergroup from the Upper Belingwean Bend Formation (L3) below it, by a major unconformity (see Fig.2.2). This Koodoovale unconformity represents a major stratigraphic break between the two greenstone volcanic episodes and implies a major time gap. This is contrary to Martin *et al.* (1993) who record no angular discordance but observe erosive channels, and clasts of the underlying Bend Formation, in the basal conglomerate of the Koodoovale Formation.

Table 2.1 - HISTORICAL STRATIGRAPHIC NOMENCLATURE OF THE ZIMBABWE CRATON

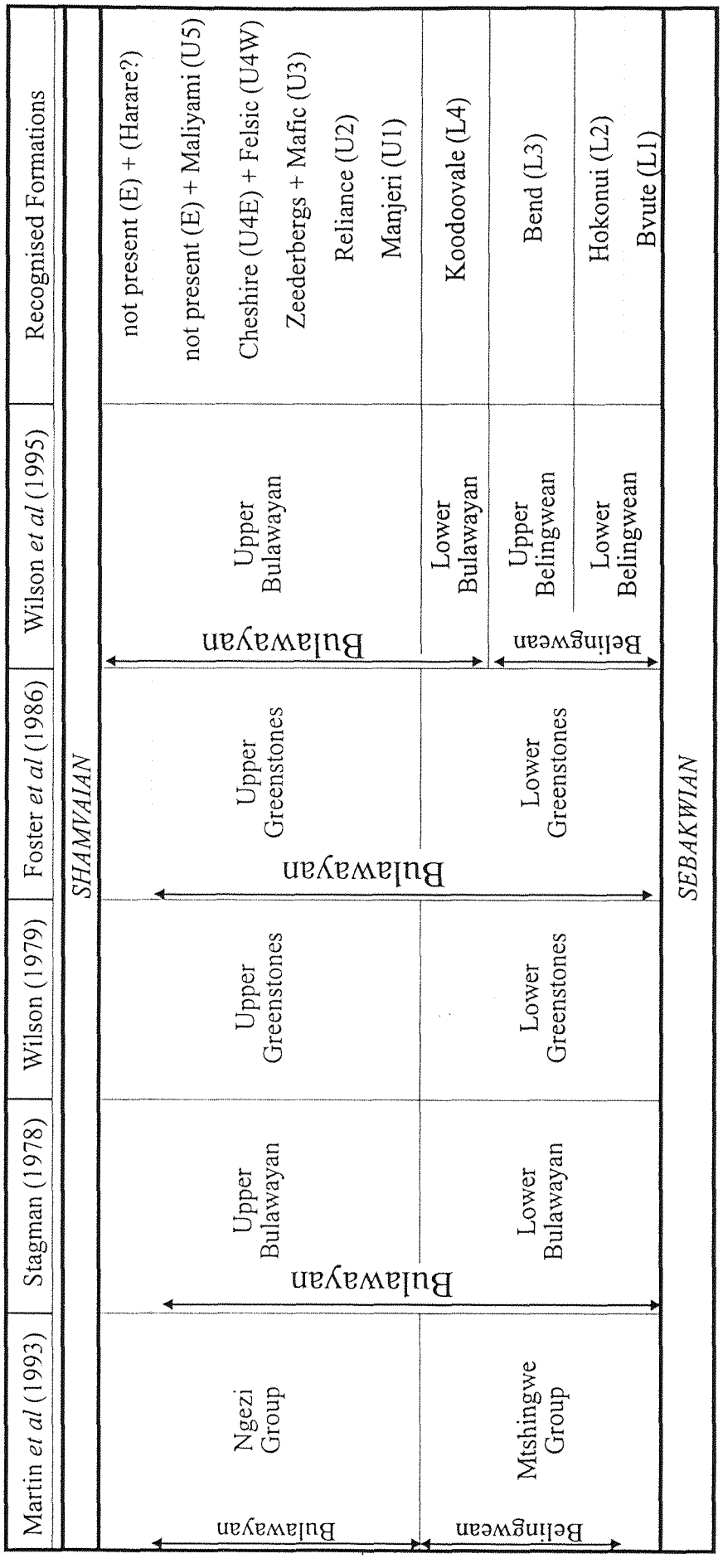

On the whole, the Upper Bulawayan Group is *c.*2.7Ga old and consists of a relatively complete cycle of mafic and ultramafic volcanism with felsic and calc-alkaline sequences occurring variably on a regional scale. These rocks form the predominant outcrop in Zimbabwean greenstone terrains today and it is this group which has allowed the craton-wide correlation of the greenstone belts, mainly by recognition of a bimodal mafic-felsic unit (U4W) within the stratigraphy. The Upper Bulawayan is marked at its base by a major unconformity. In the Mberengwa type locality, this Manjeri unconformity can be seen to lie directly on the *c.*3.4Ga Shabani Gneiss (3495 ± 60Ma, Rb-Sr, Moorbath *et al.*, 1977), indicating that by this time (*c.*2.7Ga) continental crust was evident and formed the base to the overlying greenstone succession. This report will concentrate on the nature and timing of the Upper Bulawayan volcanism, therefore a brief description of the Upper Bulawayan type lithologies follows.

The basal Manjeri Formation (U1) consists primarily of BIF with minor limestones which are stromatolitic in places (Bickle *et al.*, 1975). This is overlain by the Reliance Formation (U2) of ultramafic lavas exhibiting spinifex-textured komatiites and komatiitic high-Mg basalts (Scholey, 1992), with later development of massive and pillowed mafic lavas, limited andesites and major intercalations of BIF representing the Zeederbergs Formation (U3) (Brake, 1996). From this point the geology representing the U4 stratigraphy is different in the east of the craton (U4E) to that seen in the west (U4W). U4E comprises thick tholeiitic lavas interbedded with and overlying, fine clastic sediments, BIF and stromatolitic limestones; whilst U4W consists of mafic-felsic bimodal volcanism - exhibiting considerable reworking of the felsic volcanics in a shallow water setting, finer grained sediments and BIF. U5 is only seen in the western stratigraphy and comprises a thick calc-alkaline andesitic volcanic pile including volcaniclastics, with some basaltic and rhyolitic components. The exact position of this unit in the stratigraphy is unknown but is placed above U4W based on stratigraphic correlation with adjoining areas and other greenstone belts (Wilson, 1979) although an interdigitation of U4W and U5 may be more appropriate (Wilson *et al.*, 1995).

Broadly synchronous with the U5 and U4W volcanism is the intrusion of the Sesombi-suite tonalites (2673 ± 5Ma, Pb-Pb Kober technique, Dougherty-Page, 1994). These stocks crop out in a distinctive pattern across the western part of the craton and are recognisable by their homogeneous tonalitic nature. They exhibit very little evidence for

inclusions or assimilation of any kind and this is confirmed by a low initial-Sr value (0.7008 ± 0.0008 Wilson *et al.*, 1978) indicating a direct mantle derivation. In the north of the craton, in the Harare greenstone belt, Wilson *et al.* (1995) have recognised a suite distinct in nature from the Sesombi suite and fractionally younger (c.2.65Ga) in age, which they have called the Wedza suite (2667 ± 4Ma, U-Pb zircon, Jelsma, 1993). They believe it is the plutonic equivalent of their Harare sequence, which they recognise as being another, younger cycle different from the U4W lithology, and separated from such by the Harare unconformity (see Fig.2.2).

2.2.4) Shamvaian Supergroup

Completing the Late Archaean greenstone sequence, is the *c.*2.6-2.65Ga Shamvaian Supergroup (U6) of sediments with locally apparent felsic volcanism. A craton-wide unconformity exists between this sequence and the underlying volcanic succession.

At *c.*2.6Ga (2574 ± 15Ma, Rb-Sr, Hickman, 1978; 2601 ± 14Ma, U-Pb zircon, Jelsma, 1993) a craton-wide intrusive event represented by the Chilimanzi granites(*s.s*), indicates that the craton had become a rigid coherent mass which acted as a whole block by this time. The relatively high initial-Sr value (0.7040 ± 0.0005, Hickman, 1978), suggests derivation by anatexis, and the intrusion of the Great Dyke 150Ma later, also indicates that cratonisation had occurred by this time. Intrusion of the Mashaba-Chibi dykes, thought to be the feeders of the Upper Bulawayan U2-U3 volcanics (Wilson *et al.*, 1978), into the Tokwe segment at *c.*2.7Ga suggests that at this time the Tokwe segment itself, had become a stable nucleus for the formation of the rest of the craton.

Subsequently, dyke activity continued to occur into the Proterozoic with the most significant period at *c.*1.8Ga, characterised by the Sebanga Dykes of the Mashonaland suite in the east of the craton.

2.3) HISTORY AND CONTROVERSY IN THE ZIMBABWE CRATON

2.3.1) Models to date

Ever since the seminal paper of Macgregor (1951), debate and disagreement have raged. Macgregor recognised the importance of the granitoid complexes to their complementary greenstone belts in the granite-greenstone terrains of the Zimbabwe Craton. He considered these granitoids to have been responsible for deforming the intervening greenstone belts into the arcuate geometries observed today, through a process of diapiric intrusion and ballooning of the plutons and coigned the now famous term 'gregarious batholiths' to describe them. Later it was recognised that the granitoid terrains are in fact composite and consist of numerous phases of granitoid intruded on a temporally and spatially varying scale.

Coward (1976) and Coward *et al.* (1976) used the phrase 'billiard-ball tectonics to describe the jostling effect of the granitoids and their subsequent effect on the adjacent greenstones. This theme was continued by Wilson (1990) who perceived the effect to be present although with the 'balls' confined by a non-triangular snooker frame represented by the developing and stabilising craton.

This theme, initiated by Macgregor 40 years previously, was continued by Treloar *et al.* (1992) who considered the structural events recorded in the Zimbabwe Craton as analogous to the evolution of the Himalayan-Tibetan region over the last 50Ma. The model envisaged lateral extrusion of large parts of the Zimbabwean crust in response to collision and overthrusting of the Limpopo belt and Kaapvaal Craton, causing overthickening of the continental crust. Regional scale shears were considered to define these extruded blocks which characteristically have arcuate perimeters. However, after further consideration of this model, Treloar & Blenkinsop (1995) considered it "largely untenable", realising that some of the regional scale shears which had previously been defined were in fact composed of a number of discontinuous shears often of different generations. In place of this model a more comprehensive study and theory was defined considering the role of the different zones in the Limpopo Belt.

Consideration of the greenstone belts themselves was brought to the fore-front of discussion by Wilson (1979) in a highly acclaimed contribution invoking craton-wide correlation for the observed greenstone belt stratigraphies. For the first time (Wilson *et al.*, 1978) a similarity in the volcanic stratigraphy of all the greenstone belts was noticed. This hypothesis recognised the regional equivalence of certain horizons in spatially separated greenstone belts, and considered the volcanic stratigraphy of each to consist of a number of repeated ultramafic-mafic to mafic-felsic cycles developed to varying degrees within each setting.

This craton-wide correlation of the greenstone belt stratigraphies and the intervening granitoid suites, was seen as a landmark in the understanding of the geology of the craton and spurred a plethora of work including remapping and reinterpretation of existing data. Another important issue arising from Wilson *et al.* (1978) was that of the environment of deposition of these volcanics. Wilson *et al.* (1978), Wilson (1979) and others, recognised palaeoenvironmental features which indicated that the greenstone belts of the Zimbabwe Craton, and in particular the Belingwe belt, which had become the type locality of the Zimbabwe stratigraphic column, had been erupted through continental crust and therefore represented ensialic volcanicity most probably caused by rifting processes within the craton (Wilson, 1979). Environmental interpretation of the volcanic and interbedded sedimentary sequences was followed by Dodson *et al.* (1988) who recorded 3.8Ga detrital zircons in sedimentary horizons from greenstone belts in the south-central and extreme south of the craton indicating that at the time of formation of these greenstone belts ancient crust was exposed and being eroded. Along with supporting isotope data of Moorbath *et al.* (1977), Taylor *et al.* (1991) and Chauvel *et al.* (1993), this strongly suggested that the volcanics comprising the greenstone belts were ensialic in origin.

2.3.2) The Great Allochthon Debate

On consideration of observations in others cratons around the world, Kusky & Kidd (1992) reinterpreted the Upper Bulawayan part of the volcanic stratigraphy in the Belingwe greenstone belt to be part of an allochthonous oceanic plateau obducted onto the continental crust. This interpretation was based on structural and microstructural analysis of the rocks at the boundary between the sedimentary Manjeri formation at the base of the sequence and the

spinifex-textured komatiites of the Reliance Formation above. These authors considered these structural factors to be indicators of the decollement surface over which the allochthon was transported. This interpretation was reflected by Scholey (1992) who also considered this to be the case and 'recognised' thrust characteristics in the relevant part of the stratigraphy in some of the other sections he had investigated.

Blenkinsop *et al.* (1993) strongly disputed these suggestions, citing the enormous amount of work over many years by many different scientists which all indicated a within-continent generation for the Belingwe greenstone belt. Evidence considered included quartzose sandstone horizons intercalated within the Reliance Formation komatiites (considered to be of ophiolitic nature by Kusky & Kidd, 1992) which necessitated a proximal terrigenous source. Pb-Pb and Sm-Nd isotopic data (Chauvel *et al.*, 1993) also seemed to confirm an ensialic eruptive origin for the greenstone belts, indicating contamination by continental crust during the ascent of the komatiite magma or during its flow across the surface. This new study of an old problem allowed Blenkinsop *et al.* (1993) to refute emphatically the allochthonous oceanic plateau theory of Kusky & Kidd (1992).

A flurry of publications was led by a comment on the Blenkinsop *et al.* (1993) paper by Kusky *et al.* (1994), supporting the allochthon argument with new field data and interpretations, and a reply to this (Blenkinsop *et al.*, 1994). Bickle *et al.* (1994) also rejected the hypothesis of Kusky and co-workers on the basis that "field, stratigraphic and geochemical evidence contradict the idea". They then went on to infer that, considering the presence of interbedded shallow water sediments and zircon xenocrysts dated in the Kambalda deposits of the Yilgarn Block (Claoue-Long *et al.*, 1988) and in the Pilbara Block (Horwitz & Pidgeon, 1993), the ophiolitic origin proposed for other greenstone belts, principally in the Canadian Craton (Helmsteadt *et al.*, 1986), was "at best ambiguous".

The latest development in this particular debate, which is fundamental not just to the interpretation of one greenstone belt but of the whole craton and indeed Archaean processes recorded in cratons across the globe, is a significant contribution by Kusky & Winsky (1995). They dismiss the variable Nd-isotopic evidence of Chauvel *et al.* (1993) which is so important to the argument of Blenkinsop, Bickle and co-workers, as being well within that expected for mafic pillowed ophiolitic sequences generated proximal to continental material and assimilating terrigenous sedimentary deposits such as turbidites. Kusky & Winsky also

show detailed structural and petrographic evidence including maps and logs drawn at the localities, supporting their 'thrust sheet ophiolite' hypothesis. In contrast to others they state the "entire Manjeri/Reliance contact is intensely deformed" and suggest that one way to resolve this long-running debate would be to date the quartz-gabbros at the base of the Reliance Formation by U-Pb zircon geochronology. Should these zircons prove to be older than the minimum age for detrital zircons from the Manjeri Formation, the allochthonous oceanic plateau concept would be credible.

An interesting observation made by Scholey (1992) is that the known length of the proposed basal detachment between the Manjeri and Reliance formations is the same as the sub-parallel, intrusive Shabani Ultramafic Complex, of approximately equal age, which would probably have formed a topographic high thereby preventing the deposition of any significant thickness of volcanic lavas.

Two new models for the evolution and stabilisation of the Zimbabwe Craton have recently been advanced to challenge that built up by Wilson and co-workers. The first of these, just preceding the second, is proposed by Dirks & Jelsma (1998). They recognise significant layer-parallel shearing within units formerly considered to be banded-iron formations (BIF) such as the U1 Manjeri Formation. These strongly silicified, fine-grained, mylonitic, siliceous mica schists with a mineral lineation 'tangential to the batholith' or intruding phase, are considered to accommodate imbricate stacking of the stratigraphy leading to a series of thrust sheets with mafic and felsic components stacked one on top of the other. Dirks & Jelsma (1998) consider that this stacking would seriously disturb the equilibrium geotherm, resulting in significant perturbations within the temperature profile of the crust depending on the position and thickness of the mafic units. In trying to equilibrate these temperature differences, the equilibrium geotherm would be higher than that which existed before the imbricate thrust stacking event. The higher geothermal gradient, largely controlled by the mafic volcanic units now within the crust, is thought have been the cause of the massive crustal melting episode which led to the formation and intrusion of the Chilimanzi Suite of granites.

The second model suggests an altogether more comprehensive scenario. Kusky (1998) proposed the existence of the 'Tokwe Terrane', an ancient cratonic core of the craton similar to the Tokwe Segment of Wilson (1990). Kusky (1998) considered this 'terrane' extended NE-SW across the craton from the Zambezi mobile belt in the north-east, down into

Botswana in the south-west, and from Kwekwe in the west to a boundary in the east termed the Umtali Line linking Mutare and Zvishavane. The author also considered it to be a stable cratonic block which rifted along the Umtali Line to form the Sea of Umtali. Within this sea were formed oceanic basalts which were obducted onto the continental margin during closure along the same lineament by which the sea had opened. The belts such as the Mberengwa (Belingwe) Greenstone Belt, formed the Southern Magmatic Belt, whilst the Northern Magmatic Belt consisted of those greenstone belts such as the Midlands Greenstone belt which contained the U4W succession in their stratigraphy. These greenstone belts were considered to have calc-alkaline affinities characteristic of arc magmatism and the whole belt to represent a magmatic arc formed on the continental margin as a result of melting of a basaltic slab subducting from the north-west. 2.9-3Ga sedimentary sequences forming the Buhwa and Mweza greenstone belts were interpreted as shelf-facies shallow marine rocks formed as a sedimentary wedge on the north-west margin of the south-eastern part of the rifted continent, prograding onto the Tokwe Terrane prior to the formation of the major 2.7Ga volcanic successions. Kusky (1998) continued, suggesting that collision of the Zimbabwe and Kaapvaal cratons, resulted in orogenesis and the formation of a craton-wide system of crustal-scale strike-slip faults which provided pathways by which lower crustal and mantle fluids could escape into the upper crust. Here the fluids decreased the solidus temperature of the crust and caused major intra-crustal melting represented by the Chilimanzi Granite Suite. It is interesting to note that both Kusky (1998) and Dirks & Jelsma (1998) use major strike-slip faulting to provide the crustal shortening required for their respective models and yet one causes the Chilimanzi melting event whilst the other does not. Both these authors however, consider the Mberengwa (Belingwe) Greenstone Belt to be allochthonous and the belts such as the Midlands to be continental magmatic-arc or back-arc basin deposits.

This enthralling debate and discussion through the scientific press is one of many issues in Zimbabwean geology, some of which will be discussed later, which have occurred in the past and will continue to occur in the future. This can only lead (finally!) to a better understanding of the processes which shaped the Archaean cratons of the world, by keeping our minds open and causing us to re-examine data from a fresh, objective perspective.

CHAPTER 3 - MIDLANDS GREENSTONE BELT GEOLOGY AND STRATIGRAPHY

3.1) CURRENT UNDERSTANDING OF THE MIDLANDS GREENSTONE BELT AND ITS POSITION IN THE REGIONAL STRATIGRAPHY

3.1.1) Background to the Midlands Greenstone Belt

The location of the Midlands Greenstone Belt (MGB) can be seen in Figure 2.1. It is one of the largest greenstone belts in the Zimbabwe Craton and contains some of the best-preserved and least-altered rocks. From this point of view, it is a very good area to study, not least because 3 major rivers run across it. One of these rivers, the Sebakwe, was chosen as the study area since along its length it provides an almost perpendicular-to-strike section through one of the narrowest parts of the greenstone belt, showing all the major lithologies, and as such displays a 'condensed section' of the stratigraphy. The information given below, is the result of 5 months cumulative fieldwork conducted in two periods - November-December 1994 and September-November 1995.

Figure 3.1 shows the MGB in detail and the path of the Sebakwe River through the mapped lithologies. The main conurbation in this area, and indeed the most important one in the whole of the Midlands region, is Kwekwe. This town has been the locus of gold mining activity for a generation and is still one of the major centres for gold production in Zimbabwe. The base from which the fieldwork was conducted was Indarama Mine just north of the river.

The stratigraphy presented here (Fig.3.2) is taken from Harrison (1970), still the most recent work conducted on the stratigraphy of the Kwekwe region. The regions to the north and south were mapped and described by Robertson (1976) and Cheshire *et al* (1980) respectively, and their reports published as regional geological bulletins. The Kwekwe region has been an important area in the historical development of the Zimbabwean stratigraphy. The Sebakwe River Conglomerate first prompted Macgregor (1932) to define the Sebakwian. He considered this body to be the base of the Upper Bulawayan stratigraphy with everything below it being older and Sebakwian in age. The view that the Sebakwe River Conglomerate

Figure 3.1

Geology of the Kwekwe Region

(after Harrison, 1970 & Robertson, 1976)

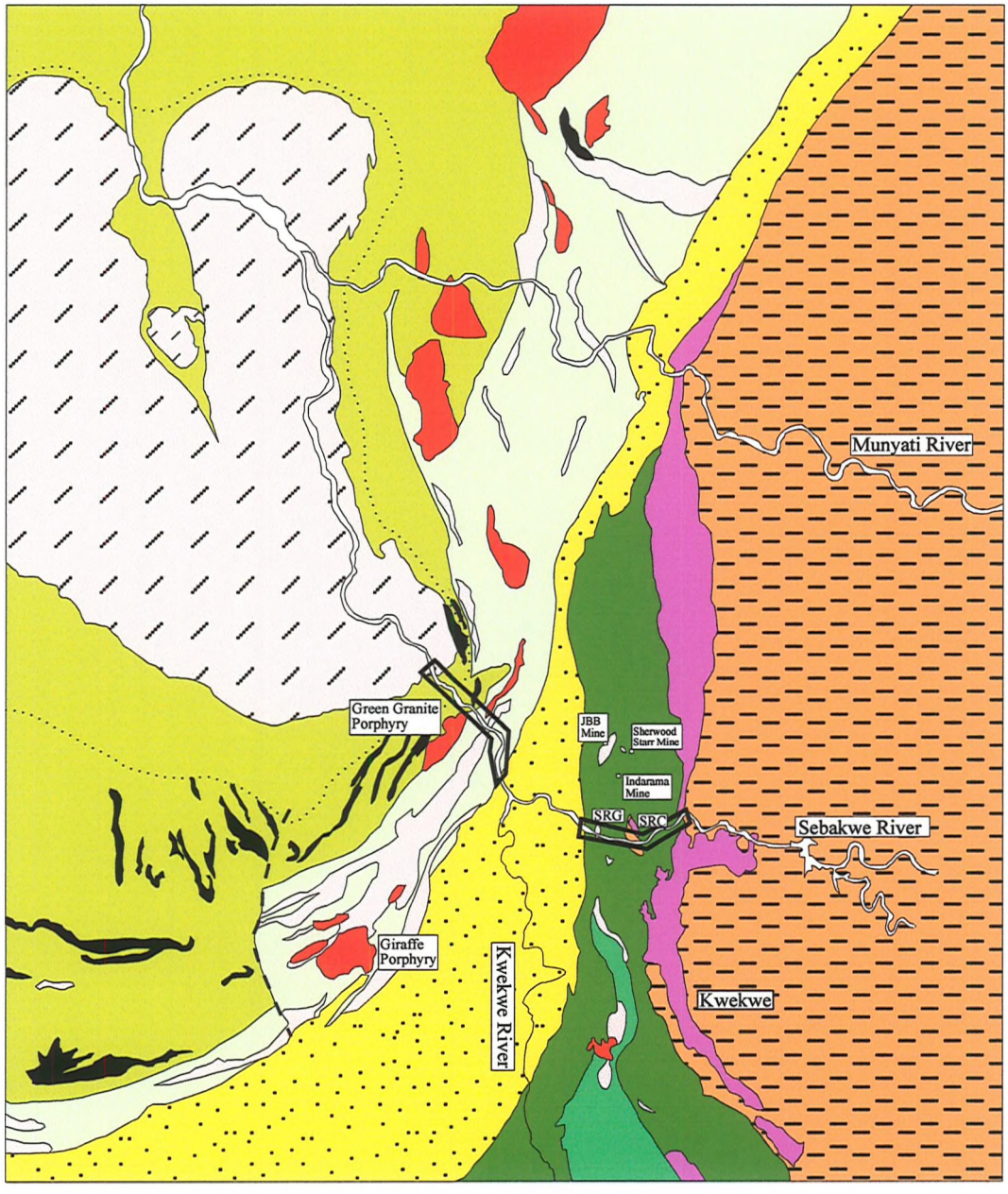

Key

0 1 2 3 4 5 miles

0 1 2 3 4 5 6 7 8 km

- Metamorphic aureole around Sesombi tonalite
- Shamvaian sediments
- Sesombi Tonalite
- Porphyries and Felsites
- Felsic volcanics of various ages
- Felsic Formation
- Agglomerates in the Maliyami Formation
- Maliyami Formation
- Mafic Formation
- Outcrop of probable Lower Bulawayan age
- Kwekwe Ultramafic Complex
- Rhodesdale Granitoid (inc. Kwekwe Gneiss)
- Main study sections

(described below) represents the base of the Upper Bulawayan stratigraphy, was contested by Harrison (1970) whose view is supported in this report.

3.1.2) The Stratigraphy of the Midlands Greenstone Belt

The stratigraphy proposed by Harrison (1970) is displayed in Figure 3.2, and has broadly speaking been borne out by this study also. Some minor differences to this are discussed in the light of the detailed stratigraphic logging conducted and these give a more complete insight into the depositional environment and nature of the magmatism.

In brief, the three volcanic formations, Mafic, Felsic and Maliyami of Harrison (1970), are considered to correspond respectively to the U3, U4W and U5 stratigraphy of Wilson *et al.* (1995), and the Mberengwa (Belingwe) type formations of Zeederbergs and Cheshire (U4E). The Maliyami U5 unit is not represented in the Belingwe (eastern) succession (see Fig.2.2). This report will follow the stratigraphy of Harrison (1970). A significant difference exists between this stratigraphic interpretation and that formulated by Wilson *et al.* (1978; 1995) and Wilson (1979). This difference relates to the position of the Maliyami Formation in the sequence. Wilson *et al.* (1995) consider it to represent the U5 subdivision as described in the previous chapter, although it is not recognised elsewhere in the craton. Whereas this isn't necessarily disputed, the corresponding stratigraphic position of the Felsic Formation is U4W. The field evidence from both Harrison and this study indicates that, based on younging indicators in the lavas, the Felsic Formation is younger than the Maliyami Formation and sits conformably above it in the stratigraphy. This variation can be explained if the relationship between the two units is one of interdigitation as suggested in figure 8 of Wilson *et al.* (1995). This would require that the course of the Sebakwe River pass through the section at a point where the Felsic Formation overlies the Maliyami Formation. Detailed structural evidence is required to determine the overall structure of this greenstone belt but until this is available, preference must be given to the interpretation for which the observations provide most warranty. To this end, it is considered that the Felsic Formation does conformably overlie the Maliyami Formation in the stratigraphy of the Midlands Greenstone Belt.

Figure 3.2
Kwekwe Regional Stratigraphy
(Harrison, 1970)

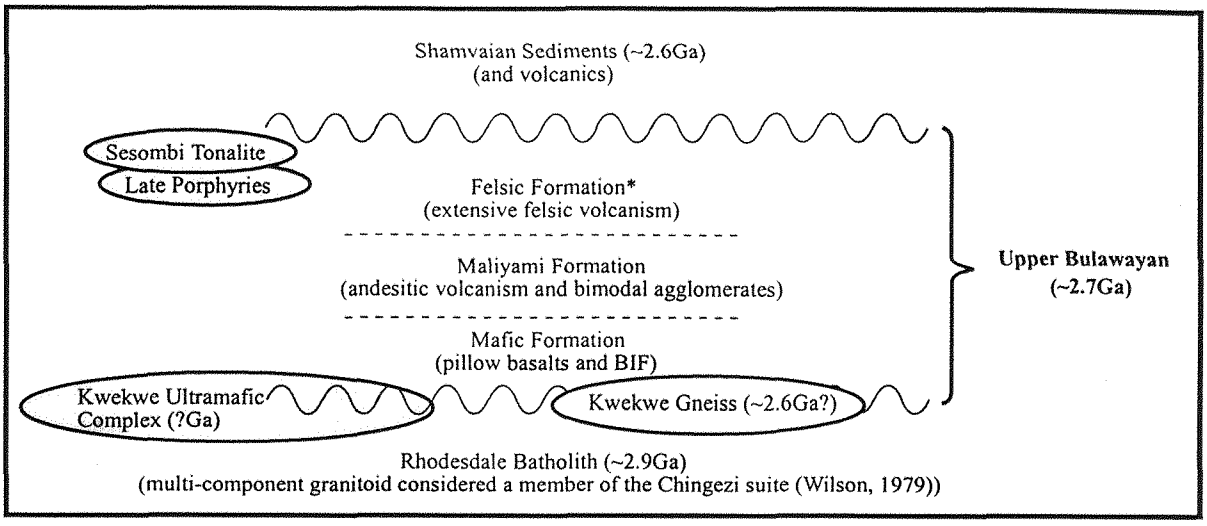

(* Note the stratigraphic position relative to the succession of Wilson *et al*, 1995)

Table 3.1

GEOCHRONOLOGY* FROM THE MIDLANDS GREENSTONE BELT

Formation/Lithology	Age (Ma)	Other Data	Referenece
Sesombi Tonalite	2633 ± 70	Sr_i = 0.7008 ± 0.0004	Hawkesworth *et al* (1975)
	2467-2614	Rb-Sr from mineral separates	Hawkesworth *et al* (1979)
	2579 +154/-173	Pb-Pb WR	Taylor *et al* (1991)
	2680	Sm-Nd T_{DM}	Taylor *et al* (1991)
	2673 ± 5	Pb-Pb zircon (Kober)	Dougherty-Page (1994)
What Cheer Formation (U4W)	2683 ± 8	U-Pb SHRIMP (2780 inheritance)	Wilson *et al* (1995)
Maliyami Formation (U5)	2663 ± 70	Sr_i = 0.7010 ± 0.0002	Hawkesworth *et al* (1975)
	2867 +171/-195	Pb-Pb WR	Taylor *et al* (1991)
	2702 ± 6	U-Pb SHRIMP	
Mafic Formation (U3)	2477 ± 140	Sr_i = 0.7034 ± 0.0006	Hawkesworth *et al* (1975)
	2380 +309/-394	Pb-Pb WR	Taylor *et al* (1991)
Rhodesdale Granitoid	2702 ± 40	Sr_i = 0.7015 ± 0.0002	Moorbath *et al* (1977)
	2976 +121/-132	Pb-Pb WR	Taylor *et al* (1991)
	2990	Sm-Nd T_{DM}	Taylor *et al* (1991)

* Rb-Sr values recalculated for a Rb decay constant of 1.42×10^{-11} yr^{-1} where necessary

An outcrop of andesites and dacites SSW of Kwekwe, was considered by Harrison (1970) to be part of the Felsic Formation, and later, in Hawkesworth *et al.* (1975), equivalence to the Mafic Formation was also suggested. Both these correlations are considered erroneous, since direct interpretation of the Harrison (1970) geological map, indicates affinity with the L4 group to be a more reasonable conclusion (Wilson, 1979).

Intimately related with and probably synvolcanic with respect to the Felsic Formation, are quartz-feldspar-porphyry intrusions such as the Giraffe and Green Granite porphyries. Clasts and matrix derived from the weathering of these intrusions are reported in the basal Shamvaian conglomerate (Harrison, 1970). Their intrusion is thought to have occurred just prior to that of the Sesombi Tonalite, synchronous with, or at the end of the volcanism.

Separating the Maliyami and Felsic Formations to the west from the Mafic Formation to the east, is the outcrop of the *c.*2.65Ga Shamvaian sediments (see Fig.3.1). These greywackes, grits, phyllites and arkoses rest unconformably on top of the volcanic succession and define four formations within the Shamvaian Supergroup as recognised by Harrison (1970), each of which is separated from the next by an unconformity. These sediments are outside the remit of this study and will not be considered in any further detail.

The outcrop of the volcanics is bounded to the east by the Rhodesdale Granitoid. This is a complex, multi-component granitoid consisting of tonalite-trondhjemite-granodiorite (TTG) lithologies of differing ages. The Rhodesdale lithology itself is truly a gneiss, showing well developed gneissose banding. Thus, when referring to this lithology the term 'Rhodesdale Gneiss' will be used whilst when referring to the mass as a whole the term 'Rhodesdale Granitoid' will be used. The most important component for this discussion is the Kwekwe Gneiss (KKG) which forms a later, possibly intrusive phase, on the western margin of the Rhodesdale Granitoid. The Rhodesdale Gneiss therefore appears to form the main lithology of a pluton, into which later phases of granitic(*sensu lato*) magma have been emplaced.

Also included in this granitoid, are remnants of an earlier greenstone episode, originally recorded as Sebakwian by Macgregor (1932) and also by Harrison (1970), but now

considered Belingwean in age (see Wilson, 1979; Wilson *et al*, 1995). Now recrystallised as fuchsite quartzites and amphibolites, these xenoliths may be all that remains of the L1-L4 stratigraphy of the MGB.

The western margin of the Rhodesdale Granitoid (including the KKG), is rimmed by the outcrop of the Kwekwe Ultramafic Complex (KUC). This body, now heavily serpentinised and carbonated, was originally a layered ultrabasic complex at least in places, as evidenced by the highly weathered (altered, but still visible) remnant layered cumulate texture. This was observed in the eastward protrusion, immediately south of the Sebakwe river (see Fig.3.1). The relationship of this layering to the attitude of the body could not be distinguished and without knowledge of this margin-layering relationship the attitude of the layering on its own is meaningless in determining the attitude of the body. The intrusion of this complex appears to be constrained by the Rhodesdale Granitoid and/or by the Sherwood Shear Zone which runs alongside it. The timing of intrusion is however, unknown but the KUC is considered to be a member of the Mashaba Ultramafic Suite (MUS) (Wilson, 1979) representing one of the magma chamber systems which fed the Bulawayan volcanism. This would therefore date it at *c*.2.7Ga.

In the west of the MGB the Maliyami Formation (U5) lavas are intruded by the Sesombi Tonalite, causing the development of a contact metamorphic aureole in the surrounding lavas. This body lends its name to a suite of rocks intruded at 2673 ± 5Ma (Dougherty-Page, 1994) and considered the plutonic equivalent of the U4W and U5 volcanism as described previously (see Fig.2.2). Contaminated granites present in the area, such as the Leith Hill stock, are thought to be the result of assimilation of greenstone belt volcanics by the Sesombi magma. However, this cannot be the case if, as is considered, the Sesombi Tonalite is pre-Shamvaian, since stocks of contaminated granite are mapped by Harrison as intruding the Shamvaian sediments. This granitic material must therefore be either Sesombi at a significantly younger age than is currently considered, or of younger origin than any previously recognised granitic component in this greenstone belt. It is proposed that, due to the history of bimodal volcanism and synvolcanic intrusion throughout the stratigraphic column, the possibility should not be ruled out, that this post-Shamvaian

granitic magma may have mixed with the post-Shamvaian metagabbros (also mapped by Harrison) to form the contaminated granite outcrops typified by the Leith Hill stock.

As discussed in the previous section, the Upper Bulawayan stratigraphy is dated at *c.*2.7Ga. Table 3.1 collates the dates so far reported in the literature, which have actually been determined from rocks of the MGB.

3.1.3) The Structure of the Midlands Greenstone Belt

A structural interpretation of the MGB is presented in Campbell and Pitfield (1994) and is shown in Figure 3.3. Previous work can be found in Macgregor (1951), and Stowe (1971; 1979).

Most of the structural interpretation of the MGB in the last 15 years has been based on interpretation of remote sensing data. On the ground, the data are more difficult to interpret since structural relationships are complex and poorly preserved in the limited exposure away from the river sections. However, in general, the structure of the Kwekwe region of the MGB can be summarised on the basis of 3 major shear zones.

The Sherwood Shear Zone (SSZ) runs parallel to the edge of the KUC and Rhodesdale Granitoid, separating them from the Mafic Formation volcanics to their west. The KUC accommodates a considerable component of the shear stress, a factor probably instrumental in the serpentinisation of this body. The SSZ appears to be the most significant of the 3 shears, both with respect to the amount of movement experienced and relationship to gold mineralisation.

The Taba-Mali Shear Zone (TMSZ) parallels the SSZ and forms the division between the Shamvaian sedimentary outcrop and the western edge of the Mafic Formation volcanics. The SSZ and TMSZ are thought to form a shear-couple, an interpretation based largely on the orientation of the BIF outcrops and duplex structures interpreted from LANDSAT imagery by Campbell & Pitfield (1994).

The Shamvaian outcrop is bounded on its western margin by the Munyati Shear Zone (MSZ). Coupled with the bounding TMSZ, these two shears are thought to define a transtensional or transpressional basin which was syn- and post-tectonically infilled by the

Figure 3.3

Major Shear Zones of the Kwekwe Region

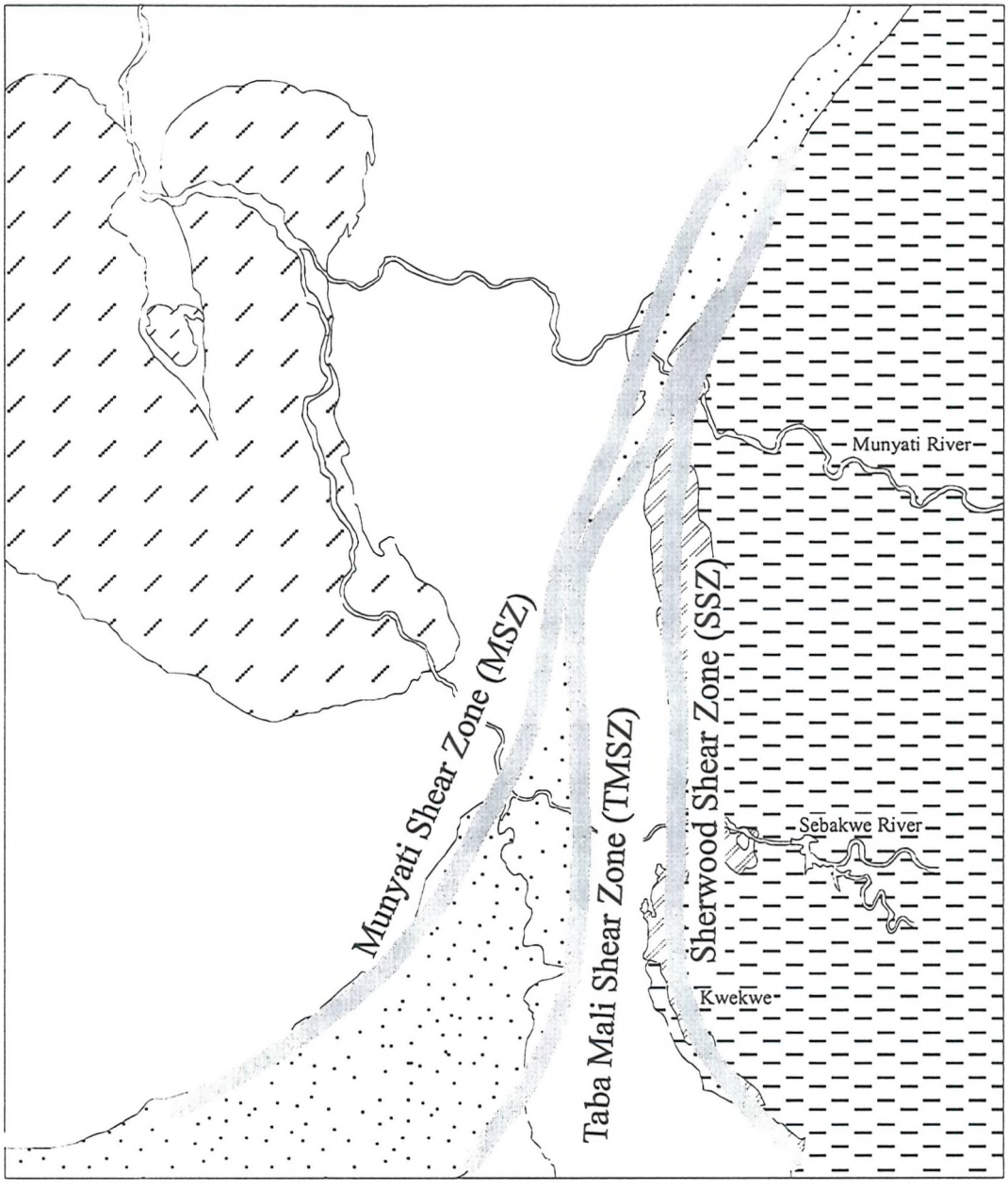

Key

0 1 2 3 4 5 miles

0 1 2 3 4 5 6 7 8 km

Shamvaian sediments

Sesombi Tonalite

Kwekwe Ultramafic Complex

Rhodesdale Granitoid (inc. Kwekwe Gneiss)

Greenstone belt volcanics

Shamvaian sediments (Campbell & Pitfield, 1994). The sediments themselves are complexly folded on a relatively small scale, some of which are syn-sedimentary (Harrison, 1970).

In contrast, the volcanics show very little evidence of intense folding. Instead the outcrops either side of the Shamvaian sediments define a broad scale synform (Harrison, 1970). This is compounded in the north-west by the intrusion of the Sesombi Tonalite into the Maliyami Formation. The broad scale synclinal structure thereby defined is in accord with the observed westerly younging Mafic Formation and the easterly younging Felsic and Maliyami Formations, and their proposed relative positions in the regional stratigraphy (see Fig.3.2).

However, recent preliminary investigations have indicated that the current models of structural control are far too simple and that the structure is a result of several stages of movement, reactivating the shear zones as well as smaller fractures (Campbell & Pitfield, 1994). Indeed, it is currently considered that the TMSZ is not a major structure (McKeagney & Blenkinsop pers.comm., 1995). This has major implications, not only for the structural history of the MGB, but also for the stratigraphy. If the TMSZ is not a major structure and does not therefore cause a major lithostratigraphic separation at its boundary with the Mafic Formation, what is the relationship between the volcanic sequence recognised as the U3 Mafic Formation, and the sedimentary sequence considered the U6 Shamvaian outcrop? It is possible for the TMSZ to be a relatively passive structure in the development of the basin and therefore not to indicate strong kinematics, but still be the site of a major lithostratigraphic boundary due to overstepping of the deposited sediments. For the purpose of this report, this contact will be considered a major unconformity until more fieldwork can be conducted to ascertain its true nature.

In a regional context, major shears such as the SSZ, TMSZ and MSZ, have been stated to have various controls, ranging from batholithic control in both a vertical (Macgregor (1951) - gregarious batholiths) and a horizontal (Coward (1976); Coward *et al* (1976) - billiard ball tectonics) sense, to a wider, cratonic control as a result of movement along the mobile belts (Wilson, 1990). The control is likely to be a combination of these processes, depending on the particular shear under investigation and its proximity to the intruding batholith and initial orientation with respect to the stress field. Recently it has been shown

that vertical kinematics due to granitoid emplacement was the major component to the stress field around the Chinamora Batholith in the Harare Greenstone Belt, and that horizontal tectonics have played only a minor part in the generation of the structures observed there (Jelsma, 1993).

3.2) FIELDWORK & PETROGRAPHY - EVIDENCE AND INTERPRETATION

3.2.1) Introduction

A traverse was undertaken along the Sebakwe river as a cross-section through the stratigraphy. The river has a roughly perpendicular-to-strike course along most of its length which enabled a thorough study of the volcanic sequence to be conducted. The traverse was broken up primarily into two sections. The first of these sections started at the contact between the Rhodesdale Granitoid and the greenstone belt magmas of the Mafic Formation and terminated at the outcrop of the Shamvaian sedimentary sequence. This traverse gives the most complete section through the Mafic Formation and will be referred to as the Mafic Formation section. The second of these major traverses began at the western edge of the Shamvaian outcrop and continued up to the Sesombi Tonalite. It allows the most complete section through the Felsic Formation to be viewed as well as giving good exposure of some of the variations exhibited within the Maliyami Formation. This section will be referred to as the Felsic-Maliyami section.

Brief investigations were also conducted into the Rhodesdale Granitoid and Sesombi Tonalite, the late porphyries and the Kwekwe Ultramafic Complex. As will be noted, the outcrop of the Shamvaian sediments was not investigated since this was considered beyond the scope of the project as the succession does not contain any volcanic material, apparent in other exposures of similar age elsewhere in the craton.

3.2.2) The Mafic Formation

This formation comprises principally mafic volcanics with interspersed BIF. Examples of ultramafic and felsic volcanics also occur, as well as sedimentary sequences (BIF`s) and a conglomeratic body (Sebakwe River Conglomerate). The felsic volcanics were considered by Harrison (1970) to be members of the Felsic Formation (section 3.2.3) erupted through the Mafic Formation lavas. This study considers them to be an integral part of the Mafic Formation sequence thereby classifying it as bimodal. A gneissic body (Sebakwe River

Gneiss) also features in the outcrop area and will be described in section 3.2.4. The whole section is intruded by late basaltic and quartz-feldspar-porphyry dykes. No andesites were found in the Mafic Formation section.

3.2.2.1) Lithologies

The main lithologies seen in the outcrop area of the Mafic Formation are pillow basalts and BIF, with some high-Mg basalts, felsic volcanics, felsic epiclastic conglomerates and grits.

The **basalts** predominantly occur as pillow lavas but also as massive flow units. The rocks young west throughout this section of the river traverse and show well preserved flows, columnar joints and younging indicators (primarily v-shaped bases to pillows). They are primarily finely crystalline and act competently in the section. Their mineralogy deviates little from the essential mineralogy of plagioclase feldspar and clinopyroxene but additionally opaque phases are common and occasionally also remnant olivine (<1%), now pseudomorphed by serpentine. Few of the rocks are truly fresh, having been metamorphosed at lower greenschist facies to epidote-sericite-chlorite-albite assemblages. The textures generally remain preserved throughout this metamorphism.

The **high-Mg basalts** show randomly orientated, clinopyroxene spinifex texture, but this is only developed on a local scale. Generally the high-Mg basalts are indicated by a negative topographic anomaly and lack of exposure. This was first realised in an exploration trench excavated by workers from the nearby Indarama Mine. The high-Mg basalts are considered to be the causative lithology of two distinct areas of negative exposure along the Mafic Formation section. As a volumetrically unimportant lithology whose exposure was limited, no samples were collected for analysis or petrography. The ultramafic lithologies, more abundant towards the contact with the Rhodesdale Granitoid, act incompetently under stress and embody most of the strain evident in the section.

The **felsic volcanics** form a minor component of the section but have a major role in the interpretation of the palaeo-eruption environment. They crop out as laterally impersistent, poorly sorted dacitic agglomerates. Clast size varies from 1-2mm to 12cm and the matrix

material is very similar to that of the clasts, indicating a proximal source. They are now pervasively epidotised and sericitised, but the remnant clastic texture is preserved. A considerable amount of carbonatisation has also occurred which may or may not relate to metamorphism and may instead, suggest alteration by pervading fluids of either late-stage magmatic origin or related to the mineralising event(s) common to the area. Sample Zimb.150 (see Log 2) is from the exposure of felsic volcanics on the Sebakwe River south-south-west of Indarama Mine. The full range of geochemistry (majors, traces, REE and Nd isotopes) and zircon geochronology, has been conducted on this sample.

It is presumably these same deposits from other parts of the area, which have been reworked and redeposited to form the **felsic epiclastic conglomerates** seen in the area (see Plate 3.1). These reworked volcanics are fine grained and the clasts are well-rounded. The deposit is largely monomictic but isolated clasts (<<1% by mode) of basalt and jaspilite indicate a local derivation for the material. These rocks are seen in Sherwood Starr mine and juxtaposed against the BIF in which JBB mine is located (see Fig.3.1). The primary mineralogy is destroyed and is now represented by finely crystalline quartz, albite, sericite, and secondary opaque phases. The clasts are distinguishable in thin section by the relative concentration of these opaque phases between the clasts and the matrix. The clastic nature is however, preserved well enough to allow preferential erosion of the matrix to leave the clasts standing proud of the surface. The presence of such sediments adds strength to the suggestion that the dacitic volcanism seen in the Mafic Formation section is contemporaneous with the basaltic volcanism.

The exposures of **BIF** form the major relief in the area, cropping out as steep ridges, and have been fractured by tectonic and/or fluid activity. These deposits are now host to economically viable gold mineralisation.

The **grits** present are usually juxtaposed against the BIF within the same sedimentary horizon. They are coarse grained, compositionally immature and clast supported, with any matrix being highly weathered and possibly feldspathic in nature.

Plate 3.1 - Felsic Epiclastic Conglomerate - showing rounded clasts with matrix of similar composition (penknife provides scale)

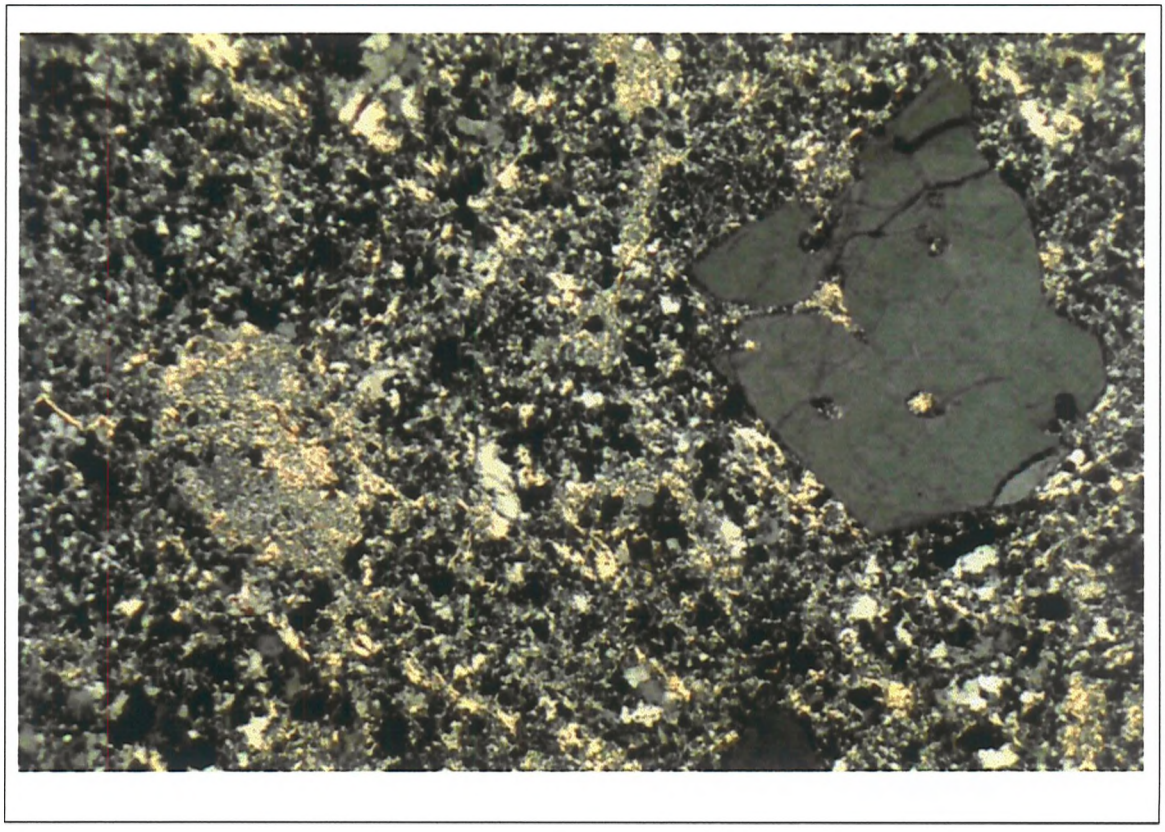

Plate 3.2 - Felsic volcanic - showing resorbed quartz, feldspar phenocrysts and low-grade greenschist facies assemblage (field of view = 3.4mm)

3.2.2.2) Interpretation

The component lithologies of the Mafic Formation and their interpretation, is summarised in Table 3.2. The principle environment of eruption is indicated by the predominance of the pillow lava and BIF lithologies. These testify to voluminous volcanism, erupted in a subaqueous environment, with relatively long periods of quiescence allowing the deposition of substantial thicknesses of BIF. Minor but important, variations on this theme are represented by the other lithologies described. The high-Mg basalts indicate that at times there is higher percentage partial melting of more primitive mantle sources and possibly even continental crustal contamination of komatiitic melts; the felsic volcanics show that the basaltic volcanism was occasionally punctuated by episodes of explosive dacitic volcanism whose evolved nature suggests assimilation of continental crust, very small scales of partial melting or fractionation of the basaltic magma; the epiclastics show that synvolcanic aqueous reworking was occurring with the material being derived locally; the coarse grained, clast supported, immature nature of the grits, suggests a local, continental crustal source. This is also evidenced by the lithology of the clasts in the Sebakwe River Conglomerate described below.

3.2.2.3) The Sebakwe River Conglomerate (SRC)

3.2.2.3.1) Lithology

This body consists of four lithologies, constituting three units. The basal unit is a gravel approximately 2.5m thick. It is possible to pick the contact with the chloritised volcanics below, although the lower half of this unit is heavily sheared. The clast material is predominantly quartz with some jaspilite pebbles.

The gravel layer is conformably overlain by finer material which is well bedded and has shaly laminations. These laminations display the relationship of this unit with the upper conglomeratic unit, indicating a rapid, mass-flow mechanism of deposition, causing scouring of the lower, finer material.

The conglomerate (*sensu stricto*) is a massive unit consisting of clasts ranging from 1cm to more than 80cm in size. The clast shape varies from very rounded to distinctly angular and indications of a shear fabric preceding that recorded by the whole body, are evident in

Table 3.2

Components of the Mafic Formation

Lithology	Interpretation
a) pillow basalts - young west throughout section - columnar joints and flows	aqueous environment and voluminous volcanism
b) BIF - significant thicknesses (100m+)	long periods of volcanic quiescence
c) high-Mg basalts - clinopyroxene spinifex locally developed	larger degree, deep mantle melting (enriched primary source?)
d) dacitic volcanics - laterally impersistent	periods of explosive volcanic activity; evolved nature may indicate residence in a magma chamber within continental crust
e) epiclastic felsic conglomerates - well-rounded to angular clasts - basaltic and jaspilitic clasts	aqueous reworking; basaltic and jaspilitic clasts suggest local derivation of material
f) grits - coarse; compositionally immature	relatively proximal to continental crustal source

Table 3.3

Components of the Maliyami and Felsic Formations

Lithology	Interpretation
a) massive and pillowed basalts and andesites - porphyrytic and vesicular	aqueous environment with much greater variation in magma composition and ejection mode compared to Mafic Formation
b) dacitic volcanics - porphyrytic and tuffaceous	extensive felsic volcanism indicating fractionation and explosive nature
c) finely bedded sediment - only ~2m thick	very little quiescence; exploited as zones of weakness for stress accommodation
d) tuffs - felsic and basaltic - bomb horizons - felsic clasts in chloritic matrix	bimodality - magma mingling causes vesiculation and eruption; bomb horizons - subaerial environment
e) oolitic limestone - intrasequence	continental shelf, shallow sea, warm water environment
f) garnet containing crystal and lithic tuffs - fining-up sequences - bands of movement - small scale folding and faulting - possibly thrusts - sulphide rich zones	gravity settling in flow mineralisation exploiting structures
g) bimodal agglomerates - siliceous clasts in basaltic matrix - clast assimmilation - main body - laterally impersistent sub-units - varying scales - associated flow-banded rhyolites	explosive volcanism and bimodality; very inconsistent - impression of moving mass of heterogeneous magma (possible volcanic vent); evolving magma chamber

some. The clast composition is rather variable but most of the lithologies can be attributed to derivation from the Rhodesdale Granitoid to the east. Mafic, felsic and jaspilitic clasts are also included. The matrix of the conglomerate, dominated by quartz and feldspar, becomes increasingly abundant towards the top of the unit as the clast input ceases and the saltation load settles out. The SRC is therefore topped by a small grit horizon before passing conformably and gradationally into a BIF.

3.2.2.3.2) Interpretation

This unit was first described by Macgregor (1932) and thought to represent the basal conglomerate of the Upper Bulawayan sequence. This interpretation is no longer thought to be correct (Harrison, 1970; this report), the unit is now considered conformable and intraformational with respect to the volcanics. The inferred mass-flow (flash-flood?) mechanism of deposition would account for the lateral discontinuity of the body, the size-range of the clasts and the immature composition of the clasts and matrix. The mafic clasts may simply have been derived from the volcanics immediately below the body but may equally have come from mafic enclaves in the Rhodesdale Granitoid (Belingwean?). The felsic clasts could have a Lower Bulawayan (L4) origin but the presence of jaspilite (Manjeri U1?) clasts suggests at least a very late Lower Bulawayan source or more likely a contemporaneous Upper Bulawayan source for the mafics, felsics and BIF. An origin combining different source areas for the different clast lithologies, and hence different chronologies, could be envisioned but seems unnecessarily complex, especially when the mass-flow nature of the deposit is considered. The main conclusion which appears inescapable, is that the TTG lithology of most of the clasts indicates derivation from the Rhodesdale Granitoid mass to the east. This must therefore have been subaerially exposed to cause its erosion, and irrefutably states that there was a continental crustal basement through which the volcanics were being erupted.

3.2.3) The Maliyami and Felsic Formations

These two formations, mapped separately by Harrison (1970), will be considered here together, since in the field they form a continuum and hence represent the evolution of the eruption environment through time. Harrison stated that the boundary between the two "is never exposed", "gradational" and "arbitrary", however, for the purpose of field mapping, an

increase in the amount of felsic material in the succession can be recognised and provides the basis for separating the two formations. This increase is gradual and necessitates a zone of uncertainty in demarcating the boundary. The characters which set these two formations apart, and on which Harrison (1970) based his classification, is the presence of bimodal agglomerates in the Maliyami Formation and extensive felsic volcanism in the Felsic Formation. The bimodal agglomerates are confined to the Maliyami Formation but felsic volcanics, although largely confined to the Felsic Formation, do occur in the former. Bimodal tuffs seem to be the equivalents of the bimodal agglomerates, being particularly prominent in the Felsic Formation and much less so in the Maliyami Formation.

3.2.3.1) Lithologies

The lithologies constituting both formations include, massive and pillowed basalts, basaltic andesites, andesites, dacites, rhyodacites, pyroclastics of various compositions, bimodal agglomerates and sediments, including an intrasequence oolitic limestone.

The **basalts and andesites** show considerable minor variation, exhibiting pillowed and massive forms with porphyritic and vesicular characteristics. Phenocrysts are usually of plagioclase although some flows have clinopyroxene phenocrysts/glomerocrysts. Few of the rocks sampled from this section were truly fresh with most exhibiting secondary amphibole replacement of the clinopyroxene and sericitisation of plagioclase. These changes are the result of the low grade greenschist facies metamorphism which has affected the whole of the greenstone belt. Later fluids have caused extensive carbonatisation of these and other rocks in the section. This metasomatism is generally restricted to parts of the section transected by a major shear such as the Taba-Mali and Munyati Shear Zones described previously.

Dacites and rhyodacites are mainly erupted as tuff deposits rather than flows, indicating pressure build up due to high viscosity and/or volatile release resulting from interaction of two or more magma pulses. They are commonly porphyritic with plagioclase phenocrysts and a fine-grained groundmass. The mineralogy is largely metamorphosed to a low grade greenschist facies assemblage of sericite, albite, and quartz. These rocks are very susceptible to carbonatisation. Their lower competency when compared to basalts and andesites leads to their exploitation during shear generation. The fluid pathways which these

shears provide cause the rock to experience flow of significant quantities of fluid. Fine-grained secondary opaque phases are also very common and are disseminated throughout the altered rocks. Some of these felsic volcanics contain quartz phenocrysts instead of, or in addition to, plagioclase phenocrysts. When present, these crystals usually show an indented and resorbed nature (see Plate 3.2). This is testimony to the change in equilibrium conditions experienced as a result of pressure decrease during eruption and/or influx of a new silica-poor batch of magma. This 'resorbed quartz' is more commonly seen in the late rhyodacitic and rhyolitic dykes which cross-cut this whole section.

Both mafic and felsic volcanics are present as **tuffs** in the Felsic-Maliyami section. The latter are the more common of the two but more frequent still are **bimodal tuffs**. This lithology is present as both felsic clasts in a basaltic matrix and the inverse of this, although the former is by far the more common. Plate 3.3a illustrates this phenomenon. It can be seen clearly, that blebs of a felsic melt have been included in a basalt. Being largely immiscible due to extreme viscosity contrasts (Philpotts, 1990), these melts have probably reacted upon association, leading to vesiculation and eruption of the heterogeneous mixture. They are, without exception, completely replaced by metamorphic and/or metasomatic assemblages as a result of their fine grain size and the reactions instigated by the association of these two contrasting magma types. The texture is still preserved and in exposure, the fragments can still be seen. The size of the material ranges from cryptocrystalline to very fine grained in the bimodal tuffs (due to the rapid nature of their cooling), up to coarse-grained when the tuff has formed as a crystal or lithic tuff.

The bimodal tuffs are the finer-grained equivalents of the **bimodal agglomerates** which characterise the Maliyami Formation. This lithology is essentially the same as the tuffs, simply containing larger clasts (see Plate 3.3b). Both variations of bimodality occur (felsic in basaltic and *vice versa*) and in some of the units assimilation is apparent as the clasts become indeterminate in shape and composition. These bimodal agglomerate units commonly have flow-banded rhyolites associated with them (see Plate 3.3c). One such unit, and the most spectacular bimodal agglomerate unit in the section, is illustrated in Log 1a & c. It is composed of laterally impersistent sub-units of bimodal associations present on varying scales from boulder agglomerates to cryptocrystalline layered mafic-felsic interleaves (Plate

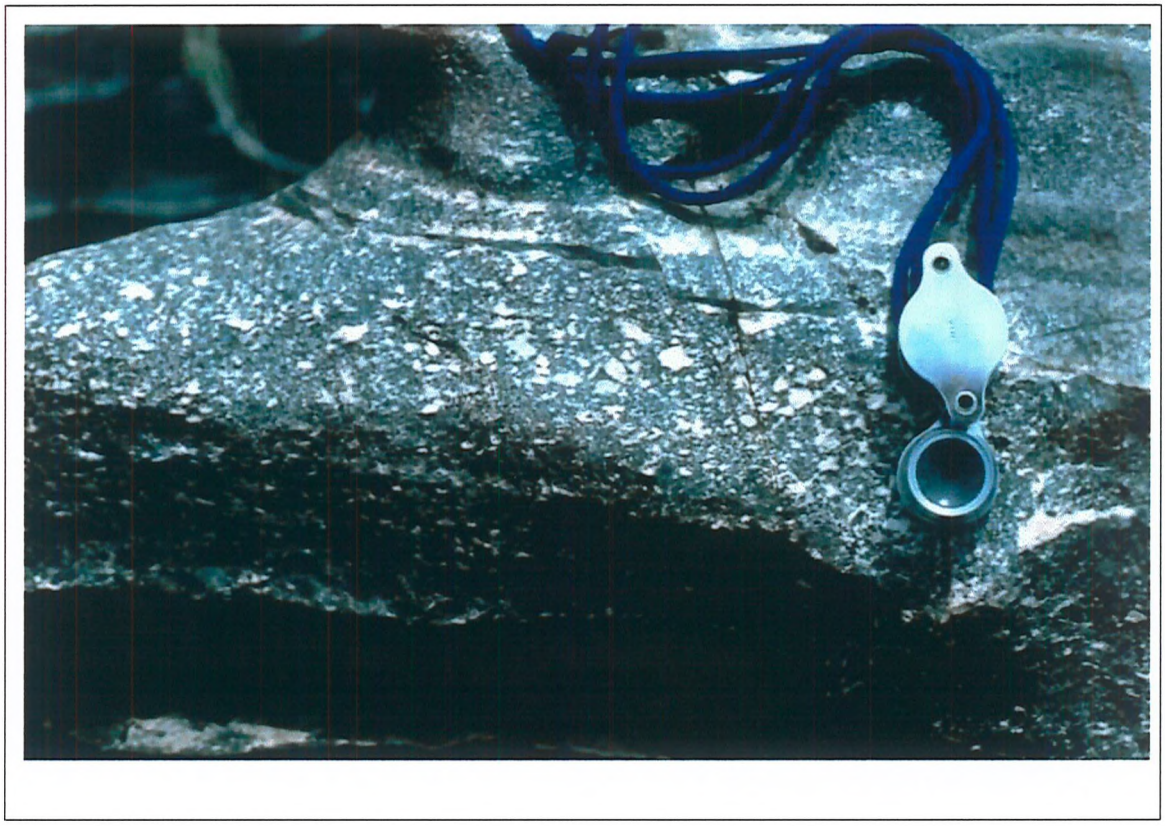

Plate 3.3a - bimodal tuff

Plate 3.3b - bimodal agglomerate - note boundary between two flows in the bottom left corner

Plate 3.3c - bimodal agglomerate and associated flow-banded rhyolite

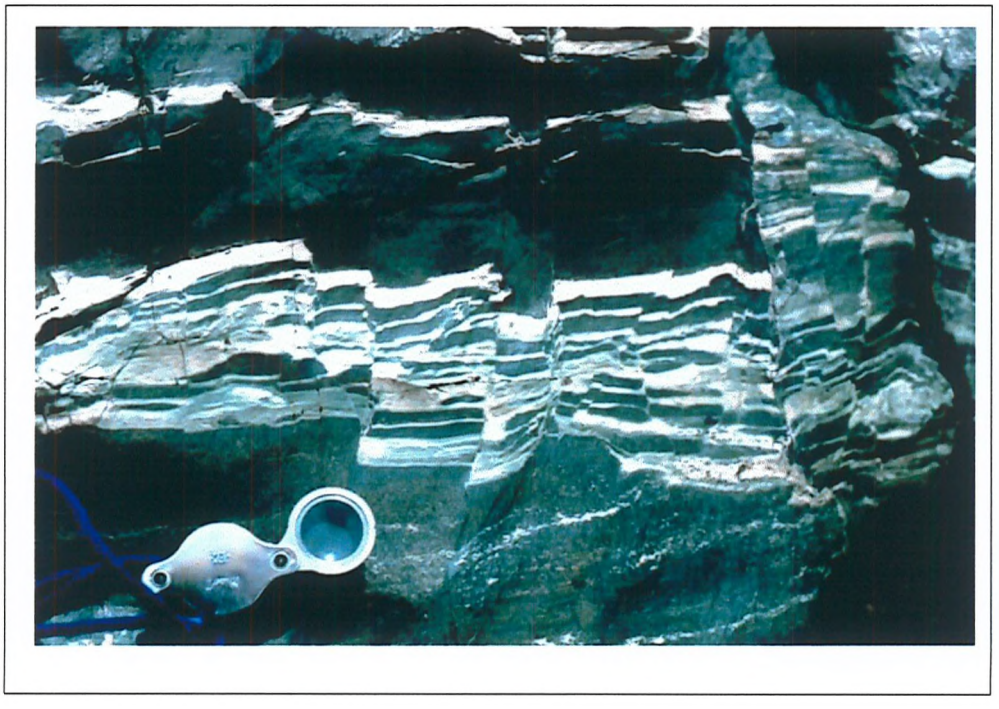

Plate 3.3d - finely layered mafic-felsic tuff interleaves in agglomerate body

3.3d). This is an incredibly heterogeneous unit as illustrated in Log 1c. Individual units are truncated at random by other units and thickness variations within individual beds are extreme. The unit seems to become more deformed with depth in the pile and in parts appears pervasively permeated by silicifying fluids.

Another tuffaceous unit present in this section through the Upper Bulawayan, is illustrated on an expanded scale in Log 1b. The most striking feature of this 10m thick unit is the presence of **garnets** as components of the lithic-tuff portion (see Plate 3.4). When present, they are concentrated at the base of the horizon and as such provide a good way up indicator. Sulphide is also common and concentrates just above the garnet-rich zone. The lithic-tuffs fine upwards into crystal-tuffs and finally into cryptocrystalline-tuffs before another horizon begins, although some of the horizons are incomplete. This unit also possesses a distinct zone of movement which indicates sinistral translation; small scale folding and faulting, including some micro-scale thrusts, resulting in repetition of the stratigraphy, can be seen in these places. This horizon is also heavily sulphidised, and whilst sulphide is present in other parts of this unit, the concentration in this zone of movement suggests that sulphide-rich fluids exploited or were related to the kinematic event.

Sediments are noticeable by their absence in the Felsic-Maliyami section, equating to only a few metres of the logged section. Small amounts are present but in significantly smaller volumes than that observed in the Mafic Formation section (Log 2). When sediments are present they are commonly finely bedded and sometimes heavily sulphidised to the extent that it is very difficult to establish their original nature. One sedimentary horizon discovered for which this was not so difficult, was an **oolitic limestone**. This surprising find, illustrated in Plate 3.5a, shows that although recrystallised the original concentric texture of the ooids has been remarkably well preserved. This limestone is significant not just in its palaeoenvironmental inference which will be discussed later, but also in its state of preservation. Present as it is, in a highly sheared section of the stratigraphy, it could be argued that it has been translocated into this position by the shear. However, it is considered that since the textural preservation is so immaculate as to conserve even the extinction cross of the ooids (see Plate 3.5b), this oolitic limestone can, at the most, have been translocated only a very short distance. The bed is 2-3m thick and the extent of carbonatisation of the adjacent felsic and basaltic rocks suggests that a) there may be more horizons of primary carbonate in

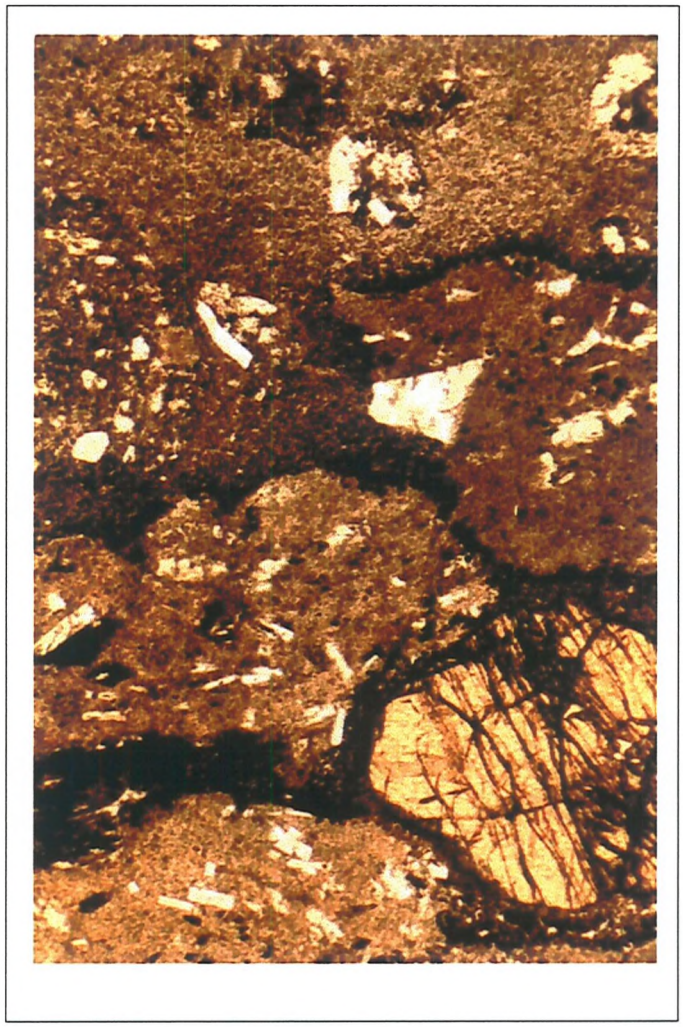

Plate 3.4 - garnet tuff horizon - showing crystal-lithic nature
(field of view = 3.4mm vertically)

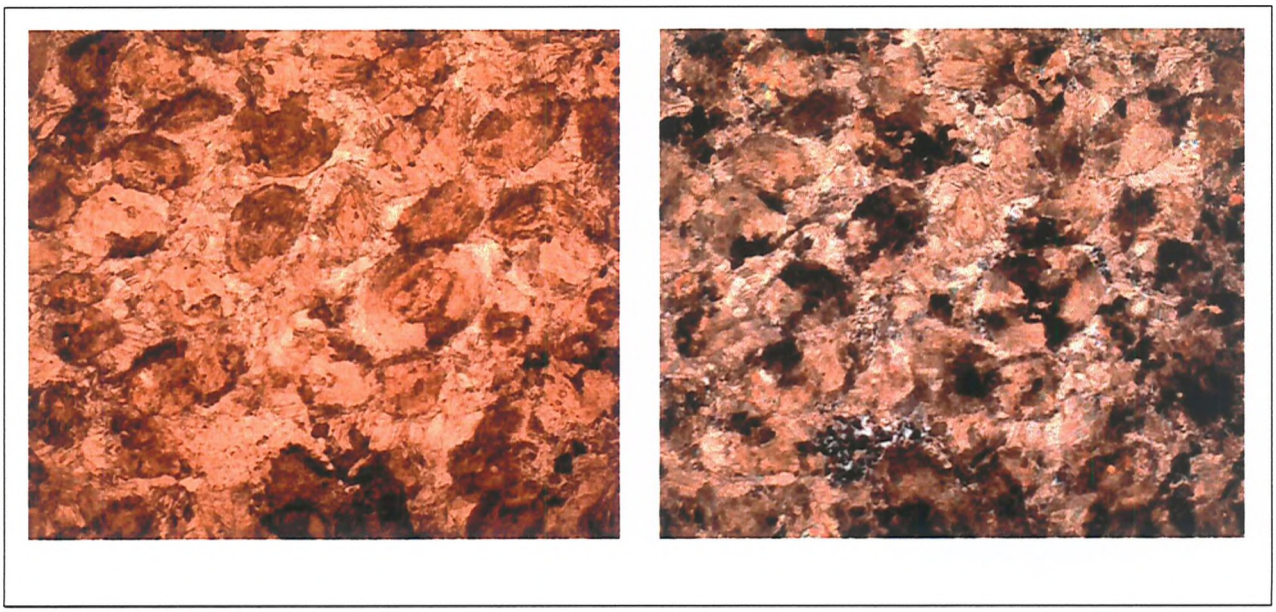

Plate 3.5 - oolitic limestone (ppl - left; xpl - right) - note well preserved optical character (extinction crosses) of ooids. (field of view ~4.6mm horizontally for each image)

this section, and b) that the texture of this oolite would have been totally destroyed if its presence was the consequence of major structural relocation, with the carbonate mobilised throughout the surrounding lithologies. It is therefore considered that this oolitic limestone is essentially intrasequence and conformable within the stratigraphy.

3.2.3.2) Interpretation

The component lithologies of the Maliyami and Felsic Formations, and their interpretation, are summarised in Table 3.3. The lavas again indicate a subaqueous environment of deposition but this time a much greater variation in the magmatic composition and ejection mode is apparent. The porphyritic lavas indicate a period of low level fractionation, whilst the vesicular variety suggests high levels of volatiles as the cause of the increase in explosive activity evidenced by the tuffs and agglomerates. The truncating relationships, varied magma types and lateral impersistence of the bimodal agglomerate body, may possibly represent a volcanic vent. This would explain the distinct impression of a moving mass of heterogeneous magma. The bimodal nature of both the agglomerates and tuffs indicates a synvolcanic relationship between the two end-member magmas, and suggests a process of magma mingling, leading to vesiculation and explosive eruption. This may or may not be combined with a periodically refilled, fractionating magma chamber below.

The voluminous felsic volcanics, possibly indicate a change in the nature and origin of magmatism with very limited periods of quiescence being represented by the thin horizons of finely bedded sediment exposed. The oolitic limestone is not exceptional and is present in other Archaean greenstone belts in other cratons such as the Superior Province in Canada and the Pilbara Block in Australia (see Eriksson (1995) and references therein). These sequences are considered to be deposited in widespread epicontinental seas which covered most of the continental crust between 3.2 and 2.0Ga ago. The preservation of the outcrop observed in the studied section is however exceptional since the ooid nature of the carbonate is unambiguously displayed. Oolitic limestones are more common after the Archaean (<2.5Ga) so the presence of this example has significant inference for the oxygen content of the environment at the time of deposition. This will be discussed in more detail in Chapter 6. Carbonates and stromatolites in general are present in other greenstone belts in Zimbabwe, notably the Harare (Jelsma, 1993) and Mberengwa (Belingwe) (Orpen & Wilson, 1981)

greenstone belts. The formation of oolitic limestone requires shallow water conditions in order to agitate the sediment at wave-base depths. Such shallow water environments would also be amenable to algae responsible for the formation of stromatolite mounds. All the evidence strongly suggests that the Midlands Greenstone Belt, Upper Bulawayan sequence was erupted through, and onto, continental crust possibly in a marginal epicontinental sea.

3.2.4) The Sebakwe River Gneiss

The Sebakwe River Gneiss (SRG) is exposed in the river due south of Indarama Mine. It has a relatively small outcrop area, only a few hundred metres across, and is mapped as impersistent both north and south of the river which exposes the body at its widest point.

Both margins of the SRG are obscured, either by the intrusion of dykes or by deformation, thus the relative age of the body to the surrounding volcanics cannot be determined.

The internal arrangement of the body is complex but can be simplified by considering the unit as an amalgamation of 3-4 phases of magma, possibly resulting from different periods of partial melting or differentiation. As such, each of the magma phases has been numbered in decreasing chronological order, i.e. Phase-1 is the oldest and Phase-4 the youngest.

3.2.4.1) Nature of the Phase Lithologies

Phase-1 is the most mafic component of this body. It is an amphibolite and as such is melanocratic. It is found as xenoliths in the Phase-2 magma usually with ragged or diffuse edges, resulting from partial assimilation. Some xenoliths, which can form large blocks up to metres in dimension, have up-turned edges (assuming the block is the correct way up) relative to an internal foliation manifest as laminations of more feldspar-rich magma (probably the Phase 2 melt) within the Phase 1 restite (see Plate 3.6b). This would seem to indicate a relative sinking of the more mafic, denser Phase-1 xenolith within the moving Phase-2 magma. In thin section (see Plate 3.6a) the rock is composed of equigranular plagioclase and blue-green pleochroic hornblende with minor (<<1%) amounts of zircon and apatite associated within and around the amphibole. In conjunction with the assemblage, the hypidiomorphic-granular texture and 120^{o} grain boundaries, indicates a mid-amphibolite facies grade for the rock.

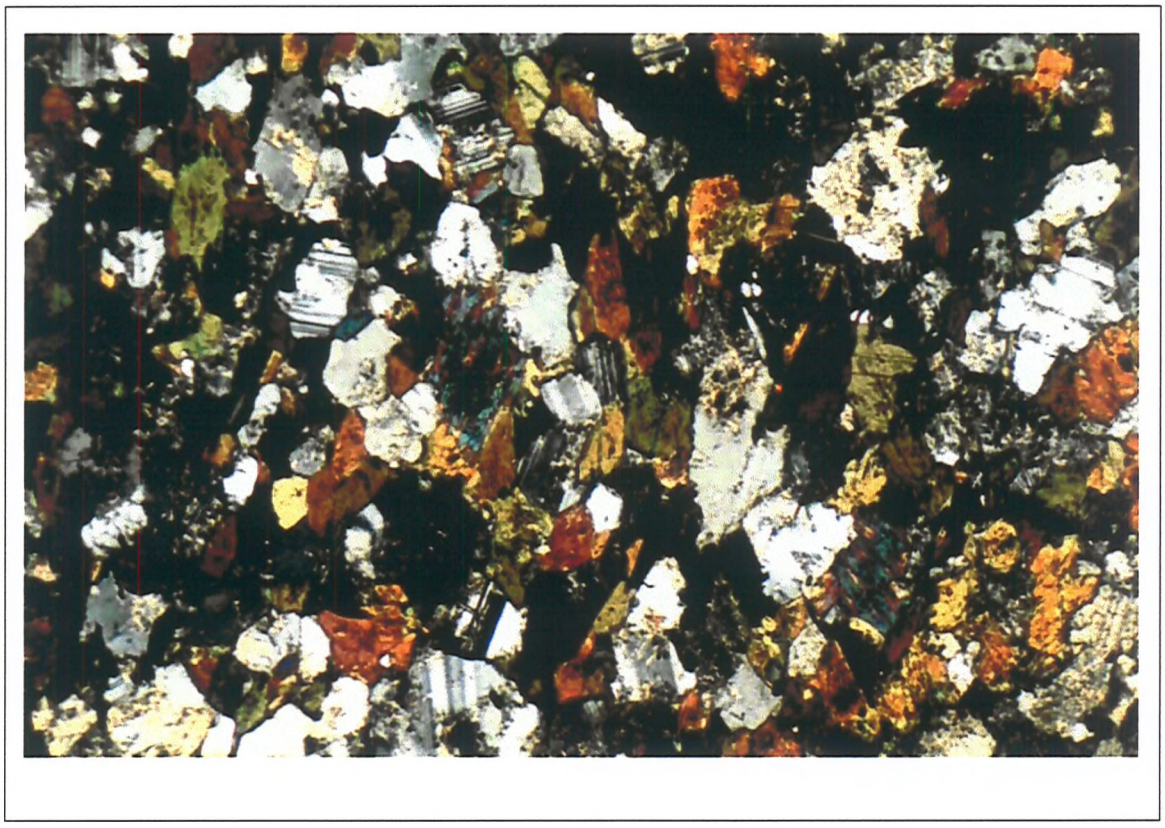

Plate 3.6a - Phase 1 Sebakwe River Gneiss - showing dominance of hornblende and plagioclase and equigranular texture with 120° crystal boundaries due to low-mid amphibolite facies metamorphism (field of view = 3.4mm)

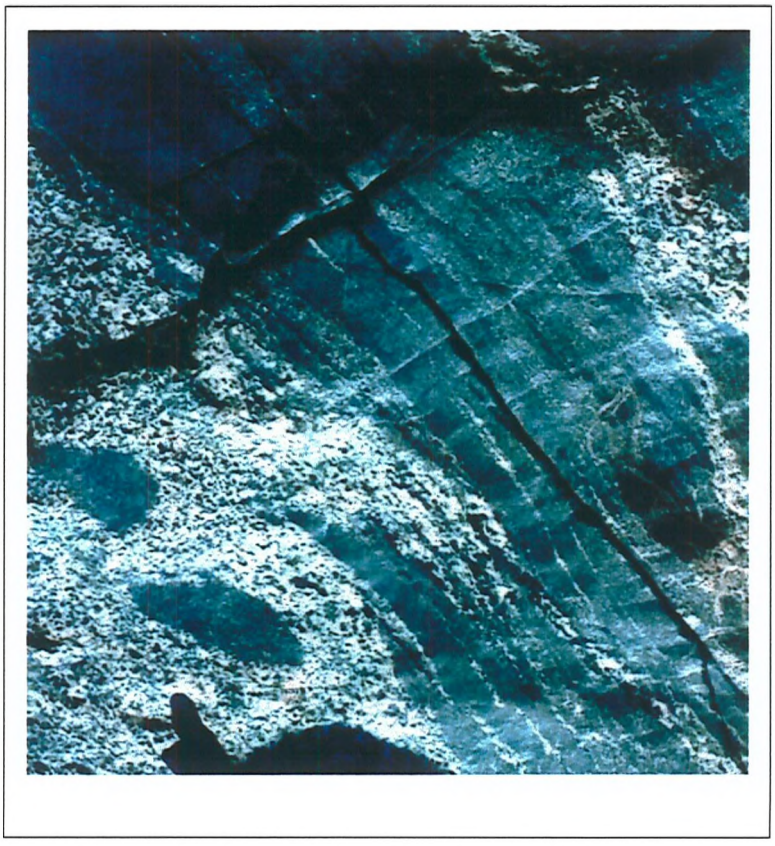

Plate 3.6b - Sebakwe River Gneiss - partial melting of Phase 1 to produce Phase 2 (field of view ~ 80cm)

Phase-2 is the dominant lithotype of the SRG and consists of a coarsely crystalline mafic-rich diorite. The dominant mineralogy (see Plate 3.6c) is biotite altering to chlorite, blue-green hornblende, quartz and plagioclase. The rock has experienced some stress, causing the amphibole to recrystallise and become polycrystalline. Quartz has reacted in a similar way and is included in the amphibole and biotite-rich domains as distinct subgrains. Biotite grains possess kinked cleavage as a result of the deformation and have also developed quartz laminae. Zircon is present predominantly enclosed in biotite, and apatite is intimately associated with the amphibole.

This phase is very heterogeneous on a very local scale and can become more quartz-rich (~15% by mode) over ~2m. This is especially apparent towards the margins of the body where the mafic mineralogy of the phase is lost but the texture largely retained. The texture is much more indicative of a primary igneous origin than the recrystallised texture displayed in Phase 1. The large feldspar and biotite crystals indicate direct crystallisation from a melt phase although the equigranular blue-green hornblende and quartz, and the alteration of biotite to chlorite, suggest subsequent metamorphism under lower amphibolite facies conditions. This phase has been selected for zircon geochronology (see sample Zimb.141, chapter 5).

Phase-3 (see Plate 3.6d) appears to be a finer crystalline, more quartz-rich version of Phase-2 and usually occurs as dykes within the earlier phase. A mantle of feldspar-rich material is developed around the intruding material as though in reaction with the Phase-2 unit. Amphibole is not present in this phase, biotite being the only mafic mineral. Quartz and plagioclase are the dominant minerals with small amounts (~3% by mode) of biotite around the margins of the grains. The plagioclase is undergoing sericitisation and the biotite is being replaced by chlorite. Deformation has resulted in quartz becoming polycrystalline although the subgrains are sometimes indistinct, and the biotite bending around the boundaries of more competent grains. A huge textural variation is displayed in Phase-3 from graphic and micrographic, to a strong (possibly flow) foliation. This is a complex phase which may yet prove to be the result of more than one magma injection.

Plate 3.6c - Phase 2 Sebakwe River Gneiss - showing plagioclase polycrystalline hornblende, quartz included in hornblende and biotite, and apatite crystallisation (field of view = 6.8mm)

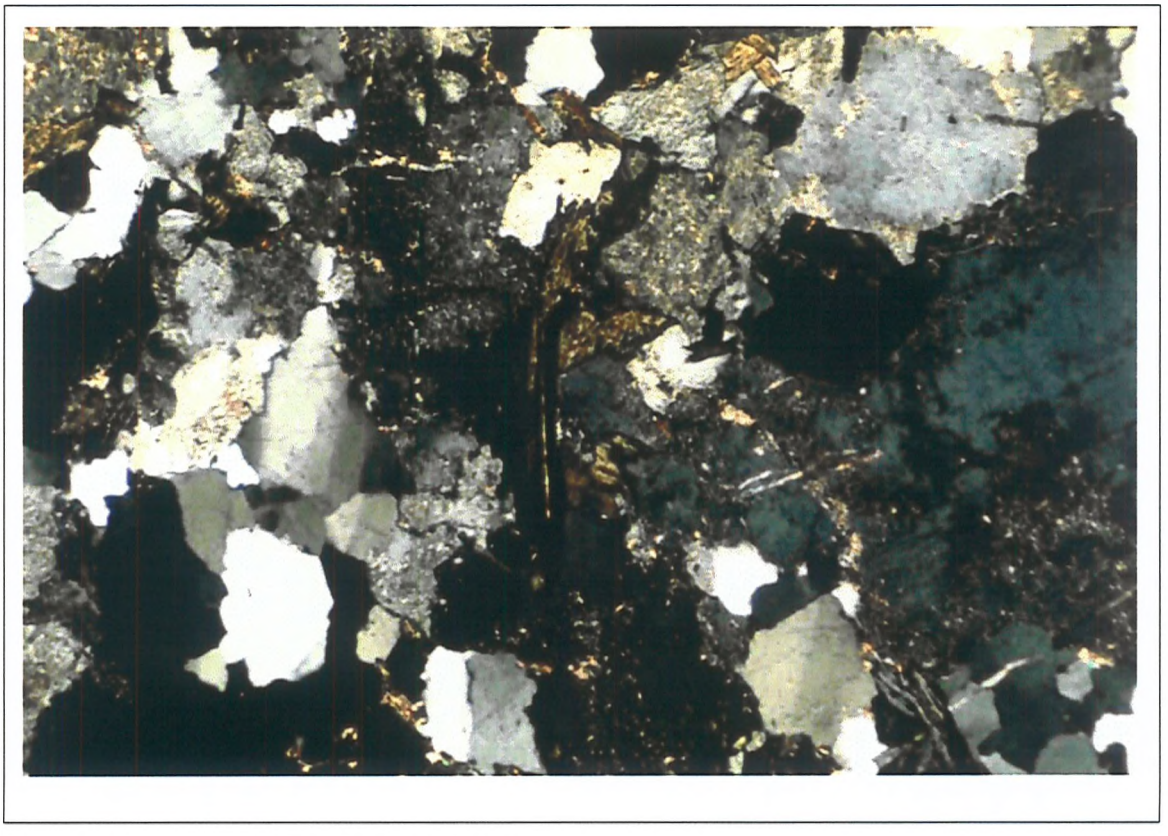

Plate 3.6d - Phase 3 Sebakwe River Gneiss - showing polycrystalline quartz, deformation of biotite being replaced by chlorite and sericitisation of plagioclase (field of view = 3.4mm)

A later pegmatitic phase, tentatively termed Phase-4, may or may not relate to the other phases but is certainly on the same scale of evolution (i.e. more evolved and lesser in volume), and cross-cuts all the other phase types.

3.2.4.2) Interpretation

The relationship of these phases is thought to resemble a differentiation model. Phase-2 is the result of a partial melting episode, from which Phase-1 is the restite. This is indicated by the mafic nature of Phase-1 and the presence of laminae within it, very similar in nature to the Phase-2 magma. These laminae are clearly apparent in exposure and are illustrated in Plate 3.6b. Xenoliths of this restite were then incorporated into the rising partial melt with the smaller xenoliths undergoing almost complete assimilation into the melt phase. Phase 2 does contain a weak deformational fabric which has aligned the xenoliths, presumably perpendicular to the direction of stress. This deformation may have been the cause of the melting and the escape of the melt from the restite phase. Phases 3 & 4 are thought to be successive differentiates of the phase 2 magma due to their more evolved nature and lesser volume.

Phases 2 and 3 can both be seen to become gradationally more quartz rich towards the margins of the body, to the extent that some of the rocks are microgranitic to rhyolitic but retain the same texture as seen previously. Other marginal rocks have lost the texture and are now cryptocrystalline. The position of these highly differentiated rocks around the margin of the SRG possibly indicates that a section through a domed magma body is being viewed.

This body is considered to be significant because although it could simply be intrusive into the volcanic sequence, none of the phase lithologies are seen anywhere else in the section. Also, the higher metamorphic grade, deformation and melt characteristics of the unit would also have affected the intruded volcanic lithologies. Therefore, the SRG *must* have had a prior history to attain the features seen. In addition, xenoliths of material very similar to Phase-1 are seen in the margin of the Rhodesdale Granitoid. This suggests that either the SRG is significantly older than first appearances might dictate, and/or the margin of the Rhodesdale Granitoid is substantially younger than is currently thought.

3.2.5) The Kwekwe Ultramafic Complex (KUC)

The nature and geochronology of this body is still obscure. It is thought to be a member of the Mashaba Ultramafic Suite (MUS) (Harrison, 1970; Wilson, 1979) of mafic and ultramafic intrusives which are considered the feeder remnants of the Upper Bulawayan volcanics. As such, the MUS is relatively dated at *c.*2.7Ga.

A brief investigation of the KUC was made, with the nature of the contact with the Mafic Formation volcanics and the anomalous sill-like protrusion just south of the Sebakwe River, of particular interest.

The southwards continuation of the northern outcrop of the KUC in the Kwekwe area, is mapped by Harrison (1970) as narrowing to the extent that upon reaching the Sebakwe River, it has virtually ceased to exist and is now represented by a narrow band of highly silicified and carbonated rocks. For this reason the relationship of this ultramafic complex with the Mafic Formation volcanics, is difficult to establish. Ultramafic flows are present in the Mafic Formation section at the point where the KUC transects the river, but these are intimately interbedded with basaltic flows of the volcanic sequence. Equivalence to the Belingwe (Mberengwa) type stratigraphy of the Reliance Formation (U2) or basal Zeederbergs Formation (U3), would therefore be a more reasonable conclusion. These ultramafic units accommodate a greater proportion of the strain, resulting in a roughly north-south shear fabric due to movement on the SSZ.

The outcrop immediately south of the river, forms a sill-like protrusion into the granitoid of the Rhodesdale complex. This part of the unit has a layered cumulate texture (see Plate 3.7) which is preserved purely by differential weathering of the cumulus and intercumulus phases. The texture is ortho- or heteradcumulate, with olivine as the most probable primary cumulus phase since this is now manifest as rusty-red, iron oxide spots. A knobbly weathering character also hints at a possible poikilitic nature. The orientation of this protrusion is unknown since the layering visible can not be taken as defining the overall attitude of the body.

Plate 3.7 - Layering in the Kwekwe Ultramafic Complex

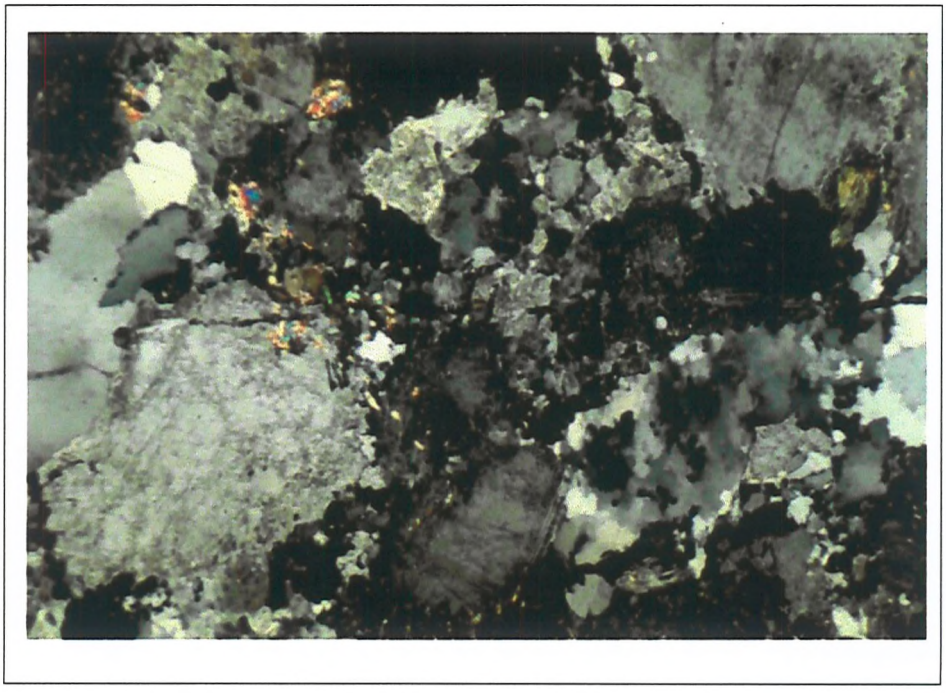

Plate 3.8 - Kwekwe Gneiss - showing strain, quartz and feldspar subgrains and low-grade greenschist facies assemblage (Field of view ~3.4mm)

3.2.6) The Rhodesdale Granitoid and Kwekwe Gneiss

The Rhodesdale Granitoid is a multi-component granitoid mass which, as discussed in section 3.2.3, undoubtedly formed the basement to the MGB. It is considered a member of the *c.*2.9Ga Chingezi Suite of granitoids (Wilson, 1979) and lies to the east of the Midlands Greenstone Belt. It is punctured by a number of granite and adamellite stocks intruded into the core of its strongly banded gneiss which exhibits well-developed melanosome and leucosome components (Harrison, 1970). Unlike the Rhodesdale Gneiss (*sensu stricto*) which has a Pb-Pb age of 2976 +121/-132Ma (Taylor *et al.*, 1991), these intruding stocks do not have absolute dates of any validity but are considered younger than the greenstone belt volcanics by Harrison (1970).

The edge of this mass is the main consideration for this discussion since it determines the chronologic relationship between the granitoid and the greenstone belt volcanism. The observations made here will therefore be discussed in detail below.

3.2.6.1) The contact of the Rhodesdale Granitoid and the Midlands Greenstone Belt.

The contact of the Rhodesdale Granitoid with the volcanic succession of the greenstone belt is best exposed on the south bank of the Sebakwe River. At this location, fingers of granitoid intruding the Mafic Formation volcanics can be seen with consequent assimilation characteristics also present. Xenoliths (or stopes?) of the volcanics in a 'frozen' state of assimilation, exhibit small blebs of the granitoid within them. The occurrence of shearing also provides evidence for this intrusive relationship and assimilation process. Most of the shearing is accommodated by the ultramafic volcanics particularly abundant here, although the whole of the mafic-ultramafic succession is considerably sheared. This succession is cross-cut by some later basaltic dykes which also cut across the contact with the granitoid, thus giving the impression of a volcanic sequence younger than the granitoid. However, the lack of any shear fabric in these dykes indicates their post-shear age. The granitoid here does not exhibit a strong shear fabric as is present in the volcanics, and in fact possesses foliation of a significantly different orientation. A shear fabric of increasing strength is apparent further into the Rhodesdale mass but this is impersistent.

Along with the finger-like intrusions, assimilation indicators and relative lack of shearing in the granitoid when compared to the greenstone belt volcanics, an important

indicator of the relative chronology between the Rhodesdale granitoid and greenstone belt volcanics, is the presence of a xenolith within this marginal zone, very similar to Phase-1 of the SRG. The conclusion drawn from this is that either the SRG is *c.*>3Ga old - allowing xenolithic incorporation into the *c.*2.9Ga Rhodesdale Granitoid, or that there is a younger (*c.*2.7-2.6Ga), marginal phase around the Rhodesdale Gneiss. This latter option is preferred and is independent of a similar conclusion arrived at by Harrison (1970) who termed this marginal phase the Que Que Gneiss (now the 'Kwekwe Gneiss'). This terminology will be followed in this report. Harrison observed that "small masses of granitic material intruded into Gold Belt rocks near the contact with the gneiss." and suggested that "the gneiss may have been remobilised during.....emplacement of the Dutchmans Pool Adamellite.", a later intrusive phase. The finger-like granitic protrusions into the Mafic Formation volcanics strongly indicate an intrusive mode for the Kwekwe Gneiss (KKG) which is therefore considered to be a later marginal phase with respect to the rest of the Rhodesdale Granitoid. This does not preclude the Rhodesdale Gneiss (*sensu stricto*) from being the basement to the Upper Bulawayan volcanics.

A sample (Zimb.226) of the Kwekwe Gneiss as mapped by Harrison (1970), was collected for zircon dating. Plate 3.8 shows the nature of this rock to be essentially a granite which has undergone a low amount of strain in the brittle-ductile regime to cause recrystallisation of the quartz and feldspar mineralogy into distinct sub-grains (Barker (1998) *pers. commun.*). The presence of a muscovite-sericite-epidote assemblage indicates low-grade greenschist facies conditions with the strain probably produced by movement along the Sherwood Shear Zone. The result of the geochronology is presented and discussed in Chapter 5. Unfortunately, due to the extremely poor exposure of the Rhodesdale Gneiss (*s.s*), it was not possible to collect a sample of this for geochemical or geochronological analysis.

3.2.7) The Sesombi Tonalite

The Sesombi Tonalite dominates much of the outcrop of the western-central region of the MGB. This is the type area for a craton-wide phase of magma probably intruded synchronously across the craton and a sample (Zimb.95/02) was taken for zircon geochronology in order to date this event.

The Sesombi intrusive is basically a homogeneous mass with some finer non-porphyritic phases. Zonation of plagioclase phenocrysts is spectacular and easily visible in hand specimen. No xenoliths of the size viewed in the Rhodesdale nor of the lithology typical of the SRG are present, only a few small (5-20cm) mafic xenoliths exhibiting deformation as a result of assimilation processes.

In thin section (Plate 3.9) the plagioclase exhibits extreme oscillatory zonation with albite and Carlsbad twinning. Large proportions of each phenocryst are sericitised according to the chemistry of the zone. Quartz is interstitial to the plagioclase and shows slight deformation. Epidote is abundant and biotite has been replaced by chlorite. Occasionally, amphibole crystals are also present. The small mafic xenoliths were not sampled.

Numerous phases of dykes intrude the Sesombi. The quartz-feldspar porphyry dykes seen throughout the Felsic-Maliyami section are seen intruding here also, indicating their relative chronology. Interestingly, a dyke very similar in nature to those seen in the Mafic Formation section can also be observed to intrude the Sesombi. Late basaltic dykes are the most abundant dyke phase, forming spectacular dark swaths, penetrating the white tonalite.

3.2.8) Late Porphyries

The Late Porphyries crop out as low relief, poorly exposed, silica-rich intrusives. The Giraffe Porphyry, in the south-west-central part of the field area, is the largest of these and the best exposed. The Green Granite Porphyry occurs just south of the river in the middle of the Felsic-Maliyami section. Both bodies contain quartz, plagioclase and amphibole as phenocryst phases, with some biotite (see Plates 3.10a & b). Both have suffered post-crystallisation replacement of their phenocryst phases which in the Giraffe porphyry, has virtually destroyed the plagioclase phenocrysts. The quartz and plagioclase groundmass in the Giraffe body is more finely crystalline than that of the Green Granite porphyry and the former also shows syntaxial overgrowths of its largely euhedral quartz phenocrysts. The Green Granite unit exhibits syntaxial overgrowths of its plagioclase phenocrysts, including subgrains of quartz in the process, whilst the quartz phenocrysts are obviously strained and are being corroded as the groundmass quartz recrystallises to form an interlocking,

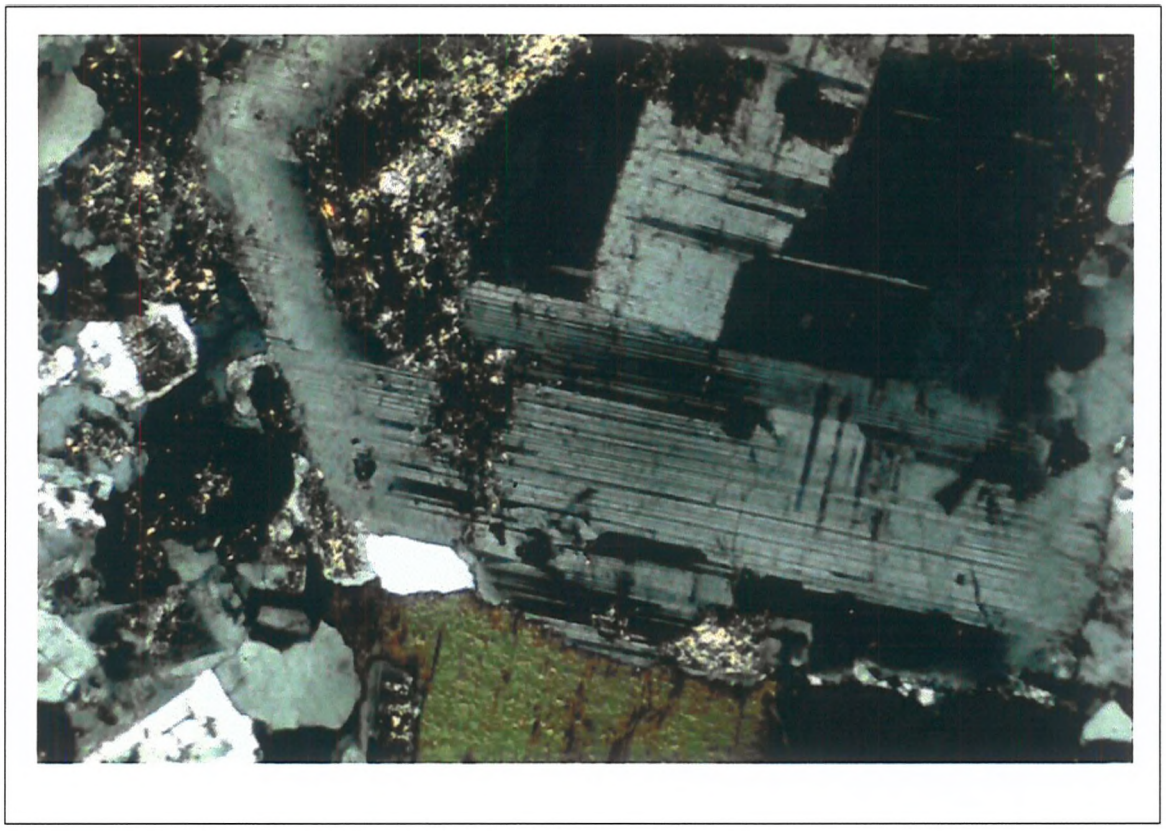

Plate 3.9 - Sesombi Tonalite - plagioclase zoning and sericitisation, biotite replaced by chlorite, and epidote (Field of view = 3.4mm)

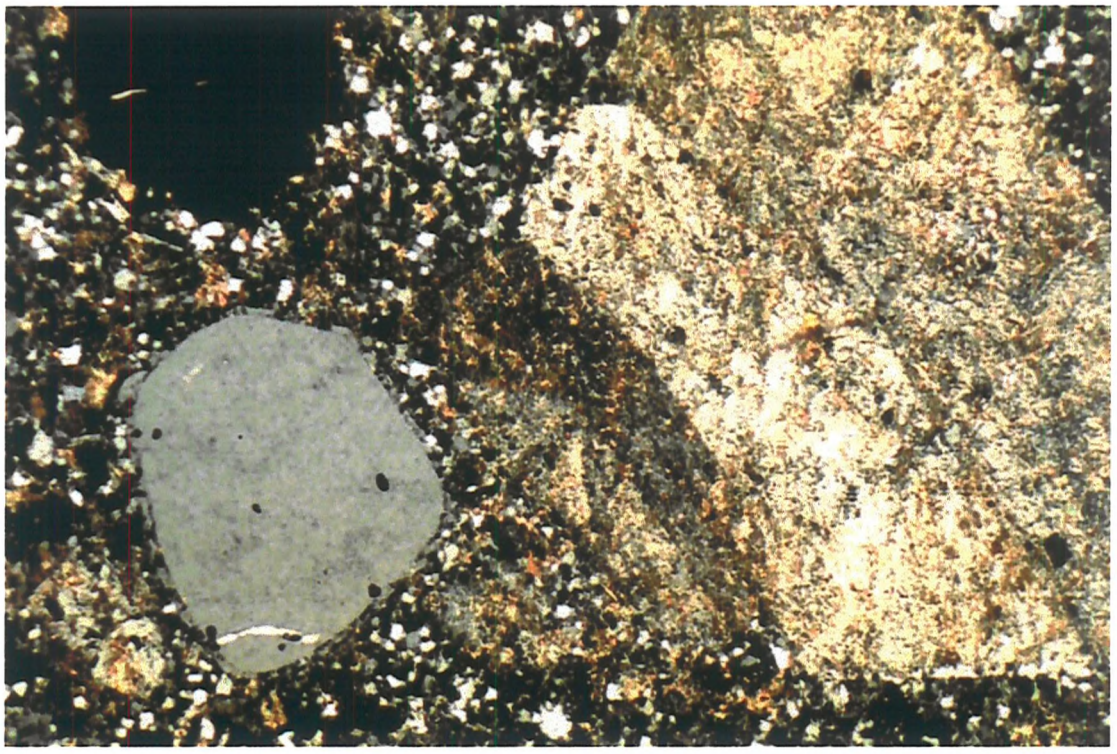

Plate 3.10a Giraffe Porphyry - showing syntaxial overgrowths of quartz phenocrysts and destroyed feldspar (field of view = 3.4mm)

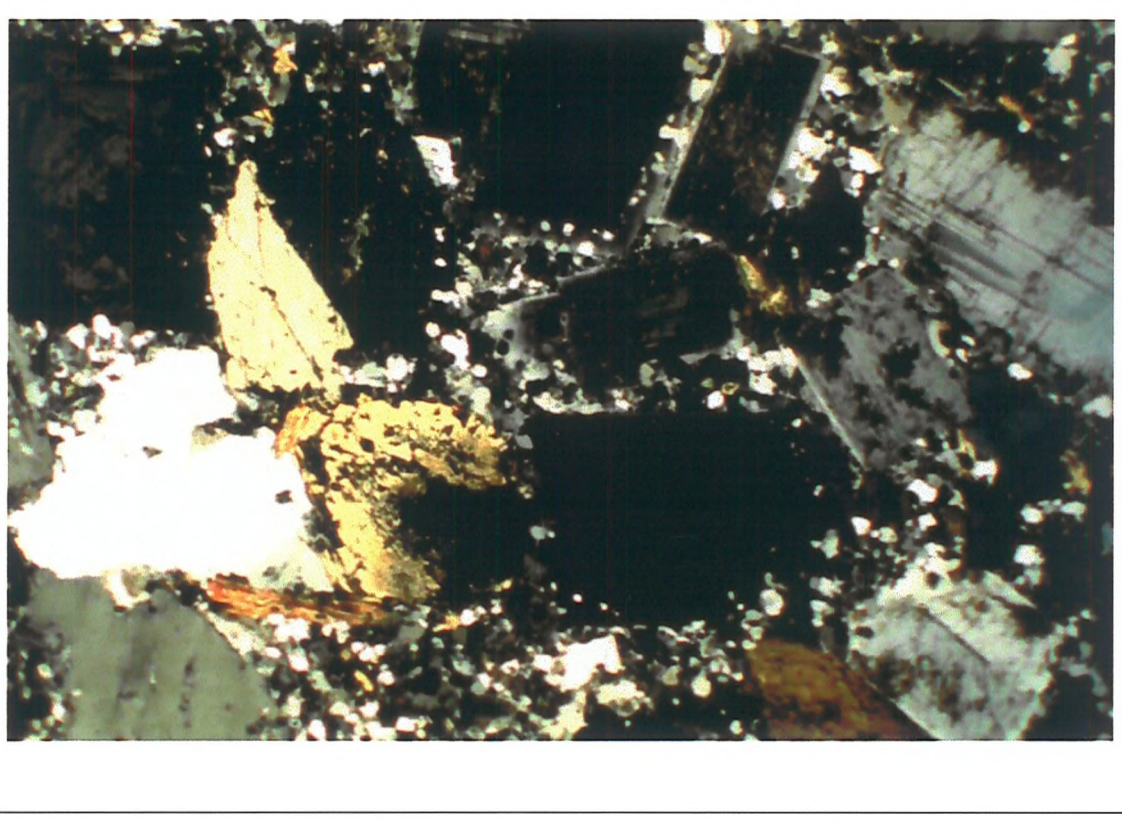

Plate 3.10b - Green Granite Porphyry - showing syntaxial overgrowths of plagioclase phenocrysts and inclusion of quartz subgrains, strained quartz and recrystallised groundmass (field of view = 6.8mm)

polycrystalline mosaic. This difference is a result of the different dynamic history each intrusion has experienced and may call into question their synchroneity.

A sample of the Giraffe Porphyry (Zimb.164) was collected for geochemistry and zircon geochronology, the results of which can be seen in Chapters 4 & 5.

CHAPTER 4 - GEOCHEMISTRY OF THE MIDLANDS GREENSTONE BELT

4.1) INTRODUCTION

Little geochemical data have been published for the Midlands Greenstone Belt (MGB). The sum total of dedicated papers numbers two, those of Harrison (1968) and Condie & Harrison (1976). The Zimbabwe Geological Survey bulletins of Cheshire *et al.* (1980), Harrison (1970), Robertson (1976) and Bliss (1970) contain some basic geochemistry but this is of small quantity and mainly concentrates on those elements now known to be easily mobilised. Although papers such as Hawkesworth & O'Nions (1977) and Sun & Nesbitt (1978) take a more regional perspective to the geochemical interpretation and contain some data from rocks from the MGB, Harrison (1968) and Condie & Harrison (1976) remain the sole contributions totally concerned with the MGB.

Major, trace, rare-earth element (REE) and Nd isotope analyses have been conducted during the course of this study. 102 samples have been analysed by X-ray fluorescence (XRF) for major and trace elements using glass beads and crushed powder pellets respectively. Inductively-coupled plasma mass spectrometry (ICP-MS) was used to analyse 64 samples for REE. From these data, the calibrated Sm-Nd ratios were used to calculate the Nd isotope data for 31 samples in conjunction with isotope dilution thermal ionisation mass spectrometry (ID-TIMS) to obtain the $^{143}Nd/^{144}Nd$ ratio of the rock. The methodology and standardisation for each of these techniques is described in more detail in Appendices B, C & D. Of the 102 samples analysed by XRF, 46 are from the volcanic stratigraphy of the Midlands Greenstone Belt and will be discussed in this text. Twenty five (25) samples of granitoid lithologies, both internal and external in relation to the greenstone belt, were analysed and some of these will be discussed. Thirty one (31) samples were considered too altered to be included or unrepresentative of primary magmatic compositions, either being tuffaceous, heavily recrystallised during metamorphism or of mixed magma origin. Alteration and metamorphism has affected the major elements more than the trace elements (see section 4.2) and as such, some of these samples, although excluded from the major element discussion, may be included in trace element, REE and Nd isotope studies.

Table 4.1 provides all the geochemical data relevant to this study. The volcanic rocks have been classified using the system of Le Maitre *et al.* (1989) - basalts 45 to 52wt% SiO_2;

basaltic-andesites 52 to 57wt% SiO_2; andesites 57 to 63wt% SiO_2; dacites 63 to 70wt%+ SiO_2 depending on total concentration of alkalis. For the compositions of interest, this classification is largely independent of total alkalis which is advantageous since the samples have suffered pervasive low-grade greenschist facies metamorphism causing mobilisation of Na and K. Only at the dacite/rhyolite boundary does the concentration of alkalis become important to the nomenclature of the rock and with this in mind all compositions with SiO_2 >70wt% will be termed rhyodacites.

The 46 samples from the volcanic stratigraphy comprise 7 basalts, 3 basaltic-andesites and 2 dacites from the Mafic Formation; 10 basalts, 4 basaltic-andesites, 5 andesites, and 4 rhyodacites from the Maliyami Formation; and 2 basalts, 4 basaltic-andesites (two bordering on andesitic in composition and plotted as such), 1 dacite and 4 rhyodacites from the Felsic Formation.

Analyses of regional and other samples may be included in Table 4.1 but are not discussed in the text. These analyses are included for completeness and for the benefit of others who may wish to utilise this data-set in the future. All samples from the volcanic stratigraphy discussed in the text are indicated in the relevant part of the stratigraphy in Logs 1a & 2.

4.2) ALTERATION, METAMORPHISM AND ANALYTICAL VARIATIONS

The volcanic and intrusive lithologies used in this study are predominantly very well preserved and very little altered. This is a characteristic of the MGB but is naturally an over-generalisation since some samples are extremely altered, especially around the major shear zones in the belt. To a large extent, initial collection of these samples was avoided but this has not prevented the collection of some highly altered samples. These have been identified and discarded from the data-set primarily on the basis of their petrography and the high percentage (>10%) of volatiles lost on ignition (LOI) during the preparation process for XRF analysis.

Metamorphism is predominantly of low-grade greenschist facies and as such it had little effect on the samples. However, where pervasive and extreme, the low-grade metamorphism has caused significant destruction of the rock texture and crystal structure with consequent disturbance of the geochemistry.

Table 4.1a - Major elements recalculated to 100% anhydrous (wt%)

BASALTS, BASALTIC-ANDESITES & ANDESITES sample no.	lithology	SiO_2	TiO_2	Al_2O_3	Fe_2O_3*	MnO	MgO	CaO	Na_2O	K_2O	P_2O_5	SO_3	TiO_2/P_2O_5	mg#	LOI	Sum before correction	correction factor
Felsic Formation																	
Z028	pillow basalt	51.1	1.0	14.9	13.5	0.2	6.7	9.0	3.4	0.1	0.1	0.1	12.6	33.1	2.8	100.5	1.00
Z029	pillow basalt	51.8	1.1	15.2	13.5	0.2	6.7	8.2	3.2	0.0	0.1	0.1	13.5	33.1	8.7	99.3	1.01
Z034	microgabbro	52.4	1.9	13.6	15.2	0.2	4.9	7.8	3.4	0.2	0.2	0.2	7.7	24.3	3.4	99.2	1.01
zimb.208	basaltic andesite	53.0	1.7	13.5	14.6	0.2	5.2	8.0	3.2	0.2	0.2	0.0	8.0	26.2	2.3	101.2	0.99
Z040	basaltic andesite	56.6	0.9	14.2	9.6	0.2	8.6	5.7	3.8	0.1	0.2	0.1	5.4	47.2	7.6	100	1.00
zimb.175	basaltic andesite	56.8	0.9	15.7	8.7	0.1	8.4	4.3	4.7	0.1	0.2	0.0	5.2	49.1	6.8	99.9	1.00
Maliyami Formation																	
Z071	basalt	45.7	2.5	13.8	20.0	0.3	7.2	9.6	0.2	0.2	0.2	0.2	9.9	26.5	2.9	99.9	1.00
Z064	porphyritic basalt	46.3	2.5	14.2	16.9	0.5	6.3	12.6	0.1	0.3	0.3	0.1	7.5	27.1	2.9	99.5	1.01
Z062	basalt	49.0	1.0	15.6	12.9	0.2	7.9	10.5	2.5	0.2	0.1	0.2	12.2	38.0	2.7	99.9	1.00
Z063	porphyritic basalt	49.5	1.3	15.1	14.3	0.2	6.3	11.3	1.3	0.0	0.1	0.4	10.7	30.6	7.8	99.1	1.01
Z072	basalt	49.5	2.6	13.1	18.2	0.2	5.1	7.7	2.2	1.0	0.2	0.0	11.8	21.9	1.3	99.5	1.01
Z073	basalt	49.4	1.6	14.2	16.6	0.3	5.5	9.9	1.8	0.4	0.1	0.2	12.0	24.9	1.7	100	1.00
zimb.188	porphyritic basalt	49.7	1.3	14.9	14.2	0.2	6.1	12.4	1.0	0.0	0.1	0.0	12.1	30.2	8.2	100.9	0.99
zimb.184	basalt	50.8	1.1	17.6	12.8	0.2	3.1	11.9	2.1	0.3	0.1	0.0	12.6	19.6	1.1	99	1.01
zimb.186	basalt	50.4	0.8	14.8	11.7	0.2	8.1	12.1	1.7	0.2	0.1	0.0	10.3	40.8	2.5	100.1	1.00
Z080	microgabbro	51.0	1.5	13.7	15.5	0.2	5.6	9.9	2.1	0.2	0.1	0.1	10.6	26.7	1.3	99.6	1.00
Z061	basalt	51.2	1.1	16.4	11.4	0.2	8.8	8.0	2.3	0.5	0.1	0.1	12.7	43.7	2.8	99.7	1.00
Z078	basalt	51.2	1.6	14.3	13.1	0.2	6.2	10.2	2.4	0.6	0.2	0.1	9.7	32.3	1.5	100	1.00
zimb.177	basalt	50.5	1.3	13.8	14.2	0.2	7.3	9.7	2.5	0.4	0.1	0.0	10.8	34.0	2.1	102	0.98
Z048	basaltic andesite	53.4	0.9	15.9	9.9	0.2	5.8	8.7	5.0	0.1	0.1	0.2	6.3	36.9	6.9	98.6	1.01
Z046	basaltic andesite	53.1	0.8	17.3	9.1	0.2	5.5	8.0	5.5	0.1	0.1	0.2	6.1	37.5	3.3	99.7	1.00
zimb.187	basaltic andesite	53.7	1.3	20.1	12.8	0.2	4.9	6.0	0.2	0.6	0.1	0.0	14.4	27.6	4.2	100.1	1.00
Z060	basaltic andesite	55.0	1.3	20.3	12.6	0.2	3.8	5.6	0.7	0.3	0.1	0.1	9.6	23.0	3.3	99.9	1.00
Z087	basaltic andesite	56.5	0.7	15.5	8.1	0.1	7.7	7.9	2.9	0.4	0.2	0.1	3.8	48.7	2.1	99.6	1.00
Z085	andesite	56.7	0.7	16.3	7.3	0.1	5.8	7.0	5.6	0.3	0.2	0.1	3.9	44.4	0.9	99.8	1.00
zimb.194	andesite	57.4	0.7	15.0	8.9	0.1	8.1	6.7	2.7	0.3	0.2	0.0	3.9	47.7	1.8	101.3	0.99
zimb.213	andesite	59.3	0.7	14.7	7.0	0.1	5.2	10.6	2.2	0.0	0.1	0.0	5.5	42.6	3.8	99.2	1.01
zimb.198	andesite	59.5	0.6	15.5	6.8	0.1	6.2	5.2	5.7	0.3	0.1	0.0	4.3	48.0	0.9	100.7	0.99
zimb.195	porphyritic andesite	59.9	0.6	15.6	6.3	0.1	5.8	5.0	6.3	0.3	0.1	0.0	3.9	48.1	0.7	101.3	0.99
Z055	andesite	61.0	0.7	16.9	7.8	0.1	5.7	4.5	3.1	0.1	0.2	0.0	4.4	41.9	3.0	99.4	1.01
Mafic Formation																	
Z004	basalt	48.3	1.3	17.0	13.8	0.2	6.2	9.3	3.7	0.1	0.1	0.0	11.7	31.1	7.9	99.8	1.00
Z018	basalt	48.8	1.0	15.5	13.9	0.2	7.7	11.4	1.3	0.0	0.1	0.1	13.0	35.5	3.0	99.7	1.00
zimb.151	basalt	50.0	0.8	15.0	12.8	0.2	7.5	11.3	2.2	0.1	0.1	0.0	13.8	37.0	2.5	100.4	1.00
Z005	basalt	50.3	1.1	14.7	13.1	0.2	7.5	11.0	1.6	0.2	0.1	0.1	11.7	36.5	1.8	100	1.00
zimb.135	basalt	50.9	1.4	14.2	14.0	0.2	6.7	9.8	2.5	0.2	0.1	0.0	12.8	32.4	3.5	100.7	0.99
Z023	basalt	51.6	1.5	14.8	14.4	0.2	5.7	8.2	3.2	0.4	0.1	0.1	12.2	28.3	3.9	100	1.00
Z006	basalt	52.1	1.0	15.5	11.2	0.2	5.8	11.5	2.2	0.1	0.1	0.3	12.9	34.1	3.4	99.5	1.01
zimb.136	basalt	51.9	1.8	13.7	17.0	0.2	6.1	7.0	1.8	0.3	0.1	0.0	12.3	26.3	7.3	100.7	0.99
Z001	basaltic andesite	52.6	1.3	17.4	12.9	0.1	7.0	2.3	6.0	0.1	0.1	0.3	12.4	35.1	6.0	101	0.99
zimb.137	basaltic andesite	52.6	1.8	13.6	17.0	0.2	5.4	7.0	2.0	0.1	0.2	0.0	11.5	24.2	5.3	101.3	0.99

Table 4.1a (cont.) - Major elements recalculated to 100% anhydrous

FELSIC VOLCANICS AND RHYOLITES																
sample no.	lithology	SiO_2	TiO_2	Al_2O_3	Fe_2O_3*	MnO	MgO	CaO	Na_2O	K_2O	P_2O_5	SO_3	TiO_2/P_2O_5	mg#	LOI	Sum before correction	correction factor
Felsic Formation																	
Z042	dacite	65.9	0.5	14.3	5.6	0.1	3.0	6.3	2.7	1.0	0.1	0.3	3.7	35.0	7.6	99.2	1.01
zimb.209	rhyo-dacite	69.8	0.4	15.2	3.6	0.1	1.6	3.3	3.4	2.6	0.1	0.0	4.0	31.3	6.0	100.5	1.00
zimb.172	rhyo-dacite	71.6	0.4	15.7	2.8	0.0	1.7	3.9	1.3	2.5	0.1	0.0	3.3	37.6	7.5	100.4	1.00
zimb.170	rhyo-dacite	71.5	0.3	15.1	2.7	0.0	1.1	5.4	1.9	1.9	0.1	0.0	2.9	28.8	7.6	100.6	0.99
zimb.161	rhyo-dacite	71.8	0.3	15.0	2.2	0.1	0.6	6.6	2.2	1.1	0.1	0.0	3.4	20.1	7.4	100.2	1.00
Maliyami Formation																	
Z066	rhyo-dacite	72.9	0.3	15.5	2.8	0.0	2.0	4.0	0.6	1.7	0.1	0.0	3.1	41.7	2.2	99.5	1.01
zimb.201	rhyo-dacite	72.4	0.3	14.9	3.2	0.0	0.8	3.8	3.6	0.8	0.1	0.0	2.7	20.2	1.7	100.3	1.00
zimb.189	rhyo-dacite	75.5	0.3	15.2	3.5	0.1	1.8	2.6	0.5	0.4	0.1	0.0	2.6	33.8	2.9	100.4	1.00
Mafic Formation																	
zimb.150	dacite	65.9	0.5	14.3	3.2	0.2	2.3	5.3	0.2	7.9	0.1	0.0	4.4	42.1	8.3	99.6	1.00
zimb.128	dacite	68.1	0.4	14.5	4.9	0.1	2.7	4.6	1.9	2.6	0.2	0.0	2.6	35.3	6.2	100.6	0.99

TUFFS AND AGGLOMERATES																
sample no.	lithology	SiO_2	TiO_2	Al_2O_3	Fe_2O_3*	MnO	MgO	CaO	Na_2O	K_2O	P_2O_5	SO_3	TiO_2/P_2O_5	mg#	LOI	Sum before correction	correction factor
Z076	recrystalised basalt	48.9	2.1	13.3	18.3	0.2	5.2	9.2	2.1	0.4	0.1	0.1	14.7	22.1	0.7	99.9	1.00
Z082	Mg basaltic tuff	52.0	0.6	14.7	10.0	0.1	13.6	4.9	3.0	0.9	0.1	0.0	4.1	57.6	3.3	99.9	1.00
zimb.197	Mg basaltic tuff	51.7	0.6	14.2	10.0	0.2	14.3	5.1	2.7	1.2	0.1	0.0	3.9	59.0	3.6	101.5	0.99
zimb.202	agglomerate	52.6	0.6	13.5	7.7	0.2	7.0	15.4	2.6	0.2	0.2	0.0	2.9	47.6	2.0	100	1.00
zimb.214	tuff	53.4	0.9	16.2	11.2	0.1	8.5	6.8	1.9	0.7	0.1	0.0	6.3	43.2	9.0	101.1	0.99
Z074	recrystalised basalt	55.1	0.9	15.7	9.7	0.3	5.0	11.6	0.6	1.0	0.2	0.0	5.1	34.2	1.9	99.7	1.00
zimb.185	clasts of agglom.	57.1	1.2	18.4	10.4	0.2	4.3	7.1	0.7	0.6	0.1	0.0	12.3	29.5	3.4	99.9	1.00
Z092	agglomerate	58.0	0.6	15.4	7.4	0.1	7.9	7.0	3.2	0.3	0.1	0.1	5.5	51.8	7.3	99.8	1.00
zimb.179	agglomerate	61.3	0.6	16.5	5.8	0.2	3.4	9.6	1.7	0.7	0.1	0.0	4.3	36.9	2.9	100.6	0.99
Z052	Siliceous crystal tuff	62.8	0.6	17.5	7.6	0.1	2.0	3.9	4.9	0.3	0.2	0.1	3.6	20.4	1.9	99.4	1.01
zimb.193	mixed magma	66.9	0.6	15.1	4.5	0.1	3.7	7.1	1.5	0.4	0.1	0.0	4.1	45.3	6.2	101.2	0.99
zimb.181	clast of agglom.	73.6	0.3	13.8	1.9	0.0	2.4	6.8	0.7	0.5	0.1	0.0	2.9	56.0	1.9	101	0.99

TOO ALTERED TO USE																
sample no.	lithology	SiO_2	TiO_2	Al_2O_3	Fe_2O_3*	MnO	MgO	CaO	Na_2O	K_2O	P_2O_5	SO_3	TiO_2/P_2O_5	mg#	LOI	Sum before correction	correction factor
zimb.138	carbonated serpentinite	43.4	0.0	1.3	10.5	0.1	41.6	3.1	0.0	0.0	0.0	0.0	0.0	79.9	19.1	100.3	1.00
zimb.219	serpentinite	45.7	0.0	0.7	7.5	0.1	44.3	1.7	0.0	0.0	0.0	0.0	0.0	85.5	13.5	100.2	1.00
zimb.220	greenstone xenolith	48.5	0.5	15.4	11.9	0.2	9.3	10.8	0.2	3.2	0.0	0.0	13.0	43.9	16.3	99	1.01
Z113	altered basalt	50.3	1.2	15.7	13.8	0.3	6.6	10.5	0.9	0.7	0.1	0.1	11.6	32.3	12.9	99.4	1.01
Z032	pillow basalt	50.9	1.1	15.5	14.0	0.2	7.7	8.2	1.6	0.4	0.1	0.3	13.1	35.4	10.5	99.4	1.01
Z027	pillow basalt	51.2	1.1	14.2	12.6	0.2	7.3	8.7	3.9	0.3	0.1	0.3	12.9	36.7	13.0	99.9	1.00
Z039	basalt	52.7	1.1	13.7	11.8	0.2	7.6	10.4	1.2	1.2	0.1	0.1	10.8	39.2	15.4	99.1	1.01
zimb.174	carbonated dacite	53.1	0.4	13.1	7.7	0.2	8.0	17.2	0.2	0.1	0.0	0.0	13.7	51.1	21.9	100	1.00
zimb.206	basaltic andesite	53.2	1.2	14.1	13.5	0.2	5.0	10.4	1.1	1.1	0.1	0.0	11.5	26.9	15.1	102	0.98
zimb.173	basaltic andesite	54.6	1.2	16.1	8.8	0.2	5.2	10.2	2.3	1.2	0.1	0.0	11.0	37.1	14.8	100.5	1.00
Z114	vesicular tuff	58.0	0.8	15.7	8.4	0.1	5.1	10.0	0.9	0.9	0.1	0.1	6.1	37.7	11.1	99.2	1.01
zimb.211	carbonated dacite	62.7	0.4	12.9	6.4	0.2	4.9	10.0	1.3	1.1	0.1	0.0	4.2	43.6	14.4	99.8	1.00
zimb.210	carbonated dacite	62.7	0.4	13.5	5.8	0.3	4.2	10.1	1.8	1.1	0.1	0.0	3.1	42.1	14.5	100.9	0.99

Table 4.1a (cont.) - Major elements recalculated to 100% anhydrous

SEBAKWE RIVER GNEISS sample no.	lithology	SiO_2	TiO_2	Al_2O_3	Fe_2O_3*	MnO	MgO	CaO	Na_2O	K_2O	P_2O_5	SO_3	TiO_2/P_2O_5	mg#	LOI	Sum before correction	correction factor
zimb.142	Phase 3	71.1	0.3	16.2	2.4	0.0	0.7	2.3	6.1	0.9	0.1	0.0	4.4	22.0	1.2	100.9	0.99
zimb.141	Phase 2	54.1	0.6	19.7	8.1	0.1	4.2	6.9	4.5	1.4	0.4	0.0	1.3	34.3	2.6	100	1.00
zimb.140	Phase 1	50.9	1.0	18.4	10.8	0.2	5.2	8.5	3.9	0.9	0.2	0.0	5.6	32.5	2.0	101.4	0.99
REGIONAL INTRUSIVES sample no.	lithology	SiO_2	TiO_2	Al_2O_3	Fe_2O_3*	MnO	MgO	CaO	Na_2O	K_2O	P_2O_5	SO_3	TiO_2/P_2O_5	mg#	LOI	Sum before correction	correction factor
Z090	Sesombi	70.8	0.3	16.1	2.4	0.0	1.1	3.7	5.3	0.3	0.1	0.0	3.4	30.2	1.3	99.6	1.00
Z091	Sesombi	70.9	0.3	16.1	2.3	0.0	1.0	3.9	5.3	0.1	0.1	0.0	3.5	30.2	1.1	99.9	1.00
zimb.248	Sesombi	71.4	0.3	15.4	2.5	0.0	0.9	3.3	4.9	1.2	0.1	0.0	4.1	26.6	0.8	101.4	0.99
zimb.95/06	Chilimanzi	72.5	0.3	14.2	2.5	0.0	0.4	1.6	3.7	4.6	0.1	0.0	3.9	15.2	0.6	100.2	1.00
zimb.95/35	'Chingezi' Granite	74.6	0.1	14.3	2.0	0.0	0.3	2.6	4.8	1.3	0.0	0.0	6.0	11.4	0.6	101.1	0.99
zimb.95/14	Tokwe River Gneiss	73.6	0.2	14.6	2.1	0.0	0.5	3.1	4.9	0.9	0.1	0.0	4.0	19.9	0.4	98.9	1.01
zimb.223	Kwekwe Gneiss 1	74.4	0.1	14.3	1.8	0.0	0.3	2.0	5.0	2.0	0.0	0.0	3.5	14.8	2.5	100.5	1.00
zimb.225	Kwekwe Gneiss 2	74.7	0.1	14.4	1.5	0.0	0.3	1.3	4.8	2.8	0.0	0.0	5.0	14.5	1.0	100.2	1.00
zimb.226	Kwekwe Geniss 3	73.8	0.2	14.8	1.9	0.0	0.4	2.1	5.4	1.3	0.0	0.0	7.0	17.6	1.0	101.6	0.98
zimb.165	Giraffe Porphyry 1	71.1	0.2	15.4	2.3	0.0	0.8	3.6	4.2	2.2	0.1	0.0	3.4	25.6	4.6	100.7	0.99
zimb.164	Giraffe Porphyry 2	71.5	0.2	15.5	2.3	0.0	1.0	3.0	4.5	1.8	0.1	0.0	3.4	30.4	4.0	100.7	0.99
zimb.156	Chicago Porphyry	82.1	0.1	13.1	0.6	0.0	0.2	0.0	0.2	3.7	0.0	0.0	12.0	26.3	2.1	99.5	1.01
zimb.246	Green Granite Porphyry	71.9	0.3	15.1	1.6	0.0	1.1	4.0	5.6	0.2	0.1	0.0	3.7	41.7	0.9	101.1	0.99

Table 4.1b - Trace element analyses (ppm)

BASALTS, BASALTIC-ANDESITES & ANDESITES

sample no.	lithology	MgO (wt%)	Ba	Rb	Sr	Y	Zr	Pb	Zn	Ni	Ti	Cr	V	Ti/Y	Ti/Zr	Zr/Y
Felsic Formation																
Z028	pillow basalt	6.7	41.0	2.9	158.0	21.9	61.9	2.3	87.6	128.9	6174.5	171.3	285.3	281.9	99.7	2.8
Z029	pillow basalt	6.7	37.5	2.1	94.8	21.1	60.6	2.1	82.5	112.5	6431.3	179.9	296.4	304.8	106.1	2.9
Z034	microgabbro	4.9	165.3	3.1	224.4	26.1	142.6	5.8	118.9	32.6	11260.3	34.2	338.1	431.4	79.0	5.5
zimb.208	basaltic andesite	5.2	297.1	2.0	273.5	24.6	132.4	4.8	112.5	39.5	10481.2	56.0	322.5	426.1	79.1	5.4
Z040	basaltic andesite	8.6	71.0	3.0	290.7	18.4	107.0	6.8	76.0	180.9	5641.3	320.3	172.8	306.6	52.7	5.8
zimb.175	basaltic andesite	8.4	117.7	1.4	352.2	15.4	96.6	7.1	86.0	267.7	5579.3	647.1	152.9	362.8	57.8	6.3
Maliyami Formation																
Z071	basalt	7.2	91.8	5.9	117.9	60.1	159.8	2.6	91.3	45.3	14790.1	53.7	402.4	246.1	92.6	2.7
Z064	porphyritic basalt	6.3	76.8	7.2	181.4	62.6	164.9	2.8	168.1	44.7	14998.0	56.6	423.4	239.6	91.0	2.6
Z062	basalt	7.9	51.7	4.5	163.8	20.3	56.6	2.1	88.6	134.7	6015.5	255.5	261.8	296.3	106.3	2.8
Z063	porphyritic basalt	6.3	12.7	1.3	151.1	27.7	79.0	2.1	102.6	98.6	7998.5	202.7	268.3	288.8	101.2	2.9
Z072	basalt	5.1	430.9	24.6	146.6	48.2	146.1	1.9	79.4	38.8	15754.6	38.1	518.4	326.9	107.8	3.0
Z073	basalt	5.5	55.6	9.9	110.5	32.9	93.2	1.3	91.6	55.3	9299.6	76.3	356.4	282.7	99.8	2.8
zimb.188	porphyritic basalt	6.1	28.8	0.0	146.2	23.7	72.1	1.4	90.0	95.5	7900.7	198.3	262.1	333.8	109.7	3.0
zimb.184	basalt	3.1	85.9	0.0	123.9	22.7	63.8	0.0	72.4	149.2	6774.4	306.9	273.2	298.8	106.1	2.8
zimb.186	basalt	8.1	88.0	3.1	218.4	17.8	46.3	2.4	103.3	102.5	4910.0	305.5	256.1	276.6	106.1	2.6
Z080	microgabbro	5.6	53.6	5.5	119.8	35.5	96.2	2.3	104.5	52.2	8971.9	144.3	340.0	252.7	93.3	2.7
Z061	basalt	8.8	94.3	13.9	108.4	19.6	60.7	1.5	82.3	140.6	6479.1	264.7	277.2	330.6	106.7	3.1
Z078	basalt	6.2	205.2	11.5	213.6	25.4	118.0	3.7	99.0	58.7	9345.4	112.5	282.6	367.9	79.2	4.6
zimb.177	basalt	7.3	58.6	8.1	154.1	26.9	73.0	1.1	95.3	80.0	7583.4	391.8	305.5	281.6	104.0	2.7
Z048	basaltic andesite	5.8	78.2	2.5	130.3	18.8	74.4	1.4	80.3	58.5	5252.1	163.3	175.4	279.4	70.6	4.0
Z046	basaltic andesite	5.5	118.9	6.9	214.3	17.0	92.8	2.8	79.2	49.4	4794.4	155.4	178.1	282.0	51.7	5.5
zimb.187	basaltic andesite	4.9	91.3	12.7	132.9	24.7	75.6	4.4	74.4	127.5	7783.4	332.1	323.2	314.9	103.0	3.1
Z060	basaltic andesite	3.8	36.0	9.5	245.1	40.7	77.2	3.4	76.5	108.1	7912.9	345.4	310.9	194.4	102.5	1.9
Z087	basaltic andesite	7.7	103.0	10.5	303.0	11.6	90.2	3.2	59.6	222.1	4256.1	382.7	143.8	366.9	47.2	7.8
Z085	andesite	5.8	71.6	7.1	178.6	10.9	110.2	3.1	70.4	180.0	4116.7	216.6	130.7	377.7	37.4	10.1
zimb.194	andesite	8.1	84.1	4.6	183.5	12.1	89.7	1.9	80.1	187.2	4200.6	317.4	148.1	347.4	46.8	7.4
zimb.213	andesite	5.2	38.3	0.0	43.7	13.3	90.0	2.4	64.4	66.8	3989.4	181.0	140.1	300.9	44.3	6.8
zimb.198	andesite	6.2	138.8	4.9	311.1	9.1	91.3	4.6	64.9	160.4	3334.2	239.1	114.7	367.2	36.5	10.1
zimb.195	porphyritic andesite	5.8	71.4	5.5	161.3	9.3	103.9	11.8	76.2	150.4	3434.2	190.1	110.5	371.3	33.1	11.2
Z055	andesite	5.7	114.5	3.6	235.8	11.1	118.8	2.9	45.3	82.4	4002.8	112.4	121.4	360.6	33.7	10.7
Mafic Formation																
Z004	basalt	6.2	31.7	2.2	81.3	24.4	82.3	1.1	102.8	138.5	7535.8	300.6	319.1	308.8	91.6	3.4
Z018	basalt	7.7	26.6	1.1	178.1	22.4	62.7	2.4	96.8	139.1	6102.4	227.2	276.7	272.4	97.3	2.8
zimb.151	basalt	7.5	50.2	0.1	215.4	17.7	41.1	1.0	82.9	183.0	4957.0	305.5	252.5	279.7	120.7	2.3
Z005	basalt	7.5	112.8	7.1	121.4	23.9	74.6	3.1	89.6	133.4	6368.6	249.8	265.0	266.5	85.4	3.1
zimb.135	basalt	6.7	119.4	3.1	97.3	26.9	78.8	1.4	70.9	59.1	8391.7	78.2	311.2	311.7	106.5	2.9
Z023	basalt	5.7	105.9	10.7	104.0	31.5	94.6	2.0	74.5	56.7	8985.4	89.6	348.4	285.3	95.0	3.0
Z006	basalt	5.8	46.7	3.9	81.3	22.4	63.9	1.4	92.4	128.4	6061.3	229.1	280.5	270.6	94.9	2.9
zimb.136	basalt	6.1	81.7	7.4	98.7	35.1	113.2	3.5	115.9	48.8	10951.9	62.4	384.1	312.1	96.8	3.2
Z001	basaltic andesite	7.0	72.3	3.4	93.0	15.0	67.8	2.6	23.1	169.8	7586.4	214.5	388.3	505.8	111.9	4.5
zimb.137	basaltic andesite	5.4	122.8	0.0	142.5	37.8	117.5	4.5	123.2	46.8	10891.4	69.0	363.3	287.9	92.7	3.1

Table 4.1b (cont.) - Trace element analyses (ppm)

FELSIC VOLCANICS AND RHYOLITES sample no.	lithology	MgO (wt%)	Ba	Rb	Sr	Y	Zr	Pb	Zn	Ni	Ti	Cr	V	Ti/Y	Ti/Zr	Zr/Y
Felsic Formation																
Z042	dacite	3.0	183.1	33.3	118.5	10.6	133.6	4.7	63.3	63.5	2827.8	128.2	87.7	266.8	21.2	12.6
zimb.209	rhyo-dacite	1.6	335.5	60.3	97.5	5.6	111.7	5.1	36.3	16.8	2147.5	32.1	47.4	383.5	19.2	19.9
zimb.172	rhyo-dacite	1.7	488.6	43.3	203.7	7.2	138.5	2.8	39.4	11.9	2150.0	57.7	28.7	299.5	15.5	19.3
zimb.170	rhyo-dacite	1.1	347.3	41.7	238.9	3.3	131.3	2.3	32.2	8.8	1907.3	61.3	22.3	576.9	14.5	39.7
zimb.161	rhyo-dacite	0.6	183.7	24.2	133.4	6.4	165.8	2.3	70.7	11.7	2033.8	40.1	29.5	317.3	12.3	25.9
Maliyami Formation																
Z066	rhyo-dacite	2.0	134.7	38.0	129.3	4.3	168.9	2.8	31.9	9.2	1873.5	19.3	26.5	435.7	11.1	39.3
zimb.201	rhyo-dacite	0.8	313.2	30.0	196.9	5.6	188.2	6.1	48.2	10.0	1792.6	44.1	14.4	322.4	9.5	33.8
zimb.189	rhyo-dacite	1.8	51.8	6.6	131.7	6.2	171.2	2.6	39.8	13.1	1731.1	31.6	27.3	278.3	10.1	27.5
Mafic Formation																
zimb.150	dacite	2.3	854.9	96.2	90.2	9.9	97.2	9.9	47.4	28.0	3189.8	218.0	67.5	321.2	32.8	9.8
zimb.128	dacite	2.7	166.5	65.1	25.5	14.1	189.7	4.6	60.9	33.5	2681.7	62.6	63.7	190.3	14.1	13.5

TUFFS AND AGGLOMERATES sample no.	lithology	MgO (wt%)	Ba	Rb	Sr	Y	Zr	Pb	Zn	Ni	Ti	Cr	V	Ti/Y	Ti/Zr	Zr/Y
Z076	recrystalised basalt	5.2	218.2	9.4	126.6	35.7	92.5	2.0	122.7	36.7	12425.2	73.3	515.1	348.0	134.3	2.6
Z082	Mg basaltic tuff	13.6	238.0	16.8	152.3	10.8	62.3	2.0	69.8	314.8	3637.3	589.7	181.1	336.8	58.4	5.8
zimb.197	Mg basaltic tuff	14.3	295.8	20.5	144.1	11.0	61.3	1.2	68.5	373.0	3485.8	612.6	158.4	317.5	56.8	5.6
zimb.202	agglomerate	7.0	105.2	1.6	351.3	7.5	71.5	3.6	70.7	163.1	3595.9	406.2	129.6	477.5	50.3	9.5
zimb.214	tuff	8.5	154.5	18.2	108.3	17.5	78.3	2.1	81.9	61.2	5635.5	177.6	202.3	322.0	72.0	4.5
Z074	recrystalised basalt	5.0	90.1	24.4	135.8	15.6	91.7	2.3	62.1	82.4	5286.2	93.8	169.6	338.9	57.6	5.9
zimb.185	clasts of agglom.	4.3	144.0	11.9	93.2	22.3	68.7	2.4	68.0	141.3	7382.7	308.0	310.5	331.4	107.4	3.1
Z092	agglomerate	7.9	93.6	9.8	203.6	8.8	86.7	4.0	62.1	155.8	3401.1	359.4	129.1	386.5	39.2	9.9
zimb.179	agglomerate	3.4	154.2	14.2	204.6	12.0	116.9	3.3	53.2	68.4	3874.3	113.5	121.4	321.8	33.1	9.7
Z052	Siliceous crystal tuff	2.0	191.1	8.9	510.5	19.8	170.9	6.7	112.4	10.2	3624.9	9.8	37.3	183.1	21.2	8.6
zimb.193	mixed magma	3.7	127.6	12.3	175.1	6.9	97.9	2.6	39.0	126.7	3378.6	183.9	92.4	486.8	34.5	14.1
zimb.181	clast of agglom.	2.4	78.9	17.0	501.5	4.2	142.1	5.4	22.3	18.6	1542.4	45.8	20.1	364.3	10.9	33.6

TOO ALTERED TO USE sample no.	lithology	MgO (wt%)	Ba	Rb	Sr	Y	Zr	Pb	Zn	Ni	Ti	Cr	V	Ti/Y	Ti/Zr	Zr/Y
zimb.138	carbonated serpentinite	41.6	15.2	0.0	17.0	0.0	5.5	1.1	26.2	2313.8	179.3	3038.8	26.8	0.0	32.4	0.0
zimb.219	serpentinite	44.3	51.0	0.0	9.9	0.0	4.5	1.8	51.2	2663.5	59.8	1921.8	15.9	0.0	13.4	0.0
zimb.220	greenstone xenolith	9.3	127.4	99.7	72.4	11.8	13.7	10.9	85.6	131.5	3147.9	323.9	230.3	266.8	229.3	1.2
Z113	altered basalt	6.6	125.4	21.3	80.7	21.4	61.2	2.3	102.4	104.2	7023.5	226.3	271.3	328.2	114.8	2.9
Z032	pillow basalt	7.7	108.7	12.9	114.4	20.2	59.7	3.1	86.2	122.6	6542.8	182.1	288.9	323.9	109.6	3.0
Z027	pillow basalt	7.3	88.6	9.5	157.4	19.4	56.7	2.2	72.9	89.6	6360.8	169.1	272.8	327.9	112.2	2.9
Z039	basalt	7.6	143.9	45.4	76.6	18.9	69.1	5.3	76.5	119.5	6313.2	334.4	253.9	334.0	91.4	3.7
zimb.174	carbonated dacite	8.0	7.5	0.0	98.5	7.9	110.8	3.4	87.7	97.1	2457.5	50.9	72.1	311.5	22.2	14.0
zimb.206	basaltic andesite	5.0	284.8	31.8	87.7	21.2	68.8	3.7	171.7	46.3	7465.1	118.3	276.9	352.6	108.5	3.2
zimb.173	basaltic andesite	5.2	229.6	21.0	174.7	21.0	71.1	3.1	60.6	90.2	7215.0	263.2	288.7	344.4	101.5	3.4
Z114	vesicular tuff	5.1	235.1	30.5	122.6	14.8	91.3	3.3	70.1	51.3	4633.5	134.3	163.8	313.1	50.8	6.2
zimb.211	carbonated dacite	4.9	131.9	29.2	121.8	8.3	110.3	5.5	49.3	75.6	2524.2	113.0	65.3	304.9	22.9	13.3
zimb.210	carbonated dacite	4.2	122.2	23.1	171.9	7.7	98.8	3.8	56.4	62.5	2553.8	78.1	62.0	333.0	25.9	12.9

Table 4.1b (cont.) - Trace element analyses (ppm)

SEBAKWE RIVER GNEISS sample no.	lithology	MgO (wt%)	Ba	Rb	Sr	Y	Zr	Pb	Zn	Ni	Ti	Cr	V	Ti/Y	Ti/Zr	Zr/Y
zimb.142	Phase 3	0.7	211.8	18.9	302.3	5.1	207.7	11.0	41.6	7.3	1840.8	36.3	28.0	360.8	8.9	40.7
zimb.141	Phase 2	4.2	411.9	29.7	218.0	72.5	81.3	10.3	119.0	33.1	3415.8	31.5	168.3	47.1	42.0	1.1
zimb.140	Phase 1	5.2	221.6	21.9	224.5	43.9	188.6	5.2	106.5	94.4	6265.7	72.9	215.4	142.7	33.2	4.3
REGIONAL INTRUSIVES																
sample no.	**lithology**	**MgO (wt%)**	**Ba**	**Rb**	**Sr**	**Y**	**Zr**	**Pb**	**Zn**	**Ni**	**Ti**	**Cr**	**V**	**Ti/Y**	**Ti/Zr**	**Zr/Y**
Z090	Sesombi	1.1	130.3	6.3	449.0	2.3	90.9	3.2	13.0	13.4	1571.4	27.9	32.5	683.2	17.3	39.5
Z091	Sesombi	1.0	118.2	3.0	452.3	3.3	85.8	4.4	12.7	11.9	1548.7	23.6	30.3	466.0	18.0	25.8
zimb.248	Sesombi	0.9	255.1	35.4	344.6	2.1	82.9	5.2	36.4	12.3	1714.2	39.1	28.2	804.8	20.7	38.9
zimb.95/06	Chilimanzi	0.4	1107.9	194.9	193.7	22.0	291.6	37.9	40.9	8.7	1854.6	44.1	18.1	84.3	6.4	13.3
zimb.95/35	'Chingezi' Granite	0.3	777.6	54.5	221.1	3.2	153.0	15.3	29.1	6.1	711.5	34.8	7.2	219.5	4.6	47.2
zimb.95/14	Tokwe River Gneiss	0.5	392.2	28.8	330.9	3.2	106.8	12.1	28.7	6.6	1212.6	35.8	10.4	373.2	11.4	32.9
zimb.223	Kwekwe Gneiss 1	0.3	545.5	57.0	162.4	4.8	104.1	11.5	31.0	7.1	835.2	31.4	9.1	174.4	8.0	21.7
zimb.225	Kwekwe Gneiss 2	0.3	480.2	76.9	151.4	12.2	112.0	34.6	23.2	7.1	598.5	26.3	3.7	49.1	5.3	9.2
zimb.226	Kwekwe Geniss 3	0.4	386.9	27.3	238.5	6.0	118.0	21.5	16.5	8.6	1238.6	28.5	7.0	206.1	10.5	19.6
zimb.165	Giraffe Porphyry 1	0.8	399.7	44.8	207.1	3.6	86.4	3.5	42.6	11.7	1428.7	51.5	26.0	401.7	16.5	24.3
zimb.164	Giraffe Porphyry 2	1.0	364.8	38.9	207.7	3.6	92.4	3.4	40.7	12.0	1429.4	36.2	26.0	396.2	15.5	25.6
zimb.156	Chicago Porphyry	0.2	426.6	74.3	31.2	12.5	115.3	17.9	6.6	5.8	722.9	108.0	0.6	57.8	6.3	9.2
zimb.246	Green Granite Porphyry	1.1	122.9	3.9	505.3	2.8	79.0	3.8	11.1	22.2	1542.4	65.6	32.2	551.4	19.5	28.2

Table 4.1c - REE analyses (chondrite normalised)

(normalisation values from Taylor & Gorton 1977)

BASALTS, BASALTIC-ANDESITES AND ANDESITES.

		Felsic Formation					Maliyami Formation basalts							
normalisation values		Zimb.028 basalt	Zimb.173 bas/and	Zimb.206 bas/and	Zimb.208 bas/and	Zimb.034 m'gabbro	Zimb.177 basalt	Zimb.184 basalt	Zimb.186 basalt	Zimb.061 basalt	Zimb.062 basalt	Zimb.064 ppy'c bas	Zimb.188 ppy'c bas	Zimb.072 basalt
0.315	La	10.86	16.36	8.72	64.59	78.88	10.39	9.38	6.51	8.09	7.54	23.33	10.01	21.68
0.813	Ce	12.81	15.93	9.89	54.78	68.63	11.87	12.12	7.36	10.07	9.89	24.62	11.61	23.59
0.116	Pr	11.17	14.88	10.33	48.94	67.21	12.29	10.93	7.59	9.57	9.14	28.14	12.13	25.07
0.597	Nd	11.26	14.12	11.15	40.62	54.26	13.15	11.25	8.19	9.94	10.71	29.38	12.91	26.10
		#N/A	#N/A	#N/A	#N/A	#N/A	#N/A	#N/A	#N/A	#N/A	#N/A	#N/A	#N/A	#N/A
0.192	Sm	11.01	12.67	12.32	27.44	34.40	13.41	11.29	8.50	10.10	10.86	30.68	13.15	26.34
0.072	Eu	10.88	12.60	10.24	22.86	27.70	13.58	12.22	9.05	12.10	12.37	27.83	12.86	23.51
0.259	Gd	10.07	10.99	10.51	20.10	18.62	12.69	10.22	8.17	9.19	11.16	28.85	12.08	23.22
0.049	Tb	10.15	10.53	10.20	15.94	18.81	13.14	10.27	8.49	9.19	11.20	29.07	12.19	23.02
0.325	Dy	9.92	10.13	9.54	13.92	15.95	12.94	9.96	8.15	8.90	10.69	26.89	12.04	21.66
0.073	Ho	9.84	10.09	9.52	12.72	16.46	13.27	9.87	8.46	8.96	10.23	26.92	12.24	21.65
0.213	Er	9.44	9.40	8.97	11.68	14.15	12.72	9.51	8.31	8.63	10.54	25.27	11.63	20.73
0.03	Tm	9.54	9.43	9.15	11.47	14.32	12.83	9.61	8.16	8.88	10.95	25.48	11.96	21.25
0.208	Yb	9.13	9.02	8.90	10.47	12.68	12.48	9.36	7.92	8.88	10.44	23.82	11.66	20.35
0.032	Lu	9.14	9.09	9.13	10.50	13.67	12.89	9.35	8.25	9.22	10.23	24.36	11.86	21.43
	La/Sm	0.99	1.29	0.71	2.35	2.29	0.78	0.83	0.77	0.80	0.69	0.76	0.76	0.82
	La/Yb	1.19	1.81	0.98	6.17	6.22	0.83	1.00	0.82	0.91	0.72	0.98	0.86	1.07
	Gd/Yb	1.10	1.22	1.18	1.92	1.47	1.02	1.09	1.03	1.04	1.07	1.21	1.04	1.14
	Eu/Eu*	1.03	1.07	0.90	0.96	1.05	1.04	1.14	1.09	1.25	1.12	0.94	1.02	0.95
	Zr/Sm	29.27	29.21	29.07	25.14	23.41	28.34	29.44	28.37	31.29	27.15	27.99	28.53	28.89
	Hf	1.34	1.64	1.46	3.10	4.59	1.79	1.29	1.09	1.26	3.65	3.49	1.64	3.27
	Ta	1.29	4.43	0.58	0.76	1.07	0.28	0.38	1.59	0.15	0.81	1.85	0.22	0.35
	Pb	4.77	2.24	2.79	4.77	5.90	0.56	1.17	0.79	1.14	4.98	1.80	1.23	1.01
	Th	0.54	0.84	0.23	3.08	5.27	0.26	0.21	0.19	0.19	1.52	0.58	0.24	0.53
	U	0.16	0.22	0.23	0.70	1.15	0.07	0.07	0.05	0.05	1.15	0.13	0.06	0.14
	Y	19.78	20.40	19.17	27.29	28.36	25.34	19.74	16.95	18.05	18.59	42.31	23.77	33.49
	Nb	2.66	3.57	3.21	13.87	18.11	3.23	2.92	2.13	2.66	5.30	7.33	3.16	6.99
	Zr/Nb	23.30	19.91	21.42	9.55	7.87	22.57	21.82	21.68	22.79	10.68	22.49	22.81	20.91
	Zr (XRF)	61.90	71.06	68.80	132.43	142.60	72.95	63.82	46.29	60.70	56.60	164.90	72.05	146.10

Table 4.1c (cont.) - REE analyses (chondrite normalised)

(normalisation values from Taylor & Gorton 1977)

	Maliyami Formation andesites					Mafic Formation				
	zimb.213	**Zimb.046**	**zimb.194**	**zimb.195**	**zimb.198**	**Zimb.135**	**zimb.136**	**zimb.137**	**Zimb.023**	**Zimb.151**
	andesite	bas/and	andesite	ppy'c and	andesite	basalt	basalt	bas/and	basalt	basalt
La	25.89	24.61	35.36	31.30	31.89	18.43	22.59	27.81	20.68	5.95
Ce	22.19	22.62	30.12	27.11	26.41	20.66	22.77	27.45	20.95	8.01
Pr	18.32	18.70	27.07	22.79	21.74	17.60	21.85	26.16	18.64	7.55
Nd	15.42	16.01	22.55	18.56	17.65	17.18	21.27	26.07	18.29	8.55
	#N/A	#N/A	#N/A	#N/A	#N/A	#N/A	#N/A	#N/A	#N/A	#N/A
Sm	11.03	11.63	13.92	11.74	10.95	15.99	20.29	24.34	16.73	8.71
Eu	10.55	11.01	12.06	10.11	9.76	15.13	17.42	21.18	14.85	9.28
Gd	8.88	9.35	10.05	8.39	7.86	13.11	17.87	21.23	14.97	8.49
Tb	7.93	8.39	7.91	6.27	5.88	13.75	17.53	21.31	14.62	8.53
Dy	7.25	7.82	6.91	5.34	4.94	13.08	17.14	20.62	13.97	8.17
Ho	7.05	7.70	6.39	4.84	4.44	13.69	17.29	20.80	14.05	7.80
Er	6.79	7.43	6.10	4.48	4.15	12.93	16.65	20.15	13.51	8.06
Tm	6.83	7.49	6.13	4.41	4.11	13.28	17.10	20.30	13.65	8.50
Yb	6.61	7.38	6.02	4.20	3.96	12.90	16.29	19.32	13.09	8.25
Lu	6.96	7.71	6.25	4.28	4.01	13.37	16.53	20.54	13.28	7.78
La/Sm	2.35	2.12	2.54	2.66	2.91	1.15	1.11	1.14	1.24	0.68
La/Yb	3.92	3.33	5.87	7.46	8.06	1.43	1.39	1.44	1.58	0.72
Gd/Yb	1.34	1.27	1.67	2.00	1.99	1.02	1.10	1.10	1.14	1.03
Eu/Eu*	1.06	1.05	1.01	1.00	1.04	1.04	0.91	0.93	0.94	1.08
Zr/Sm	42.53	41.57	33.58	46.06	43.43	25.68	29.04	25.14	29.46	19.69
Hf	1.89	1.86	1.91	2.05	1.90	2.06	2.49	3.15	1.99	1.47
Ta	0.28	0.28	0.32	0.43	0.35	0.21	0.34	0.98	0.23	0.22
Pb	2.88	1.98	1.54	10.17	2.98	1.23	2.70	2.24	1.35	0.52
Th	1.48	1.30	1.29	1.77	1.67	0.85	1.11	1.27	0.87	0.28
U	0.40	0.36	0.30	0.44	0.41	0.20	0.25	0.28	0.20	0.08
Y	14.91	16.07	13.42	10.41	9.68	24.34	36.90	42.65	24.55	17.02
Nb	3.65	3.91	4.44	4.27	3.96	4.10	5.09	5.91	4.29	2.81
Zr/Nb	24.65	23.73	20.21	24.34	23.09	19.25	22.24	19.86	22.07	14.61
Zr (XRF)	90.04	92.80	89.72	103.86	91.33	78.82	113.15	117.45	94.60	41.06

Table 4.1c (cont.) - REE analyses (chondrite normalised)

(normalisation values from Taylor & Gorton 1977)

FELSIC VOLCANICS AND RHYOLITES

	Felsic Formation					Maliyami Formation		Mafic Formation	
	Zimb.161	Zimb.170	Zimb.172	Zimb.209	Zimb.211	Zimb.066	Zimb.189	Zimb.150	Zimb.128
La	37.30	26.09	28.57	32.28	29.83	38.83	20.77	48.93	54.52
Ce	26.04	21.86	22.96	22.90	23.67	25.81	16.75	37.41	42.40
Pr	19.53	16.02	17.53	16.59	17.58	20.06	12.01	28.18	31.65
Nd	14.72	12.06	13.28	12.23	13.28	14.51	9.54	21.52	24.32
	#N/A	#N/A	#N/A	#N/A	#N/A	#N/A	#N/A	#N/A	#N/A
Sm	9.09	6.74	7.60	7.60	8.37	8.15	7.61	13.01	15.06
Eu	9.71	6.82	7.84	6.36	8.14	7.57	8.94	13.49	12.33
Gd	7.10	4.40	5.64	5.63	6.85	5.58	5.87	9.78	11.57
Tb	4.78	2.72	4.20	4.24	5.38	3.79	4.79	6.95	8.82
Dy	3.73	1.97	3.55	3.54	4.55	2.85	3.95	5.85	7.62
Ho	3.00	1.46	3.14	3.06	4.02	2.28	3.45	5.26	6.94
Er	2.56	1.21	2.87	2.80	3.62	1.92	2.98	4.88	6.62
Tm	2.23	1.05	2.56	2.65	3.45	1.73	2.85	4.73	6.51
Yb	1.99	0.98	2.37	2.54	3.33	1.64	2.63	4.55	6.32
Lu	1.95	0.97	2.09	2.51	3.41	1.61	2.61	4.58	6.83
La/Sm	4.11	3.87	3.76	4.24	3.56	4.77	2.73	3.76	3.62
La/Yb	18.77	26.57	12.08	12.73	8.95	23.62	7.90	10.76	8.63
Gd/Yb	3.57	4.48	2.38	2.22	2.06	3.39	2.23	2.15	1.83
Eu/Eu*	1.20	1.22	1.18	0.96	1.07	1.10	1.33	1.18	0.93
Zr/Sm	95.05	101.40	94.88	76.49	68.61	107.94	117.27	38.91	65.58
Hf	3.09	2.54	2.60	2.42	2.06	2.86	3.49	2.13	3.79
Ta	0.51	0.15	0.18	0.22	0.35	0.68	0.62	0.96	0.55
Pb	1.68	1.98	1.64	3.98	4.11	2.91	2.21	7.60	4.75
Th	1.99	0.81	0.87	3.87	2.01	2.19	2.24	5.61	3.66
U	0.57	0.23	0.28	1.13	0.56	0.58	0.56	1.14	1.06
Y	8.05	3.31	7.18	6.75	9.03	5.23	7.94	11.86	15.36
Nb	5.76	2.91	3.22	3.32	4.20	4.65	5.05	3.99	6.88
Zr/Nb	28.78	45.16	43.05	33.60	26.26	36.33	33.89	24.35	27.58
Zr (XRF)	165.82	131.30	138.53	111.67	110.26	168.90	171.24	97.20	189.65

TUFFS AND AGGLOMERATES

	Zimb.214	Zimb.052	Zimb.179	Zimb.181	Zimb.185	Zimb.193
	tuff	Si xl tuff	welded agg	clasts agg	clasts agg	silicified agg
La	22.12	54.21	28.14	30.47	8.10	26.72
Ce	21.80	43.38	24.12	22.36	9.41	23.61
Pr	19.58	34.04	19.84	15.63	9.76	19.23
Nd	17.83	27.37	16.38	11.39	10.22	15.45
	#N/A	#N/A	#N/A	#N/A	#N/A	#N/A
Sm	13.50	18.38	10.31	6.34	10.24	9.32
Eu	14.24	15.89	9.92	5.84	11.12	7.26
Gd	10.71	13.92	8.07	4.75	9.36	6.21
Tb	9.91	11.85	6.61	3.10	9.67	4.65
Dy	9.17	10.54	5.74	2.31	9.14	3.99
Ho	9.10	10.09	5.50	1.81	9.48	3.61
Er	8.96	9.67	5.23	1.60	9.25	3.43
Tm	9.09	9.84	5.03	1.37	8.88	3.43
Yb	9.04	9.56	4.85	1.29	8.80	3.43
Lu	9.61	10.00	5.02	1.31	9.04	3.51
La/Sm	1.64	2.95	2.73	4.80	0.79	2.87
La/Yb	2.45	5.67	5.80	23.67	0.92	7.78
Gd/Yb	1.19	1.46	1.66	3.69	1.06	1.81
Eu/Eu*	1.18	0.98	1.08	1.05	1.13	0.94
Zr/Sm	30.21	48.41	59.05	116.67	34.97	54.69
Hf	1.75	4.16	2.30	2.63	1.30	1.94
Ta	0.62	1.46	0.51	0.42	0.21	0.20
Pb	2.68	7.15	3.01	3.43	1.02	2.06
Th	0.95	4.56	1.34	1.42	0.16	1.65
U	0.24	1.20	0.31	0.37	0.04	0.41
Y	18.35	21.43	11.65	4.23	19.07	7.49
Nb	3.73	7.61	3.81	3.85	2.48	4.23
Zr/Nb	20.98	22.45	30.64	36.93	27.74	23.13
Zr (XRF)	78.30	170.90	116.88	142.11	68.73	97.87

Table 4.1c (cont.) - REE analyses (chondrite normalised)

(normalisation values from Taylor & Gorton 1977)

SEBAKWE RIVER GNEISS				REGIONAL INTRUSIVES										
	Zimb.140	Zimb.141	Zimb.142		Zimb.223	Zimb.226	Zimb.95/06	Zimb.95/35	Zimb.95/14	Zimb.091	Zimb.246	Zimb.165	Zimb.164	Zimb.156
	Phase 1	Phase 2	Phase 3		KKG1	KKG3	Chilimanzi	Chingezi	TRG	Sesombi	GGP	Giraffe	Giraffe	Chicago
La	60.43	84.36	92.17	La	87.65	116.12	259.37	97.63	59.92	21.59	13.32	21.91	21.50	117.47
Ce	45.18	68.78	60.03	Ce	54.63	74.11	189.54	60.45	37.78	18.54	13.89	19.49	17.20	77.47
Pr	63.21	70.52	37.33	Pr	36.74	46.99	131.39	42.16	27.78	13.34	11.73	13.34	13.24	50.98
Nd	54.93	63.92	24.41	Nd	24.39	30.21	87.78	27.94	17.99	10.30	9.71	10.05	10.24	32.48
	#N/A	#N/A	#N/A		#N/A	#N/A	#N/A	#N/A	#N/A	#N/A	#N/A	#N/A	#N/A	#N/A
Sm	38.03	54.73	9.43	Sm	11.39	15.20	42.19	12.40	7.65	6.31	6.07	6.03	6.35	13.87
Eu	24.27	23.34	10.42	Eu	12.43	9.34	20.53	10.44	11.51	5.94	7.11	6.04	7.21	8.21
Gd	27.17	43.81	7.32	Gd	8.18	10.46	29.55	8.56	4.49	4.13	4.06	4.13	4.39	10.50
Tb	23.45	40.92	3.82	Tb	4.47	5.24	18.54	3.57	2.70	2.67	2.62	2.66	2.75	6.68
Dy	21.00	36.97	2.84	Dy	3.06	3.68	14.53	2.35	1.89	1.96	1.81	1.96	2.07	5.83
Ho	19.66	35.04	2.34	Ho	2.26	2.61	11.72	1.44	1.52	1.50	1.35	1.53	1.58	5.46
Er	18.62	32.26	2.18	Er	2.13	2.35	10.59	1.40	1.32	1.24	1.14	1.34	1.41	6.01
Tm	18.63	31.15	1.84	Tm	1.77	2.01	9.54	1.33	1.13	1.14	0.99	1.28	1.25	6.28
Yb	17.54	28.10	1.72	Yb	1.65	1.89	8.30	1.52	1.14	1.05	0.91	1.22	1.11	6.63
Lu	17.43	27.17	1.79	Lu	1.82	1.96	7.58	1.89	1.38	1.00	0.83	1.19	1.15	7.23
La/Sm	1.59	1.54	9.78	La/Sm	7.70	7.64	6.15	7.87	7.83	3.42	2.19	3.63	3.39	8.47
La/Yb	3.44	3.00	53.50	La/Yb	53.22	61.56	31.25	64.07	52.44	20.63	14.57	17.92	19.35	17.72
Gd/Yb	1.55	1.56	4.25	Gd/Yb	4.97	5.55	3.56	5.62	3.93	3.94	4.44	3.38	3.95	1.58
Eu/Eu*	0.74	0.47	1.24	Eu/Eu*	1.27	0.73	0.57	1.00	1.90	1.14	1.40	1.19	1.34	0.67
Hf	2.42	1.97	4.37	Hf	2.45	3.44	6.73	3.65	3.71	0.90	1.06	1.36	1.42	3.31
Ta	0.42	0.56	0.24	Ta	0.91	0.27	1.16	0.39	0.33	0.08	0.10	0.23	0.24	0.98
Pb	3.31	8.89	10.24	Pb	11.47	21.23	48.01	13.90	9.75	3.60	2.74	3.00	2.52	20.18
Th	0.69	4.54	5.58	Th	10.94	20.45	31.99	12.87	6.61	1.19	0.92	1.42	1.43	13.77
U	0.26	0.82	0.60	U	2.21	1.30	8.92	1.28	0.56	0.31	0.31	0.54	0.48	1.18
Y	34.39	66.34	5.10	Y	4.79	6.01	26.83	3.24	3.25	3.32	2.80	3.56	3.61	12.51
Nb	8.96	7.15	3.65	Nb	4.54	4.01	15.22	4.78	3.46	1.45	1.10	1.78	1.66	7.50
Zr/Nb	21.04	11.38	56.94	Zr/Nb	22.90	29.40	19.16	32.02	30.87	59.19	71.64	48.66	55.76	15.38
Zr (XRF)	188.57	81.34	207.71	Zr (XRF)	104.05	117.95	291.62	153.04	106.77	85.80	78.99	86.39	92.42	115.32

Table 4.1d - REE analyses (ppm)

	BASALTS & BASALTIC-ANDESITES												
	Felsic Formation					Maliyami Formation							
	Zimb.028	Zimb.173	Zimb.206	Zimb.208	Zimb.034	Zimb.177	Zimb.184	Zimb.186	Zimb.061	Zimb.062	Zimb.064	Zimb.188	Zimb.072
La	3.42	5.15	2.75	20.35	24.85	3.27	2.95	2.05	2.55	2.38	7.35	3.15	6.83
Ce	10.41	12.95	8.04	44.53	55.80	9.65	9.85	5.98	8.19	8.04	20.02	9.44	19.18
Pr	1.30	1.73	1.20	5.68	7.80	1.43	1.27	0.88	1.11	1.06	3.26	1.41	2.91
Nd	6.72	8.43	6.65	24.25	32.40	7.85	6.72	4.89	5.93	6.40	17.54	7.71	15.58
	#N/A	#N/A	#N/A	#N/A	#N/A	#N/A	#N/A	#N/A	#N/A	#N/A	#N/A	#N/A	#N/A
Sm	2.11	2.43	2.37	5.27	6.60	2.57	2.17	1.63	1.94	2.08	5.89	2.53	5.06
Eu	0.79	0.91	0.74	1.65	2.00	0.98	0.88	0.65	0.87	0.89	2.01	0.93	1.70
Gd	2.61	2.85	2.72	5.20	4.82	3.29	2.65	2.12	2.38	2.89	7.47	3.13	6.01
Tb	0.50	0.52	0.50	0.78	0.92	0.64	0.50	0.42	0.45	0.55	1.42	0.60	1.13
Dy	3.23	3.29	3.10	4.53	5.19	4.20	3.24	2.65	2.89	3.47	8.74	3.91	7.04
Ho	0.72	0.74	0.70	0.93	1.20	0.97	0.72	0.62	0.65	0.75	1.97	0.89	1.58
Er	2.01	2.00	1.91	2.49	3.01	2.71	2.03	1.77	1.84	2.24	5.38	2.48	4.42
Tm	0.29	0.28	0.27	0.34	0.43	0.38	0.29	0.24	0.27	0.33	0.76	0.36	0.64
Yb	1.90	1.88	1.85	2.18	2.64	2.60	1.95	1.65	1.85	2.17	4.95	2.43	4.23
Lu	0.30	0.29	0.29	0.34	0.44	0.42	0.30	0.27	0.30	0.33	0.79	0.38	0.69
Hf	1.34	1.64	1.46	3.10	4.59	1.79	1.29	1.09	1.26	1.34	3.49	1.64	3.27
Ta	1.29	4.43	0.58	0.76	1.07	0.28	0.38	1.59	0.15	0.24	1.85	0.22	0.35
Pb	4.77	2.24	2.79	4.77	5.90	0.56	1.17	0.79	1.14	0.69	1.80	1.23	1.01
Th	0.54	0.84	0.23	3.08	5.27	0.26	0.21	0.19	0.19	0.19	0.58	0.24	0.53
U	0.16	0.22	0.23	0.70	1.15	0.07	0.07	0.05	0.05	0.05	0.13	0.06	0.14
Y	19.78	20.40	19.17	27.29	28.36	25.34	19.74	16.95	18.05	18.83	42.31	23.77	33.49
Nb	2.66	3.57	3.21	13.87	18.11	3.23	2.92	2.13	2.66	2.40	7.33	3.16	6.99

Table 4.1d (cont.) - REE analyses (ppm)

ANDESITES					BASALTS				
Maliyami Formation					Mafic Formation				
Zimb.213	Zimb.046	Zimb.194	Zimb.195	Zimb.198	Zimb.135	Zimb.136	Zimb.137	Zimb.023	Zimb.151
8.16	7.75	11.14	9.86	10.05	5.81	7.12	8.76	6.52	3.53
18.04	18.39	24.48	22.04	21.47	16.80	18.51	22.32	17.03	10.65
2.13	2.17	3.14	2.64	2.52	2.04	2.53	3.03	2.16	1.36
9.20	9.56	13.46	11.08	10.54	10.26	12.70	15.56	10.92	6.80
#N/A	#N/A	#N/A	#N/A	#N/A	#N/A	#N/A	#N/A	#N/A	#N/A
2.12	2.23	2.67	2.25	2.10	3.07	3.90	4.67	3.21	2.09
0.76	0.80	0.87	0.73	0.70	1.09	1.25	1.53	1.07	0.78
2.30	2.42	2.60	2.17	2.04	3.40	4.63	5.50	3.88	1.76
0.39	0.41	0.39	0.31	0.29	0.67	0.86	1.04	0.72	0.46
2.36	2.54	2.24	1.74	1.61	4.25	5.57	6.70	4.54	2.85
0.51	0.56	0.47	0.35	0.32	1.00	1.26	1.52	1.03	0.76
1.45	1.58	1.30	0.95	0.88	2.75	3.55	4.29	2.88	1.98
0.20	0.22	0.18	0.13	0.12	0.40	0.51	0.61	0.41	0.30
1.37	1.54	1.25	0.87	0.82	2.68	3.39	4.02	2.72	1.89
0.22	0.25	0.20	0.14	0.13	0.43	0.53	0.66	0.43	0.32
1.89	1.86	1.91	2.05	1.90	2.06	2.49	3.15	1.99	1.47
0.28	0.28	0.32	0.43	0.35	0.21	0.34	0.98	0.23	0.22
2.88	1.98	1.54	10.17	2.98	1.23	2.70	2.24	1.35	0.52
1.48	1.30	1.29	1.77	1.67	0.85	1.11	1.27	0.87	0.28
0.40	0.36	0.30	0.44	0.41	0.20	0.25	0.28	0.20	0.08
14.91	16.07	13.42	10.41	9.68	24.34	36.90	42.65	24.55	17.02
3.65	3.91	4.44	4.27	3.96	4.10	5.09	5.91	4.29	2.81

Table 4.1d (cont.) - REE analyses (ppm)

	DACITES & RHYODACITES															
	Felsic Formation					Maliyami Formation		Mafic Formation		Tuffs, agglomerates & mixed magmas						
	Zimb.161	Zimb.170	Zimb.172	Zimb.209	Zimb.211	Zimb.066	Zimb.189	Zimb.150	Zimb.128	Zimb.214	Zimb.052	Zimb.179	Zimb.181	Zimb.185	Zimb.193
La	11.75	8.22	9.00	10.17	9.40	12.23	6.54	15.41	17.17	6.97	17.08	8.86	9.60	2.55	8.42
Ce	21.17	17.77	18.67	18.62	19.25	20.98	13.62	30.41	34.47	17.72	35.27	19.61	18.18	7.65	19.20
Pr	2.27	1.86	2.03	1.92	2.04	2.33	1.39	3.27	3.67	2.27	3.95	2.30	1.81	1.13	2.23
Nd	8.79	7.20	7.93	7.30	7.93	8.66	5.70	12.85	14.52	10.65	16.34	9.78	6.80	6.10	9.23
	#N/A	#N/A	#N/A	#N/A	#N/A	#N/A	#N/A	#N/A	#N/A	#N/A	#N/A	#N/A	#N/A	#N/A	#N/A
Sm	1.74	1.29	1.46	1.46	1.61	1.56	1.46	2.50	2.89	2.59	3.53	1.98	1.22	1.97	1.79
Eu	0.70	0.49	0.57	0.46	0.59	0.55	0.65	0.97	0.89	1.03	1.15	0.72	0.42	0.80	0.52
Gd	1.84	1.14	1.46	1.46	1.77	1.44	1.52	2.53	3.00	2.78	3.60	2.09	1.23	2.42	1.61
Tb	0.23	0.13	0.21	0.21	0.26	0.19	0.23	0.34	0.43	0.49	0.58	0.32	0.15	0.47	0.23
Dy	1.21	0.64	1.15	1.15	1.48	0.93	1.29	1.90	2.48	2.98	3.43	1.87	0.75	2.97	1.30
Ho	0.22	0.11	0.23	0.22	0.29	0.17	0.25	0.38	0.51	0.66	0.74	0.40	0.13	0.69	0.26
Er	0.54	0.26	0.61	0.60	0.77	0.41	0.63	1.04	1.41	1.91	2.06	1.11	0.34	1.97	0.73
Tm	0.07	0.03	0.08	0.08	0.10	0.05	0.09	0.14	0.20	0.27	0.30	0.15	0.04	0.27	0.10
Yb	0.41	0.20	0.49	0.53	0.69	0.34	0.55	0.95	1.31	1.88	1.99	1.01	0.27	1.83	0.71
Lu	0.06	0.03	0.07	0.08	0.11	0.05	0.08	0.15	0.22	0.31	0.32	0.16	0.04	0.29	0.11
Hf	3.09	2.54	2.60	2.42	2.06	2.86	3.49	2.13	3.79	1.75	4.16	2.30	2.63	1.30	1.94
Ta	0.51	0.15	0.18	0.22	0.35	0.68	0.62	0.96	0.55	0.62	1.46	0.51	0.42	0.21	0.20
Pb	1.68	1.98	1.64	3.98	4.11	2.91	2.21	7.60	4.75	2.68	7.15	3.01	3.43	1.02	2.06
Th	1.99	0.81	0.87	3.87	2.01	2.19	2.24	5.61	3.66	0.95	4.56	1.34	1.42	0.16	1.65
U	0.57	0.23	0.28	1.13	0.56	0.58	0.56	1.14	1.06	0.24	1.20	0.31	0.37	0.04	0.41
Y	8.05	3.31	7.18	6.75	9.03	5.23	7.94	11.86	15.36	18.35	21.43	11.65	4.23	19.07	7.49
Nb	5.76	2.91	3.22	3.32	4.20	4.65	5.05	3.99	6.88	3.73	7.61	3.81	3.85	2.48	4.23

Table 4.1d (cont.) - REE analyses (ppm)

	SEBAKWE RIVER GNEISS			REGIONAL GRANITOIDS									
	Zimb.140	Zimb.141	Zimb.142	Zimb.223	Zimb.226	Zimb.95/06	Zimb.95/35	Zimb.95/14	Zimb.091	Zimb.246	Zimb.165	Zimb.164	Zimb.156
	Phase 1	Phase 2	Phase 3	KKG 1	KKG 3	Chilimanzi	Chingezi	TRG	Sesombi	GGP	Giraffe	Giraffe	Chicago
La	19.04	26.57	29.04	27.61	36.58	81.70	30.75	18.88	6.80	4.20	6.90	6.77	37.00
Ce	36.73	55.92	48.80	44.42	60.25	154.10	49.15	30.72	15.07	11.29	15.85	13.99	62.99
Pr	7.33	8.18	4.33	4.26	5.45	15.24	4.89	3.22	1.55	1.36	1.55	1.54	5.91
Nd	32.79	38.16	14.58	14.56	18.03	52.41	16.68	10.74	6.15	5.80	6.00	6.12	19.39
	#N/A	#N/A	#N/A	#N/A	#N/A	#N/A	#N/A	#N/A	#N/A	#N/A	#N/A	#N/A	#N/A
Sm	7.30	10.51	1.81	2.19	2.92	8.10	2.38	1.47	1.21	1.17	1.16	1.22	2.66
Eu	1.75	1.69	0.75	0.90	0.67	1.48	0.75	0.83	0.43	0.51	0.44	0.52	0.59
Gd	7.04	11.35	1.90	2.12	2.71	7.65	2.22	1.16	1.07	1.05	1.07	1.14	2.72
Tb	1.15	2.01	0.19	0.22	0.26	0.91	0.18	0.13	0.13	0.13	0.13	0.13	0.33
Dy	6.82	12.02	0.92	1.00	1.19	4.72	0.76	0.61	0.64	0.59	0.64	0.67	1.90
Ho	1.43	2.56	0.17	0.17	0.19	0.86	0.10	0.11	0.11	0.10	0.11	0.12	0.40
Er	3.97	6.87	0.47	0.45	0.50	2.26	0.30	0.28	0.26	0.24	0.29	0.30	1.28
Tm	0.56	0.93	0.06	0.05	0.06	0.29	0.04	0.03	0.03	0.03	0.04	0.04	0.19
Yb	3.65	5.85	0.36	0.34	0.39	1.73	0.32	0.24	0.22	0.19	0.25	0.23	1.38
Lu	0.56	0.88	0.06	0.06	0.06	0.24	0.06	0.04	0.03	0.03	0.04	0.04	0.23
Hf	2.42	1.97	4.37	2.45	3.44	6.73	3.65	3.71	0.90	1.06	1.36	1.42	3.31
Ta	0.42	0.56	0.24	0.91	0.27	1.16	0.39	0.33	0.08	0.10	0.23	0.24	0.98
Pb	3.31	8.89	10.24	11.47	21.23	48.01	13.90	9.75	3.60	2.74	3.00	2.52	20.18
Th	0.69	4.54	5.58	10.94	20.45	31.99	12.87	6.61	1.19	0.92	1.42	1.43	13.77
U	0.26	0.82	0.60	2.21	1.30	8.92	1.28	0.56	0.31	0.31	0.54	0.48	1.18
Y	34.39	66.34	5.10	4.79	6.01	26.83	3.24	3.25	3.32	2.80	3.56	3.61	12.51
Nb	8.96	7.15	3.65	4.54	4.01	15.22	4.78	3.46	1.45	1.10	1.78	1.66	7.50

Figures 4.1a & b display major and trace elements plotted on bivariate discrimination diagrams against Zr which has been used as an immobile comparator. Where no trends are apparent or the variation cannot be explained by a single or combination of petrogenetic processes, remobilisation is presumed and no consideration of the elements concerned will be undertaken. This discrimination largely affects the large ion lithophile elements (LILE - K, Na, Rb, Ba and Sr), which have apparently been significantly remobilised and homogenised across all volcanic compositions. No SiO_2 addition of the kind noted by Brake (1996) as occurring in the Zeederbergs Formation in the Mberengwa (Belingwe) Greenstone Belt, is apparent. Harker-type diagrams using MgO as abscissa will be used to investigate those major elements unaffected by the regional metamorphic overprint (Fig.4.4a). Aluminium shows very little variation across all compositions (13wt% to 17wt% in basalts; 13.5wt% to 17.4wt% in basaltic-andesites and andesites; 14.3wt% to 15.7wt% in dacites and rhyodacites) and is therefore of limited use in petrogenetic investigations and so will not be considered except to illustrate the compositional gaps with respect to silica, present in each formation (see Fig.4.3).

Of the trace elements (see Fig.4.1b), Rb, Sr, Pb, Zn and Ba have all been remobilised with Ni and Cr also showing a certain degree of scatter particularly in the andesites and more evolved compositions, possibly attributable to the influence of metamorphism superimposed upon an initial petrogenetic trend. Concentrations of La and Ce are sufficiently low for some samples as to bring in to question the precision and accuracy of the XRF determination, hence ICP-MS determinations will be used when considering these elements. As such, Y, Nb, Zr, Ti, and V are the most reliable trace elements of this data-set with the REE being considered a robust suite of elements. The Nb and Y concentrations for the samples were generally low.

Nb and Y have been determined by both XRF and ICP-MS for some samples and a comparison of the data shows significant variation. Figure 4.2a illustrates the fact that 1:1 correlations of Y by both techniques are only achieved at concentrations of ~20ppm. Below this, XRF/ICP-MS ratios are less than unity, decreasing to 0.6 at concentrations around 2ppm (XRF), and above 20ppm (XRF) the correlation is scattered between 1.4 and 0.8 although few samples have concentrations this high. Figure 4.2b shows the same type of plot for Nb. Here the difference is more serious. At concentrations of 9ppm (XRF) and higher, unity between the two techniques is achieved. From 9ppm down to 4ppm (XRF) the XRF/ICP-MS ratio increases almost linearly to 2.5. Figure 4.2b shows that the difference observed could be the

Figure 4.1a Major Elements vs. Zr for all Formations (XRF data)

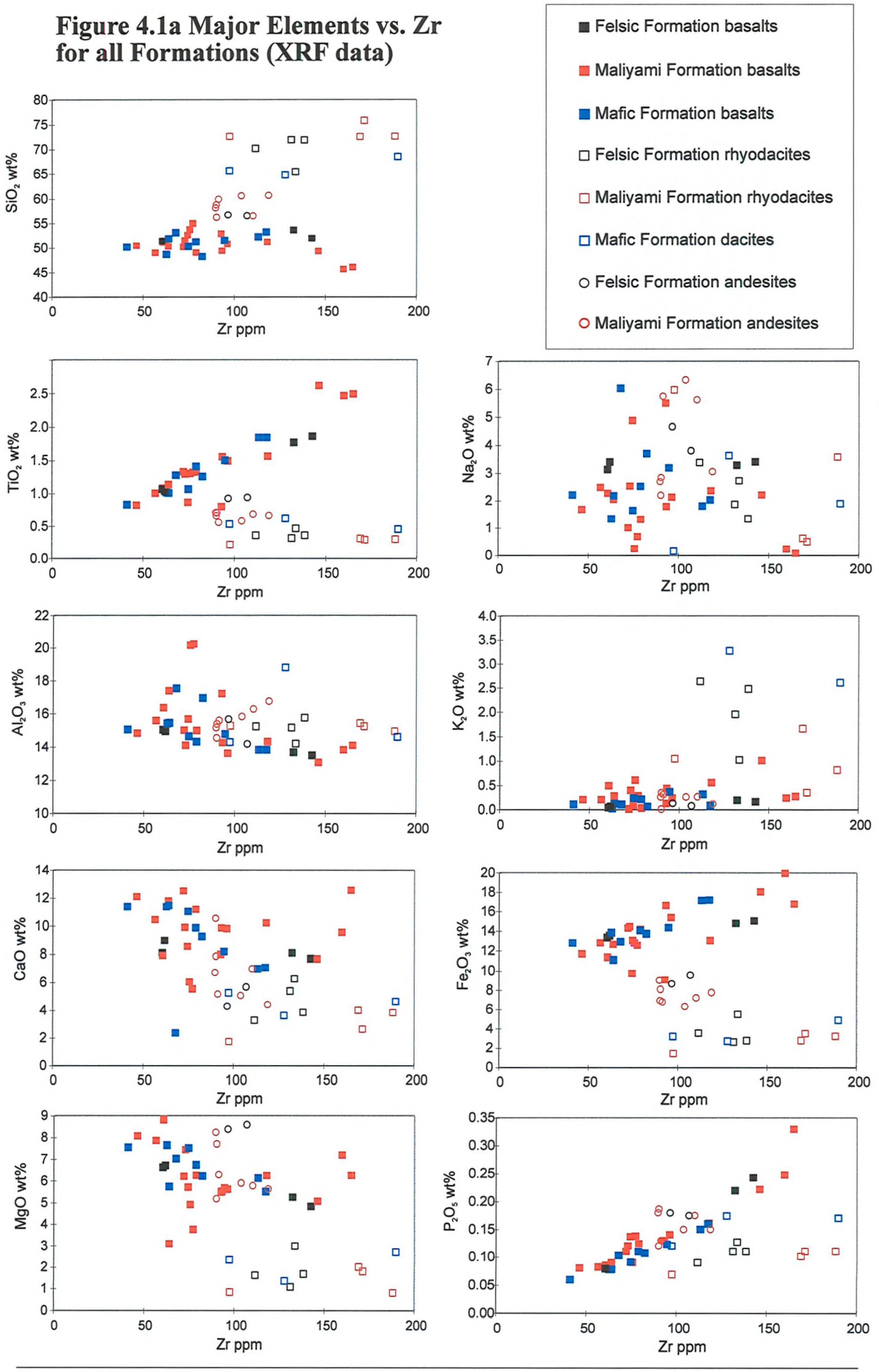

Figure 4.1b Trace elements vs Zr for all Formations (XRF data except for Nb which is ICP-MS)

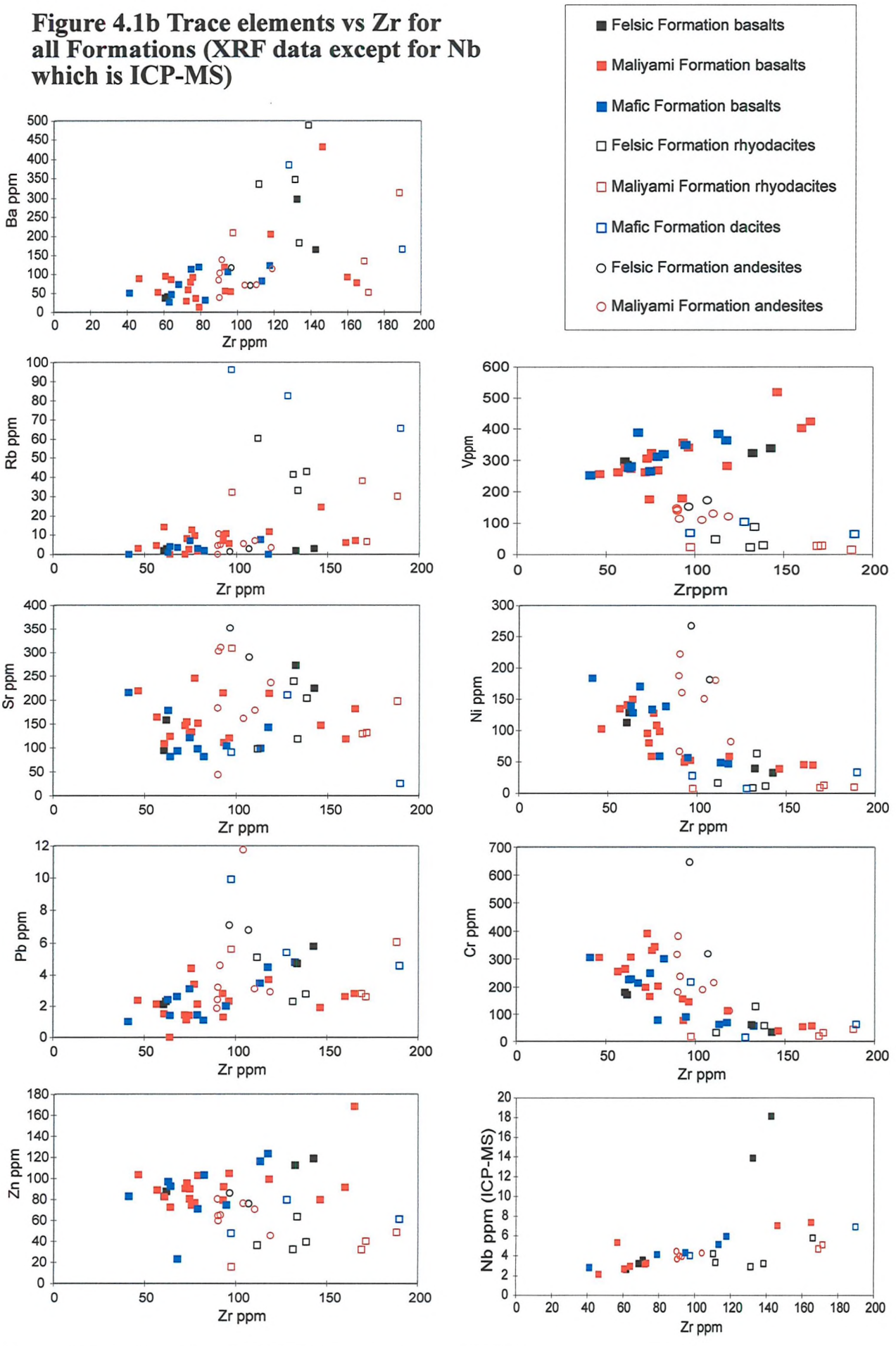

Figure 4.2 - XRF/ICP-MS comparison

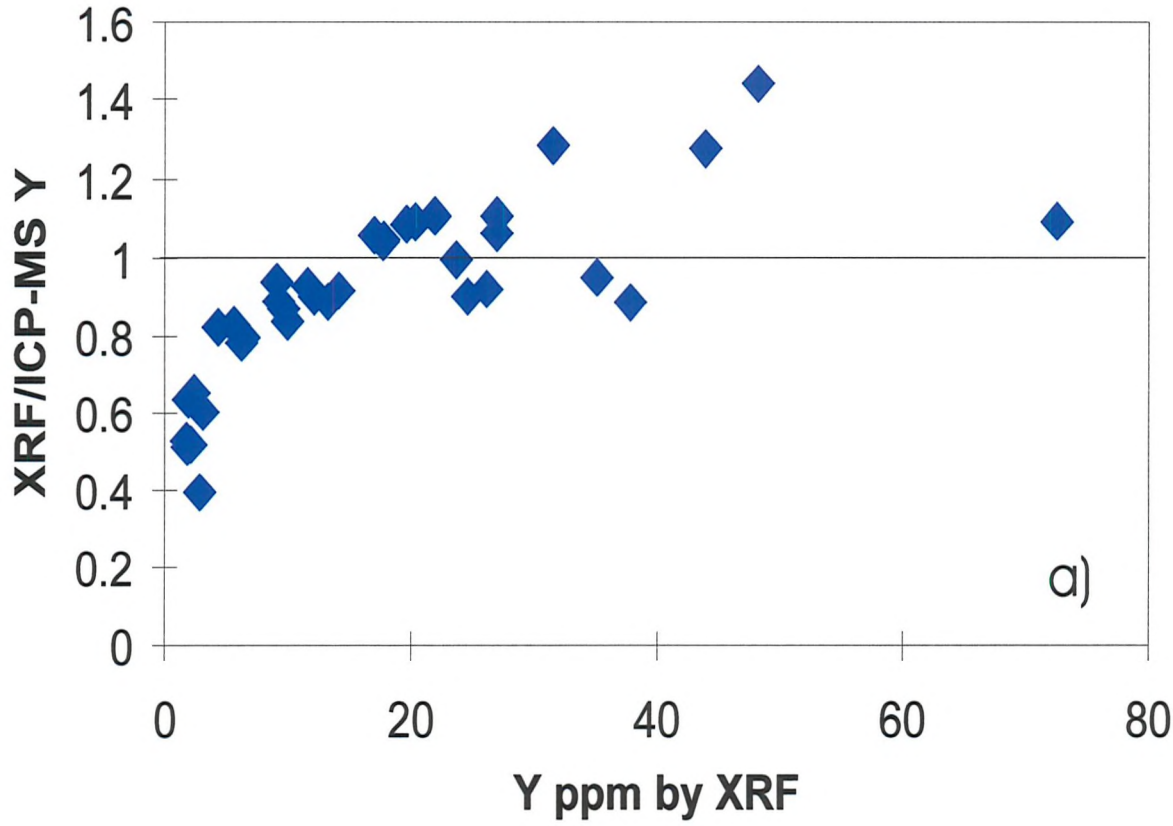

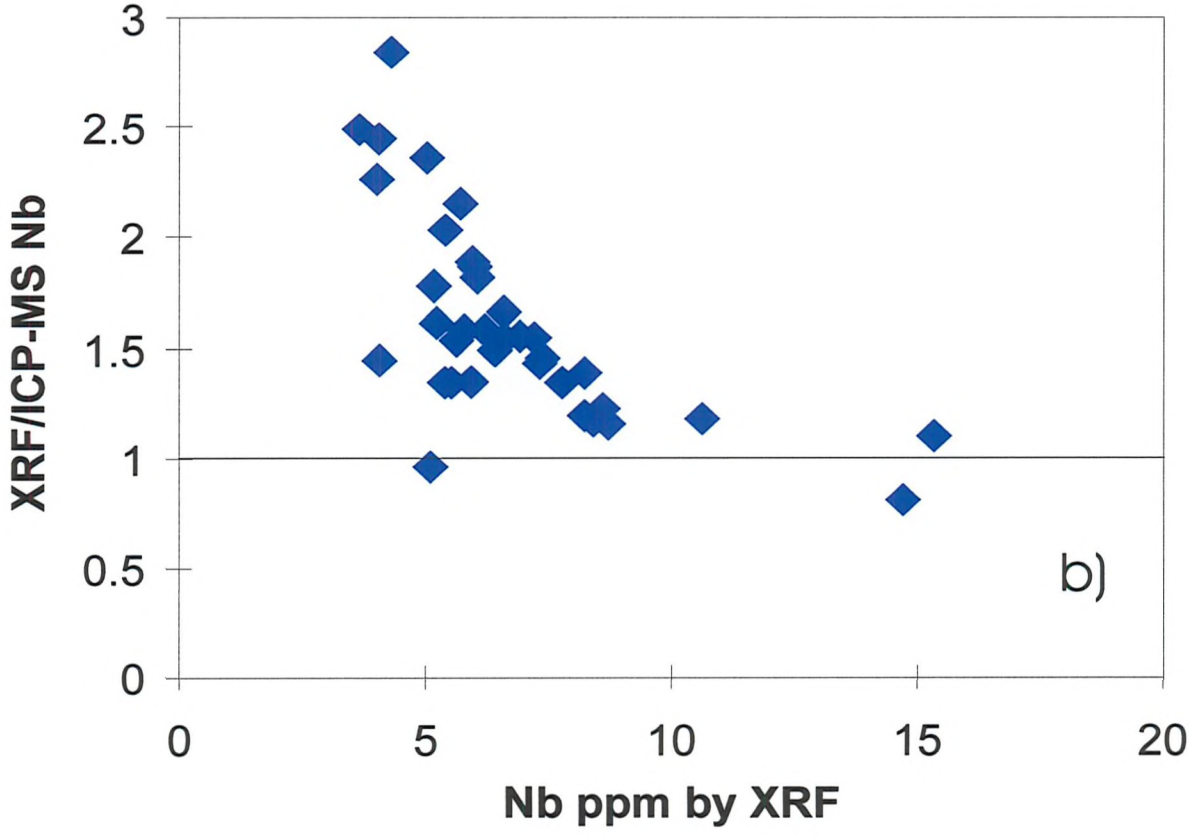

result of incomplete dissolution of accessory minerals during preparation of the solution for ICP-MS, since the XRF/ICP-MS ratio is greater than unity. However, this would not result in ratios <1 for Y (Fig.4.2a). Since no Nb-containing rock-forming mineral is likely to remain undissolved after HF/HNO_3 and HCl attack in preference to a mineral containing Y, and the elements considered were derived from the same solution, incomplete dissolution of the rock powder is considered highly unlikely. The levels of Nb and Y in the samples concerned (<9ppm Nb & <4ppm Y according to XRF) strongly suggests a calibration problem with the XRF data at low concentrations, resulting in a non-zero intercept for concentration at zero intensity of fluorescence. As a result of this, all Nb values and ratios use ICP-MS derived data, as do those samples with concentrations of Y <4ppm (XRF) (and XRF/ICP-MS ratios <<0.8).

4.3) GEOCHEMICAL METHODOLOGY

A description of the geochemistry will now follow before consideration of the relationship between formations and their possible petrogenesis. Inspection of the data in Table 4.1 indicates that specific groupings exist for some of the elements of interest (SiO_2, TiO_2, Fe_2O_3*, MgO, CaO, P_2O_5, Ti, Y, V and Zr). The distinct similarity in elemental range between the formations is also noticeable. This geochemical coherence between the lithologies of all three formations can be illustrated throughout the major and trace element diagrams plotted from here-on and strongly suggests that the processes occurring at the time of eruption of any one of the formations is a consistent process which has formed the whole of this stratigraphic section over its formation history. As a result, the data for this stratigraphy will be considered as one, plotting all the formations on one diagram in order to highlight any small differences between them and to identify outlying samples.

4.4) MAJOR ELEMENTS

4.4.1) SiO_2

Before consideration of other major elements, attention is drawn to the compositional gaps in silica concentration seen in the three formations (see Figure 4.3). A *c.*12wt% compositional gap exists in the Mafic Formation between approximately 53wt% and 65wt% SiO_2. This highlights a bimodal nature noted by this study but not by other workers. The Maliyami Formation also shows a gap, albeit at a much higher percentage of silica, with no

compositions apparent between *c.*61-72wt%. The compositional gap exhibited by the Felsic Formation is much smaller, about 8wt% between 57 and 65wt% SiO_2.

(All the major element discrimination diagrams discussed in the text from here-on are present in Figure 4.4a unless stated otherwise.)

4.4.2) TiO_2 and Fe_2O_3*

Two fractionation trends can be seen. The basalts evolve possibly by fractionating augitic clinopyroxene to give a decrease in MgO but an increase in TiO_2 and Fe_2O_3*. The andesites, starting with the same TiO_2 and Fe_2O_3* concentrations at 8wt% MgO, exhibit a trend of decreasing MgO, TiO_2, and Fe_2O_3*. This trend results in rhyodacites with very low concentrations of all three oxides.

4.4.3) CaO

The CaO versus MgO plot supports the likelihood of clinopyroxene involvement in the evolution of the basalts as CaO trends to lower values. The andesite-dacite trend also shows a small reduction in CaO concentration but the slope is shallow and spurious reductions as a result of the constant sum effect as silica increases, should not be forgotten.

Also of note, is that the scatter of data is greater for Ca than the other elements, presumably since it is more vulnerable to mobilisation under lower-greenschist facies metamorphic conditions. However, the basic trends can still be seen and initial Ca concentrations at 8wt% MgO are lower for the andesites than the basalts.

4.4.4) P_2O_5

Phosphorous shows the same pattern as TiO_2 and Fe_2O_3*; an increase in the basalts with decreasing MgO and a decrease in the andesite-dacite suite. Interestingly, unlike Fe_2O_3* and TiO_2, the andesites have higher initial concentrations of P_2O_5 than the basalts at 8wt% MgO.

4.4.5) mg#

Magnesian number (mg# - 100*(MgO/(MgO/Fe_2O_3*))) is plotted against MgO to illustrate the difference between the two fractionation trends exhibited by the basalts and

Figure 4.3 - Compositional gaps for formations of the Midlands Greenstone Belt

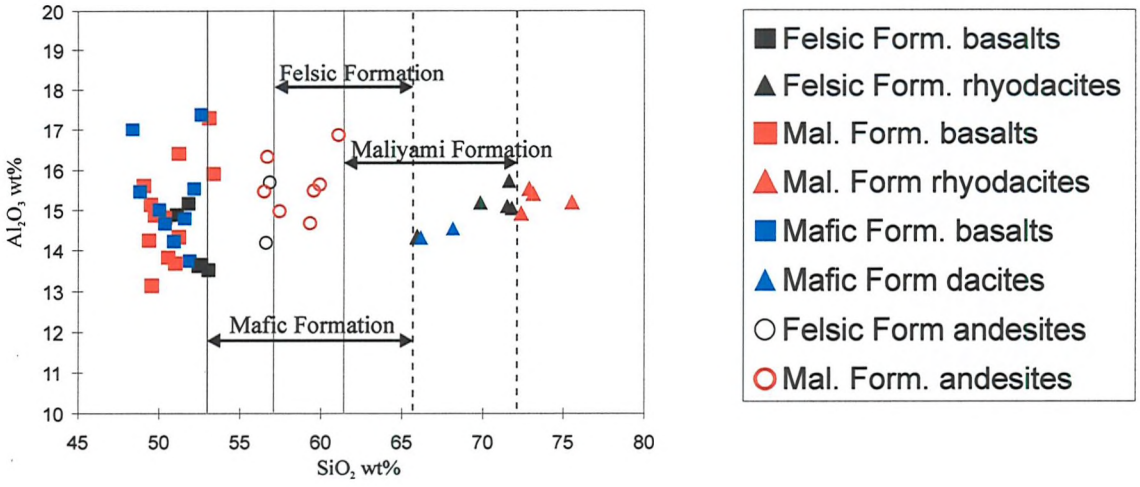

Figure 4.4a - Major Element plots

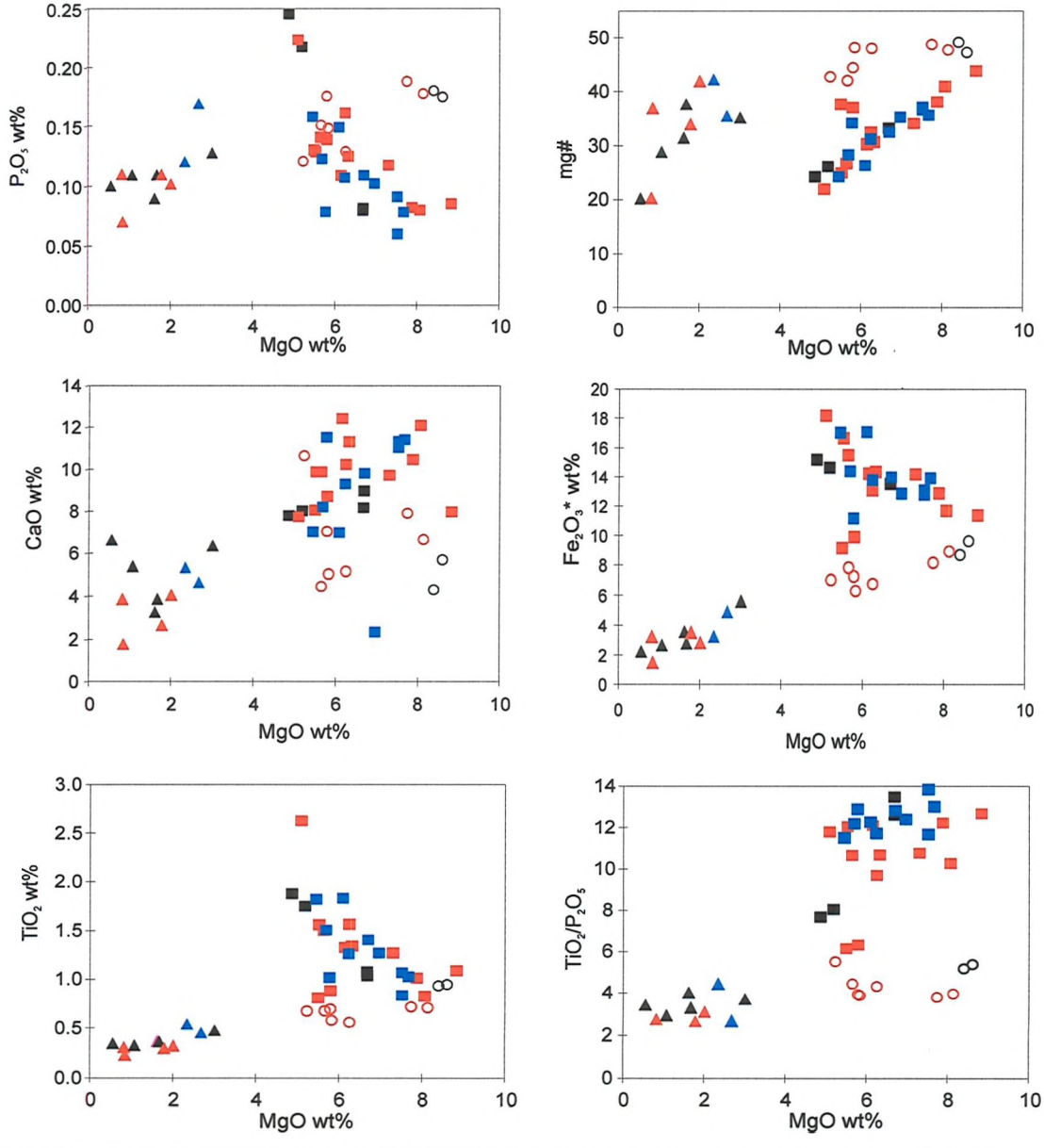

andesites. The basalts have an initial mg# of 40 at 8wt% MgO, decreasing with decreasing MgO to *c.*25 at 5.5wt% MgO, illustrating the increase in Fe_2O_3* already seen. The andesites have a higher mg# of *c.*50 at 8wt% MgO decreasing to *c.*35 at 2wt% MgO in the rhyodacites. This indicates that although Fe_2O_3* is seen to decrease, MgO is decreasing at a greater rate leading to a decreasing mg#.

4.4.6) Major element summary

Basalts and andesites show the same range of MgO concentrations (*c.*5 to 8wt%). The basalts evolve, probably by clinopyroxene fractionation towards Mg and Ca-poor, Fe, Ti and P-rich tholeiitic compositions. The andesites evolve to dacites and rhyodacites through a reduction in Mg, Fe, Ti, P and Ca (reductions due to constant summation should not be ruled out e.g. Ca and P). This strongly suggests that the samples can be considered as members of two distinct suites: basalt and andesite-dacite. This is graphically illustrated in the TiO_2/P_2O_5 vs MgO plot in Figure 4.4a which shows that the basalts retain a consistent ratio of 10 to 14 despite their obvious fractionation, and the andesite-dacite suite have TiO_2/P_2O_5 ratios starting around 6 and decrease as TiO_2 is lost through fractionation. The only exceptions to this are two high-Nb basalts (see section 4.5.5), and two basaltic-andesites which otherwise display andesitic geochemical characteristics. Both these exceptions possess lower TiO_2/P_2O_5 ratios than the rest of the basalts.

From this evidence it would seem impossible to derive the andesites by fractionation of the basalts.

4.5) TRACE ELEMENTS

The principle elements of interest are Zr, Ti, Y, Nb, P and V. The plots relating to the text are displayed in Figure 4.4b and will be described directly (rather than describing the geochemistry by element as with the majors) since no consistent abscissa is used for reference between each diagram.

4.5.1) Zr vs. Ti

Zirconium exhibits an increase in both the basalts and the andesite-dacite suite. Titanium, as seen from the major element plots, shows a decrease in the latter lithologies. Two separate trends are therefore apparent. The andesite-dacite trend projected backwards,

Figure 4.4b - Trace Element plots

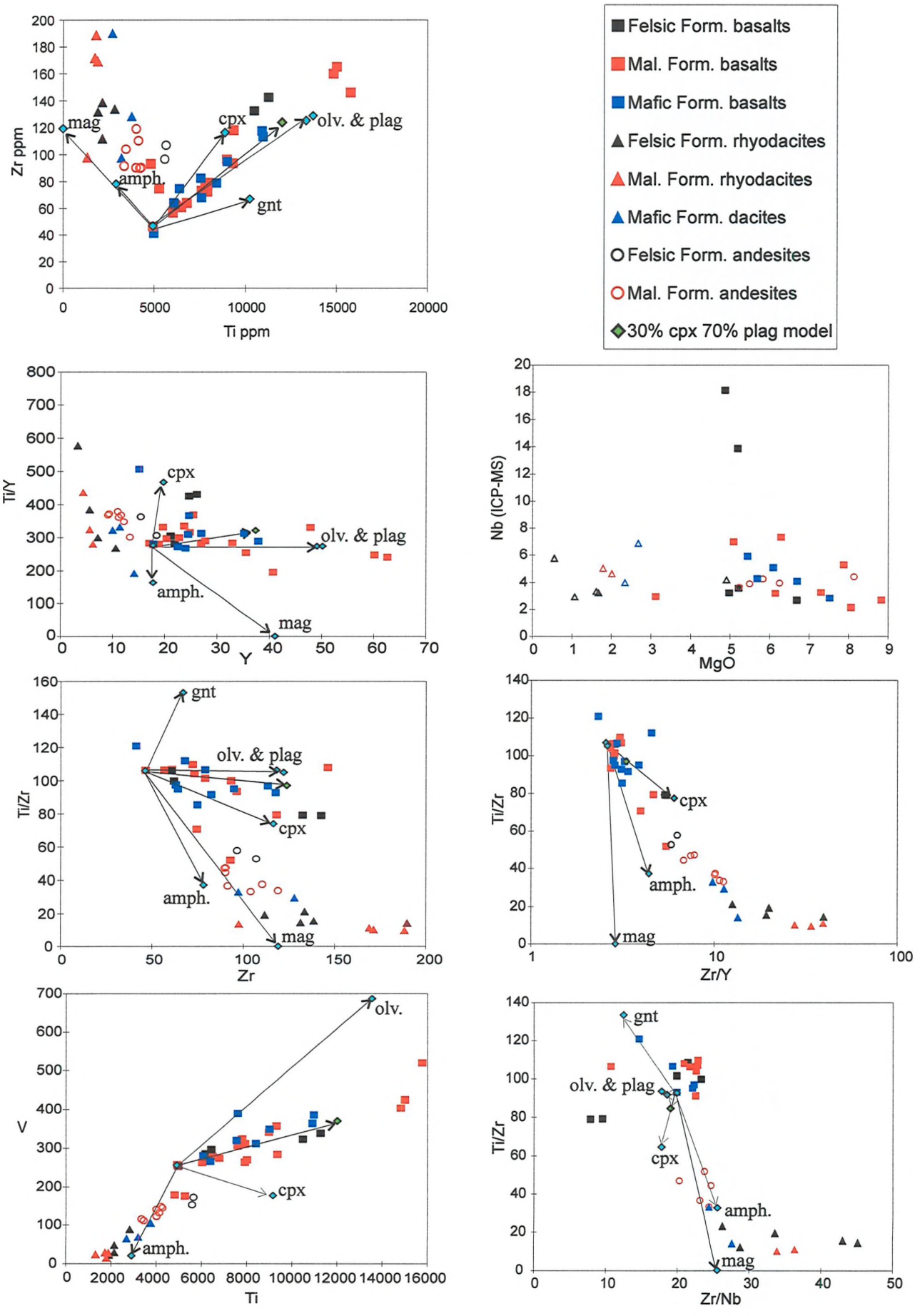

intercepts the basalt trend almost perpendicularly at a composition of 60ppm Zr and 6000ppm Ti. This corresponds to an initial basalt composition of approximately 49wt% SiO_2, typified by sample Zimb.018 in the Mafic Formation, possibly suggesting derivation from a basaltic liquid of this composition. However, other major and trace element data deny this.

At dacitic and rhyodacitic compositions Ti concentrations remain constant at around 2000ppm but Zr levels increase substantially from 110 to 190ppm.

Yttrium (not shown) reflects the behaviour of Ti and exhibits the same trends when plotted against Zr.

4.5.2) Ti/Zr vs. Zr

Ti/Zr ratios in the basalts are between 90-110. The andesites have a higher initial Zr concentration when compared to basalts with the same MgO content. Ti/Zr ratios around 50 decrease due to decreasing Ti and increasing Zr levels until a ratio of approximately 15 when the ratio remains relatively constant, decreasing to around 10 by the time rhyodacitic compositions are reached. This shallowing of the Ti/Zr trend is indicative of the cessation of drastic Ti decrease whilst Zr continues to increase.

4.5.3) V vs. Ti

Ti and V exhibit a positively correlated relationship in both the basalt and andesite-dacite suites. V increases with Ti increase in the basalts and decreases with Ti decrease in the andesite-dacite suite. It is noticeable that the andesites show lower initial starting concentrations of V when compared to basalts with the same MgO content.

4.5.4) Nb vs. MgO

The behaviour of Nb is distinctly different between the two lithological groups. The basalts show increasing Nb from 2 to 8ppm with decreasing MgO but the andesite-dacite suite exhibits slightly higher initial Nb concentrations at the same initial MgO contents and stay constant (although scattered) at approximately 4ppm Nb right through to the most evolved compositions. Of particular note are the high Nb concentrations of Zimb.034 & 208 at 18.1 & 13.9ppm respectively (ICP-MS).

4.5.5) Ti/Y vs. Y

The strong, positively correlated and constant behaviour of Ti and Y is graphically illustrated in this plot. Ti/Y ratios of 250-350 are maintained from basaltic through to rhyodacitic compositions. Only the two high-Nb samples and a rather altered basalt from the Mafic Formation have Ti/Y ratios higher than other samples of this composition. At high SiO_2 compositions, Y concentrations continue to decrease whilst Ti concentrations remain stable leading to a large increase in the Ti/Y ratio. This probably reflects the breakdown of the coherence between these two elements at extremes of fractionation.

4.5.6) Ti/Zr vs. Zr/Y

The basalts exhibit fairly consistent and chondrite-like Ti/Zr and Zr/Y ratios of 90 to 110 and 2.5 to 3 respectively. Five of them show lower Ti/Zr with higher Zr/Y ratios including samples Zimb.208 & 034 of the Felsic Formation. The andesites have lower initial Ti/Zr and higher initial Zr/Y than basalts with the same initial MgO content. Ti/Zr decreases and Zr/Y increases in the andesites through to dacitic compositions, reflecting decreasing Ti and Y and increasing Zr concentrations. At Ti/Zr and Zr/Y values around 15 and 14 respectively, Zr/Y increases markedly up to 40 whilst Ti/Zr remains stable (only decreasing to around 10) reflecting Ti stabilisation, Zr increase and Y decrease.

4.5.7) Ti/Zr vs. Zr/Nb

Ti/Zr is plotted against Zr/Nb in Figure 4.4b in order that any continental influences can be viewed against such distinctive Ti/Zr ratios. Zr/Nb ratios use ICP-MS determined Nb values as discussed in section 4.2.

The basalts generally show Zr/Nb ratios around 20 to 24. Lower ratios of 10.7 & 14.6 are seen in two samples (Zimb.062 & 151 respectively). The two high-Nb basaltic-andesites Zimb.034 & 208 have low Zr/Nb (7.9 & 9.6 respectively) but also low Ti/Zr (~79).

The andesites show the same range of Zr/Nb ratios as the basalts but lower Ti/Zr as discussed above. The rhyodacites have Zr/Nb increased from those of the andesites. Beginning around 24 they increase to 45, roughly with an increase in SiO_2.

4.5.8) Trace element summary

The andesites start with higher Zr and Nb, lower V and the same Ti and Y contents as the basalts, and evolve to rhyodacitic compositions with a decrease in Ti, Y and V, an increase in Zr and no change in the Nb concentrations. The basalts evolve to higher contents of all the trace elements.

The geochemistry thus far clearly indicates the distinction of the sampled lithologies into the two suites described. The dacites and rhyodacites appear to be the fractionation products of the andesites which are chemically distinct from the basalts and have fractionated a different assemblage. A major role for clinopyroxene in the fractionation of the basalts is suggested, however, mineral crystallisation vectors plotted on the trace element diagrams indicate that clinopyroxene alone cannot account for the trends seen. Plagioclase, olivine and hornblende vectors are also plotted as possible involved phases, calculated using distributions coefficients compiled in Rollinson (1993). The length of each vector reflects 65% fractionation of each individual mineral. These vectors show that plagioclase and/or olivine are also probably involved in the evolution of the basalts and that amphibole and an iron oxide (probably ilmenite) may be involved in the evolution of the andesite-dacite suite.

4.6) RARE-EARTH ELEMENTS (REE)

4.6.1) Basalts

The basalts exhibit REE patterns from light-rare earth element (LREE) depleted to LREE enriched. Each formation displays a similar but different set of REE patterns and so will be discussed separately.

The basalts from the Mafic Formation (see Figure 4.5a) show increasing total REE content but also increasing LREE enrichment, with increasing SiO_2. Sample Zimb.151 has the most depleted pattern (La/Sm = 0.68) and the lowest total REE content at approximately 8.5x chondrite with a silica content of 50wt% and MgO content of 7.5%. Zimb.137 has the most enriched pattern with La/Sm = 1.14 and 52.6wt% SiO_2 with total REE around 20x chondrite. A small Eu anomaly is present throughout these samples changing from positive to negative (Eu/Eu* = 1.1 to 0.91) with increase in silica.

Maliyami Formation basalts (see Figure 4.5b) all possess a depleted LREE pattern (La/Sm around 0.7 to 0.8) with a slight mid-rare earth element (MREE) enrichment and total REE contents ranging from 8.5 to 30.5x chondrite. Small positive Eu anomalies (Eu/Eu* =

Figure 4.5 - Basalt REE patterns

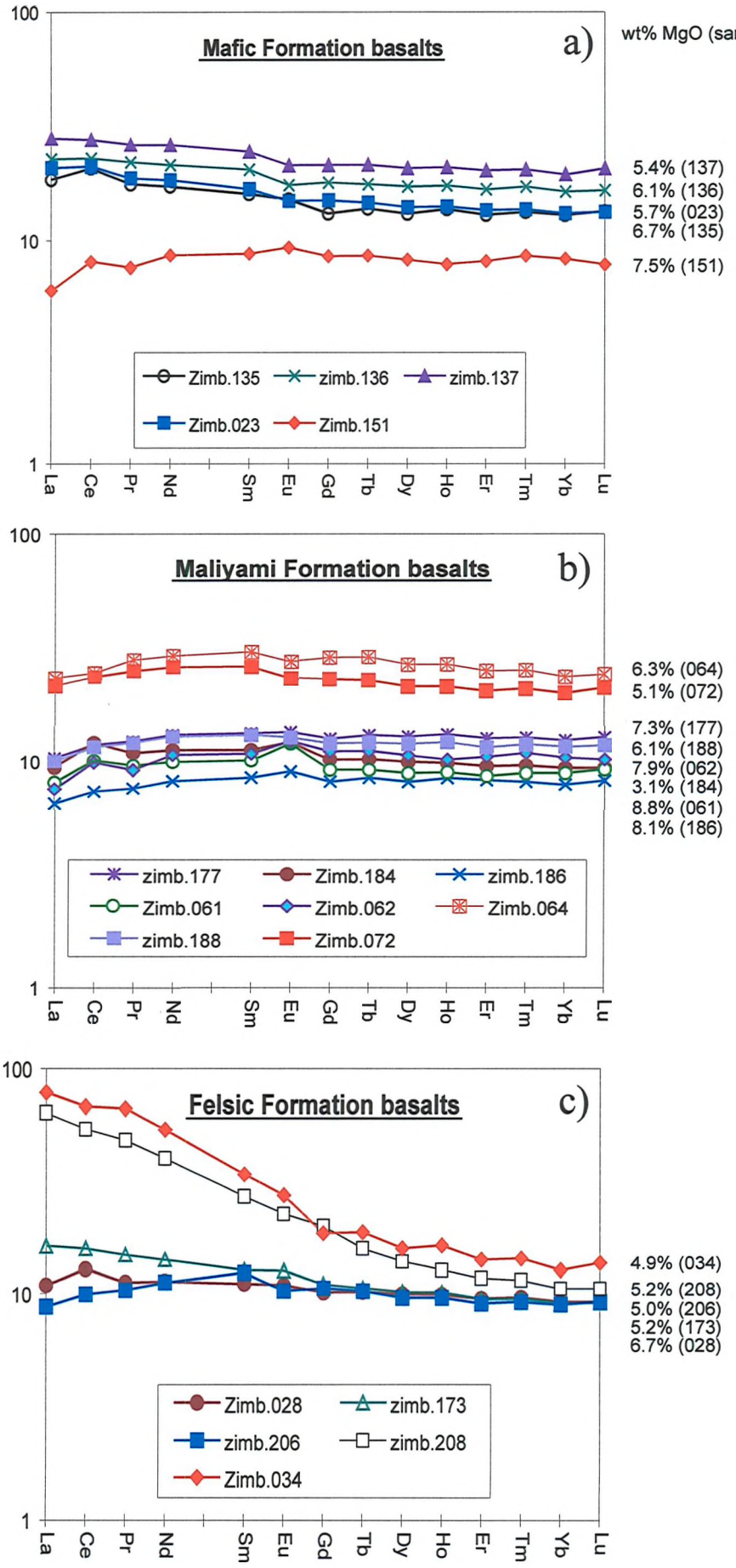

~1.1) are present in basalts with REE levels roughly 10x chondrite, but change to small negative anomalies (Eu/Eu* = ~0.94) in samples with higher REE concentrations. Zimb.046 is a basaltic-andesite that exhibits a steep REE profile with La/Sm = 2.1, Gd/Yb = 1.27 and heavy rare earth element (HREE) contents approximately 7.5x chondrite. This is not too dissimilar from the andesites (see section 4.6.2 below) and is therefore plotted with them in Figure 4.6a.

Basalts from the Felsic Formation (see Figure 4.5c) show features recognisable from both the other formations. LREE depleted to LREE enriched patterns are seen (La/Sm = 0.7 to 1.3) with total REE contents approximately 10x that of chondrite. No Eu anomalies of any significance are present. Two basaltic-andesites (Zimb.034 & 208) however, show strong LREE enrichment (La/Sm = 2.3) and mild HREE depletion (Gd/Yb = 1.5 & 1.9), with enriched total REE contents including LREE up to 80x chondrite and HREE slightly higher than the basalts (10 & 13.6x chondrite). These are the same samples with high concentrations of Nb (~15ppm).

4.6.2) Andesites and rhyodacites

Andesites from the Maliyami Formation (Figure 4.6a) exhibit increasing La/Yb (5.8 to 8.1) with increasing SiO_2 and decreasing HREE content (6.25 to 4x chondrite). No Eu anomalies are present. Zimb.213 has La/Yb = 3.9 and a HREE content of 7x chondrite despite a silica content of 59.3%, hence it has more affinity with the basaltic-andesite Zimb.046. These two samples may represent a distinct grouping separate from the other more typical andesites.

REE patterns for dacites and rhyodacites are plotted in Figure 4.6b. Those from the Mafic Formation are LREE enriched (La/Sm = 3.62 to 3.76) when compared to the basalts, with mildly depleted HREE profiles (Gd/Yb = 1.8 to 2.2) at 5 to 7x chondrite. Rhyodacites from the Felsic and Maliyami Formations are more evolved than the Mafic Formation dacites and may be considered a distinct grouping, possessing steeper REE (La/Yb = 12.1 to 26.6) but more HREE depleted (Gd/Yb = 2.2 to 4.5 at 1 to 3x chondrite) profiles. One sample from the Maliyami Formation (Zimb.189) which has the highest silica content (75.52wt%) of the rhyodacites, actually has a shallower REE profile than any of the rest, with lower LREE contents. Eu anomalies where present are small and positive (Eu/Eu* = ~1.2).

Figure 4.6 - REE patterns for Andesites and Rhyodacites

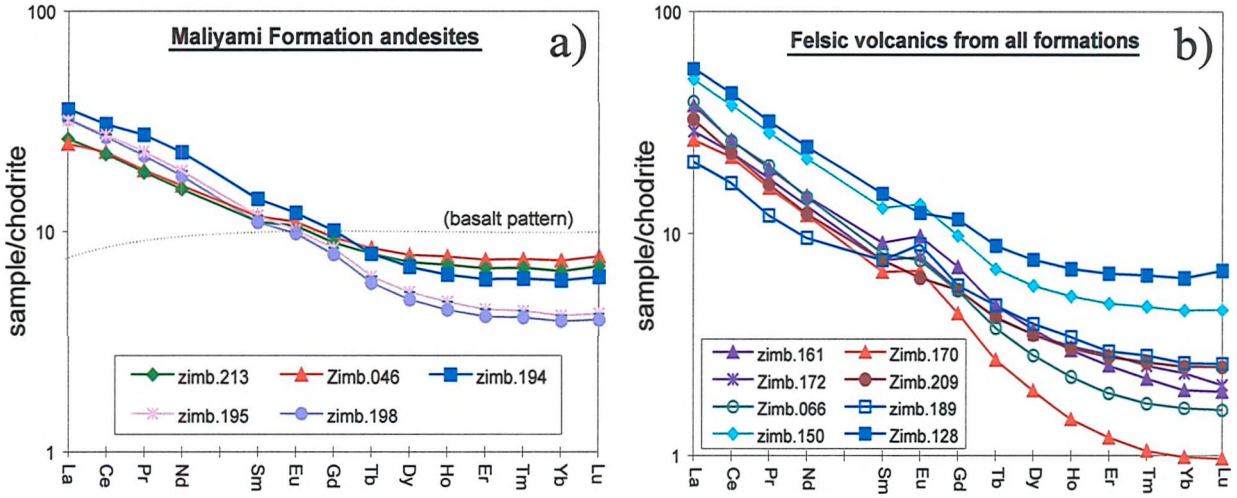

Figure 4.7 REE ratio plots

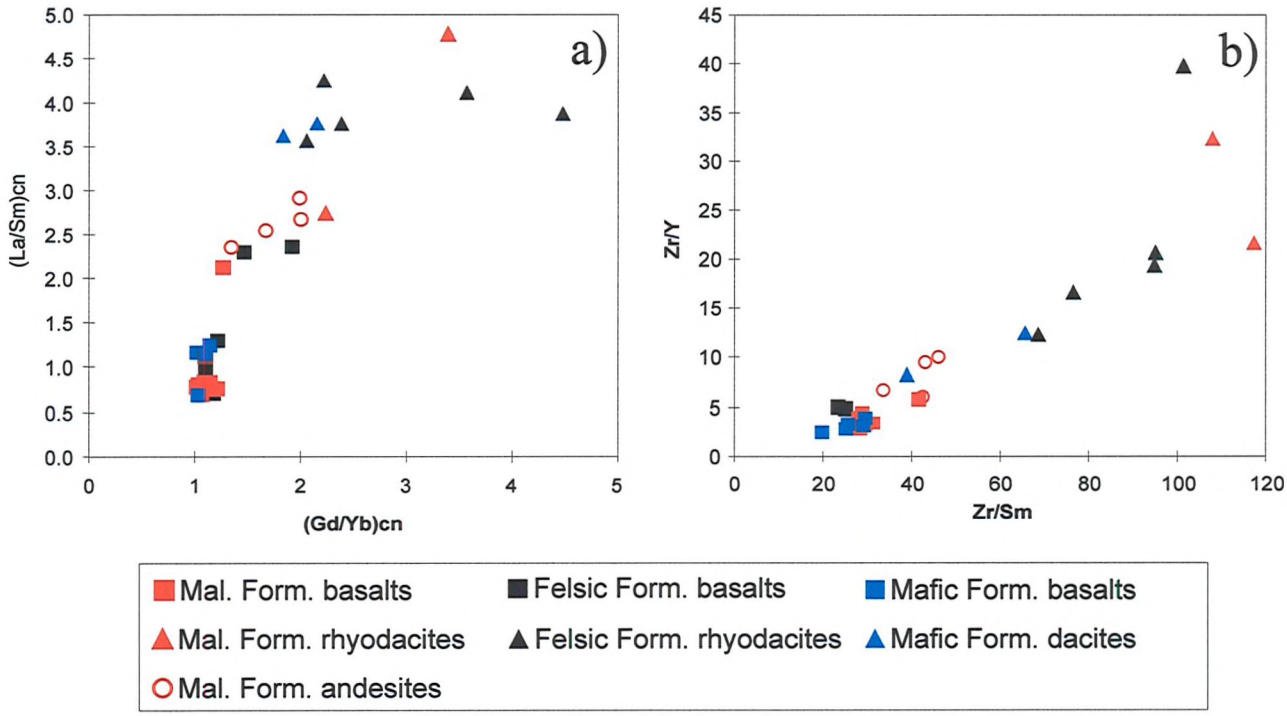

4.6.3) REE ratio plots

La/Sm vs Gd/Yb - La/Sm ratios >1 indicate LREE enrichment whilst Gd/Yb ratios >1 show HREE depletion. Such variations in REE pattern are displayed with regard to composition, on a chondrite normalised La/Sm vs Gd/Yb plot shown in Figure 4.7a. This distinguishes particularly well between the LREE depleted and undepleted basalts. The LREE enriched, HREE depleted nature of the andesites and dacites is also distinguished with basaltic-andesite Zimb.046 again illustrating affinity to andesitic geochemistry (see section 4.1 and previous geochemical plots). The two LREE enriched, high-Nb basalts (Zimb.034 & 208) also plot with the andesites as does the flat REE trending rhyodacite Zimb.189. This grouping of andesites with anomalous samples (Zimb.046, 034, 208 & 189) has La/Sm 2.1 to 2.9 and Gd/Yb 1.3 to 2.2, the higher of both ratios correlating with higher SiO_2.

The dacites and rhyodacites show two distinct groupings distinguished by much greater HREE depletion at the same LREE enrichment. The first of these has La/ Sm = 3.6 to 4.2 and Gd/Yb = 1.8 to 2.4, and the other grouping La/Sm = 3.9 to 4.8 and Gd/Yb = 3.6 to 4.5. It is not always the case that the highest silica (most evolved) samples belong to this second grouping (Zimb.161, 170 & 066) with higher Gd/Yb.

Zr/Y vs Zr/Sm - Zr/Sm ratios should reflect those of the source since each element of the pair has a very similar bulk distribution coefficient (D) (Rollinson, 1993). The ratio is therefore affected little by fractionation and melting processes until high degrees of fractionation or low degrees of partial melting, at which point the coherent relationship between the two elements breaks down. This being the case, Zr/Sm may prove very useful in evaluating whether the andesites and basalts have been sourced from the same mantle component or whether the andesites have had some influence from another component, for example continental crust, with a different more fractionated ratio. The deviations in Zr/Y have already been discussed (see section 4.5.6 and Fig.4.4b) and will not be repeated here. However, attention is drawn to the fact that in Figure 4.7b Zr is ratioed against ICP-MS derived Y unlike the ratio discussed in section 4.5.6. This Zr/Y (ICP-MS) ratio is quoted in Table 4.1c.

The basalts and basaltic-andesites form a tight grouping with Zr/Sm *c.*25 to 30 and Zr/Y 2.7 to 3.5. The two high-Nb samples (Zimb.034 & 208) also plot with very similar values indicating a strong link with the rest of the basalts when considering their origin.

The most striking feature illustrated by Figure 4.7b is that the andesites possess characteristic Zr/Sm and Zr/Y ratios of 33.6 to 46.1 and 5.8 to 10 respectively, distinctly different to the basalts and basaltic-andesites. The andesite grouping is interrupted by basaltic-andesite Zimb.046 and the least evolved, lowest silica dacite Zimb.150. The rest of the dacites and rhyodacites show very high Zr/Sm (65 to 117) possibly as a result of small-scale partial melting and/or fractionation processes which cause the 'mantle signature' relationship of the trace element pairing to break down.

4.6.4) REE summary

1) The Mafic Formation basalts show flat REE patterns around 8 to 20x chondrite, with depleted to slightly enriched LREE profiles.

2) The Maliyami Formation basalts all exhibit fairly flat but slightly LREE depleted, MREE enriched patterns.

3) Felsic Formation basalts have patterns similar to basalts from the Mafic Formation (LREE depleted to LREE enriched) with concentrations 10x that of chondrite. Two samples of basaltic-andesites show enrichment of the whole REE profile and high-Nb concentrations.

4) Maliyami andesites have LREE enriched and flat to depleted HREE profiles compared to the Maliyami basalts, with lower HREE concentrations.

5) The dacitic and rhyodacitic volcanics show a roughly correlated trend of decreasing total REE content and increasing La/Yb with increasing SiO_2 (compare Figure 4.6b & Table 4.1). One sample (Zimb.170) shows extreme HREE depletion.

6) Eu anomalies are small where present indicating the small role of plagioclase in petrogenesis and/or oxidising conditions in the magma resulting in the predominance of Eu^{3+}.

7) Trace element ratios are tabulated below

	Basalts	Andesites	Rhyodacites
$(La/Sm)_{cn}$	0.7 to 1.3	2.3 to 2.9	3.6 to 4.8
$(Gd/Yb)_{cn}$	1 to 1.2	1.3 to 2	1.8 to 2.4 & 3.4 to 4.5
Zr/Nb	20 to 24	20 to 24	24 to 45
Zr/Y	2.7 to 3.5	5.8 to 10	*c.*10 to 40
Zr/Sm	25 to 31	33.5 to 46	65 to 117

4.7) Nd ISOTOPES

Table 4.2 displays the Nd isotope data for the samples from the volcanic formations considered in this study. Nineteen samples from the volcanic stratigraphy were selected for analysis and are plotted in Figures 4.8a & b. Determinations were conducted by two methods: 1) TIMS - including isotope dilution to determine Sm/Nd, and 2) a combination of TIMS to determine $^{143}Nd/^{144}Nd$ and ICP-MS to determine Sm/Nd. It is noted that out of 12 samples determined by both methods, the results for 4 samples (Zimb.135, 028, 151 & 184) were not within error for the two techniques. All analyses determined by ID-TIMS have been accepted in preference to the TIMS/ICP-MS data. A discussion of this can be found in Appendix B.

Figure 4.8a indicates that nearly all of the volcanics have an initial $^{143}Nd/^{144}Nd$ value of between 0.50898 and 0.50931. The error bars (external reproducibility) shown are ±0.000080 (2 S.D.) for the TIMS/ICP-MS derived data, and 0.000014 (2 S.D.) for the ID-TIMS data. The two basalts analysed from the Mafic Formation have a lower calculated initial $^{143}Nd/^{144}Nd$ ($Nd_{(i)}$; *c.*0.5090) than basalts from the Maliyami and Felsic Formations resulting from their similar present day $^{143}Nd/^{144}Nd$ ($Nd_{(m)}$) and older age, allowing an increased amount of time-integrated growth when compared to basalts from the Maliyami and Felsic Formations (see Chapter 5 for geochronology). However, a dacite from the Mafic Formation (Zimb.150) and one from the Maliyami Formation (Zimb.189) both have lower initial $Nd_{(i)}$ ratios (0.508875 and 0.508847 respectively) than those for other volcanics in their respective formations at the $^{147}Sm/^{144}Nd$ ratios relevant to their composition. This indicates that they have a substantial component of non-radiogenic Nd (^{144}Nd), causing a low $^{143}Nd/^{144}Nd$.

Figure 4.8b displays the range in $^{147}Sm/^{144}Nd$ ratios for the volcanics plotted against $\varepsilon_{Nd(t)}$. This illustrates the LREE enriched (low $^{147}Sm/^{144}Nd$) patterns for the high silica members and andesites relative to their crustal/mantle signature (negative/positive $\varepsilon_{Nd(t)}$). The error bars (external reproducibility) shown are set at ±1.5 ε units (2 S.D.) for the TIMS/ICP-MS derived data, and ±0.25 ε units (2 S.D.) for the ID-TIMS data.

Apart from two dacitic/rhyodacitic rocks, the volcanics of all compositions from all formations have $\varepsilon_{Nd(t)}$ values between +1.53 and +3.49. The two dacitic/rhyodacitic volcanics (Zimb.150 &189) with low $Nd_{(i)}$ when compared to other volcanics in their formations, have

Table 4.2 - SUMMARY OF DATA FOR Nd ISOTOPE ANALYSES

Stratigraphic Formation		Sample no.	Lithology	143/144m	± 2 S.E.	Sm/Nd	± 2 S.D.	Nd ppm	147/144	± 2 S.D.	Nd(i) @ relevant age: age	143/144(i)	± 2 S.D.	εNd(t)	± 2 S.D.	T(CHUR)	error range in Ma: + 2 S.D.	- 2 S.D.	T(DM)	error range in Ma: + 2 S.D.	- 2 S.D.	Jelsma (1993) T(DM)	Isoplot v.2.90 T(DM) Ma
Felsic Formation		Zimb.161	rhyodacite	0.511396	5	0.198573	0.003971	8.8	0.120066	0.002401	2.7Ga	0.509257	53	2.42	1.04	2.46E+09	79	74	2.84E+09	74	70	2.54E+09	2680
	x	Zimb.209	dacite	0.511398	5	0.201982	0.000202	8.0	0.122127	0.000122	2.7Ga	0.509222	12	1.73	0.24	2.52E+09	4	4	2.90E+09	4	4	2.56E+09	2739
	x	Zimb.170	dacite	0.511251	5	0.184244	0.000184	7.5	0.111398	0.000111	2.7Ga	0.509266	12	2.60	0.24	2.47E+09	3	3	2.81E+09	3	3	2.48E+09	2667
	x	Zimb.028	basalt	0.512694	5	0.322019	0.000322	7.2	0.194767	0.000195	2.7Ga	0.509224	13	1.77	0.26	-4.49E+09	-	-	3.64E+09	37	37	1.93E+09	!*!?!
Maliyami Formation																							
		Zimb.066	rhyolite	0.511231	4	0.180665	0.003613	8.7	0.109234	0.002185	2.7Ga	0.509285	49	2.97	0.96	2.44E+09	62	59	2.78E+09	59	57	2.52E+09	2640
		Zimb.052	Si xl tuff	0.511587	5	0.216028	0.004321	16.3	0.130626	0.002613	2.7Ga	0.509260	57	2.47	1.11	2.41E+09	99	91	2.85E+09	92	86	2.52E+09	2671
	x	Zimb.189	rhyodacite	0.511625	4	0.257907	0.000258	5.6	0.155951	0.000156	2.7Ga	0.508847	13	-5.64	0.25	3.75E+09	14	14	3.99E+09	11	11	3.36E+09	3866
		Zimb.214	tuff	0.511893	5	0.243472	0.004869	10.6	0.147231	0.002945	2.7Ga	0.509270	62	2.67	1.23	2.29E+09	144	128	2.86E+09	131	120	2.45E+09	2639
		Zimb.194	andesite	0.511374	5	0.198455	0.003969	13.5	0.119994	0.002400	2.7Ga	0.509236	53	2.01	1.04	2.50E+09	80	75	2.87E+09	75	71	2.57E+09	2715
		Zimb.173	altered andesite	0.512391	4	0.288541	0.005771	8.4	0.174506	0.003490	2.7Ga	0.509282	72	2.91	1.42	1.69E+09	314	229	2.93E+09	284	238	2.27E+09	2541
	x	Zimb.061	basalt	0.512828	6	0.330242	0.000330	6.6	0.199747	0.000200	2.7Ga	0.509270	14	2.66	0.27	9.25E+09	-	-	3.49E+09	50	49	1.66E+09	!*!?!
	x	Zimb.072	basalt	0.512728	5	0.321010	0.000321	16.7	0.194158	0.000194	2.7Ga	0.509269	13	2.65	0.26	-5.51E+09	-	-	3.27E+09	32	32	2.20E+09	!*!?!
		Zimb.177	basalt	0.512845	5	0.327890	0.006558	7.9	0.198325	0.003966	2.7Ga	0.509312	81	3.49	1.58	1.83E+10	-	-	3.00E+09	1031	611	1.59E+09	!*!?!
	x	Zimb.184	basalt	0.512826	4	0.329706	0.000330	7.3	0.199423	0.000199	2.7Ga	0.509273	14	2.74	0.27	1.02E+10	-	-	3.43E+09	48	47	1.50E+09	!*!?!
		Zimb.188	basalt	0.512816	5	0.327672	0.006553	7.7	0.198192	0.003964	2.7Ga	0.509285	81	2.97	1.58	1.72E+10	-	-	3.26E+09	1103	658	1.78E+09	!*!?!
		Zimb.185	assimilated clast	0.512772	5	0.322244	0.006445	6.1	0.194907	0.003898	2.7Ga	0.509300	79	3.26	1.56	-1.19E+10	-	-	3.04E+09	787	519	1.81E+09	!*!?!
Mafic Formation																							
	x	Zimb.150	dacite	0.511078	5	0.191595	0.000192	12.7	0.115838	0.000116	2.88Ga	0.508875	12	-0.44	0.24	2.92E+09	4	4	3.20E+09	4	4	2.94E+09	3073
	x	Zimb.135	basalt	0.512484	5	0.305075	0.000305	10.3	0.18451	0.000185	2.88Ga	0.508976	14	1.53	0.27	1.92E+09	29	28	3.45E+09	22	21	2.28E+09	!*!?!
	x	Zimb.151	basalt	0.512892	5	0.338396	0.000338	5.2	0.204682	0.000205	2.88Ga	0.509000	14	2.01	0.27	4.79E+09	-	-	4.31E+09	99	94	1.26E+09	!*!?!
Sebakwe River Gneiss																							
		Zimb.142	P3 SRG	0.509962	4	0.134247	0.002685	14.7	0.081144	0.001623	3.55Ga	0.508056	48	0.75	0.95	3.50E+09	49	48	3.63E+09	45	43	3.38E+09	3563
	x	Zimb.141	P2 SRG	0.511884	5	0.274520	0.000275	39.4	0.166006	0.000166	3.565Ga	0.507968	14	-0.59	0.27	3.71E+09	20	20	4.01E+09	14	14	3.35E+09	3860
		Zimb.140	P1 SRG	0.511233	5	0.222704	0.004454	32.8	0.134652	0.002693	3.6Ga	0.508025	74	1.44	1.46	3.42E+09	154	141	3.66E+09	128	119	3.26E+09	3543
Regional units (and others)																							
	x	Zimb.226	Kwekwe Gneiss	0.510439	6	0.160207	0.000160	16.7	0.096847	0.000097	3.456Ga	0.508225	12	1.64	0.24	3.33E+09	3	3	3.51E+09	3	3	3.26E+09	3417
		Zimb.95/14	Tokwe River Gneiss	0.510127	6	0.136768	0.002735	10.7	0.082671	0.001653	3.455Ga	0.508238	38	1.86	0.74	3.33E+09	48	47	3.49E+09	44	43	3.24E+09	3407
		Zimb.95/35	Chingezi Gneiss	0.510557	5	0.142796	0.002856	16.7	0.086324	0.001726	2.9Ga	0.508904	43	0.63	0.85	2.86E+09	45	44	3.08E+09	42	41	2.85E+09	2977
		Zimb.95/06	Chilimanzi Granite	0.510767	6	0.154574	0.003091	52.4	0.093449	0.001869	2.64Ga	0.509140	43	-1.42	0.84	2.75E+09	50	48	3.00E+09	47	45	2.76E+09	2886
		Zimb.091	Sesombi Tonalite	0.511464	4	0.196964	0.003939	6.1	0.119095	0.002382	2.673Ga	0.509364	52	3.69	1.02	2.30E+09	72	68	2.70E+09	69	66	2.42E+09	2538
		Zimb.164	Giraffe Porphyry	0.511448	5	0.199297	0.003986	6.1	0.120505	0.002410	2.675Ga	0.509321	53	3.03	1.03	2.37E+09	77	72	2.77E+09	73	69	2.47E+09	2605
		Zimb.156	Chicago porphyry	0.510494	4	0.137303	0.002746	19.4	0.083002	0.001660	2.675Ga	0.509029	39	-2.71	0.77	2.86E+09	42	41	3.08E+09	39	38	2.85E+09	2974

x = ID-TIMS analysis
External reproducibility for ID-TIMS Sm/Nd = 0.1%; 143Nd/144Ndm = 10ppm (2.S.D.)
External reproducibility for ICP-MS Sm/Nd = 2% after normalisation to BHVO-1 = 0.2467 (2.S.D.)
CHUR values - 143Nd/144Nd = 0.512638; 147Sm/144Nd = 0.1967
DM values - 143Nd/144Nd = 0.51315; 147Sm/144Nd = 0.2137; Peucat *et al*.(1989)
Jelsma (1993) T(DM) values - 143Nd/144Nd = 0.513074; 147Sm/144Nd = 0.22021 (DePaolo,1981?)
!*!?! - Isoplot program unable to calculate age

Figure 4.8 - Nd isotope plots

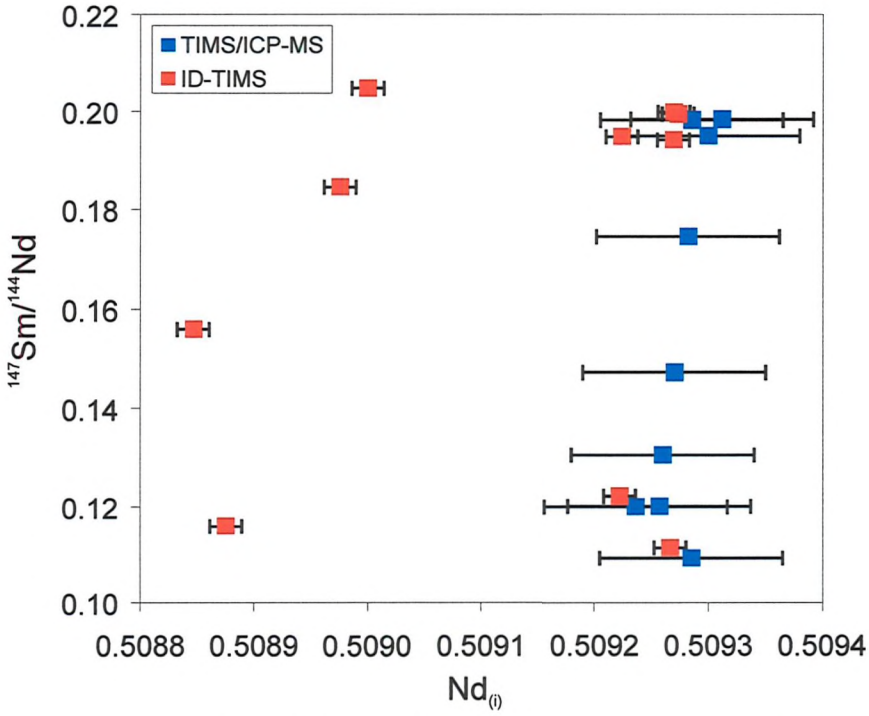

a) Initial $^{143}Nd/^{144}Nd$ vs $^{147}Sm/^{144}Nd$. Errors on ICP-MS data ± 0.000080; error on ID-TIMS = ± 0.000014.

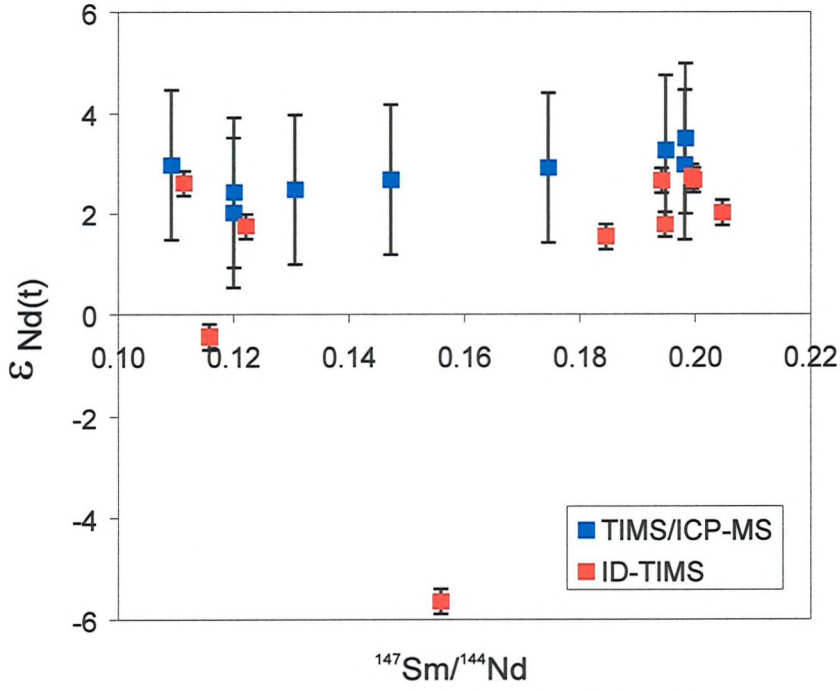

b) $\varepsilon_{Nd(t)}$ vs $^{147}Sm/^{144}Nd$. Errors on ICP-MS data = ±1.5 ε units; error on ID-TIMS ±0.25 ε units.

lower $\varepsilon_{Nd(t)}$ (-0.44 and -5.64 respectively) than that of the chondrite uniform reservoir (CHUR - zero by definition) at that time.

Table 4.2 also shows the calculated model ages for the samples. The explanation for the calculation of these values, and the reasons for the large errors, are discussed in Appendix B. Since LREE depletion is evident in the majority of the basalts, all samples have been calculated for a model age by both chondrite uniform reservoir (T_{CHUR}) and depleted mantle (T_{DM}) models. The $^{147}Sm/^{144}Nd$ and $^{143}Nd/^{144}Nd$ values of Peucat *et al.* (1989), giving an $\varepsilon_{Nd(t)}$ value of +4.1 for the depleted mantle relative to CHUR at 2.7Ga, have been used to calculate the T_{DM} model ages.

Since all T_{CHUR} determinations result in model ages that are considered too young to be realistic or produce outlandish results, only T_{DM} ages will be discussed. T_{DM} model age determinations for basalts range from approximately 3Ga to 3.5Ga (except for Zimb.151 which shows a T_{DM} model age of 4.31Ga). This is somewhat older than the andesites and rhyodacites which have T_{DM} model ages of 2.9Ga and 2.8Ga to 2.9Ga respectively. The two felsic samples with low $Nd_{(i)}$ (Zimb.150 & 189) have T_{DM} model ages of 3.20Ga and 3.99Ga respectively.

In general, the andesites and rhyodacites record a 2.8 to 2.9Ga T_{DM} model age whilst the basalts record a *c.*3.3 to 3.4Ga T_{DM} model age.

The data displayed in Table 4.2 can be used to generate an isochron for the volcanic lithologies. Figure 4.8c displays this isochron and the data used to calculate it. The spread of $^{147}Sm/^{144}Nd$ ratios is such that a good, well constrained and precise isochron can be derived. This also shows that although some of the Sm/Nd data is determined by ICP-MS, it is of sufficient quality (i.e. precision and accuracy) to be able to derive a good isochron.

Since the Maliyami and Felsic Formations clearly form a continuum in the field, a combined isochron has been generated for these two formations giving an age of 2739 ± 33Ma. This compares very well with a U-Pb zircon age of 2701 ± 6Ma (Wilson *et al.*, 1995) for a felsic volcanic from the Maliyami Formation.

From the data available (only 3 data points), it is not possible to generate a satisfactory isochron for the Mafic Formation especially since Zimb.150 possesses a contaminated signature evidenced by an $\varepsilon_{Nd(t)}$ value of -0.44. This will significantly affect the position of this data point, one which is crucial to securing the lower end of the regression

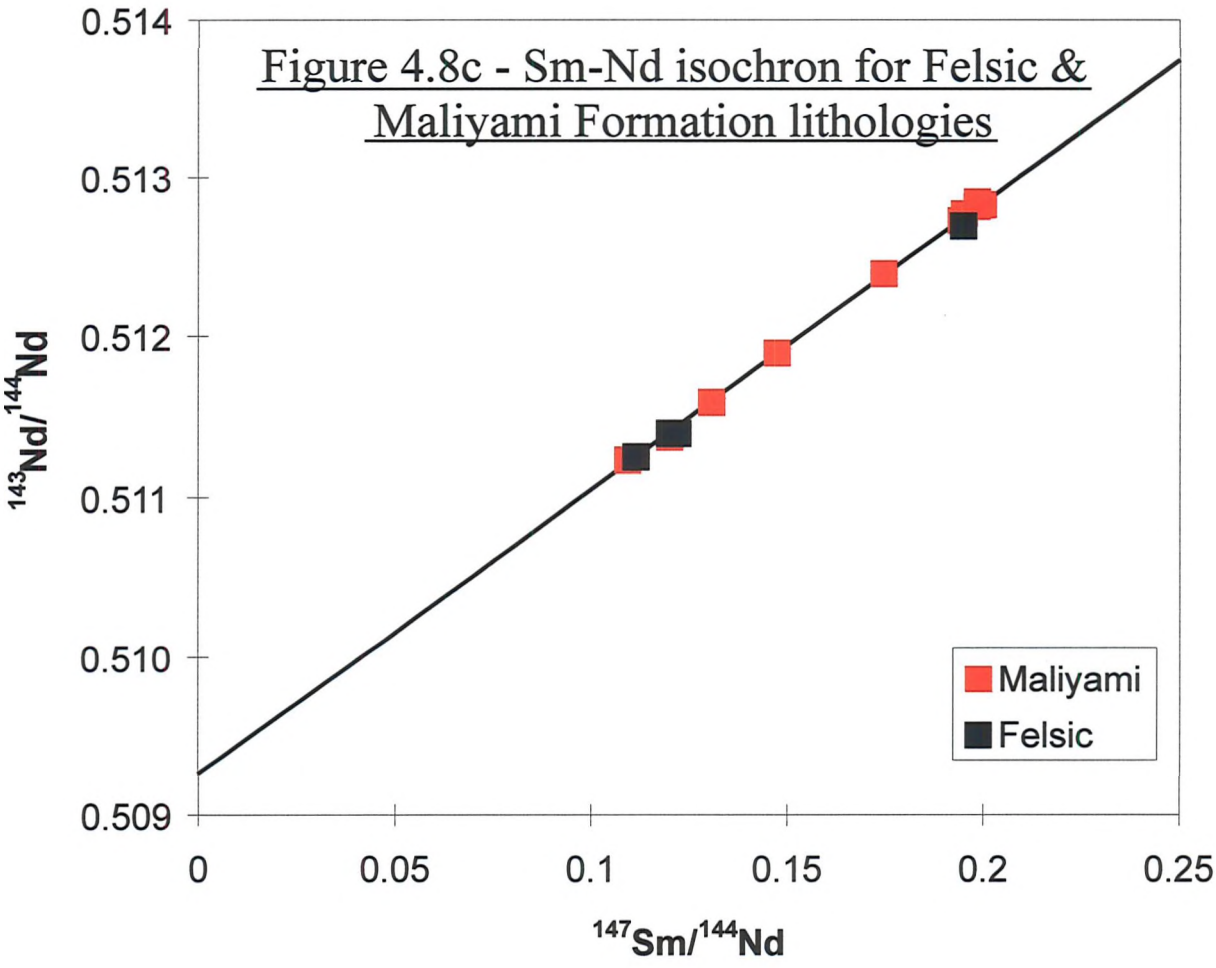

Data and calculations for isochron plot

sample	147Sm/144Nd	1 S.E.%	143Nd/144Nd	1 S.E.%	
Maliyami Formation					
zimb.066	0.109234	0.543329	0.511231	0.0004	
zimb.052	0.130626	1.019322	0.511587	0.0005	
zimb.214	0.147231	0.588531	0.511893	0.0005	
zimb.194	0.119994	0.453773	0.511374	0.0005	
zimb.173	0.174506	0.429498	0.512391	0.0004	
zimb.061	0.199747	0.051065	0.512828	0.0006	
zimb.072	0.194158	0.02704	0.512728	0.0005	
zimb.177	0.198325	0.462877	0.512845	0.0005	
zimb.184	0.199423	0.035853	0.512826	0.0004	
zimb.188	0.198192	0.414497	0.512816	0.0005	
zimb.185	0.194907	0.502034	0.512772	0.0005	
Felsic Formation					
zimb.161	0.120066	0.137841	0.511396	0.0005	
zimb.209	0.122127	0.033162	0.511398	0.0005	
zimb.170	0.111398	0.038151	0.511251	0.0005	
zimb.028	0.194767	0.055964	0.512694	0.0005	
$Nd_{(I)}$	$\varepsilon_{Nd(t)}$	T_{CHUR}	T_{DM}		
0.509226	1.80	2.15E+09	2.96E+09		

slope error =		2.72699E-05
intercept error =		3.15703E-17
Xbar=	0.16291312	
Ybar=	0.512158514	
lamda =	6.54E-12	
gradient =	0.018074306	
age (Ma) =	2739	
+/- 1 S.E. calc	4.169652368	
+/- 2 S.E.	33	(actual error)
MSWD =	15.3	
age error =	4.113691066	
Var x MSWD =	1.13693E-08	0.001738429
se x rootMSWD =	0.000106627	16.30295951

and determining the slope of the line and hence the age of the rocks. More data points are needed for this formation if an accurate Sm-Nd isochron is to be determined.

4.8) SEBAKWE RIVER GNEISS (SRG)

REE plots for the samples from the SRG are displayed in Figure 4.9. Each sample shows a Eu anomaly, slightly negative in Zimb.140 (Eu/Eu*= 0.74), distinctly negative in Zimb.141 (Eu/Eu*= 0.47) and positive in Zimb.142 (Eu/Eu*= 1.24). All exhibit LREE enriched, HREE depleted profiles with Zimb.142 also exhibiting a decrease in the total REE when compared to the other two samples. Zimb.140 (Phase 1) has REE concentrations 60x chondrite for the LREE decreasing to 20x chondrite in the HREE reflecting a La/Yb ratio of 3.44. Zimb.141 (Phase 2 - the main phase) shows slightly increased total REE with 85x chondrite for the LREE and 30x chondrite for the HREE, reflecting a decreased La/Yb ratio of 3.00. Zimb.142 (Phase 3) shows massive REE depletion when compared to the other samples and although reaching LREE concentrations of around 90x chondrite, HREE concentrations reach <2x chondrite giving a La/Yb ratio of 53.5.

A similar variation is displayed by the trace elements. Niobium, Ti and V all exhibit decreases in concentration from Zimb.140 to 142. Yttrium is more concentrated in Phase 2 than Phase 1 and Phase 3 shows very low Y concentrations of just 5.58ppm (ICP-MS). Zirconium shows the inverse of this. More Zr is present in Phase 3 than the other two and Phase 2 shows the least at 81.34ppm indicating decoupling of Zr from the REE. The reason for this is unknown. These Zr and Y variations on the pattern of decreasing Ti, V and Nb dictate the trace element ratios observed. Hence where Zr and Y might ordinarily be expected to increase with increasing silica, they do not and explanation of this difference is probably fundamental to deciphering the generation history of the rock.

Nd isotope determinations are shown in Table 4.2. Care must be taken when considering data from rocks of this age and/or any rocks which may have experienced more than one period of melting or high-grade metamorphism, since one of the fundamental premises on which Nd isotope determinations are interpreted is that the Sm/Nd ratio has not changed since formation of the rock. These rocks, clearly continental crustal rocks and melts there-of, may not satisfy this assumption and hence $\varepsilon_{Nd(t)}$ values of +1.5 to -0.6 may simply be an average after several melting events and incorporation of mixed continental and mantle components.

Figure 4.9 - REE patterns for the Sebakwe River Gneiss

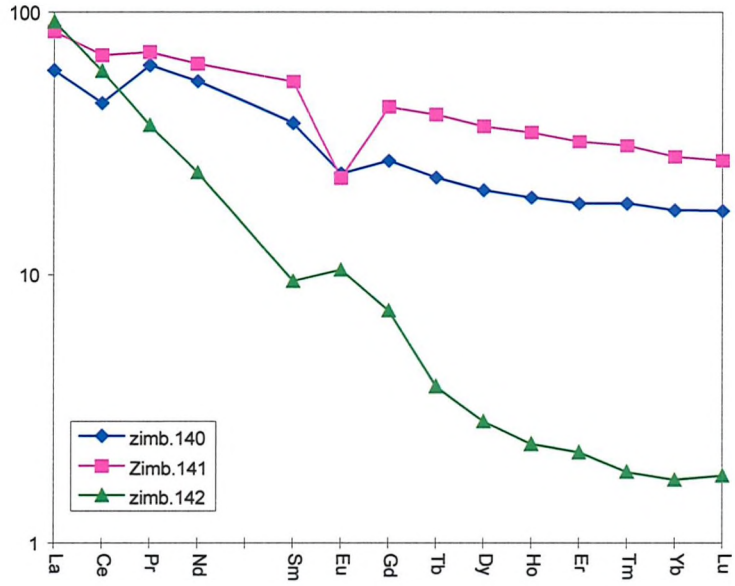

Figure 4.10 - REE patterns for the Regional Granitoids

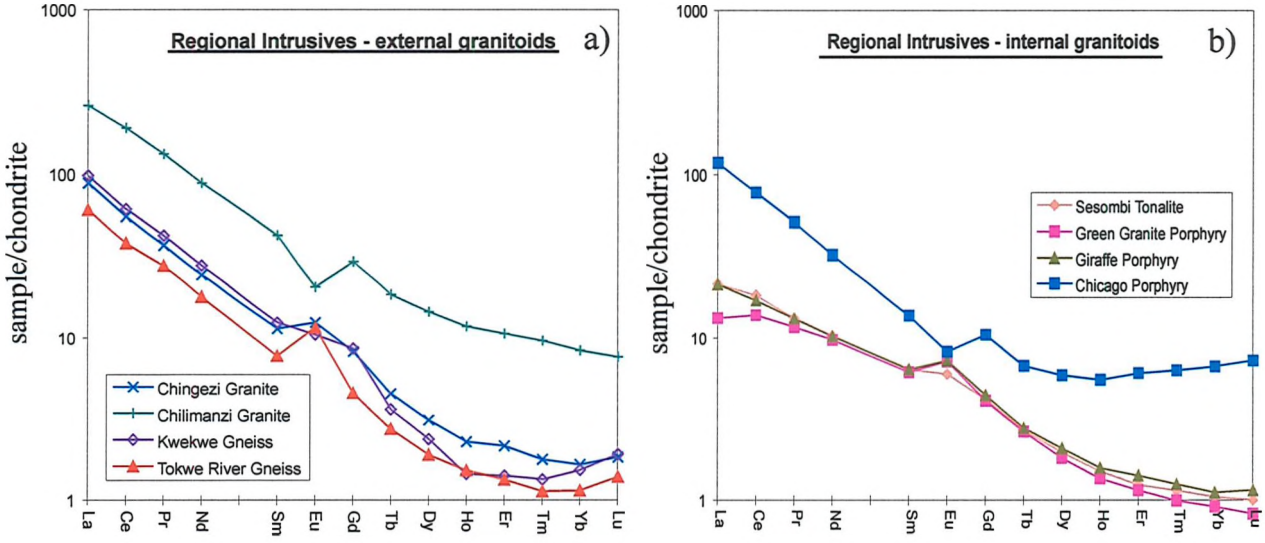

Zimb.141 has been dated by zircons (see Chapter 5) and provides the basis on which the relative ages for Zimb.140 and 142 were 'guestimated'. Errors due to age differences may therefore be present for these two samples but will have only a small effect on the $\varepsilon_{Nd(t)}$ and model age values. The T_{CHUR} model age for Zimb.141, the main phase of this gneissic unit, is slightly older than the zircon age at *c.*3.7Ga. Zimb.140 gives a younger T_{CHUR} model age of *c.*3.42Ga with a *c.*150Ma error. This is younger than that for Zimb.141 which is considered to be a partial melt from this amphibolite. The discrepancy in model ages between these two samples possibly reflects other partial melting episodes which may have disturbed the Sm-Nd isotope systematics. Zimb.142 has a T_{CHUR} model age of 3.5Ga ± 50Ma not too dissimilar to the approximated age (3.55Ga) used to calculate $\varepsilon_{Nd(t)}$ for this sample.

4.9) RELEVANT REGIONAL GRANITOIDS

Figure 4.10 displays the REE patterns for the regional granitoids analysed during this study. These include the Tokwe River Gneiss from the Tokwe Segment in the south of the craton, a member each of the Chingezi and Chilimanzi suites, the Kwekwe Gneiss - the marginal phase of the Rhodesdale Granitoid adjacent to the Midlands Greenstone Belt, the Sesombi Tonalite and three members of the Late Porphyries considered to be the intrusive equivalent to the felsic volcanics seen in the Felsic Formation (Harrison, 1970). These samples will be considered here in two groups; the granitoids from the rest of the craton including the Kwekwe Gneiss (Fig.4.10a), and those internal to the Midlands Greenstone Belt - the Sesombi Tonalite and Late Porphyries (Fig.4.10b). Most of these samples have been dated by the single zircon technique described in Chapter 5.

The Tokwe River Gneiss has a strongly LREE enriched, HREE depleted pattern (La/Sm = 7.83, Gd/Yb = 3.93, La content ~60x chondrite) with a positive Eu anomaly (Eu/Eu* = 1.9). The Chingezi Gneiss exhibits a similar pattern without the Eu anomaly (La/Sm = 7.87, Gd/Yb = 5.62) but with higher total REE contents (LREE up to 100x chondrite). The Kwekwe Gneiss also reflects a similar pattern to the Tokwe River and Chingezi gneisses (La/Sm = 7.64, Gd/Yb = 5.55) and also shows similar total REE content (La = 116x chondrite) with a small negative Eu anomaly (Eu/Eu* = 0.73). The Chilimanzi Granite sample has a similar LREE ratio to the other granitoids (La/Sm = 6.15) but has less depleted HREE (Gd/Yb = 3.56) and an enhanced negative Eu anomaly (Eu/Eu* = 0.57).

An interesting upturn in the HREE pattern of the HREE depleted external granitoids may be explained through a role for garnet either on the liquidus during crystallisation, or more likely in the source during melt generation. REE patterns for garnets commonly show less enrichment for Yb and Lu than for Ho, Er and Tm (Bea, 1996) reflecting the higher Kd`s of these latter elements in garnet.

As might be expected, the trace element characteristics of these rocks offer no clue as to their origin due their highly evolved and fractionated nature resulting in high Zr/Y and Zr/Nb and low Ti/Zr ratios. The Chilimanzi Granite however, has Zr/Nb ~19 indicating an origin as conventionally perceived (Wilson, 1979), through crustal anatexis.

The Sesombi Tonalite and Giraffe and Green Granite members of the Late Porphyries, have virtually identical REE concentrations and patterns. The Green Granite Porphyry (Zimb.246) shows slightly lower La concentrations and consequent La/Yb and La/Sm ratios but that apart, average ratios for these three granitoids are La/Yb ~20, Gd/Yb ~4.2 and La/Sm ~3.4. Total REE concentrations are 20x chondrite for La down to 1x chondrite for the HREE and the Eu anomaly is small but positive with Eu/Eu* ~1.3. The Chicago Porphyry is quite different. It shows stronger LREE enrichment (La/Sm = 8.47), less HREE depletion with a flatter HREE profile (Gd/Yb = 1.58), a negative Eu anomaly (Eu/Eu* = 0.67) and greater total REE contents (>100x chondrite for La).

Trace element ratios of the internal granitoids are similarly high in comparison with the external granitoids. The Chicago Porphyry is noticeable in having a low Zr/Nb ratio of 15.4 indicative of a crustal origin. This similarity with the Chilimanzi Granite is also reflected in its REE pattern (see description above and Fig.4.10). From these data a relationship between these two intrusions might be hypothesised but resorbed quartz phenocrysts in the Chicago Porphyry suggest a closer relationship with the other Late Porphyries. This intrusion is however heavily altered, precluding a definitive conclusion from petrographic study.

Nd isotope determinations are available for all the above samples except the Green Granite Porphyry. The values have been calculated using ages determined by zircon geochronology conducted during this study, or by relative dating. The results show that the more regional granitoids of the Tokwe River, Chingezi and Kwekwe gneisses and the Chilimanzi Granite, all possess $\varepsilon_{Nd(t)}$ values between -1.42 to +1.86. Antiquity of the Kwekwe Gneiss is indicated by the T_{CHUR} determination of 3.33Ga (or 3.51 T_{DM}) for this sample. The T_{CHUR} model age for the Tokwe River Gneiss appears young at 3.33 but a T_{DM}

model age of 3.49Ga comes closer to that determined by zircon geochronology. A T_{CHUR} result of 2.86Ga for the Chingezi Gneiss sample supports the perceived idea on the timing of this craton-wide event whilst a similarly derived result of 2.75Ga for the Chilimanzi Granite is somewhat older than expected according to convention.

The Nd isotope results for the Sesombi Tonalite and Giraffe Porphyry are within error of each other with $\varepsilon_{Nd(t)}$ of 3.69 ± 1.02 and 3.03 ± 1.03, and T_{DM} model ages of 2701 ± 70Ma and 2767 ± 70Ma respectively. The T_{CHUR} values for these samples are considered too young at *c.*2.3Ga to represent the age of Nd separation from its mantle parent. The Chicago Porphyry shows older T_{CHUR} and T_{DM} model ages at 2.86 and 3.08Ga respectively, and an $\varepsilon_{Nd(t)}$ value of -2.71 reflecting its crustal (low) Zr/Nb ratio.

4.10) ORIGIN AND EVOLUTION OF THE MIDLANDS GREENSTONE BELT LITHOLOGIES - INTERPRETATION AND DISCUSSION OF THE GEOCHEMISTRY

4.10.1) Trace Element Ratio Interpretation

Table 4.3 displays characteristic trace element ratios for various mantle and crustal components. This indicates that the basalts generally conform to chondritic trace element ratios with TiO_2/P_2O_5=10-13, Zr/Sm=25-30, Zr/Nb=20-24, Ti/Y=250-350, Ti/Zr=90-110 and Zr/Y=2.5-3.5. Zr/Nb is slightly high when compared to chondrite and may indicate the level of fractionation suffered by the basalts. The two high-Nb basalts from the Felsic Formation (Zimb.034 & 208) have Zr/Sm=23-25 strongly indicating a chondritic mantle origin although most of the other ratios for these samples indicate an influence from continental crust, including Zr/Nb of 8 to 10. Smaller percentage melting of a deeper mantle source would produce the high-Nb concentrations and Ti/Y ratios present.

The andesites show distinctly different trace element ratios to the basalts justifying separation of the lithologies into a basalt and andesite-dacite suite. TiO_2/P_2O_5 and Ti/Zr are substantially lower (*c.*5 & 35-50 respectively) which along with their high Zr/Sm (35-45) and Zr/Y (~6) indicates their evolved nature. Zr/Nb ratios however, are identical to the basalts suggesting no influence from continental crust in their generation which would lower this ratio. Since Ti/Y ratios remain approximately chondritic (300-370) garnet in the source may

Table 4.3 Trace element ratios for Midlands Greenstone Belt Volcanic Lithologies and various crustal and mantle components

Component	TiO2/P2O5	Zr/Sm	Zr/Nb	Ti/Y	Ti/Zr	Zr/Y
Chondrite	10.6-11.8	25-29	16-20	280-310	95-115	2.5-4.5
Primitive Mantle	11.6-12.3	23.9-28.9	12-17.8	246-283	109-118	2.3-2.5
MORB	12.5	c.27	25.7-35.2	250-300	100-102	2.5-3
Upper Cont. Crust	.....	42.2	7.6	81.8	9.5	8.6
Lower Cont. Crust	.....	22.1	11.7	189.3	51.4	3.7
Bulk Cont. Crust	.....	28.6	9.1	161.9	32.4	5
Archaean Cont. Crust	.....	31.3	.....	166.5	24	6.9
Archaean Bulk Crust	.....	29.4	.....	189.3	36	5.3
Mafic Form. Basalts	11.5-13	25.1-29.5	19.2-22.9	266-312	91.6-111.9	2.8-3.4
(Zimb.151)	*13.8*	*19.7*	*14.6*	*280*	*121*	*2.3*
Maliyami Form. Basalts	9.7-12.7	28.3-31.3	20.9-22.8	253-368	93-110	2.6-3.1
(Zimb.186)	*10.25*	*28.4*	*21.7*	*277*	*106*	*2.6*
Felsic Form. Basalts	12.6-13.5	29.1-29.3	19.9-23.3	282-305	100-106	2.8-2.9
(Zimb.034 & 208)	*7.7-8.1*	*23.4 & 25.1*	*7.9 & 9.6*	*431 & 426*	*79 & 79.1*	*5.5 & 5.4*
Maliyami Form Andesites	3.8-5.5	33.6-46.1	20.2-24.7	301-378	33.1-47.2	6.8-11.2
Felsic Form. Andesites	5.2-5.4	.....	.....	307-363	52.7-57.8	5.8-6.3
Mafic Form. Dacites	2.7	65.6	27.6	190	14.1	13.5
(Zimb.150)	*4.4*	*38.9*	*24.3*	*321*	*32.8*	*9.8*
Maliyami Form. Rhyodacites	2.7-3.1	107.9	36.3	322-436	9.5-13.5	33.8-39.3
(Zimb.189)	*2.6*	*117.3*	*33.9*	*278*	*10.1*	*21.6*
Felsic Form. Rhyodacites	2.9-4	68.6	26.3-45.2	267-577	12.3-21.2	12.6-39.7

Chondrite, Primitive Mantle & MORB from Rollinson (1993)
Continental crustal values from Taylor & McLennan (1995)

Table 4.4 Distribution coefficients used in modelling

	Olivine	Plag.	Garnet	Clinopyx.	Amph.
Y	0.01	0.03	9	0.9	1
Ti	0.02	0.04	0.3	0.4	1.5
Zr	0.012	0.048	0.65	0.1	0.5
Nb	0.01	0.01	0.02	0.005	0.8
V	0.06	(no value)	(no value)	1.35	3.4
La	0.0067	0.19	#N/A	0.57	0.5442
Ce	0.006	0.111	0.03	0.092	0.843
Pr	#N/A	#N/A	#N/A	#N/A	#N/A
Nd	0.0059	0.09	0.07	0.23	1.3395
	#N/A	#N/A	#N/A	#N/A	#N/A
Sm	0.007	0.072	0.29	0.445	1.8035
Eu	0.0074	0.443	0.49	0.474	1.5565
Gd	0.01	0.071	0.97	0.556	2.0165
Tb	#N/A	#N/A	#N/A	0.57	#N/A
Dy	0.013	0.063	3.17	0.582	2.0235
Ho	#N/A	#N/A	#N/A	#N/A	#N/A
Er	0.0256	0.057	6.56	0.583	1.74
Tm	#N/A	#N/A	#N/A	#N/A	#N/A
Yb	0.0491	0.056	11.5	0.542	1.642
Lu	0.0454	0.053	11.9	0.506	1.5625

Kd's from Rollinson (1993)

not be a factor since much higher Ti/Y would be expected. This would appear to suggest the influence of a mineral with almost identical distribution coefficients for Ti & Y.

The dacites and rhyodacites show fractionated trace element ratios for all the pairings considered.

4.10.2) Evolution of the Basalts

Before consideration of initial generation, the fractionation of each lithological suite will first be examined since each suite has been shown to have a coherent history.

The geochemistry of the basalts of the Midlands Greenstone Belt strongly indicates a role for augitic clinopyroxene in their evolution. Mineral vectors on trace element diagrams in Figure 4.4b show that augite alone cannot be responsible for the fractionation trends seen and that plagioclase and/or olivine must also have played a significant role. Modelling of this trend using Rayleigh fractionation has been conducted using sample Zimb.186 (Maliyami Formation) as a starting composition since it has the highest MgO content of the basalts. Distribution coefficient (Kd) values compiled in Rollinson (1993) are reproduced in Table 4.4 and are used to model the end-member composition of Zimb.137 (Mafic Formation), a basalt with some of the highest trace element contents. A result of 65% fractionation of a 30% clinopyroxene : 70% plagioclase assemblage fits the observed trend very well (see Fig.4.4b).

Fractionation of 70% plagioclase might be expected to produce significant negative Eu anomalies in the resulting liquid but this is offset to a certain extent by the low Kd for Eu in clinopyroxene (0.474) thereby delaying the development of a significant Eu anomaly until *c.*70% fractionation (see Fig.4.11a) of this assemblage. Slightly oxidising conditions might also be postulated to allow plagioclase fractionation without producing a significant Eu anomaly. The increases in TiO_2, Fe_2O_3*, P, Zr, Y, V, and Nb, and decreases in MgO, CaO, Ni and Cr support the possibility for the modelled assemblage. Olivine is not seen in any of the thin sections which argues against it being on the liquidus at the time of crystallisation of the basalt, especially since some of the samples clearly show a quench texture (e.g. Zimb.006, 062 & 151) and would therefore be expected to show the fractionating assemblage. This lack of olivine is in itself evidence that the basalts have undergone a substantial amount of fractionation, to the extent that the olivine-clinopyroxene cotectic has been left in favour of the clinopyroxene-plagioclase cotectic.

Examination of the REE allows refinement of the model. However, it must be remembered that there is an age difference between these samples and that the chemistry of the samples may therefore reflect one of three models: fractionation of a single magma pulse for each formation; 'snapshots' of the fractionation process for more than one magma pulse; or different degrees of partial melting to generate each sample. It is considered more likely that the samples from each formation represent 'snapshots' from the fractionation of a number of magma pulses. The occurrence of a single process between each injection is not therefore a foregone conclusion and must be considered when modelling the data.

The Maliyami Formation basalts prove the easiest to model by the assemblage determined thus far. Using a starting composition of Zimb.186 the pattern and concentration of REE can be modelled for Zimb.177 after 40% fractionation of the clinopyroxene-plagioclase assemblage (see Figure 4.11a). Zimb.072 & 064 would require 70 to 75% fractionation respectively to achieve the levels of REE concentrations seen but lack the negative Eu anomaly expected after this degree of fractionation. Both samples are considerably altered and REE enrichment as a result of hydrating fluids may be a factor. The similar REE geochemistry and tightly constrained Zr/Nb, Zr/Y and Zr/Sm ratios (see Figure 4.7c) for all the basalts of the Maliyami Formation, indicate that these samples were possibly derived from a single melting episode rather than from a series of melts or separate partial melting events.

The Mafic Formation basalts can also be modelled by 40% fractionation of clinopyroxene & plagioclase starting with Zimb.135 and fractionating through to Zimb.137 (see Figure 4.11b). Zimb.151 is clearly more 'primitive' than Zimb.135 but was not used as a starting composition for fractional crystallisation since to do so would not derive the LREE enriched patterns exhibited by the other samples. Zimb.151 is considered to be more reflective of the source composition after melting has derived Zimb.135 since it also comes later in the succession. The origin of both of these samples will be considered shortly.

Understanding the fractionation of the basalts from the Felsic Formation is more problematic. Only 4 samples are available for this and they form two pairs, one (Zimb.028 & 029) showing flat REE patterns and the other being LREE and Nb enriched (La/Sm = 2.3, Zimb.034 & 208, see Fig.4.5c). It is not possible to relate the pairs by 40% fractionation of a clinopyroxene-plagioclase assemblage as is the case for the other two formations. Modelling of the enrichment in Y, Zr, Ti and Nb is possible by 60-65% fractionation of this assemblage

Figure 4.11 - Fractional crystallisation models

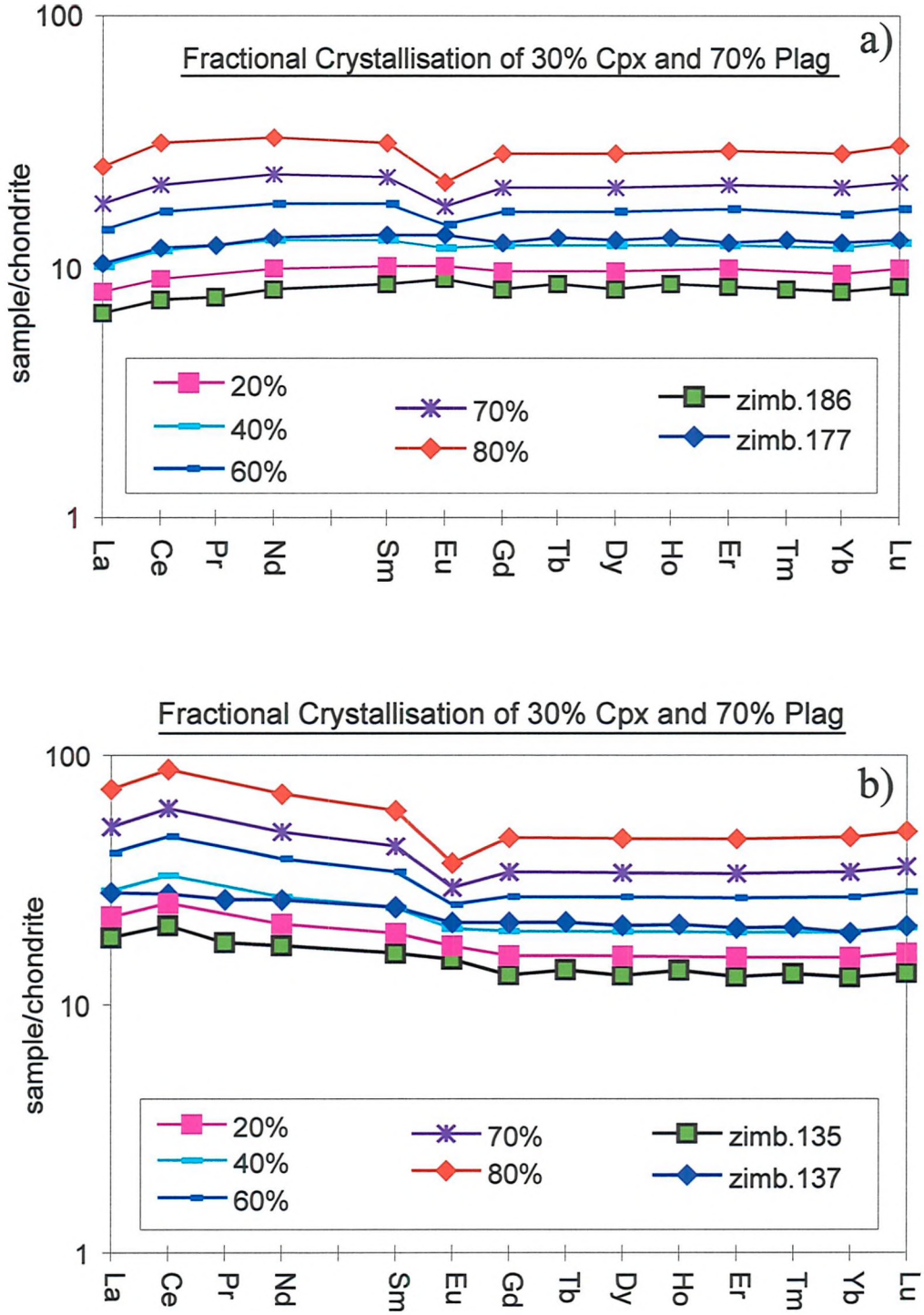

but this does not produce anything like the REE patterns seen. Inclusion of small amounts of garnet in the fractionating assemblage in place of plagioclase does produce the REE patterns seen but requires extraordinary levels of crystallisation (*c.*90%) that could clearly not occur and result in a rock of basaltic-andesite composition. Also, Y levels do not decrease as would be expected. The origin of these samples is therefore not considered to be in fractionation from Zimb.028.

The REE patterns Zimb.173 & 206 are shown in Figure 4.5c. These are heavily altered samples and may reflect fluid alteration mobilising the LREE since both these samples have high volatile contents (~15%) and are substantially altered (see Table 4.1a 'Too altered to use' for major element data). However, despite this they have coherent trace element and REE characteristics and are considered to represent fractionation or other primary petrogenetic phenomena.

At this point therefore, it is not possible to resolve the evolution of the Felsic Formation basalts since enough examples are not available. Their close relationship with the geochemistry of the basalts from both the Maliyami and Mafic Formations however, strongly favours the same fractionation process. The high Nb, LREE enriched samples clearly have a different origin to the rest of the Felsic Formation basalts and this will be discussed later.

4.10.3) Evolution of the Andesites and Rhyodacites

The lack of suitably accurate and numerous Kd values for the REE between minerals and andesitic melts, precludes modelling of the REE patterns directly. However, from the major and trace element chemistry, fractionation of ilmenite may be suspected to have a significant influence on the evolution of the andesites. Decreasing TiO_2, Fe_2O_3, Y and V support this and decreasing CaO, MgO, P_2O_5 and Ni suggest involvement of another phase, possibly clinopyroxene or amphibole although static Nb concentrations throughout the range of compositions, argue against the latter since distribution coefficients for Nb in amphibole are 1.3 and 4 for andesitic and rhyodacitic liquids respectively (Rollinson, 1993). To evolve the rhyodacites from the andesites, HREE depletion and LREE enrichment are required, a role which only garnet could really fulfil in andesitic magmas. The level of garnet fractionation would be crucial to the REE profile generated due to its very high Kd values for the HREE (see Table 4.4) and would require some kind of 'buffer' mineral to prevent rapid excess HREE depletion. Such a mineral would normally be plagioclase, with low Kd values

for all the REE. However, crystallisation of both plagioclase and garnet would be highly unusual. It would appear therefore that it is very difficult to evolve the rhyodacites by fractional crystallisation from the andesites despite the geochemical coherence these lithogroups display. Involvement of continental crust could be a factor and high Zr, low Ti/Zr and negative $\varepsilon_{Nd(t)}$ values indicating assimilation of a continental crustal component provide support for this view. However, Zr/Nb ratios should be sensitive to assimilation processes since continental crust has a low Zr/Nb ratio around 10, yet the ratios for all the rhyodacitic volcanics increase to between 26 and 45.

4.10.4) Origin of the Midlands Greenstone Belt Volcanics

The source and mechanism by which the basalts, andesites, dacites and rhyodacites of the Midlands Greenstone Belt were derived is a central question to looking at not only the origin and evolution of the greenstone belt, but also to determining possible palaeotectonic models for its generation. A number of possibilities exist for the origin of these rocks. The basalts could have been derived from direct partial melting of a mantle source or fractionation of ultrabasic and high-Mg magmas similar to those seen in the Mberengwa (Belingwe) Greenstone Belt. The andesites may have an origin in fractionation of the basalts, mixing of basalts and rhyodacite magmas or direct partial melting of a basaltic source transformed to amphibolite. The rhyodacites may have resulted from fractionation of the andesites, direct melting of continental crust or small scale partial melting of an originally igneous, amphibolite source.

These questions will be addressed in the following sections and possible models for the palaeotectonics suggested at the end and in more detail in Chapter 6.

4.10.4.1 Mberengwa (Belingwe)-Midlands comparison

In the regional scheme of greenstone belt lithostratigraphic correlation in Zimbabwe, the Mafic Formation is correlated with the Zeederbergs Formation of the Mberengwa (Belingwe) Greenstone Belt (Wilson *et al.*, 1995). The komatiites of the underlying Reliance Formation are not present in the Midlands (see Fig. 2.2). An origin for the basalts of the Midlands Greenstone Belt through fractionation of a komatiite or komatiitic basalt is therefore a possibility. The source and generation of komatiites is discussed in Scholey (1992) and Brake (1996) and will not be discussed here. Figure 4.12 displays various major

Figure 4.12 - Midlands/Mberengwa (Belingwe) comparison

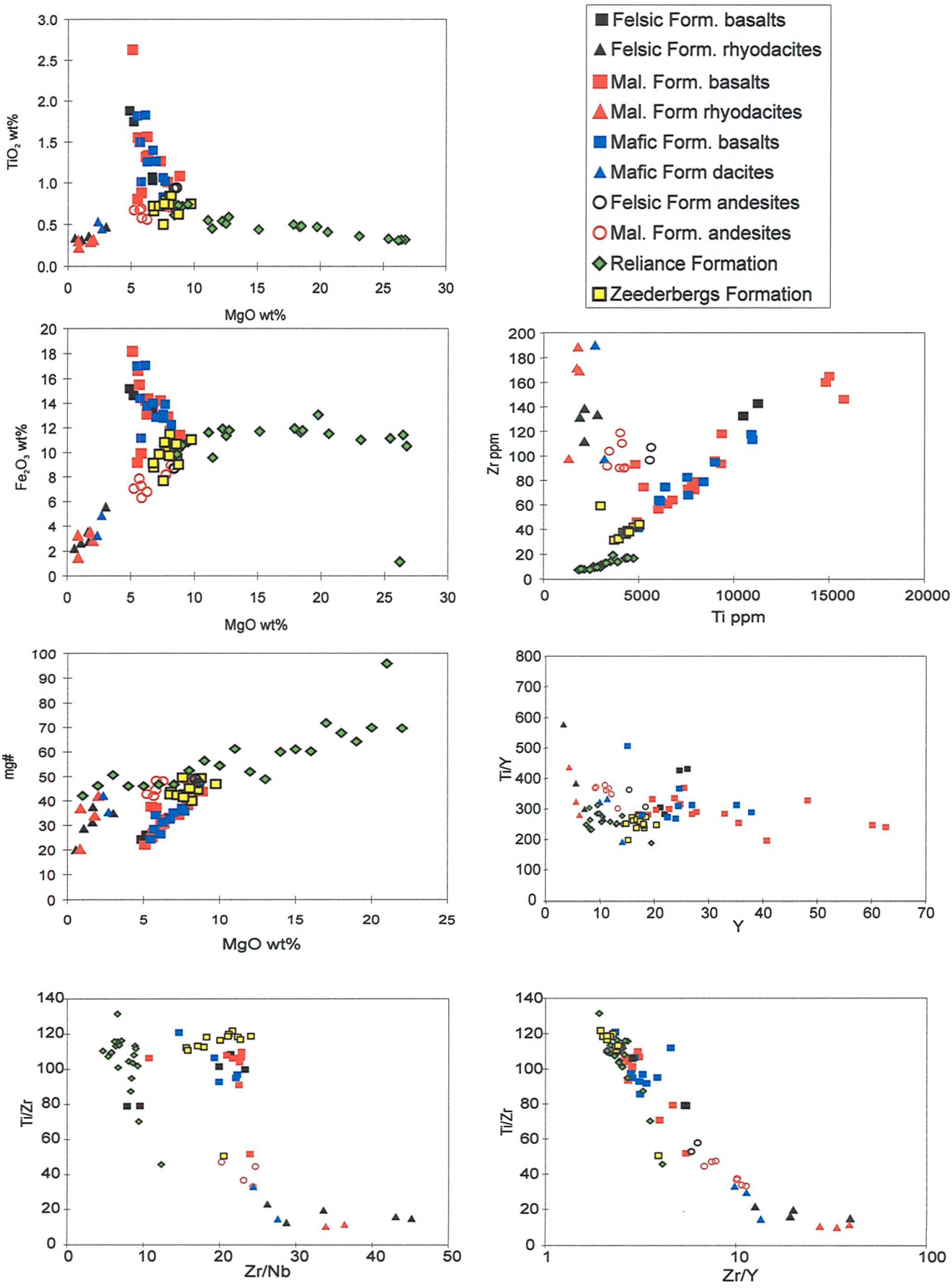

and trace element diagrams showing Reliance and Zeederbergs ultramafic and mafic lithologies compared with lithologies analysed during this study. Brake (1996) divided the basalts of the Zeederbergs Formation into two types based on their Al_2O_3 content; Type II basalts have distinctively low Al_2O_3 contents. None of these samples were plotted in Figure 4.12 since no samples from this study reflect their low Al_2O_3 nature. The Reliance Formation samples cover komatiitic, siliceous high-Mg basalt and tholeiitic basalt compositions and were compiled from Scholey (1992).

Numerous studies have been conducted on the petrochemistry of the Mberengwa (Belingwe) lithostratigraphy including Nisbet *et al.* (1977); Nisbet *et al.* (1982); Scholey (1992), numerous contributions in Bickle & Nisbet (1993); Brake (1996) and Silva (1998). All of these studies have concluded that the Reliance Formation komatiites are derived from melting within a mantle plume with the related basaltic lithologies derived by either low pressure fractionation of olivine, clinopyroxene, plagioclase ± Fe-Ti oxides, or smaller scale partial melts of a source with a composition similar to that which formed the komatiites but at lower pressure. The Type I and Type II Zeederbergs basalts of Brake (1996), are distinguished on the basis of their Al_2O_3, FeO*, TiO_2 and P_2O_5 contents and CaO/Al_2O_3 and Al_2O_3/TiO_2 ratios. He considered that Type II were not related to the Type I basalts or komatiites of the Reliance Formation, but were derived from Al-depleted komatiites. Type I basalts are considered by Scholey (1992), Bickle *et al.* (1993) and Brake (1996) to be descended from primary magmas similar to the Reliance Formation komatiites, by fractional crystallisation of olivine and minor Cr-spinel (and later clinopyroxene) with assimilation of 1-2% continental crustal material. This signature of *c.*1% crustal contamination in the Reliance/Zeederbergs succession was noted by Chauvel *et al.* (1993). Most recently, Silva (1998) has related the two types of Zeederbergs basalts as defined by Brake (1996) to different pressures of fractionation; Type II forming at higher pressures than Type I. She also confirmed the primary control of olivine fractionation on the high-Mg magmas and divided the Type I Zeederbergs into Series A & B basalts. Series A was derived directly from the Reliance Formation and Series B, forming the majority of the Zeederbergs Formation, was derived from a primitive or depleted mantle source similar to that from which the Reliance Formation was derived, with garnet and/or clinopyroxene in the residue. The geochemistry of the Reliance and Zeederbergs lithologies are therefore obviously intimately related.

Figure 4.12 suggests that the Zeederbergs and Reliance Formation lithologies share a close compositional relationship with the Midlands lithologies. TiO_2 and Fe_2O_3* vs MgO major element plots show that the Reliance Formation lithologies trend to the point of intersection of the basalt and andesite-dacite suites of the Midlands Greenstone Belt. The Zeederbergs samples scatter around this 'triple-junction'. A plot of mg# vs MgO also shows this strong coherence with the andesite-dacite suite matching the trend of the Reliance Formation to mg# of *c.*35 at 2wt% MgO whilst the Midlands basalts form a separate trend splaying off to mg# of *c.*20 at 5wt% MgO. The point at which these trends separate is approximately mg# 50 and 10wt% MgO. The Zeederbergs basalts scatter at values just below these. Plots involving Nb show the Zeederbergs and Midlands basalts have significantly lower Nb concentrations than the Reliance lithologies but this may reflect differences in analytical accuracy and precision for Nb between the three studies. The data in the Ti/Zr vs Zr/Nb plot in Figure 4.12 contains XRF data for Nb for both the Zeederbergs and Reliance lithologies and ICP-MS data for those samples from the Midlands Greenstone Belt. This would suggest questions regarding the accuracy of the Reliance Formation Nb XRF data of Scholey (1992). As such, it is difficult to assign any significance to the differences in Zr/Nb ratios shown.

Ti/Zr ratios for all three lithostratigraphies are roughly the same, approximately 70 to 120 for Reliance and Midlands samples with the Zeederbergs being consistently around 110 to 120. This coherent nature is also displayed in the Zr vs Ti plot although the Reliance Formation shows slightly different fractionation, trending to lower Zr levels at similar Ti concentrations to Zeederbergs basalts. A strong inter-relationship between the Reliance, Zeederbergs and Midlands lithologies is also shown by Ti/Zr and Zr/Y ratios. The plot has a logarithmic x-axis to maximise the visible spread in the Zr/Y data since high Zr/Y ratios (up to 40) for the andesite-dacite-rhyodacite suite causes compression of the basalt data using a linear scale. Ti/Y ratios for all lithologies are chondritic until extremes of fractionation in the Midlands rhyodacites break the strong Ti-Y correlation seen throughout the fractionation sequence, resulting in high Ti/Y ratios (400 to 600).

The basalts of the Midlands Greenstone Belt would therefore appear to show strong similarities to the geochemistry of the Zeederbergs Formation Type I basalts and evolved Reliance Formation lithologies. They have however, evolved differently whilst still maintaining the trace element ratios shown by all three lithotypes. The andesite-dacite suite

may be derived initially from this suite of mafic lithologies but has certainly evolved in a very different way. The critical composition at which these evolutionary pathways may have diverged is approximately 8wt% MgO, 10wt% Fe_2O_3*, mg# 50, 6000ppm Ti, 60ppm Zr and 20ppm Y.

4.10.4.2 Primary generation

Another option is that the basalts from the Midlands Greenstone Belt are of totally separate origin to those from Mberengwa (Belingwe). In light of recent palaeotectonic interpretations this may be feasible. Kusky (1998) forwarded the hypothesis that the Tokwe Segment as defined by Wilson (1990) is significantly larger than recognised and infact forms a large stable continental block at the heart of the craton approximately 3.2Ga in age. He considered that this 'Tokwe Terrane' rifted in a NE-SW direction forming the Sea of Umtali with consequent formation of oceanic basalt and plateau sequences. During subsequent closure, these oceanic sequences were obducted onto the margin of the Tokwe Terrane to form allochthonous greenstone belts typified by the Mberengwa (Belingwe) Greenstone Belt. To the NW of the Tokwe Terrane, subduction below the terrane margin resulted in arc volcanism seen as the dacitic and rhyodacitic volcanics of the Midlands Greenstone Belt. This scenario, if proved correct, precludes a relationship between the basalts of the Midlands Greenstone Belt and those in the Mberengwa (Belingwe) Greenstone Belt in the south of the craton.

Basalts

Condie & Harrison (1976) suggested that the Mafic Formation tholeiites could be generated by 20% equilibrium partial melting of a lherzolite source with 15% clinopyroxene, 50% olivine and 35% orthopyroxene. Figure 4.13a and Table 4.5 show the results from modelling of this scenario using Zimb.135 as the melt composition generated and the lherzolite composition and Kd values quoted in Condie & Harrison (1976). The model fits the data very well, strongly supporting this as a mechanism of generation. Zimb.151 collected from higher in the succession, is probably a result of continued melting of this now depleted lherzolite source. The Maliyami formation basalts, also displaying LREE depleted profiles, are considered to result from the continuation of this process.

Figure 4.13a - Modal batch melting of lherzolite using composition and Kd's from Condie & Harrison (1976)

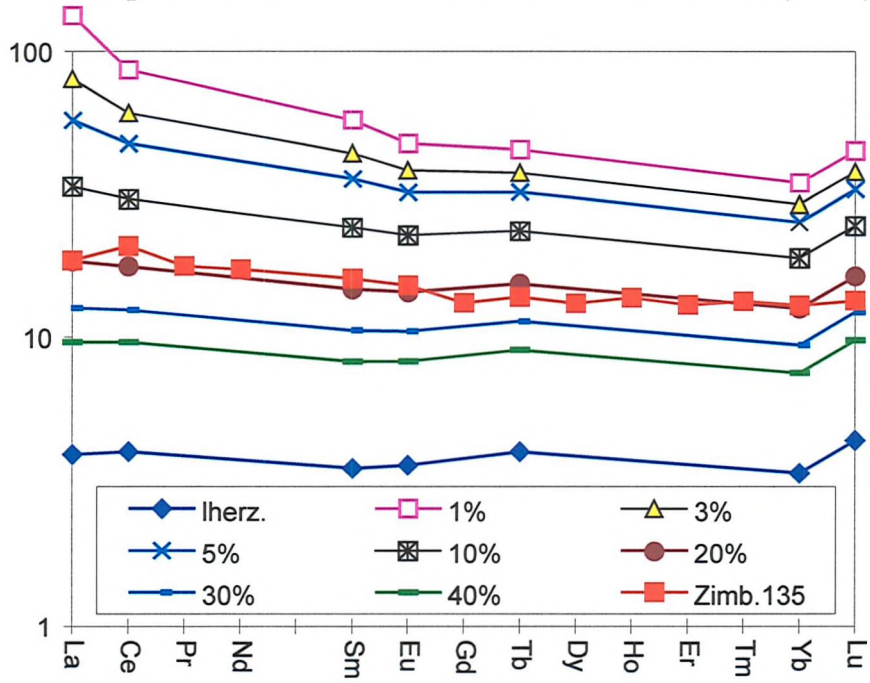

Table 4.5

D Calculations

	% Olivine	% Cpx	% Plag	% Opx
Mode	50%	15%	0%	35%

Basaltic Kd values after Condie & Harrison (1976)

	Olivine	Clinopx	Plag	Orthopx	D
La	0.01	0.05	0.1	0.03	0.02
Ce	0.01	0.1	0.1	0.05	0.04
Pr	#N/A	#N/A	#N/A	#N/A	#N/A
Nd	#N/A	#N/A	#N/A	#N/A	#N/A
	#N/A	#N/A	#N/A	#N/A	#N/A
Sm	0.01	0.2	0.1	0.05	0.05
Eu	0.01	0.3	0.6	0.05	0.07
Gd	#N/A	#N/A	#N/A	#N/A	#N/A
Tb	0.015	0.3	0.1	0.08	0.08
Dy	#N/A	#N/A	#N/A	#N/A	#N/A
Ho	#N/A	#N/A	#N/A	#N/A	#N/A
Er	#N/A	#N/A	#N/A	#N/A	#N/A
Tm	#N/A	#N/A	#N/A	#N/A	#N/A
Yb	0.02	0.3	0.1	0.1	0.09
Lu	0.02	0.3	0.1	0.1	0.09

(#N/A = not available)

Batch melting of Lherzolite

				Percentage melt						
	lherz.	D	Zimb.135	1%	3%	5%	10%	20%	30%	40%
La	3.95	0.02	18.43	132.60	79.99	57.27	33.49	18.29	12.58	9.59
Ce	4.05	0.04	20.66	85.86	60.96	47.26	30.25	17.59	12.40	9.58
Pr	#N/A	#N/A	17.60	#N/A	#N/A	#N/A	#N/A	#N/A	#N/A	#N/A
Nd	#N/A	#N/A	17.18	#N/A	#N/A	#N/A	#N/A	#N/A	#N/A	#N/A
	#N/A	#N/A	#N/A	#N/A	#N/A	#N/A	#N/A	#N/A	#N/A	#N/A
Sm	3.55	0.05	15.99	57.23	43.83	35.51	24.09	14.66	10.53	8.22
Eu	3.64	0.07	15.13	47.33	38.09	31.86	22.62	14.32	10.47	8.26
Gd	#N/A	#N/A	13.11	#N/A	#N/A	#N/A	#N/A	#N/A	#N/A	#N/A
Tb	4.04	0.08	13.75	45.07	37.40	31.96	23.44	15.29	11.34	9.02
Dy	#N/A	#N/A	13.08	#N/A	#N/A	#N/A	#N/A	#N/A	#N/A	#N/A
Ho	#N/A	#N/A	13.69	#N/A	#N/A	#N/A	#N/A	#N/A	#N/A	#N/A
Er	#N/A	#N/A	12.93	#N/A	#N/A	#N/A	#N/A	#N/A	#N/A	#N/A
Tm	#N/A	#N/A	13.28	#N/A	#N/A	#N/A	#N/A	#N/A	#N/A	#N/A
Yb	3.41	0.09	12.90	34.40	29.06	25.16	18.83	12.53	9.39	7.51
Lu	4.42	0.09	13.37	44.65	37.72	32.66	24.45	16.27	12.19	9.75

The Felsic Formation basalts display essentially flat REE patterns (see Fig.4.5c). Melting of a new, undepleted lherzolite or chondritic source in the same way as that which produced the Mafic and Maliyami basalts is considered a possibility. Generation of the high-Nb, LREE enriched basalts Zimb.034 & 208 by smaller percentage and/or deeper partial melting is considered a strong possibility for their origin.

Andesites

Equilibrium partial melting of an eclogite source thought to be from the Mafic Formation, was also suggested by Condie & Harrison (1976) for generation of the Maliyami Formation andesites. Figure 4.13b and Table 4.6 show the results for just such a model, indicating that a 20% partial melt of Zimb.151 with 50% clinopyroxene, 20% garnet and 30% amphibole in the mode produces roughly the REE pattern seen in sample Zimb.194. The fit for La is not as good as for some of the other elements but this is due to the fact that the chosen starting material has a LREE depleted pattern. The difference in fit for the modelled Sm and Eu concentrations is probably due more to the exact Kd values than the model itself. Zimb.198 can be produced in a similar way after 25% partial melting of eclogite with 70% clinopyroxene and 30% garnet in the mode.

Dacites and Rhyodacites

Two origins are possible for the dacites and rhyodacites. Firstly, they could be generated simply through fractionation of the andesites. This would have to involve amphibole and/or garnet to allow depletion of total REE and increase of the La/Yb ratio. Garnet on the liquidus is evidenced by garnet in Zimb.052 (see Plate 3.4), a tuff from the Maliyami Formation. However, whether this has significant relevance to the petrogenetic mechanism is subject to some debate (see discussion in section 4.11).

Secondly, they could be generated by direct partial melting of a similar source to that which produced the andesites. Figure 4.13c and Table 4.7 show the results for modelling of equilibrium modal melting of an eclogite with 70% clinopyroxene and 30% garnet in the mode. Using Zimb.170 as an example end-member it can be seen that the fit is quite good at low percentages (1-10%) of melting, indicating that this is a very viable way of generating these high-silica melts. This will be discussed further in section 4.11.

Figure 4.13b - Modal batch melting of Zimb.151 using composition and Kd's from Condie & Harrison(1976)

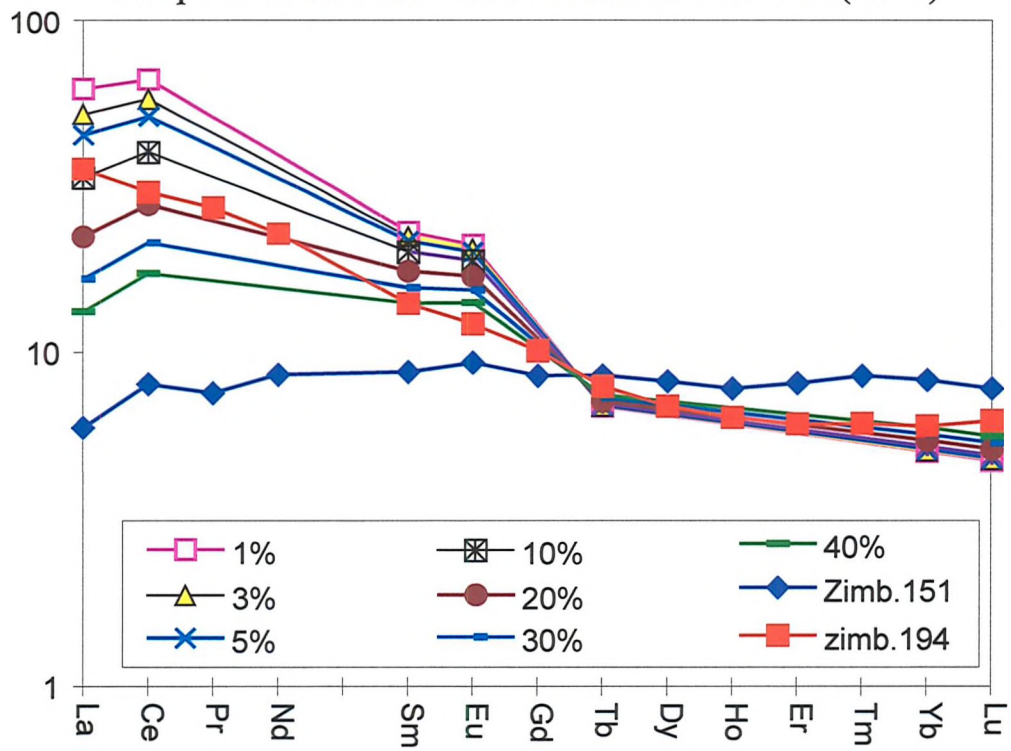

Table 4.6

D Calculations

	% Garnet	% Cpx	% Plag	% Amph.
Mode	20%	50%	0%	30%

Basaltic Kd values after Condie & Harrison (1976)

	Garnet	Clinopx	Plag	Amph.	D
La	0.01	0.05	0.1	0.2	0.09
Ce	0.01	0.1	0.1	0.2	0.11
Pr	#N/A	#N/A	#N/A	#N/A	#N/A
Nd	#N/A	#N/A	#N/A	#N/A	#N/A
	#N/A	#N/A	#N/A	#N/A	#N/A
Sm	1	0.2	0.1	0.25	0.38
Eu	1	0.3	0.6	0.3	0.44
Gd	#N/A	#N/A	#N/A	#N/A	#N/A
Tb	5	0.3	0.1	0.3	1.24
Dy	#N/A	#N/A	#N/A	#N/A	#N/A
Ho	#N/A	#N/A	#N/A	#N/A	#N/A
Er	#N/A	#N/A	#N/A	#N/A	#N/A
Tm	#N/A	#N/A	#N/A	#N/A	#N/A
Yb	7	0.3	0.1	0.3	1.64
Lu	7	0.3	0.1	0.3	1.64

(#N/A = not available)

Batch melting of Zimb.151

				Percentage melt						
	zimb.151	D	zimb.194	1%	3%	5%	10%	20%	30%	40%
La	5.945	0.09	35.359	61.85	51.97	44.82	33.34	22.05	16.47	13.15
Ce	8.010	0.11	30.116	66.26	57.77	51.21	39.89	27.66	21.17	17.14
Pr	7.546	#N/A	27.074	#N/A	#N/A	#N/A	#N/A	#N/A	#N/A	#N/A
Nd	8.548	#N/A	22.553	#N/A	#N/A	#N/A	#N/A	#N/A	#N/A	#N/A
	#N/A	#N/A	#N/A	#N/A	#N/A	#N/A	#N/A	#N/A	#N/A	#N/A
Sm	8.709	0.38	13.917	22.84	22.12	21.44	19.91	17.42	15.48	13.94
Eu	9.281	0.44	12.065	20.83	20.32	19.83	18.71	16.81	15.26	13.98
Gd	8.486	#N/A	10.051	#N/A	#N/A	#N/A	#N/A	#N/A	#N/A	#N/A
Tb	8.527	1.24	7.906	6.89	6.92	6.94	7.01	7.15	7.30	7.45
Dy	8.167	#N/A	6.907	#N/A	#N/A	#N/A	#N/A	#N/A	#N/A	#N/A
Ho	7.802	#N/A	6.390	#N/A	#N/A	#N/A	#N/A	#N/A	#N/A	#N/A
Er	8.060	#N/A	6.098	#N/A	#N/A	#N/A	#N/A	#N/A	#N/A	#N/A
Tm	8.497	#N/A	6.130	#N/A	#N/A	#N/A	#N/A	#N/A	#N/A	#N/A
Yb	8.251	1.64	6.023	5.05	5.09	5.13	5.24	5.46	5.70	5.96
Lu	7.778	1.64	6.250	4.76	4.80	4.84	4.94	5.14	5.37	5.62

Figure 4.13c - Modal batch melting of Zimb.151 using composition and Kd's from Condie & Harrison (1976)

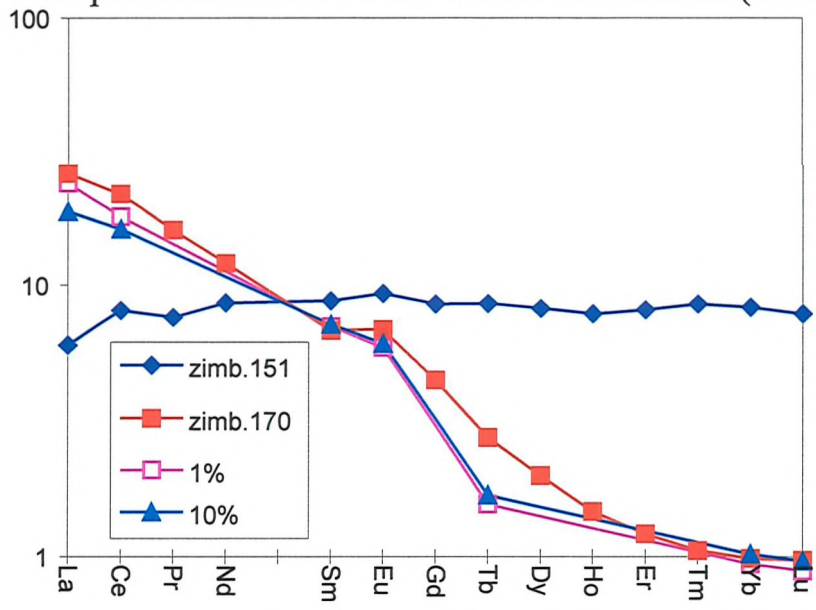

Table 4.7

D Calculations

	%Garnet	% Cpx	% Plag	% Amph.
Mode	30%	70%	0%	0%

Basaltic Kd values after Condie & Harrison (1976)

	Garnet	Clinopx	Plag	Amph.	D
La	0.1	0.3	0.1	0.0	0.24
Ce	0.3	0.5	0.1	0.9	0.44
Pr	#N/A	#N/A	#N/A	#N/A	#N/A
Nd	#N/A	#N/A	#N/A	3	#N/A
	#N/A	#N/A	#N/A	#N/A	#N/A
Sm	3	0.5	0.1	3.99	1.25
Eu	3	1	0.6	3.4	1.60
Gd	#N/A	#N/A	#N/A	5	#N/A
Tb	15	1.5	0.1	0.3	5.55
Dy	#N/A	#N/A	#N/A	6	#N/A
Ho	#N/A	#N/A	#N/A	#N/A	#N/A
Er	#N/A	#N/A	#N/A	6	#N/A
Tm	#N/A	#N/A	#N/A	#N/A	#N/A
Yb	25	2	0.1	4.9	8.90
Lu	25	2	0.1	4.5	8.90

(#N/A = not available)

Batch melting of Zimb.151

				Percentage melt						
	zimb.151	D	zimb.170	1%	2%	3%	5%	7%	9%	10%
La	5.945	0.24	26.092	24.01	23.30	22.62	21.39	20.28	19.28	18.81
Ce	8.010	0.44	21.857	17.97	17.75	17.53	17.11	16.71	16.33	16.15
Pr	7.546	#N/A	16.018	#N/A	#N/A	#N/A	#N/A	#N/A	#N/A	#N/A
Nd	8.548	#N/A	12.059	#N/A	#N/A	#N/A	#N/A	#N/A	#N/A	#N/A
	#N/A	#N/A	#N/A	#N/A	#N/A	#N/A	#N/A	#N/A	#N/A	#N/A
Sm	8.709	1.25	6.744	6.98	7.00	7.01	7.04	7.07	7.10	7.11
Eu	9.281	1.60	6.818	5.82	5.84	5.87	5.91	5.96	6.00	6.03
Gd	8.486	#N/A	4.399	#N/A	#N/A	#N/A	#N/A	#N/A	#N/A	#N/A
Tb	8.527	5.55	2.717	1.55	1.56	1.58	1.60	1.63	1.66	1.67
Dy	8.167	#N/A	1.972	#N/A	#N/A	#N/A	#N/A	#N/A	#N/A	#N/A
Ho	7.802	#N/A	1.458	#N/A	#N/A	#N/A	#N/A	#N/A	#N/A	#N/A
Er	8.060	#N/A	1.206	#N/A	#N/A	#N/A	#N/A	#N/A	#N/A	#N/A
Tm	8.497	#N/A	1.048	#N/A	#N/A	#N/A	#N/A	#N/A	#N/A	#N/A
Yb	8.251	8.90	0.982	0.94	0.94	0.95	0.97	0.99	1.01	1.02
Lu	7.778	8.90	0.967	0.88	0.89	0.90	0.91	0.93	0.95	0.96

Magma mixing

There is plenty of evidence in the Midlands Greenstone Belt for direct interaction of compositionally heterogeneous magmas. These are manifest as bimodal tuffs and agglomerates particularly the 'Agglomerate body' of Log 1c (see sleeve at rear of thesis). With so much interaction, magma mixing *has* to be considered as a possible generative factor in the origin of some of the lithologies sampled.

The first question has to be "Can the andesites be derived directly by mixing of the basalts and rhyodacites?" The answer to this is an emphatic "No!". Aside from the fact that all the major and trace element plots would show straight mixing lines between the two end-member compositions, magma mixing theory indicates that the mingling and mixing of two magmas of such disparate compositions is highly unlikely. At more than a few percent rhyolite the two magmas will not mix properly and will be erupted as pods of felsic melt within the basalt. These are exactly the bimodal eruption textures seen in the Maliyami and Felsic Formations. Viscosity differences between the two magmas are large. Injection of hot, low viscosity basalt into a cooler, more viscous and semi-crystalline rhyodacite, results in cooling, crystallisation and consequent increase in viscosity of the basaltic member until it reaches a point where it is effectively solid. This occurs rapidly with mixtures containing only a small percentage of basaltic melt and causes small blebs of basalt to behave as solid xenoliths within the evolved magma. This texture of small basaltic blebs, was observed in the Sesombi Tonalite. Intimate mingling of the two magmas is required to reduce the diffusion distance for both heat and chemical components and allow mixing. However, this requires the mafic component to be mingled as small blebs, at which point the bulk viscosity contrast between the two is such that the small blebs act as solid xenoliths and no mixing will occur (see Philpotts (1990) for discussion on magma mixing).

It is therefore believed impossible, based on physical and chemical parameters, to mix a basalt such as Zimb.151 with a rhyodacite such as Zimb.170 and form an andesite such as Zimb.194. However, intimate mingling (rather than mixing) of magmas *does* occur in the Midlands Greenstone Belt and so mixing may still be a factor between less extreme end-member compositions. It is noticeable that not all REE patterns for andesites and rhyodacites possess the same La/Yb. Zimb.213 & 046 both possess significantly flatter REE profiles (La/Yb = 3.9 & 3.3 respectively) than Zimb.194 (La/Yb = 5.9) and cross-cut it. REE patterns resulting from simple mass-balance mixing calculations between Zimb.151 (basalt) and

Zimb.194 (andesite) are shown in Figure 4.14 and Table 4.8 and indicate that Zimb.213 & 046 could quite possibly be the result of mixing between these two magma types in the proportions 50-30% basalt and 50-70% andesite. Viscosity contrast between these two magmas would be low, promoting mixing. Low mg# (<60) of the mafic component also aids mixing (Philpotts, 1990), values possessed by basalts and andesites in this study. Trace elements such as Zr, Ti and Y however, do not correlate to such a mixing model which either suggests that the model is poor or that the composition as seen now has been affected by subsequent fractionation as a result of temperature and chemical contrasts.

Figure 4.15 shows that it is also possible to generate most of the dacitic and rhyodacitic volcanics by mixing of Zimb.194 (andesite) and 170 (rhyodacite; see Table 4.9). This includes Zimb.193 which in hand specimen particularly, clearly has a heterogeneous character. In fact the only sample for which it is difficult to model a mixing or generative origin in light of its highly evolved composition, is Zimb.189 which has a flatter REE trend than any of the other rhyodacite samples (La/Yb = 7.9) and yet the highest silica content of any. A considerable influence from continental crust is indicated by this sample, possessing an ε_{Nd} of -5.64, which would normally be expected to increase the La/Yb ratio and further illustrates the disturbed nature of this sample. Trace element characteristics of the rhyodacites do allow a mixing model as suggested, for some of the samples although noticeably not for those from the Maliyami Formation which shows the greatest amount of association (mingling) between contrasting magma types. This would suggest that although REE profiles can be generated by mixing models trace element concentrations suggest this is not often the method of formation. However, as stated previously, geochemical evidence for this process is likely blurred by consequent fractionation. The large amounts of magma mingling evident in the Midlands Greenstone Belt would suggest that mixing *has* to have occurred even if only on a relatively small scale.

Using the results above, an origin for the Midlands Greenstone Belt basalts can be envisioned by equilibrium partial melting of a mantle lherzolite source resulting in slightly LREE enriched, flat and finally LREE depleted REE profiles. This same source was probably sampled during eruption of the Maliyami Formation giving the same LREE depleted patterns and T_{DM} signature around 3.2Ga (see section 4.10.5). The andesites may have been generated by equilibrium partial melting of an eclogite source and the rhyodacites by a smaller scale partial melt of the same source. Mixing of basalt with andesite may have resulted in the

Figure 4.14 - Mixing curves between basalt and andesite

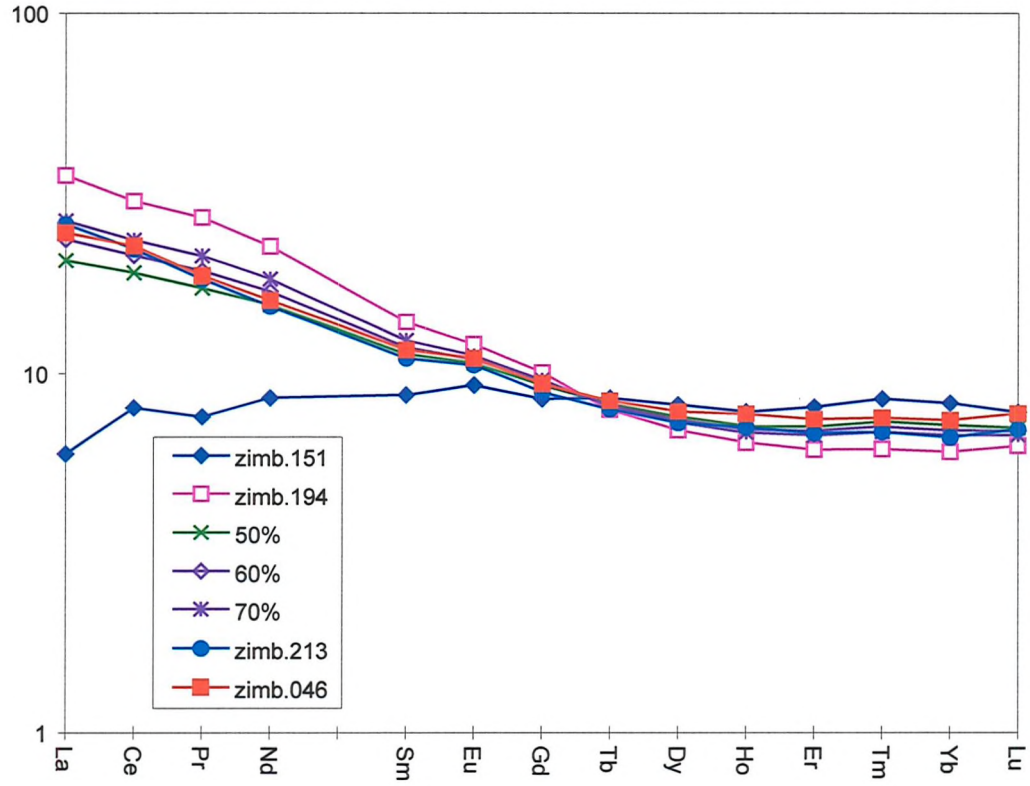

Table 4.8

Magma mixing calculations

	Percent andesite in mixture						
	zimb.151	zimb.194	50%	60%	70%	zimb.213	Zimb.046
La	5.95	35.36	20.65	23.59	26.53	25.89	24.61
Ce	8.01	30.12	19.06	21.27	23.48	22.19	22.62
Pr	7.55	27.07	17.31	19.26	21.22	18.32	18.70
Nd	8.55	22.55	15.55	16.95	18.35	15.42	16.01
	#N/A	#N/A	#N/A	#N/A	#N/A	#N/A	#N/A
Sm	8.71	13.92	11.31	11.83	12.35	11.03	11.63
Eu	9.28	12.06	10.67	10.95	11.23	10.55	11.01
Gd	8.49	10.05	9.27	9.43	9.58	8.88	9.35
Tb	8.53	7.91	8.22	8.15	8.09	7.93	8.39
Dy	8.17	6.91	7.54	7.41	7.29	7.25	7.82
Ho	7.80	6.39	7.10	6.95	6.81	7.05	7.70
Er	8.06	6.10	7.08	6.88	6.69	6.79	7.43
Tm	8.50	6.13	7.31	7.08	6.84	6.83	7.49
Yb	8.25	6.02	7.14	6.91	6.69	6.61	7.38
Lu	7.78	6.25	7.01	6.86	6.71	6.96	7.71
La/Sm	0.68	2.54	1.83	1.99	2.15	2.35	2.12
La/Yb	0.72	5.87	2.89	3.41	3.97	3.92	3.33
Gd/Yb	1.03	1.67	1.30	1.36	1.43	1.34	1.27

Figure 4.15 - To show that mixing between andesite and rhyodacite end-members can account for the majority of rhyodacite REE profiles

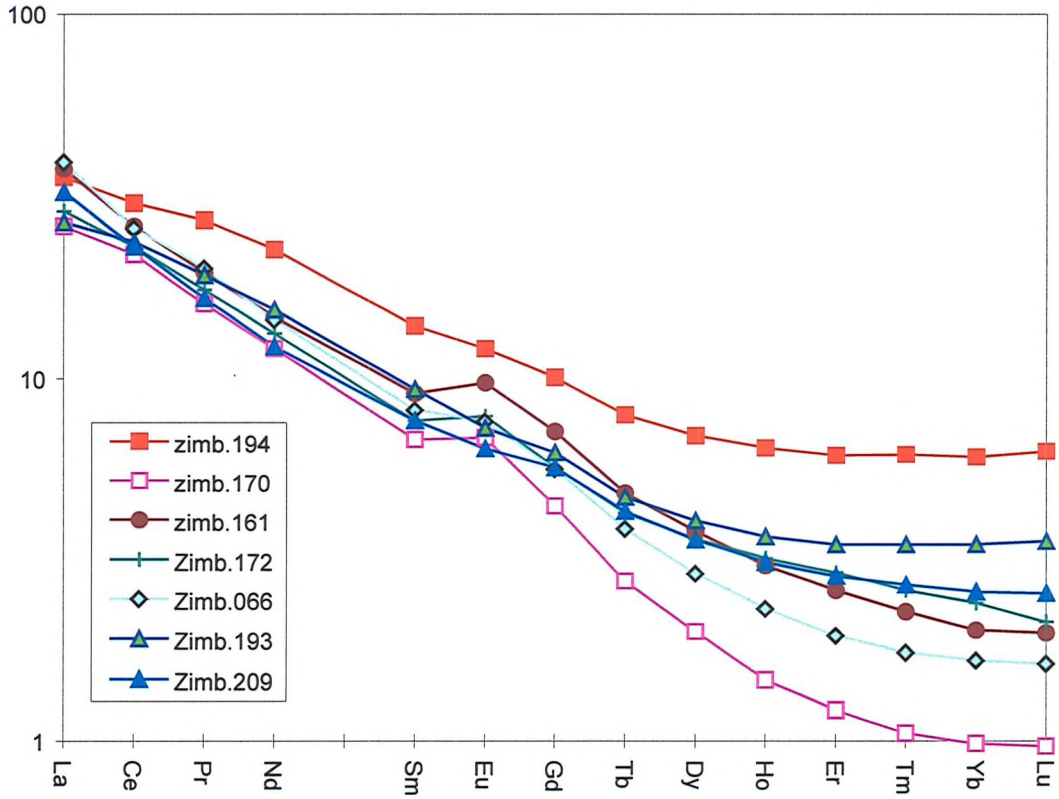

Table 4.9

Magma mixing									
	end-members		samples with compositions between end-members						
	zimb.194	zimb.170	zimb.161	Zimb.172	Zimb.209	Zimb.066	zimb.150	Zimb.128	Zimb.193
La	35.36	26.092	37.30	28.57	32.28	38.83	48.93	54.52	26.72
Ce	30.12	21.857	26.04	22.96	22.90	25.81	37.41	42.40	23.61
Pr	27.07	16.018	19.53	17.53	16.59	20.06	28.18	31.65	19.23
Nd	22.55	12.059	14.72	13.28	12.23	14.51	21.52	24.32	15.45
	#N/A	#N/A	#N/A	#N/A	#N/A	#N/A	#N/A	#N/A	#N/A
Sm	13.92	6.744	9.09	7.60	7.60	8.15	13.01	15.06	9.32
Eu	12.06	6.818	9.71	7.84	6.36	7.57	13.49	12.33	7.26
Gd	10.05	4.399	7.10	5.64	5.63	5.58	9.78	11.57	6.21
Tb	7.91	2.717	4.78	4.20	4.24	3.79	6.95	8.82	4.65
Dy	6.91	1.972	3.73	3.55	3.54	2.85	5.85	7.62	3.99
Ho	6.39	1.458	3.00	3.14	3.06	2.28	5.26	6.94	3.61
Er	6.10	1.206	2.56	2.87	2.80	1.92	4.88	6.62	3.43
Tm	6.13	1.048	2.23	2.56	2.65	1.73	4.73	6.51	3.43
Yb	6.02	0.982	1.99	2.37	2.54	1.64	4.55	6.32	3.43
Lu	6.25	0.967	1.95	2.09	2.51	1.61	4.58	6.83	3.51
La/Sm	2.54	3.869	4.11	3.76	4.24	4.77	3.76	3.62	2.87
La/Yb	5.87	26.573	18.77	12.08	12.73	23.62	10.76	8.63	7.78
Gd/Yb	1.67	4.480	3.57	2.38	2.22	3.39	2.15	1.83	1.81

formation of the basaltic-andesites and the same process between andesite and rhyodacite may have formed the less silica-rich rhyodacites and dacites. Mixing of the basalts and rhyodacites could *not* have formed the andesites. Mixing was likely accompanied by rapid crystallisation and consequent fractionation as a result of the various temperature and viscosity changes. Simultaneous fractionation would only help to further blur the nature of the process occurring. A mixing model possibly explains the strange change in vector for the rhyodacites in the Zr, Ti, and Y plots. Here initial formation of high-Zr, low-Y rhyodacites such as Zimb.066, formed by small scale partial melting of a garnet containing source, may have mixed with lower-Zr, higher-Y rhyodacites such as Zimb.172, derived from fractionation of andesites.

4.10.5) Interpretation of Nd isotope data

On the whole, all of the volcanics of the Midlands Greenstone Belt stratigraphy exhibit positive $\varepsilon_{Nd(t)}$ values. Only Zimb.150 (Mafic Formation dacite) & 189 (Maliyami Formation rhyodacite) show negative $\varepsilon_{Nd(t)}$ values indicative of continental crustal assimilation (see Figure 4.8b). This is extreme in Zimb.189 implying significant disturbance of its Sm/Nd isotope systematics. Largely therefore, continental crustal influences appear to be small if present.

Chondritic uniform reservoir (T_{CHUR}) model ages are clearly too young to represent Nd separation ages for these rocks which reflects the LREE depleted nature of the basalts. As such, no significance is placed on the T_{CHUR} determinations and depleted mantle (T_{DM}) model ages are considered instead.

T_{DM} model ages suggest older events than the rocks themselves record. The basalts record a *c.*3.3 to 3.4Ga age at which the Nd they contain separated from the mantle reservoir. The andesites and rhyodacites of the Maliyami and Felsic Formations possess much smaller errors and record a *c.*2.85Ga mantle separation age. Zimb.189 is the only exception but at 3.99Ga, this probably records the continental crustal influence it has obviously suffered.

It is possible that the older T_{DM} model ages of the basalts could reflect the age of a contaminant, for example the Kwekwe Gneiss, through which the volcanics have been erupted. A number of features would be expected if this were the case. A decrease of $\varepsilon_{Nd(t)}$, increase of model age, increasing Nd and decreasing $Nd_{(i)}$ would be expected. A decrease in

$\varepsilon_{Nd(t)}$ is shown by the volcanics, decreasing to +1.53 in Zimb.135 (Mafic Formation basalt), and so may reflect crustal contamination. Calculation of $\varepsilon_{Nd(t)}$ of the Kwekwe Gneiss at 2.7Ga shows it to be -8.25, a low enough value to require only a very small amount of contamination to produce the +3.49 to +1.73 range of $\varepsilon_{Nd(t)}$ values seen in the 2.7Ga volcanics. Chauvel *et al.* (1993) demonstrated that incorporation of <1% continental crust explained the change from +3.2 to +0.4 $\varepsilon_{Nd(t)}$ in the Reliance Formation komatiites, a greater range of values than those seen here. Less than 1% contamination of Zimb.186 by Zimb.226 (Kwekwe Gneiss) would not significantly change the REE profile of the basalt. It is therefore possible to generate the variation in $\varepsilon_{Nd(t)}$ seen in the volcanics of the Midlands Greenstone Belt by simple continental crustal contamination. This would not significantly affect the REE profiles of the individual rocks and therefore does not explain the origin of the evolved samples. This approach also therefore, rules out generation of the andesites and/or dacites by massive crustal contamination of basalt.

Such small amounts of crustal material would also account for the variation in $Nd_{(i)}$ seen in the volcanics, and at such low levels, contamination would not affect the Nd concentration unduly.

At such low levels of contamination however, one must question the likelihood of it happening at all. Could *c.*0.5% crustal contamination be mixed with the magmas and be consistently apparent over the 200Ma generative lifetime of the Midlands Greenstone Belt basalts? Zimb.150 (dacite) & 189 (rhyodacite) illustrate that contamination *is* occurring by their negative $\varepsilon_{Nd(t)}$ values. An alternative method of generating the variable $\varepsilon_{Nd(t)}$ values shown by the basalts, is by sampling of a heterogeneous mantle component. Such a process would be expected to result in variable $Nd_{(i)}$ due to variable Sm-Nd depletion, at similar Nd concentrations. Also, a correlation between increasing $\varepsilon_{Nd(t)}$ and increasing depletion at a certain model age would be expected.

Figures 4.16a&b illustrate the differences in the expected effects of crustal contamination and sampling of a variably depleted mantle component. The first of these shows that there is very little variation in the $Nd_{(i)}$ of the 2.7Ga volcanics. Such a plot ($Nd_{(i)}$ vs 1/Nd) was used by Moorbath *et al.* (1997) to illustrate isotopic homogenisation at time *t*, producing a straight line correlation. This does not apply here since $Nd_{(i)}$ is calculated for the age of the rock and therefore expected to produce a straight line if all the rocks are of the

Figure 4.16a $Nd_{(i)}$ vs 1/Nd

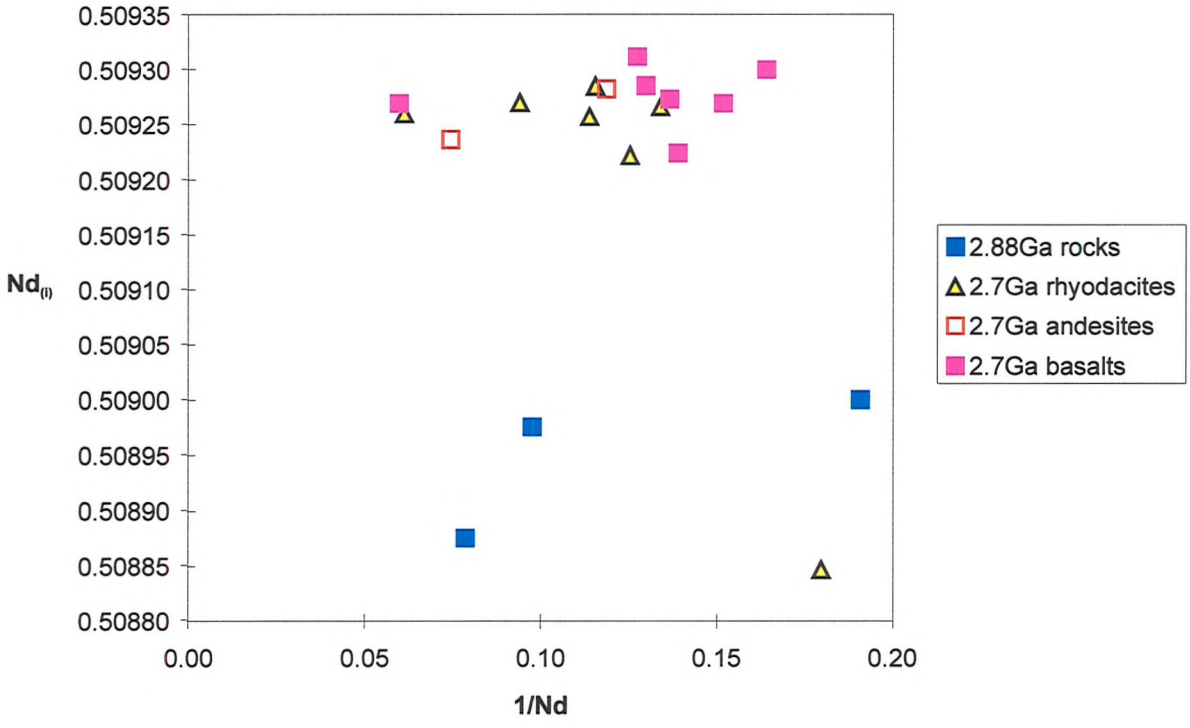

Figure 4.16b T_{DM} vs $\varepsilon_{Nd(t)}$

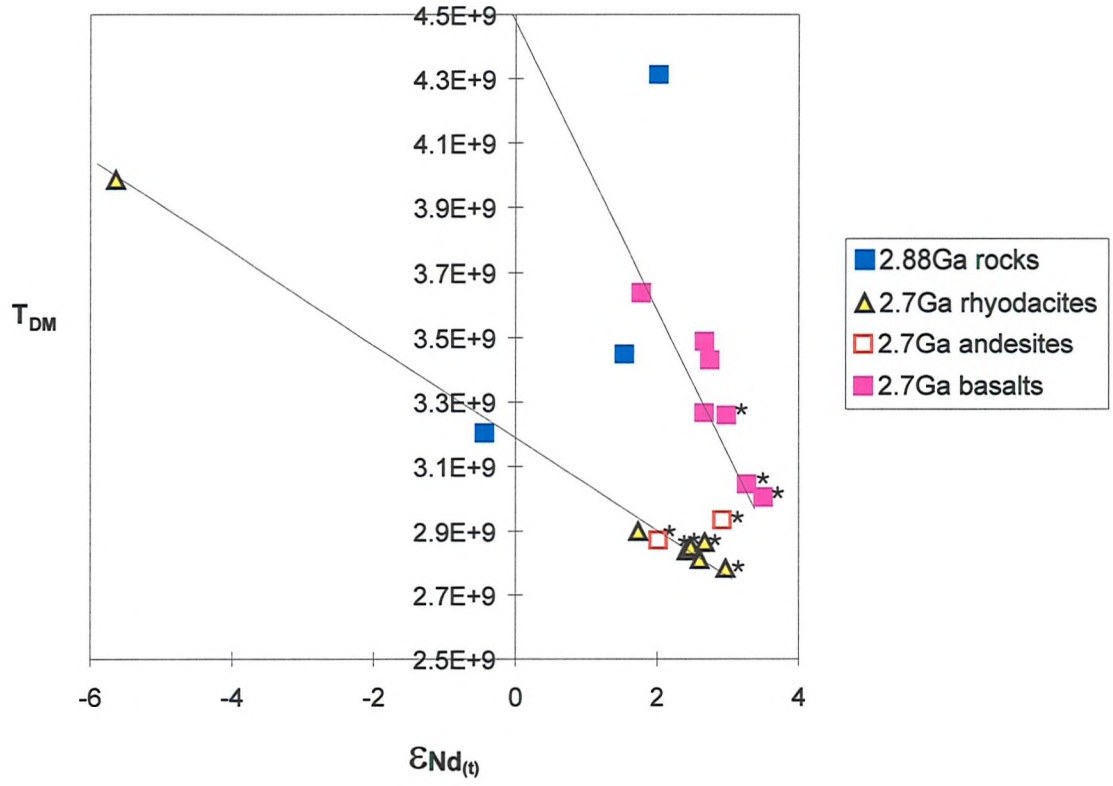

(* = ICP-MS analysis for Sm/Nd)

same age. Also, the rocks have not suffered a major tectonothermal event of the kind suffered by the Early Archaean samples studied by Moorbath *et al.* (1997), the rocks of the Midlands Greenstone Belt being essentially fresh with only a minor low-grade greenschist facies overprint. By producing this straight line, Figure 4.16a actually provides support that the rocks of the Maliyami and Felsic Formations are indeed *c.*2.7Ga old, and this is exemplified by the fact that Zimb.189 plots with significantly lower $Nd_{(i)}$ than the rest of the 2.7Ga volcanics due to its contaminated nature. A straight (horizontal) line correlation for the Mafic Formation may be hypothesised although only two samples are available for this, with Zimb.150 plotting with low $Nd_{(i)}$ in a similar fashion to Zimb.189 as a result of contamination.

Figure 4.16b (T_{DM} vs $\varepsilon_{Nd(t)}$) appears to suggest a correlation between increasing T_{DM} and decreasing $\varepsilon_{Nd(t)}$ which would strongly suggest crustal contamination. However, analytical precision is a large factor in this diagram as a result of the $1/\lambda$ component in the calculation of the T_{DM}. Analyses by ID-TIMS have 2σ (external) error bars only as large as their symbols on Figure 4.16b but those samples whose Sm/Nd was determined by ICP-MS can have 2σ external errors between ± 0.6 & 1.1Ga T_{DM}. This easily accounts for the variation in the T_{DM} values and therefore no confident interpretation can be placed on the displayed trend of decreasing $\varepsilon_{Nd(t)}$ with increasing T_{DM} until all samples have been determined by ID-TIMS. However, it is noticeable that those samples analysed by ID-TIMS, still roughly define a trend of increasing model age with decreasing $\varepsilon_{Nd(t)}$, supporting the possibility of crustal involvement.

Assimilation and fractional crystallisation processes (AFC - O'Hara & Matthews, 1981) are much more complex and precise than contamination models discussed here and may provide more accurate answers to this problem.

Having conducted Nd isotope and Sm/Nd ratio determinations by both TIMS/ICP-MS and TIMS (including ID-TIMS), an analytical factor may be considered involved with the generation of such high T_{DM} model ages, especially since any minor variation is magnified greatly ($1/\lambda = 1.53 \times 10^{11}$) to achieve the result. However, data produced by ID-TIMS (see Table 4.2/2 in Appendix B), although different (i.e. not within error of the ICP-MS derived data for some samples), is of a high quality and is considered accurate. This indicates that analytical error is not a factor in generating the high T_{DM} model ages and that these ages are

real. Other explanations for these variations will be considered later. Alternatively, the specific $^{147}Sm/^{144}Nd$ and $^{143}Nd/^{144}Nd$ values used for the calculation of the depleted mantle model ages are significant, illustrated by T_{DM} model ages calculated using the values quoted in Jelsma (1993) and the Isoplot program of Ludwig (1980) (see Table 4.2). Both these sets of values produce T_{DM} results too young to be considered reasonable and indeed, in the case of the Isoplot program, fail to produce any result at all. The Peucat *et al.* (1989) values used are therefore considered the most relevant.

4.10.6) Sebakwe River Gneiss

It is difficult to relate the chemistry of the multiple phases which this unit contains. Phase 2 (Zimb.141) can be seen in the field to be a derivative of Phase 1 (Zimb.140). The origin of Phase 3 (Zimb.142) is less certain but the cross-cutting field relationship with the other two phases and more evolved nature strongly suggests derivation by continued differentiation or through another partial melting episode. This being the case, the massive depletion in HREE and Y, along with a small (*c.*3%) decrease in Al_2O_3, can most likely be accounted for by garnet fractionation or retention in the source since amphibole and apatite do not have the Kd credentials required to generate the REE pattern seen (see Fig.4.9). Alternatively, zircon fractionation may be considered as a possible cause but the high Zr content of Phase 3 (208ppm) would appear to preclude this as a solution.

$\varepsilon_{Nd(t)}$ values for the Sebakwe River Gneiss at the time of its formation are probably meaningless due to being the source for subsequent melting events. However, $\varepsilon_{Nd(t)}$ evolved through to 2.7Ga produces values ranging form -4.1 to -12.1. As basement to the greenstone belt, these values would allow small amounts of assimilation to cause the variations in $\varepsilon_{Nd(t)}$ seen in the volcanics.

4.10.7) Relevant Regional Granitoids

Of the regional granitoids analysed, the only samples of real concern in regard to the Midlands Greenstone Belt volcanics are the internal granitoids and Kwekwe Gneiss.

The Kwekwe Gneiss indicates its basement credentials by similarity to the Tokwe River Gneiss, an $\varepsilon_{Nd(t)}$ value around unity and a modal age of *c.*3.5Ga. The internal granitoids of the Sesombi Tonalite and Late Porphyries all exhibit remarkably similar characteristics in

all aspects of their geochemistry. $\varepsilon_{Nd(t)}$ values of *c.*3.5 and T_{DM} model ages of 2.7 to 2.75Ga indicate direct derivation at this time from a depleted mantle source. As such, these granitoids can be considered small-scale melts of primary mantle components with no influence from continental components. The exception is the Chicago Porphyry (Zimb.156) which has obvious crustal contamination evidenced by its REE pattern, $\varepsilon_{Nd(t)}$ of -2.7 and a model age around 3Ga.

4.11) GEOCHEMICAL DISCUSSION

The evidence gathered from all the data presented here is subject to interpretation and inconclusive. No single scenario fits all the observed data. However, some scenarios are considered more likely than others in the light of current understanding. The basalts of the Midlands Greenstone Belt may well have relation to the komatiites, siliceous high-Mg basalts and tholeiitic basalts of the Mberengwa (Belingwe) Greenstone Belt as described by Scholey (1992), Bickle *et al.* (1993), Brake (1996) and Silva (1998). This being the case, a marginal plume model of generation may be considered.

Magma mingling has occurred but homogeneous mixing would only have been successful where the mingled magmas have relatively similar composition and were intimately mingled by turbulent intrusion, thereby decreasing temperature, viscosity contrasts and diffusion distance for both heat and chemical components. The results of unsuccessful mixing are evident throughout the Maliyami and Felsic Formations as bimodal agglomerate and tuff deposits. Successful mixing is considered to have occurred between basalts and andesites; andesites and dacites/rhyodacites; and possibly also between dacites and rhyodacites. Evidence for this is also seen in thin section in the form of resorbed quartz phenocrysts and free quartz in the andesites. These bimodal and mixed magma relationships are evidence for increased volcanic activity during the eruption of the Maliyami Formation, allowing interaction of different magmas possibly from different sources. Other evidence suggesting increased volcanic activity is provided by the narrow range of trace element ratios for the Maliyami Formation basalts, indicating derivation during a single magma formation event. The wider range of ratios shown by the Mafic and Felsic Formation basalts indicates

that the data for these formations are the result of the accumulation of more than one period of magmagenesis.

Generation of the volcanics must therefore account for three compositions; basalt, andesite and rhyodacite. Basalt can be generated by melting of a lherzolitic source, either depleted or not but if T_{DM} model age determinations are to be believed, this source is heterogeneous in its depletion and substantially older than the volcanics being generated from it. Such a component of sub-continental lithospheric mantle (SCLM) has been recognised under the Tokwe Segment by Nägler *et al.* (1997). A heat source would be needed at 2.9 and 2.7Ga to allow melting of this SCLM at this time.

The andesites provide a problem. They may have had a similar parent to the basalts, containing 10wt% MgO, 6000ppm Ti, 60ppm Zr and mg# = ~50 but then evolved along a different fractionation path; the basalts crystallising clinopyroxene and plagioclase whilst the andesites additionally fractionated ilmenite, amphibole and/or garnet. They cannot be generated by mixing between basalts and rhyodacites, nor by significant contamination of basaltic magma by continental crust, nor by simple fractionation of the basalts. Whether the solution could be a combination of scenarios, for example very small levels of crustal contamination adding water and oxidising the initial basalt melt and thereby driving it onto a fractionation pathway including ilmenite, amphibole and/or garnet, is unknown.

Amphibole and or garnet must be involved in andesite origin and/or evolution in order to generate the observed REE patterns. If amphibole/garnet fractionation is not accepted as a model, these minerals are required in the source. Partial melting of an eclogite with the composition of the Mafic Formation basalts, can produce the andesite geochemistry seen. However, Barker & Arth (1976) suggested that due to an increased geothermal gradient in the Archaean, generation of garnet containing rocks such as eclogite and garnet-amphibolite was not possible since the required pressures were not generated before melting occurred. Arth & Barker (1976) illustrated that it was possible for fractionation of amphibole to generate the observed chemistry of TTG magmas. Wyllie and co-workers however, have showed over a number of studies (e.g. Wolf & Wyllie, 1994; Wyllie *et al.*, 1997) that dehydration of amphibolite at low temperatures (<750°C) and depths of only 10kbars leaves a garnet residue which explains the extreme HREE depletion seen in Archaean rhyolites and tonalites. Most of these workers infer or calculate 10-20% partial melting to achieve rhyolite compositions and indeed Rapp *et al.* (1991) indicate that a small volume of rhyolitic magma resulting from 10%

partial melting of an amphibolite source requires only 100-1000 years to segregate from its source as long as it has a high enough water content. These calculations also assume a static tectonic environment which may or may not have been the case.

The presence of garnet in the volcanic section provides an interesting problem. Is it a primary liquidus mineral or the result of assimilation of Al-rich sediments? Garnet is seen to be present on the liquidus during the eruption of the dacitic tuff sample Zimb.052 (see plate 3.4) but this may not have petrogenetic implications. Deer *et al.* (1982) compile evidence from a number of researchers on the crystallisation and role of garnet in andesitic and dacitic magmas. Almandine garnets are common in magmas of this composition and generally show an appreciable spessartine (Mn) component (up to 20%). Keesman *et al.* (1971) showed that almandine is unstable at low pressures and high temperatures and must therefore be the result of crystallisation at depth around the crust-mantle boundary (9-18kbar) prior to eruption. Henson & Green (1973) suggested that garnets may be evidence for mixed crustal lithologies in the source region of the andesites and dacites since they were most likely the result of admixing of pelitic rocks which have not equilibrated fully with the whole of the magma body. However, the general absence of negative $\varepsilon_{Nd(t)}$ values for the rocks of the Midlands Greenstone Belt, argues strongly against this proposal and suggests that the garnet in these samples is a primary liquidus phase.

Generation of the dacites and rhyodacites may be two fold. Fractionation of amphibole, plagioclase and ilmenite from andesites may result in the dacites but primary generation may also be required as suggested by rhyodacitic volcanics with strongly depleted HREE and high Ti/Y (*c.*500); a similar composition to the Sesombi Tonalite. Primary generation may occur by smaller scale (1-10%) partial melting of the same source as that which formed the andesites. Such compositions were shown by Martin (1993) to be possible as a result of melting a subducting basaltic slab prior to dehydration reactions. Whilst the geochemistry of this scenario is recognised, the palaeotectonic interpretation which this implies is not considered a foregone conclusion. Barker & Arth (1976) showed that melting of a basaltic pile transformed to amphibolite could also produce the bimodal successions often seen in Archaean terrains. Although these authors suggested this would be most likely to occur in a rift situation, this interpretation is largely free of palaeotectonic implications. A more complete discussion of previous studies and palaeotectonic interpretations is left until Chapter 6.

Minor variations in $\varepsilon_{Nd(t)}$ values for the volcanics indicate very limited crustal assimilation (<1%) which may or may not therefore have occurred at all. This being the case, $\varepsilon_{Nd(t)}$ relates to the source and the minor variations would reflect heterogeneity within this source.

The two high-Nb, LREE enriched samples (Zimb.034 & 208) are most likely the result of small amounts of deeper mantle melting. This would generate the high Nb concentrations and low Zr/Nb and Ti/Zr ratios seen. These samples possess high Ti and also high Zr concentrations resulting in low Ti/Zr ratios (~79), indicating a preferential enrichment scheme for these two samples of Nb > Zr >Ti. A small amount of crustal contamination may therefore be involved in generating the high Zr and consequent low Ti/Zr ratios without significantly lowering the Zr/Nb ratio. These samples display free-quartz in thin section but unfortunately Nd isotope data is not available.

Cessation of volcanic activity is marked by the intrusion of the Late Porphyries and the Sesombi Tonalite. These granitoids show characteristics indicating direct derivation by small-scale melting of a basaltic source with a residual garnet component in the same way as rhyodacite Zimb.170, without any continental crustal influence.

CHAPTER 5 - ZIRCON GEOCHRONOLOGY - METHODS AND APPLICATION

5.1) INTRODUCTION

This chapter is divided into 2 parts. The first part will describe the principles behind zircon geochronology, both from the mineral characteristics and analytical points of view. The theory behind zircon dating, including the structural and chemical characteristics of zircons, will be discussed in order that a better understanding of their formation can be achieved. The principles and problems involved in their analysis will also be discussed after a brief résumé of the features visible under back-scattered-electron and cathodoluminescence imaging techniques.

The second part of this chapter will then concentrate on the samples involved in the study, including their morphology, image-interpretation and analysis. The geological interpretation of these new dates will be left for discussion in Chapter 6.

PART 1 - AN INTRODUCTION TO U-Pb ZIRCON IMAGING, ANALYTICAL TECHNIQUES AND INTERPRETATION

5.2) MINERAL CHARACTERISTICS AND ZIRCON GEOCHRONOLOGY - THE THEORY BEHIND THE PRACTICE

5.2.1) Physical and chemical characteristics of zircon - the traditional viewpoint

Zircon ($ZrSiO_4$) is generally a late crystallising phase from a refractory magma or fluid, for example granitic-pegmatites and nepheline-syenites, and is most commonly found in granodioritic to granitic intrusives and their related volcanics. It is a member of the tetragonal crystal system and is compositionally a solid solution of the end-members hafnon ($HfSiO_4$) and zircon (Ramakrishnan *et al.*, 1969). HfO_2 content of zircon is usually around 1-2wt% but can reach 31wt% (Deer *et al.*, 1966). Xenotime is also isostructural with zircon and as such Y^{3+} and P^{5+} readily substitute for Zr^{4+} and Si^{4+} (Speer, 1980; Benisek & Finger, 1993). U^{4+} and Th^{4+} are common substituting cations for Zr^{4+} and cause destruction of the zircon lattice through recoil of their nuclei after α-emission (Nasdala *et al.*, 1996), during decay to their respective radiogenic products ^{206}Pb, ^{207}Pb and ^{208}Pb. This lattice destruction is

exacerbated by the size of the Pb^{2+} ion, much expanded in comparison to the U^{4+} or Th^{4+} ions (see Table 5.1), and the temperatures generated locally around the decay particles (Deer *et al.*, 1966).

Table 5.1* - Table of ionic radii for elements commonly substituting for Zr^{4+}

(N.B. co-ordination number = 8)

Element	Ionic radii (Å)	Charge	size/charge ratio
Zr	0.84	4+	0.2100
Hf	0.83	4+	0.2075
La	1.16	3+	0.3867
Lu	0.98	3+	0.3267
U	1.00	4+	0.2500
Th	1.05	4+	0.2625
Pb	1.29	2+	0.6450

*Ionic radii values from Shannon (1976)

This physical and chemical disturbance to the crystal causes metamictisation, a breakdown in the crystal structure of pristine zircon. Along with cracking, metamictisation allows easier access for metamorphic and hydrothermal fluids which alter the trace element composition of the crystal. This has particular significance for U, Th and Pb with concomitant implications for geochronological analysis. REE are also ubiquitous in zircons and display a characteristic HREE-enriched pattern as a result of the lanthanide contraction in ionic size allowing HREE to be far more readily accepted into the zircon structure than LREE (see Table 5.1). The difference in ionic size, in conjunction with the charge imbalance, is also the reason why U^{4+} is accepted into the structure of a growing zircon and Pb^{2+} is not. This exclusion of Pb enables precise ages to be calculated by the U-Pb decay system, and is also one of the reasons that the Lu-Hf system is less effective since in this system both parent and daughter isotopes are already present in the zircon before decay. Also, the small amount of Lu in zircon relative to the mass of the crystal, the length of the half-life ($3.8x10^{10}y^{-1}$) for the Lu-Hf decay scheme and the amount of Hf present in zircon, are all factors which favour the use of the U-Pb system for the purpose of dating zircons.

Pristine zircon has a high blocking temperature (>900°C for pristine zircon: Lee *et al.*, 1997) and commonly forms as a late stage refractory mineral in evolved magmas at temperatures not much greater than this. Hence, the age determined from a crystal generally represents the age of crystallisation of the magma rather than a period in its cooling history. This also means that the mineral is quite resistant to dissolution and assimilation, and to complete resetting of the Pb/U ratio by complete Pb loss. However, in contradiction to this robust nature in the face of magmatic processes, zircon is known to lose Pb during metamorphic, hydrothermal and weathering processes. This results in a change in the Pb/U ratio, causing a discordant plot on a concordia diagram (see section 5.3.2).

The high temperature of crystallisation for zircon in conjunction with a high blocking temperature, enables the mineral to resist the process of assimilation by another magma hot enough to melt the host rock in which it resides. Consequently any primary zircon crystallising from this new magma will preferentially nucleate on the xenocryst remaining after assimilation of the host rock. The result is a composite zircon with a xenocrystic core of older zircon and a new magmatic rim. These two phases of zircon can and will most probably contain, different trace element abundances, imparting a characteristic trace element pattern to that part of the zircon with its own distinct age. From back-scattered electron (BSE) images generated on a scanning electron microscope (SEM), it can clearly be shown that under the correct conditions, zircons do begin to melt when undergoing assimilation (Hanchar & Miller, 1993). This resorption causes embayment and general rounding of the crystal faces, truncating any growth patterns present. When interpreting BSE or cathodoluminescence (CL) images (another commonly used imaging technique producing similar results), it is these truncations to the fine growth-zones, representing changes in concentration of elements with higher atomic number, which enable different crystal sectors to be recognised. Crystal sectors are here defined as additional phases of zircon of whatever age, which crystallise on pre-existing zircon as indicated by truncation or other geologically significant juxtapositions. Sectors may or may not display different ages, simply representing a hiatus in crystallisation during which conditions altered such that a different morphology of crystal was favoured reflecting subtle changes in magma chemistry.

These structural sectors, representing distinct breaks in crystallisation, and often totally different events, should not be confused with the chemical sector zoning described by Dowty (1976) and Watson & Liang (1995).

5.2.2) Recent advances in zircon understanding

Numerous studies have placed varying importance on the effect of physical and chemical criteria in determining the trace element composition and morphology of zircon crystals. Pupin (1980) devised a table in which the change of morphology of a euhedral zircon was shown to be chiefly a function of temperature and agpaicity or peralkalinity ((Na+K)/Al) of the magma. He argued that the morphology of a zircon could be related to a particular kind of granite and thereby indicated the petrogenetic process involved in its generation. Information on the crystallisation period of the crystal, water content of the magma, chemical and temperature variations of the crystallising medium, types of associated accessory minerals, and comparative petrology - the petrogenetic relationship of two juxtaposed bodies, were all considered possible conclusions from studies of the crystal morphology.

However, more recent studies have shown that other factors may play a more dominant role in determining the morphology of a zircon. Vavra (1990) considered zircon supersaturation to be a major control. On cathodoluminescence (CL) images, low zircon supersaturation was indicated by widely spaced zones interrupted by dissolution surfaces and considered to cause the preferential growth of [100] relative to [110]. High zircon supersaturation led to the development of narrowly spaced oscillatory zonation without dissolution surfaces and the preferential growth of [110] relative to [100]. Benisek & Finger (1993) disagreed; they considered the trace element composition of the melt to be the dominant factor. Using observations of the magmatic oscillatory growth zoning seen in the crystals, U was strongly suspected of producing an adsorptive growth blocking effect on [110], leading to [110] dominant crystals as [100] grew out of existence (see Figure 5.05). Granitic melts high in U, Th, Y, REE, and P relative to Zr, were considered predestined to crystallise zircons with large [110] prisms due to the coupled substitution:

$$Y(REE)^{3+} + P^{5+} \longrightarrow Zr^{4+} + Si^{4+}$$

Figure 5.05 - Growth blocking of [110] and preferential growth of [100]

(Benisek & Finger (1993)

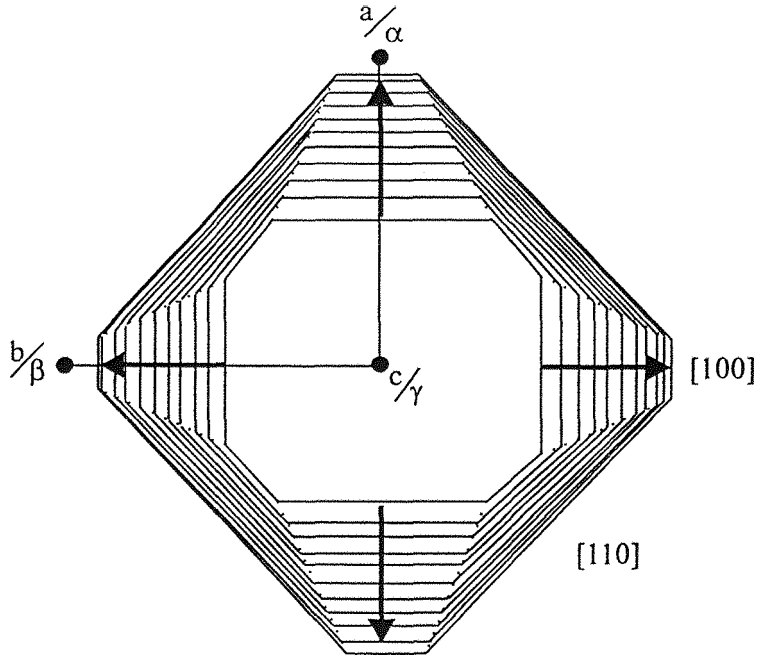

However, Y-rich oscillatory zones with both enriched and depleted P contents were observed within the same crystal, casting doubt on the causatory link of this substitution. Benisek & Finger (1993) also recognised that narrow-spaced oscillatory zoning may arise from non-equilibrium partitioning of the relevant elements between the melt and the crystal face, whilst the larger scale chemical zonation of increasing U and Hf concentrations from core to rim, was probably dependent on the melt chemistry and would therefore broadly follow equilibrium Kd relations. Non-equilibrium crystallisation was indicated by the reduction of Hf in the U and Y-rich zones (bright areas on BSE images), a fractionation occurrence contrary to the incompatible nature of all three elements. The oscillations were therefore considered to represent local chemical gradients within the melt immediately adjacent to the crystal face. They also recognised compositional sector zoning between [100] and [110], as an important factor in their normal magmatic growth, observing that [100] preferentially incorporated Y, REE, U and Th, relative to [110], thereby producing a growth blocking effect on the [110] prism face. Concentration of these elements towards the rim of the zircon probably reflected the fractionation processes occurring in the magma at the time of crystallisation. They concluded that temperature (considered by Pupin (1980) to be a factor) does not have an effect on zircon morphology which is therefore a poor

geothermometer, and that zircon supersaturation of the melt was also probably insignificant. They did however concede, that a slow cooling magma (causing low zircon supersaturation) or high temperature (causing increased cation mobility), were likely to reduce the growth blocking effect and cause [110] growth in relatively U-rich melts, and conversely that a cooling melt would lead to concentration of the incompatible elements concerned (assuming no crystallisation of other accessory minerals which might remove U and Y, nor input of fresh magma) and therefore the predominance of the [110] prism (by stunting growth). Loth & Höll (1996) used these observations extensively in interpreting the crystallisation history of a magma through internal variations in the morphology of the zircon crystals imaged by CL.

Pidgeon (1992) observed that these chemical characteristics were changed by recrystallisation of the oscillatory zoned zircon. Uranium, Th, and Pb were all noted to be lost during recrystallisation, leading to the production of extremely stable unzoned zircon. Later events which might normally be expected to cause Pb-loss, did not seem to have this effect thereby allowing the retention of a concordant or only slightly discordant age. A date obtained on this recrystallised zircon is probably close to the primary crystallisation age of the rock since Benisek & Finger (1993) recognised the presence of recrystallisation most frequently in those granites which had experienced a protracted cooling history. They also noticed that recrystallisation was only rarely seen in zircons whose host rock had experienced amphibolite facies metamorphism. These two observations indicate that recrystallisation generally occurs under very high temperature conditions. If no high-grade metamorphic events have been suffered by the rock, an age determined on recrystallised zircon probably represents an age just after the initial crystallisation of the rock. A date from a partially recrystallised zircon will therefore represent a weighted average of the two components involved, and a mixture between the true crystallisation age and a period early in its cooling history.

Important experimental work has been conducted by Watson and co-workers. Watson (1996) considered Zr diffusion to be the major controlling factor in zircon dissolution and growth but also discussed the importance of factors such as the volume and spatial distribution of the reservoir of melt with which the crystal interacts, the initial size of the crystal (when considering dissolution) and the duration of the thermal event. He concluded that failure of the melt to coalesce, large zircons (and/or their occlusion in major phases) and

a very brief or relatively cool magmatic event, are all influential factors leading to inheritance of zircon within rocks.

Cherniak *et al.* (1997a) showed that the diffusion rate of REE in zircon was sufficiently slow as to be considered negligible thereby allowing the development and retention of sector and oscillatory zoning by preferential incorporation of REE on certain faces; a feature controlled by the lanthanide contraction which results in the strong LREE depleted pattern for zircon (see Table 5.1).

More importantly for the geochronologist, Watson *et al.* (1997) studied the extent to which Pb was incorporated into zircon during its crystallisation and found that this was, to all extents and purposes, negligible, but interestingly noted that zircons grown under hydrothermal conditions contained much higher levels of common-Pb. They concluded therefore, that this was also likely to be the case in nature and that this might prove a useful 'fingerprint' to the identity of hydrothermal zircon. Within igneous zircons, high activity of P was also seen to have a significant effect on the common-Pb uptake of a crystallising zircon.

5.2.3) Back-Scattered-Electron-Imaging of Zircons - examples and interpretation

With the advent of high-precision, high-spatial resolution U-Pb zircon geochronological techniques such as SHRIMP and LA-ICP-MS, imaging of zircons prior to analysis has become increasingly important. The importance lies in knowing *exactly* what is being analysed. As discussed above, zircons are one of the most resistant minerals to dissolution, resorption and remelting and as such, often exhibit three or more separate phases of growth which may or may not have occurred at significantly different times. Using high-spatial resolution methods of analysis these individual phases can be distinguished and a more complete, and frequently complex, history can be determined.

When viewed by back-scattered-electron (BSE) or cathodoluminescence (CL) imaging, zircons often exhibit a series of zones or patches of varying intensity on a grey-scale. Lighter patches represent higher average atomic number, primarily Hf (and secondarily U) in the case of BSE, or REE (primarily Dy^{3+}) in the case of CL (Hanchar & Miller, 1993). Recently a number of publications have discussed these zoning features of zircons and what they mean chemically and for U-Pb zircon age intepretations. Some of this work will now be discussed using BSE images of zircons extracted from samples in this study. The aim of this discussion is to highlight some of the chemical and structural features of zircon. These

features, their interpretation and effect on the analyses will be considered for each of the samples analysed in this study.

Plate 5.1 shows classic, primary magmatic, oscillatory-zoned zircon defined by greater or lesser concentrations of Hf. This may be recrystallised in places, during which process, extraneous U, Th and Pb are displaced from the lattice leading to a homogeneous structure (Pidgeon, 1992; see Plates 5.2a&b). When more than one phase of zircon is present, or the high-U zones in a phase are significantly broad, radioactive decay of the U^{4+} to the larger Pb^{2+} ion, coupled with the destructive disturbance of the U nuclei recoiling after α-emission, causes a volumetric expansion of the zircon in that zone thereby radially cracking the surrounding low-U zircon (Lee & Tromp, 1995; see Plates 5.3a & b). Such cracks are also often seen radiating from an inherited core (see Plate 5.4). Features such as the intense oscillatory zoning exhibited in parts of Plate 5.5, are proposed by Vavra (1990) to be due to high supersaturation of the melt with respect to zircon. However, some patterns, such as the convolute zoning seen in Plate 5.6 are harder to explain by any theory. Twinning in zircon was found to be fairly common in the samples used for this study and under BSE imaging can be quite spectacular (see Plate 5.7).

These are some of the more basic interpretative characteristics seen in zircons during BSE or CL imaging and Table 5.2 summarises these features.

5.3. - U-Pb ZIRCON ANALYTICAL TECHNIQUES

5.3.1) Introduction

U-Pb and Pb-Pb geochronology of zircons has been used in this study because it has a number of advantages over other systems. Firstly, the system is relatively robust during metamorphic and fluid processes, especially when compared to the Rb-Sr system. This represents a significant advantage in a craton, having experienced a pervasive low-grade metamorphism with some regional and many local, increases. Secondly, the precision possible using this isotope system as determined from accessory minerals, easily exceeds that determined from any of the other geochronological isotope systems for rocks of this age. Thirdly, U-Pb dating of zircon is possible using techniques with high-spatial resolution, whilst still maintaining reproducible, high-precision results.

Plates 5.1-5.3 - Interpretation of zircon zonation patterns under BSE imaging

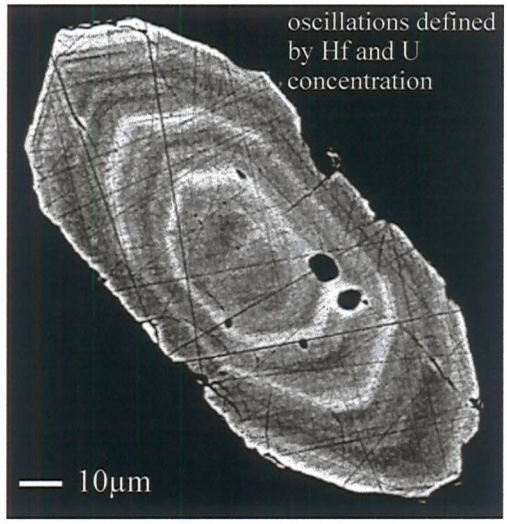

Plate 5.1 - classic, primary magmatic oscillatory zonation

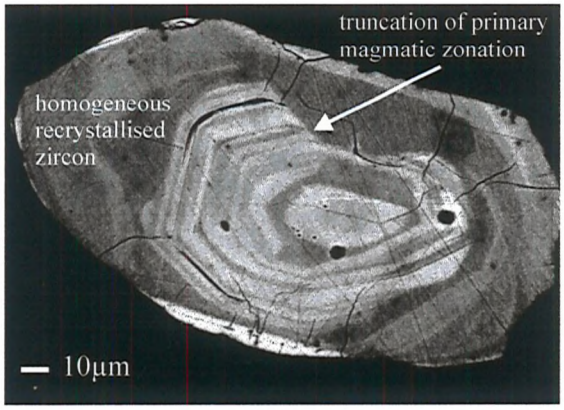

Plate 5.2a - recrystallised zircon

Plate 5.2b - patchy recrystallised zircon

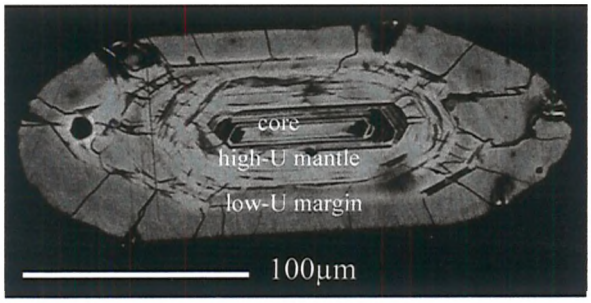

Plate 5.3a - 3 phases of zircon: inner xenocrystic core with high-U mantle causing cracking of outer low-U margin

Plate5.3b - zircon with high-U mantle causing radial expansion cracking of outer low-U zircon

Plates 5.4-5.7 - Interpretation of zircon zonation under BSE imaging

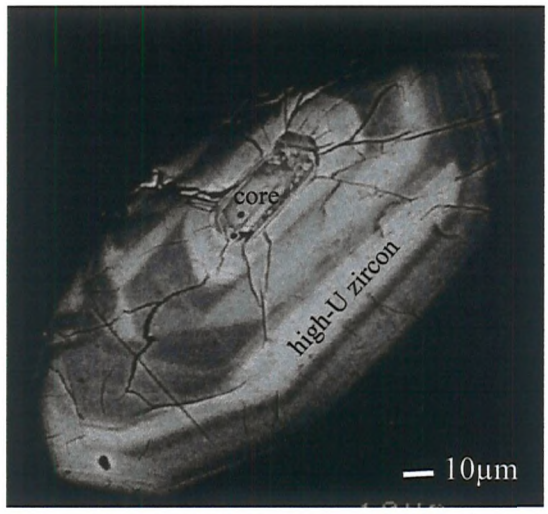

Plate 5.4 - radial expansion cracks through rest of grain indicate xenocrystic core significantly older than other phases

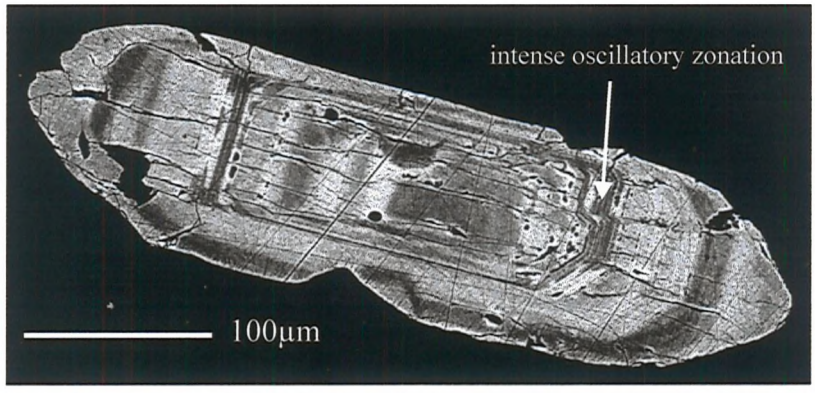

Plate 5.5 - closely spaced oscillatory zoning indicating high zircon supersaturation of the melt

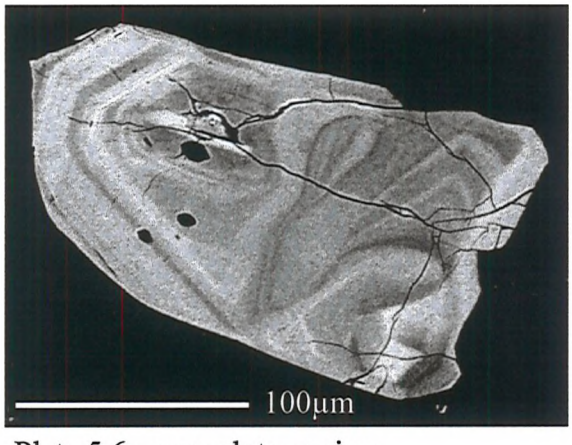

Plate 5.6 - convolute zoning

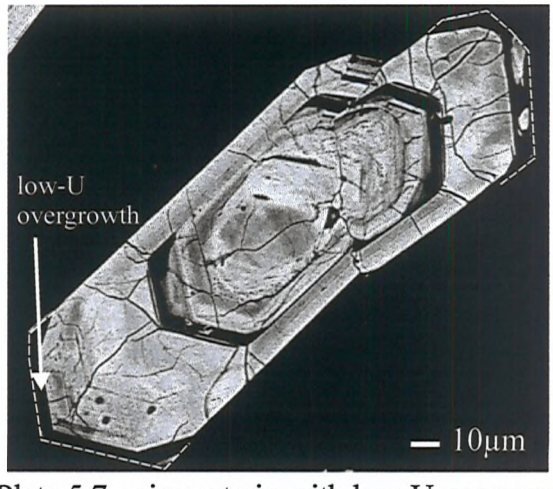

Plate 5.7 - zircon twin with low-U overgrowth

Table 5.2*

GEOMETRY AND INTERPRETATION OF ZIRCON ZONATION PATTERNS UNDER BSE AND CL IMAGING
1) Concentric zoning a) euhedral zones, commonly finely oscillatory - igneous growth during a single episode - widely spaced or diffuse - low zircon supersaturation in melt (Plate 5.1) - closely spaced - high zircon supersaturation in melt (Plate 5.5) b) rounded cores - multiple episodes of metamorphic growth
2) Distinct anhedral cores - core is inherited, truncation of core represents resorption or abrasion surfaces; rim represents a new stage of growth (Plates 5.3a & 5.4)
3) Multiple, euhedral discrete cores - igneous clustering (synneusis)
4) Euhedral rims - final growth in melt or fluid
5) Rounded, multifaceted rim zones - final growth during metamorphism
6) Truncation of interior zones a) high-angle truncations - fracture surfaces, either from sedimentary transport or cataclasis b) low-angle truncations - may result from sedimentary abrasion (rounding) or resorption (igneous, metamorphic or fluid) c) embayments - resorption; may indicate site of a totally resorbed inclusion or an arrested stage of rapid growth.
7) Sector zoning - relatively rapid igneous growth
8) Patchy and/or unzoned zircon with or without complex outer boundaries - recrystallisation (Plates 5.2a&b)
9) Highly irregular, curving, thin zones that pinch out (includes fillings of embayments) - unknown origin (Plate 5.6)
10) Cracking a) radial - decay of high-U zone or core with expansion against external low-U zone (Plates 5.3a&b & 5.4) b) concentric - decay of high-U zone with expansion against internal low-U zone

(*adapted from Table 1 in Hanchar & Miller, 1993)

During crystallisation of zircon, U^{4+} and Th^{4+} are taken into the lattice structure of the crystal, substituting for Zr^{4+} by virtue of a similar size/charge ratio (see Table 5.1). As the magma cools beyond the blocking temperature of zircon (>900°C, Lee *et al.*, 1997), the amount and ratio of the substituting elements remain fixed. With time ^{238}U and ^{235}U decay to ^{206}Pb and ^{207}Pb with half-lives of $4.46x10^{9}y^{-1}$ and $7.04x10^{8}y^{-1}$ respectively (Faure, 1986). Pb^{2+} (1.29Å) does not fit into the Zr^{4+} (0.84Å) site and may leave the crystal under suitable conditions. This Pb-loss is usually partial but if complete, total resetting of the U-Pb geochronometer results.

^{232}Th decays to ^{208}Pb with a half-life of $1.4x10^{10}y^{-1}$. Th^{4+} is not included in as high concentrations as U^{4+} and is therefore usually not considered in geochronometric studies of zircon. However, in younger terrains such as the Alps and Himalayas, excess ^{230}Th, a daughter nuclide in the ^{238}U-^{206}Pb decay scheme, included in the crystal structure during crystallisation, results in U-Th-Pb disequilibrium. This excess Th has to be corrected for in young lithologies for the true U-Pb age to be realised. In older rocks, decay of ^{238}U over time equilibrates any discrepancies caused by excess ^{230}Th.

5.3.2) Concordia, Discordia and the role of Pb-loss - are zircons forever?

Wetherill (1956a&b) devised the concordia diagram (Fig.5.1) to exhibit, on a single diagram, three radioisotopic ratios ($^{206}Pb/^{238}U$; $^{207}Pb/^{235}U$; $^{207}Pb/^{206}Pb$) attainable from zircon, in order that cross correlation could be used to investigate the rigidity of the data. In essence it shows the evolution of the radiogenic isotope ratios with time and illustrates the effect that Pb-loss (discordance) has on the system.

From Table 5.1 it can be seen that the difference in size/charge ratio between Zr^{4+} and Pb^{2+} is very significant and is the reason Pb is largely excluded from the structure of a growing zircon crystal. Conversely, this is also the reason for many of the problems of analysis related to this technique, due to loss of radiogenic-Pb from the lattice during metamorphism and/or alteration. Pb-loss in zircons is usually only a partial process, not all the Pb is lost, but can cause a large decrease in the Pb/U ratio. The U-Pb data from zircons plotted on a concordia diagram, can be interpreted to provide information on not only their age, but also the history of the zircon since its crystallisation (see Fig.5.1). A fairly comprehensive review of concordia diagrams and the conditions under which Pb-loss occurs was recently presented by Mezger & Krogstad (1997) to which the reader is referred since

Figure 5.1 - Pb-loss mechanisms on concordia diagrams

(relevant references - Tilton (1960); Wetherill (1963); Mezger & Krogstad (1997); Steiger & Wasserburg (1969))

1) Episodic Pb-loss

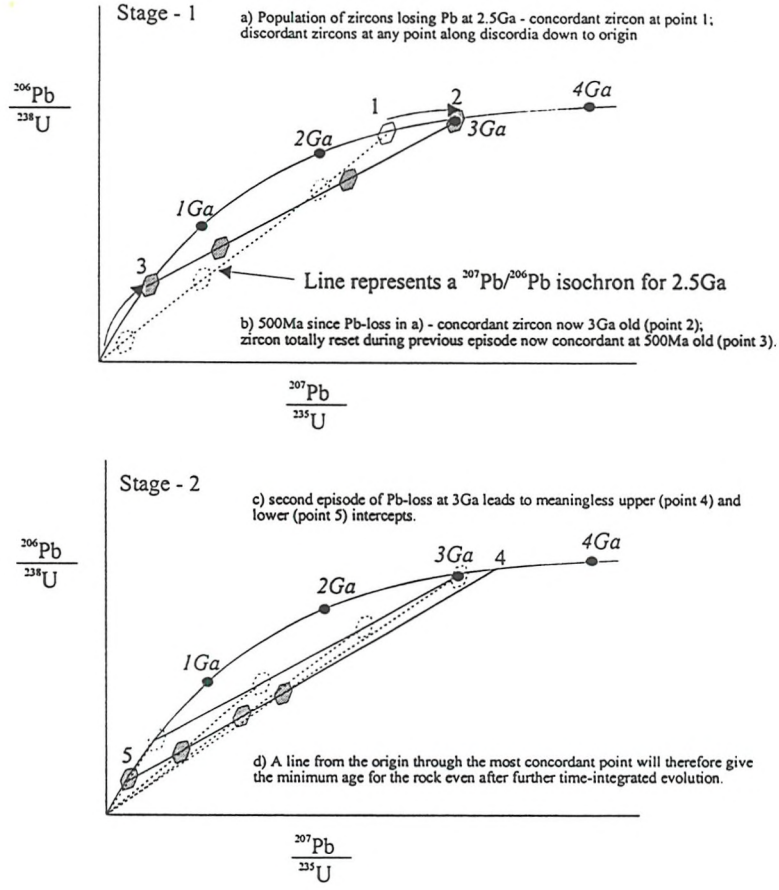

2) Episodic Pb-loss superimposed on continuous Pb-loss by volume diffusion

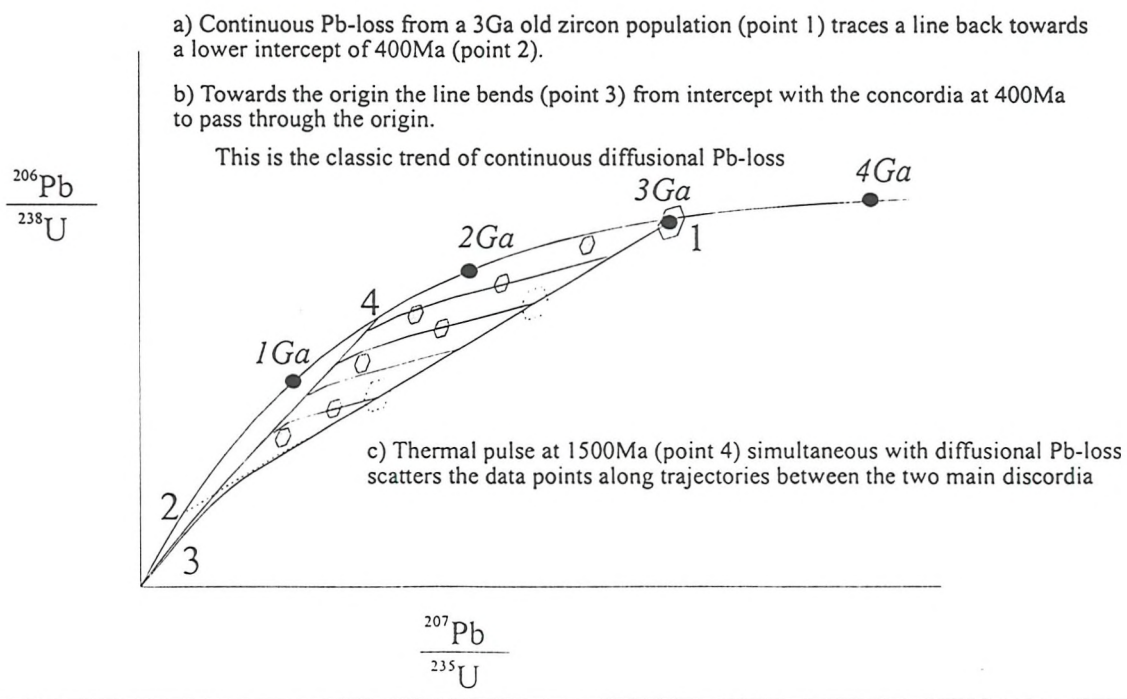

any explanation here would simply be a duplication. However, Figure 5.1 is provided as an illustration and quick reference to the interpretation of this fundamental diagram.

Mezger & Krogstad (1997) concluded that there are four important temperature domains in the history of a zircon crystal. At <600°C, below the annealing temperature of zircon, metamictisation occurs through destruction of the lattice by α-emission and fission processes, allowing Pb-loss by alteration, leaching (including weathering, Stern *et al.*, 1966) and possibly even diffusion from the metamict material. At ~600-650°C annealing of the damaged lattice causes significant Pb-loss by exclusion. This is usually only partial, rather than completely resetting the geochronometer. Between 650-1000°C no appreciable Pb-loss occurs since Pb diffusion within the pristine crystal lattice is too slow, but at temperatures >1000°C this may become possible. Another domain at temperatures even higher than this may well be added in consideration of the dissolution/resorption, reprecipitation and consequent total resetting of the U-Pb clock which can occur at very high metamorphic grades and melting events. However, also noted was the fact, so infuriating to zircon geochronologists, that these enigmatic crystals "seem to lose Pb for no apparent geological reason"! They also concluded that the interpretation of lower intercept ages on concordia diagrams is at best ambiguous. Placing trust in such an interpretation is highly speculative, especially since other geochronological systems using other minerals are much better at highlighting the age of the metamorphic or alteration event which caused the Pb-loss.

It is for reasons of establishing concordance that it is particularly important to consider which analytical technique is employed in determining the ratios necessary to date zircons. A number of techniques are currently being used and a brief discussion of each will now follow.

5.3.3) Analytical techniques employed in U-Pb zircon geochronology

The **Kober** technique (Kober, 1986) uses a single zircon, wrapped in a Re boat (two Re filaments encapsulating the grain), as the source during thermal ionisation mass spectrometry (TIMS). The principle is to step-heat the zircon in a two-stage process, to a temperature at which the emitted $^{207}Pb/^{206}Pb$ ratio is constant. The Pb is 'evaporated' from the zircon without changing the isotope ratio as the evaporation front progresses through the crystal. During the first 'conditioning' stage, the $^{207}Pb/^{206}Pb$ ratio fluctuates, a feature

attributed to loosely bound Pb at the margin of the zircon - either due to enclosed common-Pb, or radiogenic-Pb leaving the damaged zircon structure. After this has burnt off, the temperature is increased until the emitted $^{207}Pb/^{206}Pb$ ratio reaches a constant value. More than one 'plateau' value may be obtained and these can be interpreted to represent more than one phase of crystallisation within the zircon. To resolve multiple phases however, requires shorter periods of analysis to prevent averaging of the isotope ratios from different sectors, and this inevitably compromises precision (Dougherty-Page & Foden, 1996).

The main benefits of the technique are that very little preparation of the sample is required - no chemistry or abrasion is involved - and the use of TIMS allows very precise data to be collected with relative speed and efficiency. This technique therefore enables quick and relatively easy access to precise geochronological data. The major drawback to the method however, is that only $^{207}Pb/^{206}Pb$ ratios can be collected and hence concordancy has to be assumed. In reference to Figure 5.1, it can be seen that a discordant zircon will inevitably yield a Pb/Pb ratio which indicates an age too young for the zircon unless zero age Pb-loss has occurred (e.g. weathering). Dougherty-Page & Foden (1996) argue that this can be taken into account and the concordancy of the zircon verified by the stability of the analysed ratio; conditioning of the grain prior to data collection increases concordancy by removing metamict material and assumption of concordance is valid if several heating steps reproduce the same age.

Also, this technique is indiscriminate of the internal three-dimensional structure of the crystal. From the discussion above, consideration of the internal form of the zircon is seen to be vital. Areas of recrystallisation, resorption and differences in width within any particular sector will all affect the result since the evaporation of the grain takes place uniformly from the outside in, only increasing along cracks in the grain which themselves allow access to sectors of the crystal which may not relate to the rest of the zircon through which the evaporation front is moving (Chapman & Roddick, 1994). Dougherty-Page & Foden (1996) have resolved these problems by employing an increased number of heating steps of shorter duration and selecting crack-free grains, and have shown that it is possible to use the evaporation technique to obtain a primary magmatic age from zircons known to contain xenocrystic components.

A new technique in U-Pb analysis is **Energy-dispersive Miniprobe Multielement Analyser** (EMMA). This system is "basically a desktop miniprobe XRF" (Cheburkin *et al.*, 1997), for the "analysis of trace elements in single mineral grains". It has detection limits U, Th and Pb ~10ppm and is a non-destructive, rapid (3-6mins per analysis) technique requiring virtually no sample preparation. It has a relatively small spatial resolution (<50μm) and an instrumental intragrain reproducibility of no greater than ±4% (less than the inter-grain chemical variability usually exhibited by zircons). However, one major drawback is that the instrument cannot resolve the difference between radiogenic and common-Pb since it does not measure the isotopic ratios, only the concentrations of the elements. Some appreciation of the common-Pb content can be achieved by plotting U concentration against total Pb. The intercept on the y-axis is interpreted as the amount of common-Pb in ppm, but with understanding of the intricacies of zircon form and composition ever increasing, complexities irresolvable by the EMMA technique, may yet prove to be too limiting. The results from this technique represent maximum formation ages due to the common-Pb problem. This is less of a problem in zircon work, where the amount of common-Pb is minimal, than it is for minerals such as monazite which include Pb during crystallisation. This equipment finds a niche in high-volume reconnaissance work, providing cheap and rapid 'ball-park' indicators for mineral ages. This can then be followed up using more expensive and time-consuming but precise methods.

Step-wise Pb leaching (Frei & Kamber 1995) is a technique used to selectively discriminate between radiogenic and common-Pb in order to increase the precision of the data. A series of acid digestion steps are performed, involving HBr, HCl, HNO_3 and HF acids. After each step the leachate is taken and prepared for TIMS analysis, resulting in a set of data for one crystal representing the isotopic composition of different U-Pb domains within the crystal. The data can then be compiled to give a precise age for the crystal, including discriminating between zircon of different ages.

Sensitive High Resolution Ion Microprobe (SHRIMP) (Compston *et al.*, 1986) is the most precise high-spatial resolution technique for U-Pb geochronology of accessory minerals currently available. It combines an ion-beam spot size of ~20μm with precision of <5%. Because of cost, this equipment is of limited availability. It also suffers from the fact

that the ion beam produces a number of ionic and molecular species which have to be corrected for, necessitating a significant amount of data manipulation. However, this technique is currently favoured by most because of the precision, spatial resolution and relatively rapid data acquisition.

Laser-Ablation Inductively Coupled Plasma Mass Spectrometry (LA-ICP-MS) (Hirata & Nesbitt, 1995), is a relatively new technique and rapid improvements are being made in its development as a mainstream method of data acquisition. The benefits of this method include limited sample preparation time, rapid analysis (10sec period of acquisition) and hence low cost per analysis, a high spatial resolution (~10-20μm) and good precision (~3% RSD (1σ) $^{207}Pb/^{206}Pb$).

Limitations of this technique currently include the apparent intragrain variability of the U concentration and U-Pb fractionation during analysis, causing variable Pb/U ratios. This, in conjunction with noted heterogeneities in the concordancy of individual spot-analyses within a single grain (Schärer & Allègre, 1982; Williams *et al.*, 1984), causes the Pb/U ratios to exhibit 10-20% precision (1σ). Intragrain heterogeneities are also a problem for the SHRIMP technique but these heterogeneities are precisely resolvable by this method whilst with laser-ablation they simply add to the problem of fractionation. Also problematic at the moment is the control of penetration rate by the laser. The question of 3-D resolution is a problem because the lasers currently utilised (UV Nd:YAG) for the analysis ablate the zircon at such a rate that multiple phases of zircon may be sampled in the duration of a single acquisition. Decrease of power limits penetration but also decreases the amount of material ablated and therefore results in decreased precision due to detection and background problems.

Mercury provides a problem for the common-Pb correction. ^{204}Hg constitutes 23% of atomic Hg and must be subtracted from the ^{204}Pb analysis. This should mean that the ^{204}Pb analysis is reduced to zero since in theory no common-Pb is contained in zircons. However, background ^{204}Pb is present and results in a remnant common-Pb remaining after correction for Hg. This remnant can be corrected for by subtracting the average value for the detection limit calculated after analysis of 20 gas blank ratios acquired just prior to the zircon data. This should then cancel out any necessity for a common-Pb correction. However, some zircons do contain common-Pb but the correction process described above, followed by correction of the

$^{206}Pb/^{204}Pb$ and $^{207}Pb/^{204}Pb$ ratios for this remnant common-Pb, will result in the correct U-Pb and radiogenic Pb-Pb ratios for the zircon. Unfortunately this does not totally solve the problem. Due to variations in the background intensity of ^{204}Pb at any point in time, the detection limit correction for background Pb may be too high or, more seriously, too low for any one analysis. If the detection limit value used in the correction is too high, the calculated common-Pb content becomes negative and this is simply defaulted to zero, indicating no common-Pb correction. If however, the detection limit calculated prior to acquisition of the zircon data is lower than that present at the time of analysis, the correction will not get rid of all the background ^{204}Pb and this will be used in the common-Pb corrections, thereby biasing the final ratios. Some zircons do appear to contain Hg. This is either contained in their structure or, most likely, results from processing of the sample to separate the zircons. Heavy liquid separation using di-iodomethane (methylene iodide) is the likely culprit and indicates that the grains must be washed in HNO_3 acid before analysis in the same way as those prepared for ID-TIMS dissolution (see Appendix A). The presence of significant quantites of Hg is not ideal and hinders accurate correction.

The main benefit of LA-ICP-MS is however, the ability to detect U and Pb isotopes simultaneously, meaning that a concordia plot can be generated and the concordancy of the zircon assessed. This is a significant advantage over the Kober and EMMA techniques and with continued development, some of the problems with this technique will hopefully be solved thereby providing ready access to reliable geochronological data.

Isotope Dilution Thermal Ionisation Mass Spectrometry (ID-TIMS) (Krogh, 1973), or the 'conventional' method of dating as it is commonly called, is still considered the best technique for U-Pb geochronology of accessory minerals. It is the most precise method but is *very* labour intensive. Improvements in the procedure in recent times include magnetic separation and air-abrasion of the crystals before dissolution to remove any metamict, altered or second phase zircon material (Krogh 1982a&b), in order to increase the concordancy of the final analysis. Laboratory apparatus and procedure must be meticulously clean to extract the best results from this method. This tried and trusted technique formed the mainstay of the geochronology conducted for this thesis, and was performed at the NERC Isotope Geosciences Laboratory (NIGL), one of the world's leading laboratories in the execution of

this process. A full description of the method and procedure employed can be found in Appendix A.

PART 2 - ZIRCON GEOCHRONOLOGY OF THE MIDLANDS GREENSTONE BELT AND RELEVANT REGIONAL GRANITOIDS

5.4) INTRODUCTION

Having discussed the intricacies of zircon systematics, this section will describe the samples used for and data resulting from U-Pb zircon geochronology by isotope dilution-thermal ionisation mass spectrometry (ID-TIMS), conducted over a period of 7 months at the NERC Isotope Geoscience Laboratory (NIGL), Keyworth, Nottingham, under the guidance of Dr.Steve Noble. This data will be interpreted with regard to BSE imaging conducted on these samples and a final conclusion given for the age of the rock and its magmatic and metamorphic history. The relevance to the regional geological interpretation will be discussed in Chapter 6.

The samples selected for dating were chosen for their stratigraphic importance or, as in the case of the Sebakwe River Gneiss, simply to find out where in the stratigraphic column it belonged. Five samples were selected from the Midlands Greenstone Belt and four from other regionally important lithologies. These are tabulated below, their grid references given in Appendix F and their field details described below.

Zircon samples from the Midlands Greenstone Belt

Sample number	Lithology
Zimb.95/02	Sesombi Tonalite
Zimb.164	Giraffe Porphyry
Zimb.150	Dacitic volcanic from the Mafic Formation
Zimb.141	Sebakwe River Gneiss (Phase 2)
Zimb.226	Rhodesdale Granitoid/Kwekwe Gneiss

Zircon samples from regional granitoids within the Zimbabwe Craton

Sample number	Lithology
Zimb.95/06	Chilimanzi Granite
Zimb.95/09	Leucosome within Tokwe Gneisses
Zimb.95/14	Tokwe River Gneiss
Zimb.95/29	Chingezi Suite Granitoid

5.5) SAMPLE DESCRIPTION

5.5.1) The Rhodesdale Granitoid/Kwekwe Gneiss - Zimb.226

This multi-component granitoid forms the basement east of the Midlands Greenstone Belt volcanics (see Fig.3.1) and has been described previously (see section 3.2.6 and Plate 3.8). It is comprised of a number of tonalite-trondjhemite-granodiorite (TTG) and gneissic units of different chronologies. The main phase constituting the batholith has been dated at ~2.9Ga (Pb-Pb, Taylor *et al.*, 1991) and has conventionally been considered a member of the *c.*2.9Ga Chingezi Suite (Wilson, 1979). It contains remnants of a previous greenstone episode which are considered to be all that remains of the L1-L4 Belingwean stratigraphy in the Midlands region (Wilson *et al.*, 1995). The sample used in this study was collected approximately 2.6km into the granitoid mass from the contact with the greenstone belt and is therefore technically from the Kwekwe Gneiss as mapped by Harrison (1970). It is granitic to granodioritic in composition and exhibits recrystallisation of quartz and feldspar reflecting a small amount of strain.

Six zircons were selected for analysis, comprising two morphologies: one oblate prismatic, the other rods with aspect ratios of 3-4:1 (see Table 5.3).

5.5.2) The Sebakwe River Gneiss - Zimb.141

This gneissic unit is of limited regional extent, being found in an 800m section of the Sebakwe River approximately 2.1km west of the contact of the greenstone belt volcanics and the Rhodesdale Granitoid. It therefore does not form part of a region-wide intrusive phase.

It is a complex unit of unknown chronology which has, until now been un-named and largely ignored except for brief descriptions given in the bulletins of the Zimbabwe Geological Survey (Harrison, 1970; Campbell & Pitfield, 1994). Of the three phases present, Phase 2 is considered to represent the main magmatic event forming this unit and was dated for this reason. It is dioritic in composition.

Seven zircons were selected for analysis, their morphologies including oblate prismatic, rods with aspect ratios of 3:1 and amorphous fragments. Two of the oblate prismatic grains were distinctly mauve in colour.

5.5.3) Tokwe River Gneiss - Zimb.95/14

Zircons were also extracted from a sample of the Tokwe River Gneiss and a leucosome component sampled from within the Tokwe Gneisses of the Tokwe Segment, in order that a good zircon date could be obtained for the Tokwe Segment and the results from the Midlands Greenstone Belt compared with the oldest rocks so far known in the craton.

The Tokwe River Gneiss has been described and dated by Hawkesworth *et al.* (1975) using the Rb-Sr method and by Taylor *et al.* (1991) using the same samples for a Pb-Pb determination. The sample used in this study was collected separately and is petrographically a foliated quartz, plagioclase, biotite gneiss with development of subhedral epidote and a little chlorite replacing biotite. The locality details for this sample are given in Appendix F.

Five zircons were selected ranging from colourless to mauve, transparent or translucent, fragments and needles. The description of each grain is recorded in Table 5.3.

5.5.4) Leucosome of Tokwe Gneiss - Zimb.95/09

This leucosome component was present within the Tokwe Gneisses of the Tokwe Segment and as such represents either a melt pod from migmatisation of the gneisses or the result of a melting/metamorphic event affecting the Sebakwian rocks now included as xenoliths within the Tokwe Gneisses. The locality details are given in Appendix F but unfortunately no material for petrographic study was available.

Eight zircons were selected for analysis each having a distinct translucent red-brown colour and bipyramidal to oblate prismatic morphology, save one which exhibited a transparent pink-brown colour and was a sub-circular, flat fragment.

5.5.4) 'Chingezi Suite' Granitoid - Zimb.95/29

As one of the main regionally intrusive suites forming the chronological framework of the craton, a sample of the Chingezi gneisses was sampled and dated (see Appendix F for locality details). Petrographically it is not a gneiss. Euhedral plagioclase crystals 1-3mm in size are randomly arranged within a quartz groundmass and exhibit simple albite twins with sericitisation of their more Ca-rich centres. The quartz crystals are strained, exhibiting complex polycrystalline arrangements with serrated edges to the sub-grains. Heavily chloritised biotite crystals are deflected around quartz and feldspar. Some epidote and

muscovite is apparent which along with the sericitisation, indicates a low-grade greenschist metamorphic overprint. Evolution of the magma during crystallisation is indicated by albite margins to the plagioclase and development of microcline as a mesostasis mineralogy in pockets of melt trapped interstitial to quartz and plagioclase. This is taken to indicate a fairly closed system of crystallisation with a granitic magma evolving from a tonalite to a granodiorite.

Five zircons were dissolved for analysis, two of which were small (50x20μm) rods or stubs with aspect ratios of ~3:1 and three of which were ovoid or sub-spherical, polygonal grains.

5.5.5) Chilimanzi Granite - Zimb.95/06

This suite is the youngest intrusive granitoid suite in the Zimbabwe Craton and signifies stabilisation of this continental crustal block through anatexis of pre-existing crustal material. To date, the most precise age for this event is 2601 ± 14Ma (Jelsma, 1993) obtained by multi-grain analysis of zircons. Sampling of this suite (see details in Appendix F) allows a complete stratigraphic framework to be constructed with some of the main regional granitoids included for comparison with ages published by other workers.

Petrographically, this sample is similar to the Chingezi sample but more evolved, being classified as a granite *sensu stricto*. More K-feldspar is present in the form of orthoclase and microcline with plagioclase being significantly reduced when compared to Zimb.95/29. This increase in K is also exhibited in the increased development of biotite mica. Quartz is ubiquitous and is often occluded in K-feldspar. Minor epidote coupled with sericitisation of the plagioclase, illustrates the low-grade greenschist facies overprint. Exsolution of orthoclase to perthite is also occurring.

Nine crystals were chosen for dissolution, six possessing a tear-drop shaped or rounded morphology, two being needle fragments and one a small grain with a simple, tetragonal shape.

5.5.6) Giraffe Porphyry - Zimb.164

This intrusive stock has been described earlier (see section 3.2.8 and Plate 3.10a) and is a member of the Late Porphyries thought to have been intruded at the very end of the

Maliyami Formation volcanism. As such, it should provide a very good constraint for the end of the Upper Bulawayan in the Midlands Greenstone Belt.

Four zircons were selected for analysis all of which were pink-brown in colour and of simple tetragonal morphology.

5.5.7) Sesombi Tonalite - Zimb.95/02

This well known granitoid, described in section 3.2.7, has been dated by others (Hawkesworth *et al.*, 1975; Taylor *et al.*, 1991; Dougherty-Page, 1994), each using a different technique (Rb-Sr; Pb-Pb WR & Pb-Pb Kober respectively). A U-Pb zircon age should therefore provide a definitive age as well as a good comparison between the four different techniques.

Two separate batches of zircons were run for this sample. All zircons were pink or pink-brown in colour with a simple, tetragonal morphology. They proved to be particularly hardy crystals in the face of air abrasion with pyrite, taking many hours to abrade satisfactorily, and as such were considered good candidates for precise, concordant data.

5.5.8) Dacitic volcanic from the Mafic Formation - Zimb.150

The recognition of intraformational felsic volcanics in the Mafic Formation volcanic succession provides an unparalleled opportunity to record a direct, absolute age for this sequence. Thought to represent the lower-Upper Bulawayan in the Midlands Greenstone Belt, the extraction of zircons from this sample potentially allows the exact relationship to the rest of the volcanic stratigraphy to be determined.

Petrographically, this dacitic volcanic is a lithic-tuff. It has suffered sericitisation and carbonatisation often in the form of rhombic dolomite crystals.

Seven zircons were dissolved and analysed, all with morphologies varying little from a simple, tetragonal theme.

5.6) RESULTS AND DATA DISCUSSION

The U-Pb ID-TIMS results will now be discussed and compared with BSE images for the sample when present. It should be noted that the images provided are not images of the grain prior to analysis but members of the same (or different) populations simply illustrating

the features present in these grains. Also, none of the grains are precisely orientated although most images represent sections parallel to the *c*-axis and the prism faces.

The data have all been reduced and regressed using the Pbdat and Isoplot programs of Ludwig (1980). All common-Pb has been corrected for and removed with the composition of the laboratory blank determined at the time of analysis (see Table 5.3). Justification for this is two-fold; 1) according to U-Pb geochronological theory for zircon, Pb is excluded during its formation and therefore should not be present (This has been shown not to be totally correct especially for hydrothermal zircons (Watson *et al.*, 1997)); 2) procedural blanks during the time the samples were prepared, were very variable due to a reduction in the extraction efficiency of the laboratory fume-hood and degradation of the hotplate coating. This resulted in procedural blanks as low as 2.5pg (representative of the normal level of fall-in common-Pb) and as high as 164pg! All common-Pb measured was therefore removed as laboratory blank with any small remainders being removed using a Stacey & Kramers (1975) model-Pb composition relevant to the projected age of the sample. All errors quoted are 2σ unless stated otherwise.

Most of the samples show lower intercepts on concordia around 900Ma and lower. This is considered to be either a result of continuous Pb-loss by volume diffusion (Tilton, 1960) or a function of the interplay of a number of complex Pb-loss events. Mezger & Krogstad (1997) give a complete discussion of the reasoning behind this conclusion and the reader is referred here for further explanation. As such, no geological significance is applied to the lower intercepts of any of the samples and will therefore not be considered further.

5.6.1) The Rhodesdale Granitoid/Kwekwe Gneiss - Zimb.226 (Fig.5.2)

Figure 5.2a presents the concordia diagram for this granitoid mass. No BSE images were available. Sample blank common-Pb values varied from 14.07-110.82pg thereby causing low $^{206}Pb/^{204}Pb$ ratios of 142 to 656. Of six points analysed, five have been regressed to give an age of 3456 ± 6Ma with an MSWD = 1.4. One point has been excluded (but still plotted in Fig.5.2) on the basis of its discordancy and lack of co-linearity with the rest of the grains. Inclusion in the regression leads to an age of 3467 ± 33Ma and an MSWD of 5.2. Although other points are equally, and indeed more discordant and no analytical reason for exclusion can be forwarded, it is considered that this increased MSWD indicates the influence of factors other than those analytical (Wendt & Carl, 1991; Kalsbeek, 1992; Wendt, 1992)

TABLE 5.3 - REDUCED DATA FOR U-Pb ID-TIMS ZIRCON GEOCHRONOLOGY OF ZIMBABWEAN SAMPLES (ANALYSED 1997)

			Concentrations†				Atomic Ratios				Ages			Errors				
Fraction*	Fraction Description~	Weight (µg)	ppm U	ppm Pb	pg common Pb	206/204§ (raw)	206*/238# (rad.)	207*/235# (rad.)	207*/206*# (rad.)	206*/238 Age (Ma)	207*/235 Age (Ma)	207*/206* Age (Ma)	206*/238 %err	207*/235 %err	207*/206* %err	Rho 6/8-7/5	discordance‡ %
Sebakwe River Gneiss - Zimb.141																	
z141-27	rod/stub; ar = 3:1	1.3	241.3	174.2	20.38	539	0.567137	23.3718	0.298885	2896	3243	3464.5 ± 2.1	1.08	1.10	0.14	0.992	25.6
z141-31	amorphous fragment	1.9	39.6	35.1	15.15	223	0.700109	30.5412	0.316387	3421	3504	3552.4 ± 3.2	2.71	2.74	0.21	0.997	5.6
z141-25	mauve, oblate prism	2.6	109.2	92.7	12.29	933	0.690048	30.0321	0.315650	3383	3488	3548.8 ± 1.8	0.63	0.64	0.12	0.983	7.1
z141-23	oblate prism	2.0	98.0	82.0	7.84	951	0.683346	29.3789	0.311813	3357	3466	3529.9 ± 1.8	0.59	0.60	0.12	0.981	8.5
z141-24	oblate prism	1.5	206.6	173.7	7.79	1514	0.691419	29.8542	0.313157	3388	3482	3536.6 ± 1.7	0.41	0.43	0.11	0.967	7.2
z141-26	rod/stub; ar = 1.5:1	1.7	3184.4	353.0	10.89	2268	0.079939	3.4399	0.312096	496	1514	3531.3 ± 1.7	0.36	0.38	0.11	0.958	89.3
z141-22	mauve, oblate prism	1.5	164.0	129.7	155.49	84	0.664425	28.5999	0.312189	3284	3440	3531.8 ± 8.9	9.51	9.65	0.58	0.998	11.0
Tokwe River Gneiss - Zimb.95/14																	
95/14-15	mauve, transl. fr	1.0	208.6	168.1	2.68	2327	0.691218	28.1586	0.295457	3387	3425	3446.6 ± 1.7	0.34	0.36	0.11	0.955	2.8
95/14-17	mauve, transp. needle fr	0.8	307.8	197.4	7.27	1070	0.575601	21.7094	0.273543	2931	3171	3326.5 ± 1.8	0.51	0.53	0.12	0.975	22.0
95/14-19	pink-mauve, transp. needle	1.0	360.2	239.1	3.24	2867	0.562480	21.7734	0.280749	2877	3174	3367.1 ± 1.7	0.27	0.29	0.11	0.931	22.9
95/14-18	mauve, transp. needle	1.0	669.2	418.5	22.18	1005	0.546694	21.0350	0.279060	2811	3140	3357.7 ± 1.9	0.61	0.63	0.12	0.982	25.2
95/14-20	colourless transp. needle fr.	1.0	261.4	210.8	10.73	976	0.693943	28.3167	0.295950	3398	3430	3449.2 ± 1.8	0.64	0.65	0.12	0.984	2.3
Rhodesdale Granitoid/Kwekwe Gneiss - Zimb.226																	
z226-12	oblate prism	1.2	354.5	241.1	53.47	289	0.550033	21.2258	0.279881	2825	3149	3362.3 ±3.2	2.14	2.19	0.21	0.996	24.7
z226-30	rod; ar = 4:1	1.4	287.5	120.4	40.60	229	0.346922	11.0809	0.231655	1920	2530	3063.5 ± 6.5	2.73	2.88	0.41	0.991	56.5
z226-14	rod; ar = 4:1	0.9	961.4	391.5	88.33	237	0.358293	11.2141	0.226999	1974	2541	3031.0 ± 6.7	2.69	2.85	0.42	0.990	55.5
z226-10	oblate prism	1.2	215.0	157.1	14.07	656	0.598364	23.5424	0.285354	3023	3250	3392.5 ± 2.0	0.87	0.89	0.13	0.989	17.3
z226-11	rod; ar = 4:1	1.0	548.7	283.5	110.22	142	0.399686	13.7424	0.249370	2168	2732	3180.8 ± 8.9	4.83	5.04	0.56	0.994	48.2
z226-13	rod/stub; ar = 3:1	0.7	576.0	405.8	47.10	319	0.569783	22.2461	0.283167	2907	3195	3380.5 ± 2.9	1.92	1.95	0.19	0.996	21.6
Leucosome of Tokwe Gneiss - Zimb.95/09																	
95/09-09	rbrown, transl. bipyr.	12.1	262.8	198.6	5.52	19216	0.647620	24.9426	0.279332	3219	3306	3359.2 ± 1.6	0.37	0.38	0.11	0.962	5.9
95/09-10	rbrown, transl. bipyr; ar=5:1	7.7	239.6	174.7	5.73	10516	0.629586	24.0342	0.276868	3148	3270	3345.4 ± 1.6	0.20	0.23	0.11	0.887	8.9
95/09-11	rbrown, transl., oblate prism	5.5	263.9	203.8	62.46	968	0.664817	25.6200	0.279496	3286	3332	3360.1 ± 1.8	0.63	0.65	0.12	0.983	3.4
95/09-12	pbrown, transp. sub-circ. flat fr.	7.5	215.0	167.9	2.50	18285	0.673448	26.0248	0.280274	3319	3347	3364.5 ± 1.6	0.25	0.28	0.11	0.925	2.0
95/09-13	rbrown, transl., oblate prism	16.3	257.0	253.7	9.14	21612	0.848998	32.7598	0.279855	3962	3573	3362.1 ± 1.6	0.25	0.27	0.11	0.921	-23.5
95/09-14	rbrown, transl. bypyr; ar = 1.5:1	5.1	291.9	219.0	5.67	8731	0.642787	24.6608	0.278253	3200	3295	3353.2 ± 1.6	0.19	0.22	0.11	0.874	6.8
95/09-16	rbrown, transl, oblate prism	5.3	225.4	174.3	2.87	12137	0.664096	25.5245	0.278756	3283	3329	3356.0 ± 1.6	0.22	0.24	0.11	0.900	3.6
95/09-28	rbrown, transl. prism	11.3	292.9	224.5	8.89	13508	0.656248	25.3063	0.279678	3253	3320	3361.1 ± 1.6	0.23	0.25	0.11	0.909	4.6
Dacite of Mafic Formation - Zimb.150																	
z150-13	tetragonal prism	0.5	143.6	96.7	13.49	192	0.557112	15.7814	0.205448	2855	2864	2870.0 ±5.6	3.07	3.12	0.34	0.994	1.4
z150-12	tetragonal prism	0.6	172.5	84.1	12.95	208	0.406649	11.6351	0.207515	2200	2576	2886.2 ± 5.1	2.81	2.85	0.31	0.994	27.7
z150-09	tetragonal prism	1.0	91.1	58.9	5.54	496	0.558992	16.0092	0.207713	2862	2877	2887.8 ± 3.2	1.01	1.03	0.20	0.982	0.5
z150-10	tetragonal prism	0.7	139.3	88.8	12.54	260	0.535465	15.2714	0.206846	2764	2832	2881.0 ± 4.3	2.20	2.23	0.26	0.993	4.9
z150-11	tetragonal prism	1.8	95.4	63.1	8.20	662	0.558457	15.9473	0.207107	2860	2874	2883.1 ± 2.4	0.81	0.83	0.15	0.984	0.8
z150-14	tetragonal prism	1.1	169.4	104.5	14.91	393	0.512971	14.6129	0.206606	2669	2790	2879.1 ± 3.1	1.41	1.43	0.19	0.991	8.9
z150-28	tetragonal prism	0.6	172.0	100.0	22.78	153	0.492277	14.0314	0.206724	2581	2752	2880.0 ± 7.0	4.13	4.18	0.43	0.995	12.6

TABLE 5.3 (continued)

'Chingezi Suite' Granitoid - Zimb.95/29																	
young																	
z95/29-12	sub-spherical, polygonal	0.5	84.7	48.5	11.66	127	0.511558	12.8673	0.182427	2663	2670	2675.1 ± 9.5	4.94	5.00	0.58	0.993	0.3
z95/29-10	oblate prism	0.5	281.4	135.1	38.38	113	0.419123	10.2629	0.177593	2257	2459	2630.5 ± 12.0	6.02	6.12	0.73	0.993	19.4
z95/29-11	oblate prism	0.5	285.3	146.3	22.92	193	0.465458	11.4941	0.179099	2464	2564	2644.6 ± 6.6	3.14	3.19	0.40	0.992	10.1
old																	
z95/29-14	needle fr;ar = 3:1	0.5	650.7	338.1	26.56	352	0.450268	12.2171	0.196787	2396	2621	2799.7 ± 3.6	1.65	1.68	0.22	0.992	20.4
z95/29-09	stub; ar = 2.5:1	0.5	446.3	217.8	56.87	122	0.426762	11.4696	0.194922	2291	2562	2784.1 ± 9.7	5.56	5.65	0.60	0.995	24.9
Chilimanzi Granite - Zimb.95/06																	
95/06-13	oblate prism	1.0	227.4	148.5	21.18	362	0.535533	13.2958	0.180064	2765	2701	2653.5 ± 5.9	1.60	1.65	0.35	0.977	-6.7
95/06-22	oblate prism	1.0	77.1	56.5	5.07	405	0.496537	12.2557	0.179013	2599	2624	2643.8 ± 4.4	1.21	1.24	0.27	0.977	1.3
95/06-23	oblate prism	1.0	291.5	162.4	26.31	319	0.448925	10.9786	0.177367	2390	2521	2628.4 ± 4.6	1.82	1.85	0.27	0.989	11.2
95/06-24	oblate prism	1.0	246.3	131.9	17.95	375	0.438282	10.7364	0.177666	2343	2501	2631.2 ± 3.9	1.51	1.54	0.24	0.988	13.2
95/06-25	needle fr; ar = 4:1	1.0	130.3	56.1	14.75	182	0.313882	7.5493	0.174438	1760	2179	2600.7 ± 8.8	3.28	3.35	0.53	0.987	38.4
95/06-27	oblate prism	1.0	236.7	146.0	8.41	794	0.499129	12.2227	0.177604	2610	2622	2630.6 ± 2.4	0.67	0.68	0.14	0.978	1.2
95/06-28	oblate prism	1.0	189.9	113.7	27.72	206	0.451820	10.8920	0.174841	2403	2514	2604.5 ± 6.9	2.94	2.99	0.42	0.990	11.3
95/06-26	tetragonal prism	1.0	130.6	60.9	39.61	99	0.396586	9.6907	0.177222	2153	2406	2627.0 ± 14.0	7.13	7.22	0.83	0.993	21.6
Giraffe Porphyry - Zimb.164																	
zimb164-1	oblate prism	3.4	70.4	40.0	10.20	637	0.513009	12.9005	0.182381	2669	2672	2674.6 ± 2.7	0.77	0.79	0.17	0.978	0.4
zimb164-2	oblate prism	1.4	110.0	62.2	10.10	405	0.510648	12.8667	0.182744	2659	2670	2677.9 ± 3.7	1.21	1.24	0.22	0.984	0.8
zimb164-6	pbrown oblate prism	1.4	86.3	49.8	8.26	388	0.512823	12.9402	0.183009	2669	2675	2680.3 ± 5.1	1.18	1.23	0.31	0.969	0.3
zimb164-5	pbrown sub-spherical	1.9	67.8	38.1	60.08	85	0.505262	12.6477	0.181549	2636	2654	2667.1 ± 16.0	8.69	8.82	1.00	0.994	2.1
Sesombi Tonalite - Zimb.95/02																	
young																	
95/02b8	pbrown prism	0.9	212.8	76.8	5.00	657	0.329033	7.2922	0.160738	1834	2148	2463.5 ± 3.6	0.74	0.78	0.22	0.961	37.6
95/02-20	pale-pink oblate prism	0.5	131.3	72.6	13.20	130	0.503808	12.3328	0.177540	2630	2630	2630.0 ± 7.5	3.64	3.69	0.45	0.992	-0.3
95/02b12	pbrown prism	1.0	173.1	77.2	4.30	808	0.404635	9.4561	0.169492	2190	2383	2552.6 ± 3.4	0.66	0.70	0.20	0.957	21.3
old																	
95/02b7	pbrown prism	1.1	74.6	74.6	3.20	579	0.484265	12.0093	0.179860	2546	2605	2651.6 ± 4.6	0.80	0.85	0.28	0.945	6.0
95/02b9	pbrown prism	1.2	134.8	67.7	1.80	1475	0.446730	10.8951	0.176883	2381	2514	2623.9 ± 2.3	0.30	0.33	0.14	0.909	14.0
95/02b10	pbrown prism	1.1	137.6	63.9	13.20	293	0.413567	10.0197	0.175714	2231	2437	2612.8 ± 5.2	1.92	1.96	0.31	0.987	20.6
95/02b11	pbrown prism	1.0	113.4	43.5	3.20	591	0.354882	8.2541	0.168687	1958	2259	2544.7 ± 3.5	0.75	0.79	0.21	0.964	33.2
95/02-21	pink tetragonal prism	0.7	221.4	110.2	25.20	159	0.448182	10.9835	0.177739	2387	2522	2631.9 ± 71.	3.31	3.36	0.43	0.992	13.5

* All fractions non-magnetic at 20 degrees tilt angle on a Frantz LB-1 Separator at 1.7 amps.
~rbrown = red-brown; pbrown = pink-brown; transl. = translucent; transp. = transparent; fr = fragment, sub-circ. = sub-circular; ar = aspect ratio; bipyr. = bipyramid
† Maximum errors are ± 20%. Weights were measured on a Cahn C32 microbalance.
# Measured ratio corrected for fractionation.
§ Corrected for fractionation and spike.
** 207Pb/235U - 206Pb/238U error correlation coefficient calculated following Ludwig (1980).
‡ N.B. discordance calculated as average of percentage deviation from concordant 206Pb/238U - 207Pb/235U values for projected age
The laboratory blank Pb composition is 206Pb/204Pb = 18.19: 207Pb/204Pb = 15.58: 208Pb/204Pb = 38.5.
Quoted errors are 2 sigma (% for ratios, absolute for ages)

Figure 5.2 - Rhodesdale Granitoid/ Kwekwe Gneiss (Zimb.226)

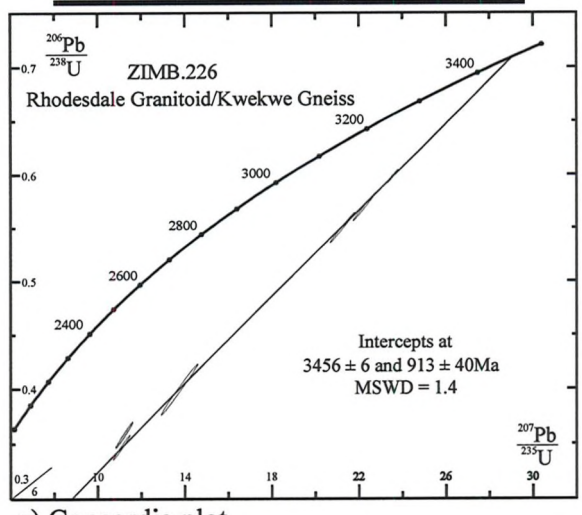

a) Concordia plot

Figure 5.3 - Sebakwe River Gneiss (Zimb.141)

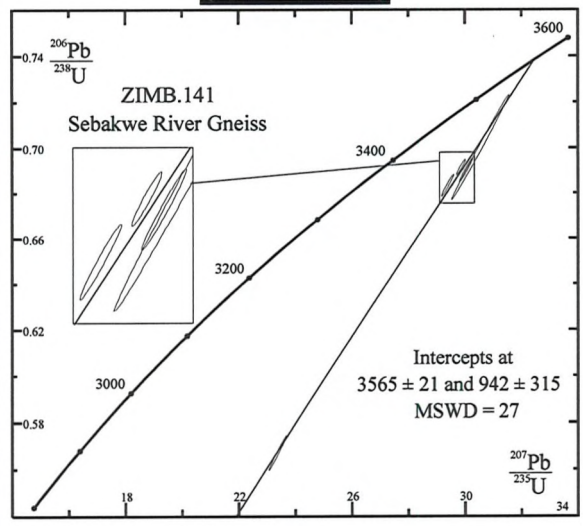

a) Concordia plot

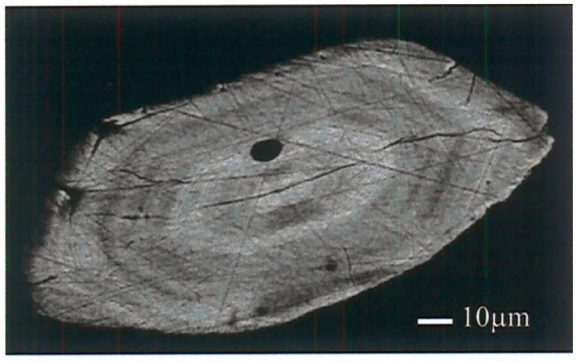

5.3b) primary magmatic oscillatory zonation (N.B. note lack of core or 2nd phase zircon)

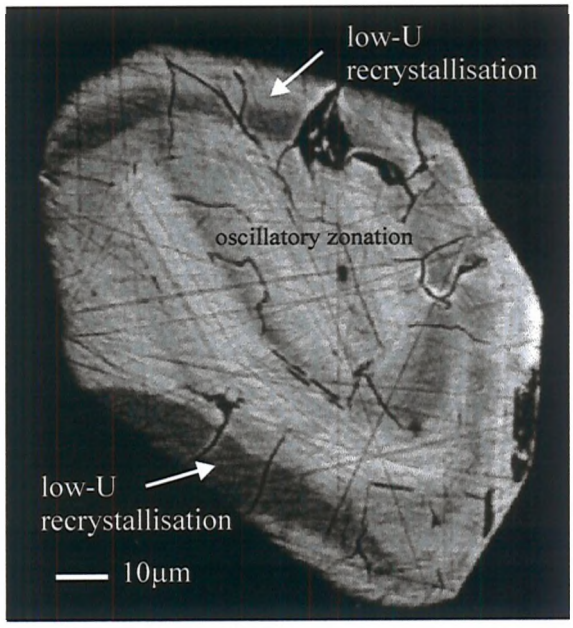

5.3c) crystal termination

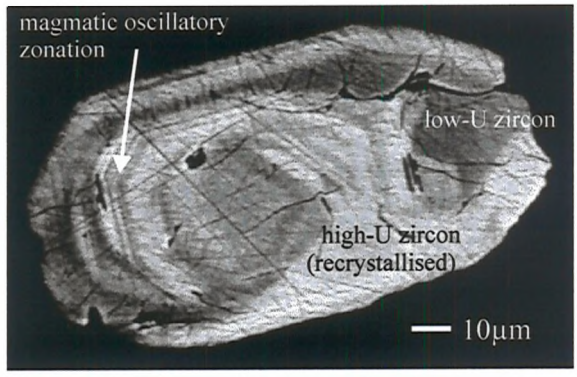

d) primary magmatic zircon showing recrystallisation

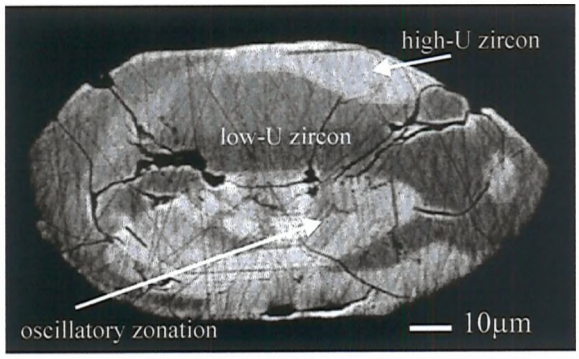

e) primary magmatic zircon with recrystallisation and radial expansion cracks

and therefore justifies its exclusion. A complex Pb-loss history such as episodic Pb-loss superimposed on continuous Pb-loss would account for this digression from the main discordia (see Fig.5.1 and section 5.6.3 for more detail). More importantly, the other points show a remarkable co-linearity indicating similar reaction to the Pb-loss events suffered and hence represent more reliable indicators of the true age.

5.6.2) The Sebakwe River Gneiss - Zimb.141 (Fig.5.3)

A five point regression has resulted in an age of 3565 ± 21Ma and an MSWD = 27 for this sample (Figure 5.3a). Two points have been omitted from the regression and the diagram. One plots almost at the origin with 89% discordance due to extreme Pb-loss resulting from decay of its *c.*3200ppm U component. The other point plots on the discordia but has a very large error ellipse due to the high common-Pb component in the analysis (155.49pg: see Table 5.3), resulting in a very low $^{206}Pb/^{204}Pb$ ratio (~84) and very high $^{206}Pb/^{238}U$ and $^{207}Pb/^{235}U$ errors (~10% each). Aside from this sample the rest had reasonable sample blank values between 7.79 and 20.38pg with $^{206}Pb/^{204}Pb$ ratios between 200-2250 and errors on Pb/U ratios <1% and ~0.1% for $^{207}Pb/^{206}Pb$ ratios.

Some back-scattered-electron (BSE) images of these grains are also presented in Figure 5.3. These show a number of features. Fig.5.3b shows primary magmatic zoning similar to that seen in Plate 5.1. Figure 5.3c is the termination of a larger zircon whilst figures 5.3d&e are both whole crystals as indicated by the primary magmatic zoning which can still be seen. *No sectors representing zircon of a different age are present.* Each of these figures exhibits some degree of recrystallisation which has 'softened' the zonation patterns and indeed obscures the majority of the grain in figures 5.3d&e. This recrystallisation has led to the development of broad bands with high or low average atomic number manifested as light or dark-grey areas respectively. It is therefore concluded that these zircons represent primary magmatic grains which have since been recrystallised slightly.

The high MSWD quantifies the scatter exhibited by the four points nearer concordia. This is considered to reflect a geological factor causing the scatter. However, despite this imprecision, taking into consideration the lack of multiple phases of zircon illustrated in the BSE images, the result is considered to represent the crystallisation age of the rock within the error limits defined.

5.6.3) Tokwe River Gneiss - Zimb.95/14 (Fig.5.4)

Common-Pb values for these fractions were between 2.68-22.18pg with $^{206}Pb/^{204}Pb$ ratios ranging from 976 to 2867. Errors on the calculated radiogenic ratios are ~0.5% for Pb/U ratios and ~0.1% for $^{207}Pb/^{206}Pb$ ratios (see Table 5.3). Four out of the five points analysed have been regressed to give an age of 3455 ± 2 (MSWD = 1.7), as plotted in Figure 5.4a. A remarkable similarity exists between the result for this sample and that for Zimb.226 (Rhodesdale Granitoid/Kwekwe Gneiss), and like this sample the data for the omitted point is good. However, inclusion of this point in the regression escalates the MSWD to 280, indicating a clearly erroneous correlation. The two points nearer the concordia (2-3% discordance) tie the upper intercept very well. The amazing co-linearity of the lower two points with the upper more concordant points, is striking considering the extent of their discordance (23-25%). The four points included in the regression have therefore all responded to the Pb-loss process(es) in exactly the same way as indicated by their co-linearity. The excluded point has clearly behaved differently, although coherently, in response to these same or different processes. This may be due to its position in the rock relative to major phases allowing greater fluid flow around this grain (c.f. Sergeev *et al.*, 1995; Bacon, 1989), thereby suffering more/different Pb-loss events in comparison to the rest (c.f. Fig.5.1).

BSE images for this sample are displayed in Figures 5.4b-e. They indicate the presence of primary magmatic zoning (Fig.5.4b) often with a high-U centre causing radial cracking, and marginal recrystallisation or possibly second phase addition after resorption (Figs.5.4c&d). Some spectacular cores are present in some grains (see Fig.5.4e) causing extensive radial cracking. In relevance to the ID-TIMS analyses, this indicates that abrasion should have removed the marginal recrystallisation. Further, the data suggest that no cores were occluded in the selected grains since no older component was detected.

5.6.4) Leucosome of Tokwe Gneiss - Zimb.95/09 (Fig.5.5)

One point was excluded from the regression for this sample since it displayed reverse discordance. High $^{206}Pb/^{238}U$ and $^{207}Pb/^{235}U$ ratios, causing the point to plot above concordia (not shown), is the result of failure of the sample and spike solution to mix properly. Hence, when correcting the data for the spike contribution, too much U is removed and the sample appears to have 'gained' Pb. This therefore renders the fraction analytically deficient and justifies its omission from the regression.

Figure 5.4 - Tokwe River Gneiss (Zimb.95/14)

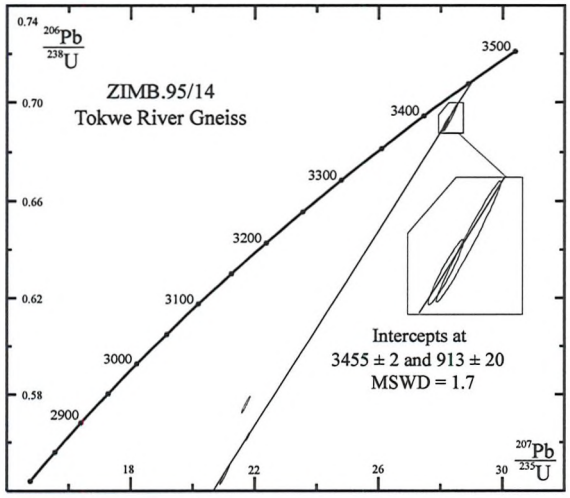

a) Concordia plot

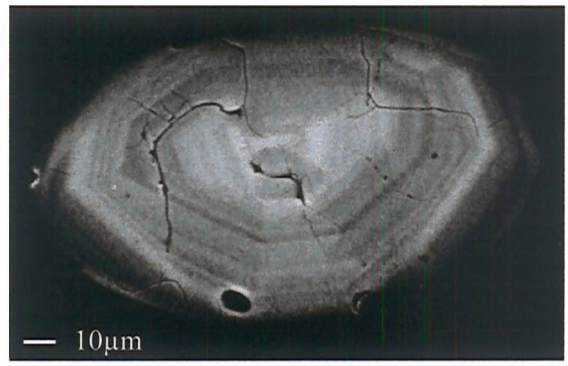

b) primary magmatic oscillatory zonation

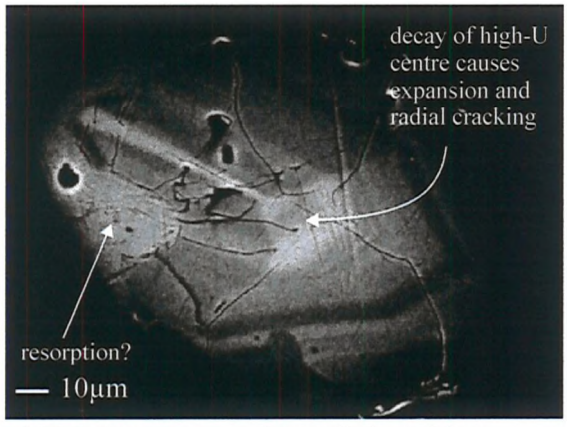

c) high-U centre causing radial cracking. Also shows a recrystallised portion to rim possibly representing a resorption event

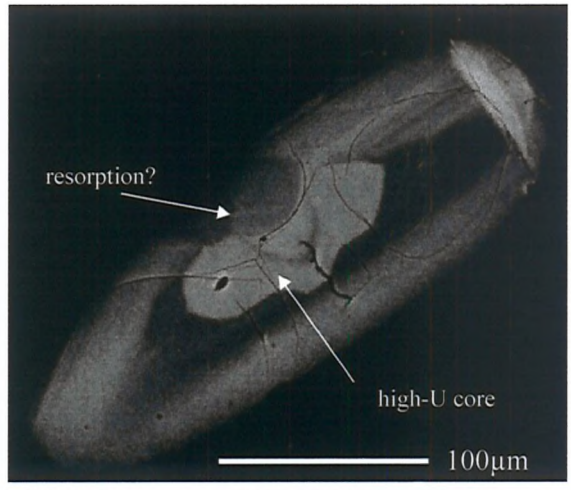

d) high-U centre with possible re-entrant resorption feature

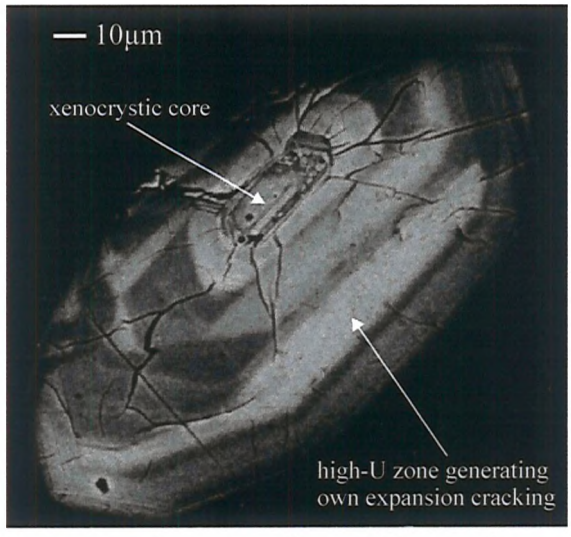

e) xenocrystic core causing radial expansion cracking

Figure 5.5 - Leucosome of Tokwe Gneiss (Zimb.95/09)

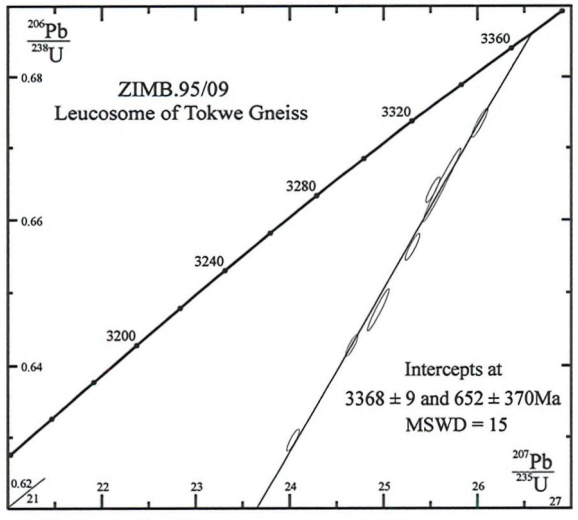

a) Concordia plot

Figure 5.6 -'Chingezi Suite' Gneiss (Zimb.95/29)

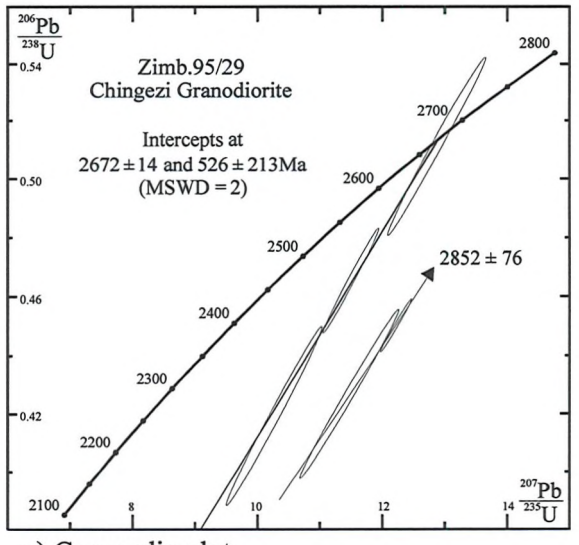

a) Concordia plot

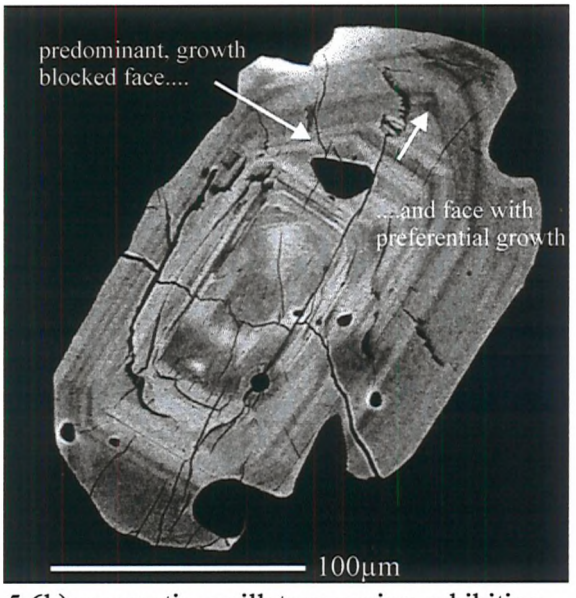

5.6b) magmatic oscillatory zoning exhibiting preferential face growth

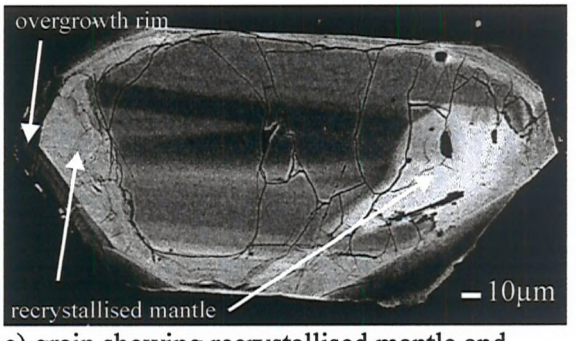

c) grain showing recrystallised mantle and overgrowth rim

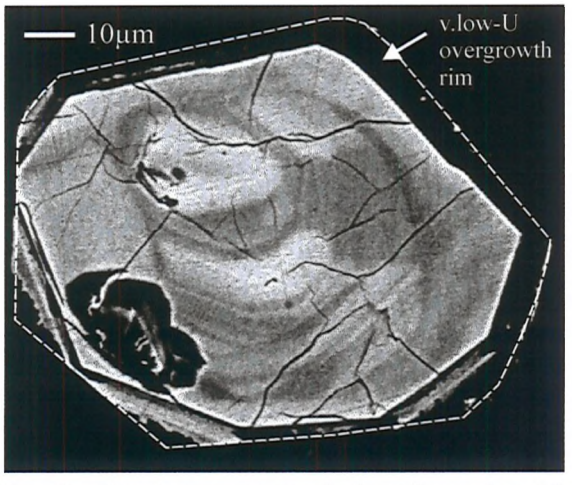

d) grain showing overgrowth rim of very low-U zircon

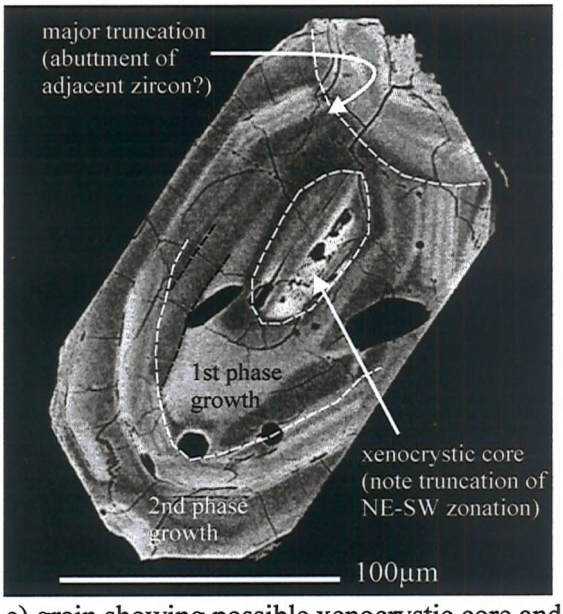

e) grain showing possible xenocrystic core and 2 phases of magmatic overgrowth

The remaining seven points define a regression (see Fig.5.5a) with possibly significant scatter (MSWD = 15). The spread of data along the discordia define it well, keeping the precision on the age high at ±9Ma, but the scatter of the points possibly indicates internal complexity to the zircons. Unfortunately, BSE images of these zircons, which may have provided evidence for this, were not available for interpretation. However, a closer look at the data indicates a more palpable culprit for the high MSWD. Table 5.3 shows that this sample contained the largest grains (5.1-16.3 μg) and some of the lowest sample blanks (2.5-9.14pg (one at 62.46)), resulting in the highest $^{206}Pb/^{204}Pb$ ratios of any of the samples (8700-21,600 (one at 967)). As such, it was possible to achieve greater precision on the $^{206}Pb/^{204}Pb$ ratio during analysis and this is reflected in the size of the errors propagated through to the calculated $^{206}Pb/^{238}U$, $^{207}Pb/^{235}U$ and $^{207}Pb/^{206}Pb$ ratios. These extremely small errors result in very little overlap between error ellipses and a consequent apparent increase in scatter indicated by an MSWD = 15. If the errors were increased by just a small amount to approximately 0.5%, still substantially less than other analyses in this study, the MSWD would be substantially reduced.

In summary, it is considered that an age of 3368 ± 9Ma is a reflection of the crystallisation age of the rock. The very small differences in the Pb-loss response of individual grains coupled with very precise data acquisition, results in a relatively high MSWD as a function of the precision of the data.

5.6.5) 'Chingezi Suite' Granitoid - Zimb.95/29 (Fig.5.6)

The sample-blanks for this granitoid were all quite high, ranging from 12-57pg. This resulted in very low $^{206}Pb/^{204}Pb$ ratios (~100) with understandably high errors on the calculated $^{206}Pb/^{238}U$, $^{207}Pb/^{235}U$ and $^{207}Pb/^{206}Pb$ ratios (see Table 5.3). Consequently, the error ellipses displayed in Figure 5.6a are very large and aid the low MSWD value of 2. The points are however reasonably co-linear and define two distinct discordia. The first, at 2672 ± 14Ma, is interpreted to be the age of crystallisation with the second discordia at *c.*2850Ma being xenocrystic.

Figures 5.6b-e illustrate the different physico-chemical features seen in these zircons under BSE imaging. Primary magmatic zonation (Fig.5.6b) is well represented but has often suffered recrystallisation (Fig.5.6c) and later overgrowth forming a rim of younger material (Fig.5.6c&d) relative to that making up the main grain. A xenocrystic core is indicated in

Figure 5.6e which also exhibits a complex relationship between oscillatory zoned phases, possibly suggesting two phases of crystallisation aside from the core and recrystallised rim (see Fig.5.6e for explanation). Figure 5.6b also illustrates well the preferential growth of one face relative to another. This may indicate a process of preferential trace element incorporation analogous to that suggested by Benisek & Finger (1993). Two distinct morphologies were picked and it was the small stubs/rods with aspect ratios of ~3:1 which proved to be xenocrystic.

BSE images of these zircons illustrate that, although occasionally simple (Fig.5.6b), the zircons in this sample are often quite complex and strongly favour prior imaging of the exact grains to be analysed in order to select those by which the different growth phases may be properly deciphered.

5.6.6) Chilimanzi Granite - Zimb.95/06 (Fig.5.7)

The sample-blank values for Zimb.95/06 were quite variable, ranging from 5.1 to 39.6pg Pb. Of eight fractions analysed one sample was omitted from the regression (not shown in Fig.5.7a) because it plotted above the concordia, suggesting non-equilibration of the sample and spike. The other seven fractions define two possible parallel discordia (see Fig.5.7a); one at 2633 ± 4Ma, the other at 2642 ± 9Ma (MSWD = 2.1). Only two points define this younger discordia, hence no MSWD value. However, no analytical reason to separate these points exists and it is probably arbitrary to distinguish these separate discordia since they are within error of each other. As such, all seven fractions have been included in a single regression resulting in an age of 2634 ± 17Ma, the fairly high MSWD of 16 reflecting the scatter caused by the two sub-parallel points.

The BSE images for this sample show extensive recrystallisation to be commonplace. Figure 5.7b exhibits initial primary magmatic oscillatory zonation being recrystallised to form ragged patches of un-zoned zircon. It is believed that this has gone to completion in Figure 5.7c which also shows the growth of a high-U margin. Whether this is a distinctly separate growth phase or simply a chemical change is unclear but exhibits the concentric cracking suggested by Lee & Tromp (1995) to be due to expansion of high-U zircon during metamictisation, against an inner low-U phase. Xenocrystic cores are present in this sample (Figure 5.7d) but apparently not occluded in the fractions picked for analysis. On the basis of this image interpretation and the work of Pidgeon (1992) (who stated that recrystallisation

Figure 5.7 - Chilimanzi Granite (Zimb.95/06)

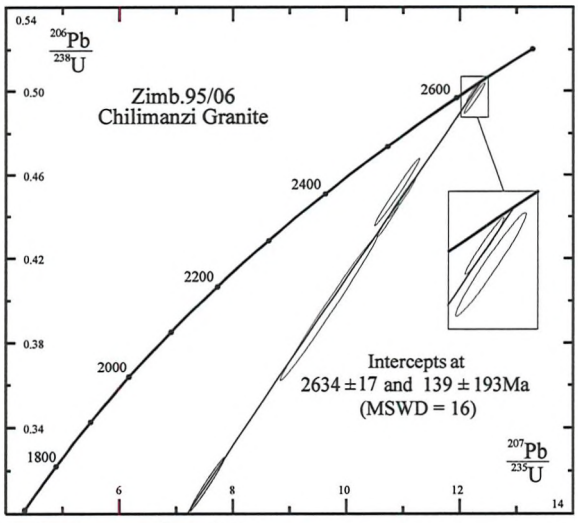

a) Concordia plot

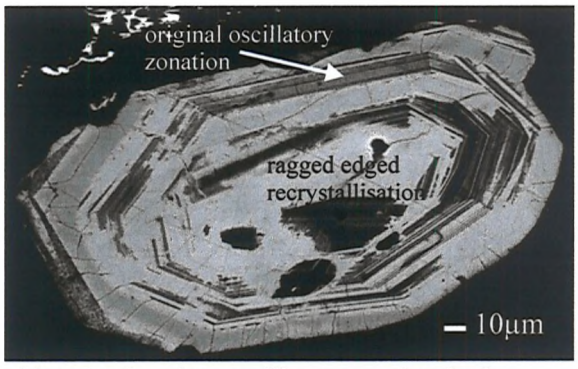

b)grain showing oscillatory zoning in the process of recrystallisation

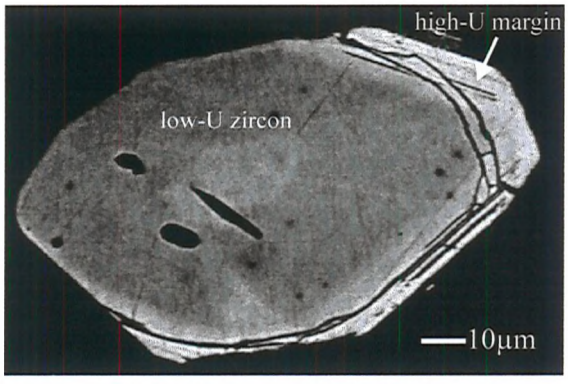

c) recrystallised zircon with high-U zone causing concentric expansion cracking against inner low-Ub zircon

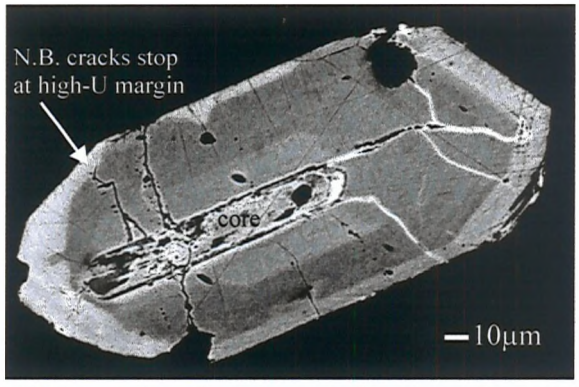

d) zircon showing xenocrystic core and related radial expansion cracks

occurs just after initial crystallisation and may reflect a mixture of the true crystallisation age and a period in a protracted cooling history), the possibility should not be rejected that the older, more constrained of the two discordia defined above, represents a more accurate interpretation of the initial crystallisation age for this Chilimanzi Suite granite.

5.6.7) Giraffe Porphyry - Zimb.164 (Fig.5.8)

This sample produced the most definitive result of the study. Four fractions were analysed, three of which have been plotted in Figure 5.8a. The fourth point was omitted due to a 60pg common-Pb component causing a very low $^{206}Pb/^{204}Pb$ ratio and a concomitant large error ellipse. All the grains were low in U with concentrations ranging from 70 to 110ppm. Due to an acknowledged error in the systematics by which the regression program calculates the intercepts and their errors, the age and error for these three concordant points was calculated as a weighted average of their $^{207}Pb/^{206}Pb$ ages. The result of 2677 ± 6Ma (MSWD = 2.4) is a direct reflection of the crystallisation age of this intrusion and this is verified by the BSE image shown in Figure 5.8b. All the zircons for this sample exhibited simple, primary magmatic oscillatory zonation with no xenocrystic cores, recrystallisation or rim overgrowths.

5.6.8) Sesombi Tonalite - Zimb.95/02 (Fig.5.9)

The results from this sample, expected to show concordancy and provide a definitive answer for the age of the rock, were very surprising. Figure 5.9a shows the concordia plot for the Sesombi tonalite, the type lithology for the regionally intrusive Sesombi Suite. Two distinct discordia may be interpreted from the data. The geological interpretation of this is discussed in Chapter 6.

Two batches of zircon were run. The first batch, prepared at the same time as the rest of the samples in this study, had high common-Pb components due to the high level of fall-in blank experienced at that time. The second batch was prepared a year later and did not suffer to the same extent. As a result, only two fractions from the first batch of chemistry (the two with the largest error ellipses in Fig.5.9a) had small enough errors to be suitable for consideration in the plot. The common-Pb values for the eight fractions used in Figure 5.9a ranged from 1.8 to 25.2pg. Three of them define a discordia at 2626 ± 8Ma (MSWD = 0.47) and the other five regress to 2668 ± 17Ma (MSWD = 4.3). This 62Ma difference is

Figure 5.8 - Giraffe porphyry (Zimb.164)

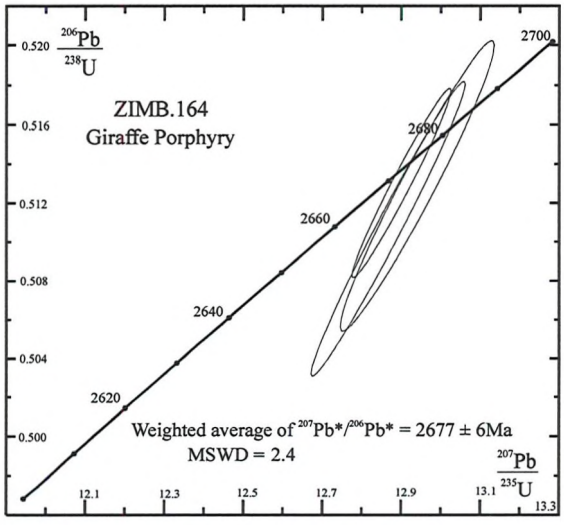

a) Concordia plot

b) grain showing primary magmatic oscillatory zoning. Note lack of cores, rims and recrystallisation

Figure 5.9 - Sesombi Tonalite (Zimb.95/02)

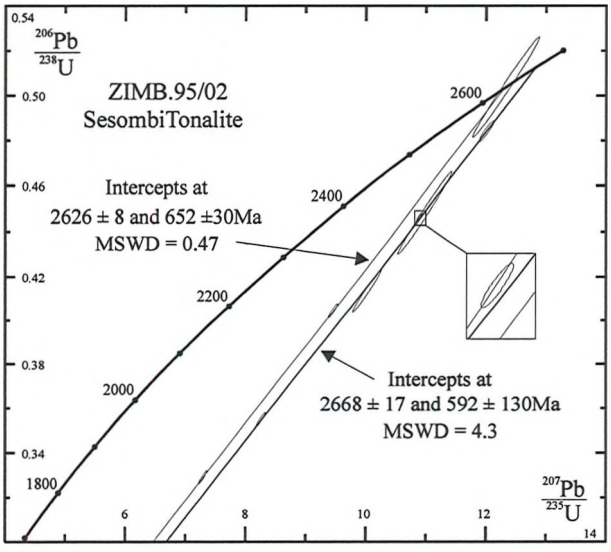

a) Concordia plot

b) single phase, oscillatory zoned zircon

considered significant enough to justify interpretation of two discordia. Combination of the data to form a single regression creates a result of 2658 ± 34Ma (MSWD = 57). The low precision and high MSWD render this result at best unlikely, especially when compared to the dual discordia results. Although no analytical difference exists between the two groups of zircon and no difference in their morphology was noted, the interpretation of two discordia is favoured based on the precision of the results and the large difference between the two ages. If the older result is accepted as the age of the rock, a possible interpretation for the younger date is that at this time a major thermal event caused total Pb-loss in some of the zircons which have, like the rest, since suffered a continuous process of Pb-loss by volume diffusion (Tilton, 1960; Lee *et al.*, 1997)). It would therefore have to be presumed that the zircons suffering this *c.*2620Ma Pb-loss event were not occluded or protected by major mineral phases. However, total resetting of the U-Pb geochronometer in zircon is extremely rare and probably possible only by complete dissolution and reprecipitation of the zircon (Mezger & Krogstad, 1997). Also, if such an event had occurred, the other rocks sampled from the Midlands Greenstone Belt would also be expected to show the effects. A total Pb-loss event at c.2620Ma is therefore not considered possible. This leaves the possibility that there are two distinct population of zircons of different age within this sample.

The image interpretation of the BSE images does not help solve the dilemma. Figure 5.9b is an example of a typical zircon from the Sesombi Tonalite. It displays single phase magmatic, oscillatory zoned zircon and no other features. This does not rule out the possibility that two different phases of zircon exist, but merely shows that they are not both present in the same crystal. However, that one zircon population could be included in the magma of another, without suffering any Pb-loss, recrystallisation or overgrowth, is considered highly unlikely.

5.6.9) Dacite from the Mafic Formation - Zimb.150 (Fig.5.10)

Of seven zircon fractions analysed, all have been included in the regression plotted in Figure 5.10a. Three of them plot very close to concordia, the centre of all three being just below. The common-Pb component of the analyses vary from 5.54 to 22.78pg and they regress to 2880 ± 8Ma (MSWD = 7.9).

The BSE images of the zircons belies the simple nature to the concordia plot. At least three distinct phases of zircon are present: xenocrystic cores, homogeneous unzoned and

Figure 5.10 - Dacite from the Mafic Formation (Zimb.150)

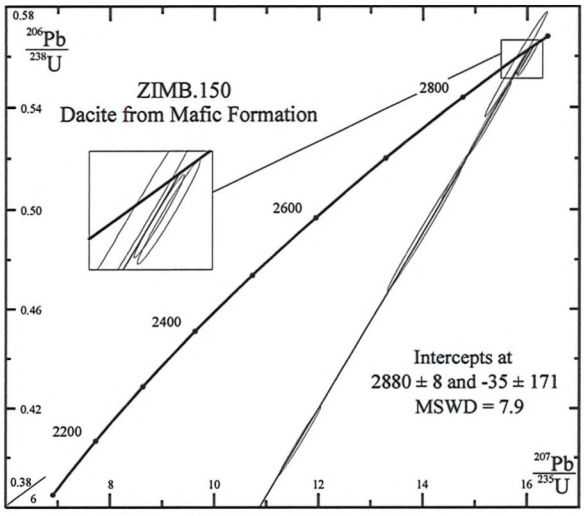

a) Concordia plot

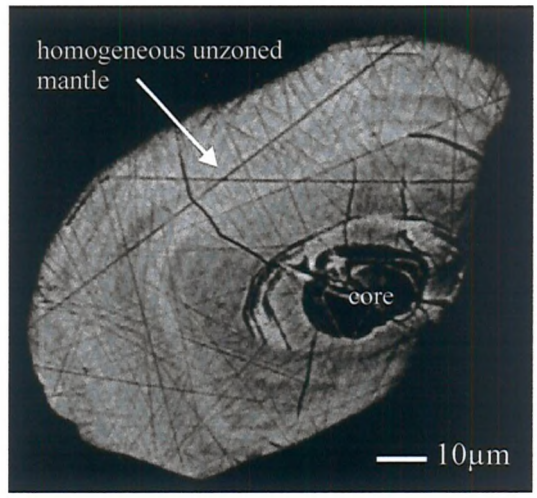

b) zircon showing xenocrystic core and homogeneous unzoned mantle

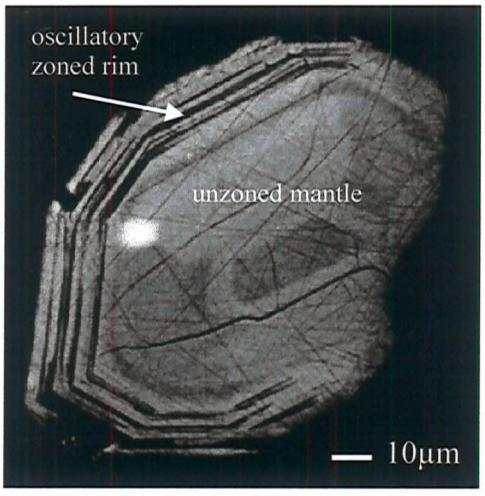

c) grain exhibiting unzoned centre and oscillatory zoned rim

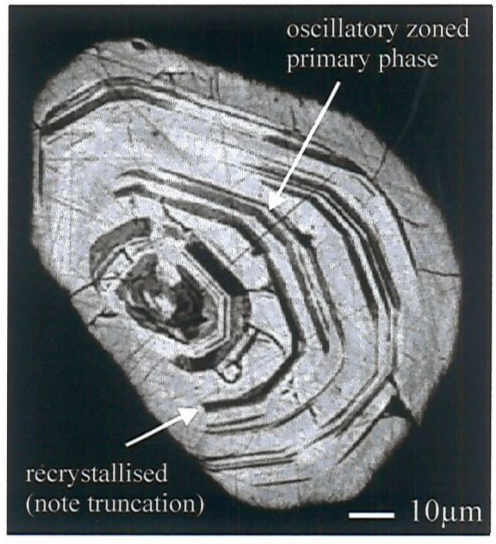

d) oscillatory zoned primary phase and homogeneous recrystallised rim

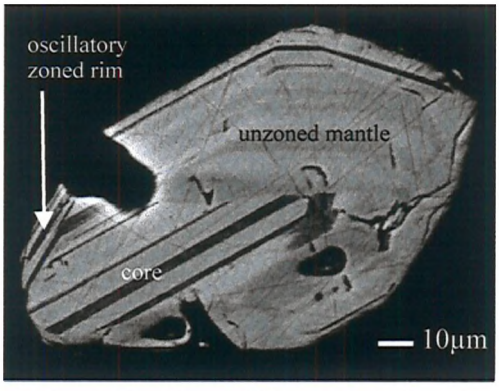

e) zircon showing oscillatory zoned core clearly truncated by unzoned mantle zircon

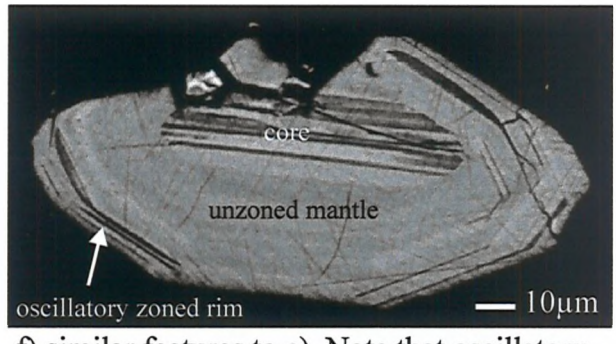

f) similar features to e). Note that oscillatory zoned zircon forms the rim in both

oscillatory zoned zircon. The unzoned material generally forms the mantle to the grain, irrespective of the presence of a core (see Figs.5.10b&c). The oscillatory zoned zircon sometimes forms a rim phase to the unzoned material (Fig.5.10c) but the opposite may also be true (Fig.5.10d). The cores are often composed of oscillatory zoned zircon exhibiting clear truncations between this and the homogeneous, unzoned mantle (Figs.5.10e&f), with more oscillatory zoned zircon forming the rim. The homogeneous component is assumed to represent recrystallised zircon since Cherniak *et al.* (1997b) recognised that diffusion of U, Th and in part Pb, was too slow to allow growth of homogeneous zircon, i.e. that oscillatory zones of high and low concentrations of U must form.

In light of these BSE images, it is possible that the result shown in Figure 5.10a represents xenocrystic cores. However, to achieve this, total separation from all other phases of zircon would be needed. This is considered unlikely considering the very small size of the cores, the random nature of the abrasion process and the expected variations in core-shape when considered in three dimensions. Each analysis would be expected to show small variations in the amount of second phase zircon remaining on each core after abrasion, and hence result in a significant amount of scatter on a concordia plot. The crystallisation age of the rock is therefore interpreted to be 2880Ma.

5.7) SUMMARY OF GEOCHRONOLOGICAL RESULTS

1) Sebakwe River Gneiss - is 3565 ± 21Ma old (MSWD = 27)

2) Rhodesdale Granitoid/Kwekwe Gneiss - is 3456 ± 6Ma old (MSWD = 1.4)

3) Tokwe River gneiss - is 3455 ± 2Ma old (MSWD = 1.7)

4) Leucosome of Tokwe Gneiss - is 3368 ± 9Ma old (MSWD = 15)

5) Dacite from the Mafic Formation - is 2880 ± 8Ma old (MSWD = 7.9)

6) Giraffe Porphyry - is concordant at 2677 ± 6Ma old (MSWD = 2.4)

7) 'Chingezi Suite' Granitoid - is 2672 ± 14Ma old (MSWD = 2) with *c.*2850Ma inheritance

8) Chilimanzi Granite - is 2634 ± 17Ma old (MSWD = 16) (or possibly 2642 ± 9Ma (MSWD = 2.1) with an event (recrystallisation?) at 2633 ± 4Ma)

9) Sesombi Tonalite - records two distinct ages - 2668 ± 17Ma (MSWD = 4.3) most probably representing the crystallisation age, and 2626 ± 8Ma (MSWD = 0.47) whose precise interpretation is unsure

CHAPTER 6 - DISCUSSION

6.1 FIELDWORK

6.1.1 Implications for the environment of deposition

An aqueous environment of deposition is obviously indicated by the voluminous pillow lavas seen in the Midlands Greenstone Belt and other greenstone belts in the Zimbabwe Craton and around the world. Well-bedded, sorted and fine grained sediments including BIF of probable hydrothermal origin (Eriksson *et al.*, 1994), also testify to the presence of substantial quantities of water. Field evidence in the Midlands Greenstone Belt however, also indicate that this water was fairly shallow. Coarse sediments, including the boulder conglomerate of the Sebakwe River Conglomerate and coarse quartz-rich grits, are good evidence for fairly shallow conditions, allowing rapid deposition of the sediment load as the river tributary feeding this environment entered the quiet, open waters of the depositional environment. BIF however, indicates that at times this siliciclastic input ceased, allowing background and chemical sedimentation to occur in a low energy environment.

More than this however, the presence of an oolitic limestone strongly suggests a change to a shallow water, higher energy environment since wave-base agitation is required to generate the concentric ooids (Beukes, 1977). The widespread occurrence of epicontinental seas from 3.2 to 2.0Ga (Eriksson, 1995) would provide the ideal environment in which to deposit the lithologies of the Midlands Greenstone Belt. This has significant implications for the oxygen content of the environment at least with regard to this locality if not representative of this time. The formation of the oolitic limestone found in the Maliyami-Felsic section, requires the presence of oxygen-producing bacteria and/or algae resulting in free oxygen within the water allowing carbon to act as an oxygen sink (Eriksson, 1995). This situation is more common in the Proterozoic and indeed, is thought characteristic of this time period. Massive crust production in the Late Archaean is thought to have resulted in the formation of large, oxygen-rich, epicontinental seas and hailed the generation of large quantities of oxygen in these expansive, warm shallow water environments by bacteria. Fedo & Eriksson (1996) interpret such a shelf-facies environment for the extensive sedimentation preserved in the Buhwa Greenstone Belt, and although dominantly volcanic, a similar continental shelf environment is envisioned for the Midlands Greenstone Belt.

The environment was also sub-aerial at times as evidenced by pyroclastic textures in the andesitic and dacitic volcanics. Tuffs and lapilli-tuffs (Blenkinsop *pers. commun.*, 1995) found in parts of the section attest to subaerial eruptions, suggesting that at times the volcanoes producing these deposits had at least their vents above water.

6.1.2 Implications for palaeotectonics

The most significant lithologies indicating possible palaeotectonic conclusions, are the quartz-rich grits, Sebakwe River Conglomerate and ooilitic limestone. The first two of these vehemently proclaim extreme proximity to a continental crustal source of material. Metre-sized boulders of tonalite-trondhjemite-granodiorite lithologies must have been deposited very rapidly after the unusual amount of water required to transport them, lost its carrying energy on entering a larger, much quieter lagoon, bay, basin or sea. Although finer, the grits are still of significant grain size (~0.5-1mm) and must have originated from a proximal sialic source. The oolitic limestone, is indicative of shallow, agitated water, typical of epicontinental seas in the Proterozoic. This probably suggests a continental margin environment.

The field evidence therefore collectively suggest deposition and eruption of the stratigraphy within a shallow basin, lagoon or marginal sea (possibly epicontinental) which records increasing energy of the environment (mingled magmas) and oxygenation of the water (oolitic limestone) over a 200Ma period, periodic siliciclastic input and background exhalative-hydrothermal sedimentation (BIF).

6.2 GEOCHRONOLOGY

6.2.1 The Sebakwian comes home: Geochronological implications for the generation and evolution of the Midlands Greenstone Belt

The date obtained for the Kwekwe Gneiss (3456 ± 6Ma) is identical to that for the Tokwe River Gneiss (3455 ± 2Ma, see Chapter 5). This directly recognises the presence of rocks of Tokwean age in the Midlands Greenstone Belt. Macgregor (1951) considered the Rhodesdale Granitoid to be *c.*3Ga in age recognising it as older than the Sebakwe River Conglomerate which he concluded marked the base of the volcanic stratigraphy. The mafic xenoliths within the Rhodesdale Granitoid he therefore referred to as Sebakwian and the

production of a 3456Ma age for the Kwekwe Gneiss, one of the granitoid phases comprising the Rhodesdale Granitoid, brings this terminology back into the stratigraphy in this part of the craton. More so with the Sebakwe River Gneiss. This small granitoid mass, dated at 3565 ± 21Ma, is clearly of ancient origin but the amphibolite phase which melted to produce the second (dated) phase can clearly be surmised to be 3.6-3.8Ga old. The Sebakwian (*sensu stricto*) it would seem, is back on the Sebakwe river.

The surrounding volcanics, the Mafic Formation of Harrison (1970), have yielded a U-Pb zircon result of 2880 ± 8Ma and are therefore the first rocks of Lower Bulawayan/Belingwean age directly recorded in the Midlands Greenstone Belt. This also rules out the correlation of the Mafic Formation with the U3 Zeederbergs basalts of the Mberengwa (Belingwe) Greenstone Belt (Wilson, 1979; Wilson *et al.*, 1995). It is noticeable that nowhere on the published geological maps is the Mafic Formation juxtaposed against the Maliyami or Felsic Formation. Only in one place, to the north of the area considered in this study, does the What Cheer Formation, considered by Robertson (1976) as the lateral equivalent of the Mafic Formation, lie next to the Felsic Formation. This in itself displays anachroneity if this equivalence is correct.

The presence of the Sebakwe River Gneiss with its Tokwean/Sebakwian date, produces a problem in interpreting the structural make-up of this part of the greenstone belt. Irrespective of the 2880Ma age now obtained from the surrounding rocks, the volcanics of the Mafic Formation must now be interpreted to lie unconformably or with structural disconformity, upon the Sebakwe River Gneiss. Campbell & Pitfield (1994) consider this gneissic body to occupy the core of an anticline with a shear down its eastern margin. They find little evidence of shearing on the western contact of the gneiss, whilst the eastern contact is more strongly sheared but poorly exposed. This agrees with the observations made in this study (see section 3.2.4). Campbell & Pitfield (1994) consider the gneiss to be a fragment of the basement gneisses which is exposed as a result of shearing-out of the east dipping limb of a NW oriented anticline-syncline fold pair. This explains why all the observed pillow lavas indicate younging to the west, since the easterly younging limb of the anticline has been sheared-out (see Figure 6.1). An alternative explanation, or maybe in addition to one sheared margin, is the possibility that although now sheared, the contact of the volcanics with the Sebakwe River Gneiss represents a regional unconformity of the nature seen between the Shabani Gneiss and Manjeri Formation in the National Monument section of the Mberengwa

Figure 6.1

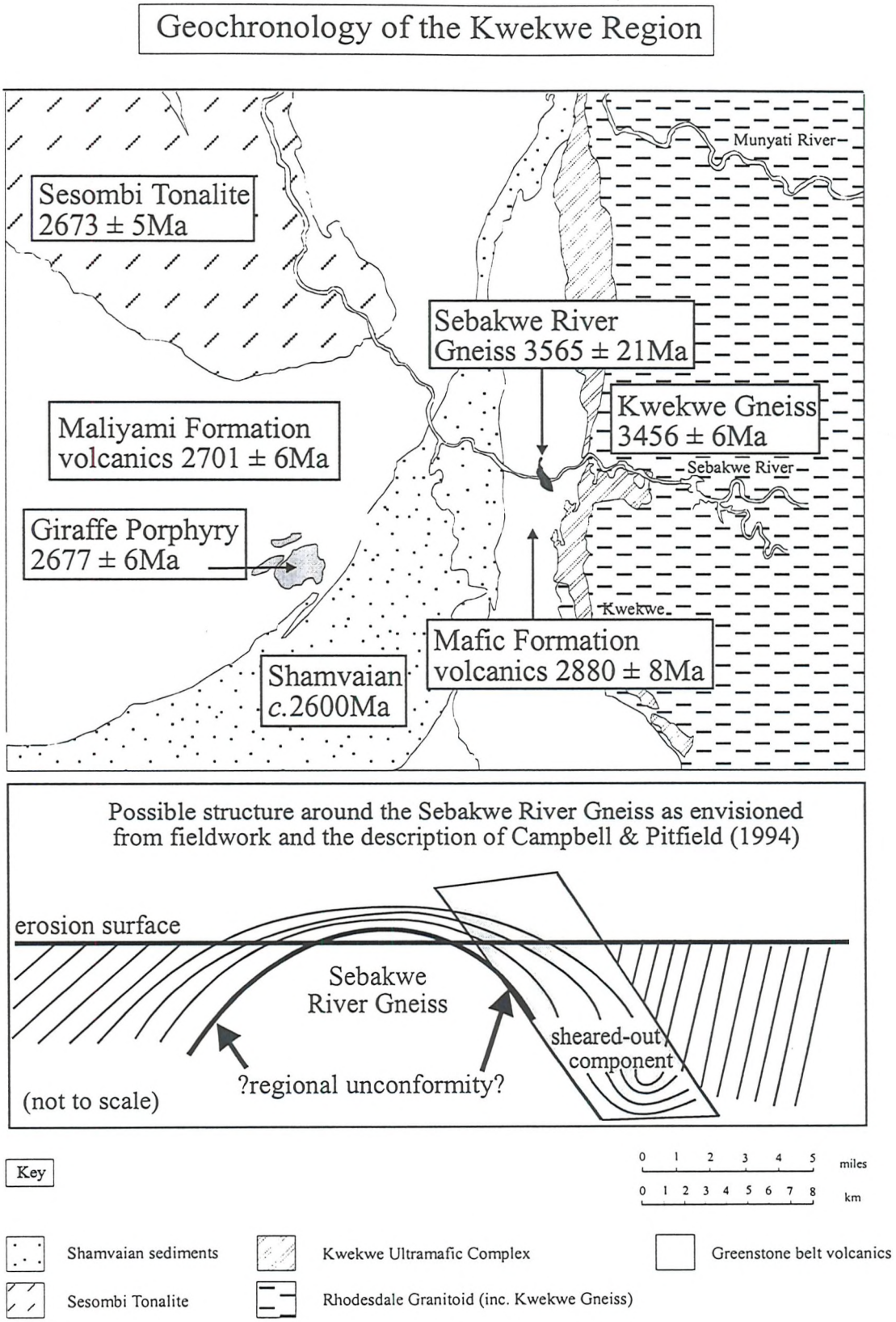
Geochronology of the Kwekwe Region
Munyati River
Sesombi Tonalite
2673 ± 5Ma
Sebakwe River
Gneiss 3565 ± 21Ma
Kwekwe Gneiss
3456 ± 6Ma
Sebakwe River
Maliyami Formation
volcanics 2701 ± 6Ma
Giraffe Porphyry
2677 ± 6Ma
Kwekwe
Mafic Formation
volcanics 2880 ± 8Ma
Shamvaian
c.2600Ma
Possible structure around the Sebakwe River Gneiss as envisioned
from fieldwork and the description of Campbell & Pitfield (1994)
erosion surface
Sebakwe
River Gneiss
sheared-out
component
?regional unconformity?
(not to scale)
Key
0 1 2 3 4 5 miles
0 1 2 3 4 5 6 7 8 km
Shamvaian sediments
Kwekwe Ultramafic Complex
Greenstone belt volcanics
Sesombi Tonalite
Rhodesdale Granitoid (inc. Kwekwe Gneiss)

(Belingwe) Greenstone Belt. Although of different age in the Midlands (*c.*2.9Ga instead of *c.*2.7Ga), this is considered a distinct possibility.

The Upper Bulawayan volcanism, dated at 2701 ± 6Ma (U-Pb zircon) by Wilson *et al.* (1995) using a felsic volcanic from the Maliyami Formation, gives credibility to the 2739 ± 33Ma age obtained from a Sm-Nd isochron in this study for the volcanics of the Maliyami-Felsic succession. The cessation of Upper Bulawayan volcanism is constrained by an age of 2677 ± 6Ma obtained for the Giraffe Porphyry. This sub-volcanic Late Porphyry has strong geochemical affinities with the rhyodacites from the Felsic Formation and has representative clasts in the basal conglomerate of the Shamvaian sediments in the Midlands Greenstone Belt (Harrison, 1970). As such, it provides a good minimum age for the volcanism and correlates well with the Sesombi Tonalite dated at 2668 ± 17Ma in this study and conventionally considered to be at least synchronous and most probably slightly younger than the Late Porphyries. A Pb-Pb zircon age of 2673 ± 5Ma obtained for the Sesombi Tonalite (Dougherty-Page, 1994) would appear to agree with this and provides the most precise and probably accurate date so far attained for this granitoid.

The dates produced in this study would therefore appear to significantly reappraise the geochronologic composition of the Midlands Greenstone Belt, and by consequence, its structure (see Figure 6.1). In light of the geochronological interpretation provided, major structural kinematics have to be inferred to juxtapose the 2880Ma Mafic Formation in its present position alongside the 2.7Ga stratigraphy of the Maliyami and Felsic Formations. Dating of mineralisation present within both these chronostratigraphies at 2.67Ga (Darbyshire *et al.*, 1996) may be taken to indicate the current juxtaposition by this time. The intrusion of the Chicago Porphyry through the Mafic Formation section would also appear to date this juxtaposition to before 2677Ma (assuming a similar age to the Giraffe Porphyry). This, along with the roughly vertical attitude of the rocks, indicates that a significant amount of structural repositioning must have occurred in a relatively short space of time between the end of the Felsic Formation volcanism and the intrusion of the sub-volcanic porphyries. The time available for this currently stands at 24Ma (2701-2677Ma) but since the older of these ages is from rocks lower in the stratigraphy (Maliyami Formation), this time-zone must be less than this and 10-15Ma is possibly more representative of the time available. Evidently a major

ground-based structural study needs to be conducted on the Midlands Greenstone Belt to help resolve some of these problems and consider the hypotheses proffered here.

In section 3.2.6.1 it was stated that the Kwekwe Gneiss (the marginal phase of the Rhodesdale terrain) was considered intrusive into the margin of the Midlands Greenstone Belt. This is in contravention to the conventional wisdom which states that the Rhodesdale Granitoid as a whole formed the basement to the Midlands Greenstone Belt. The 3456 ± 6Ma age for the Kwekwe Gneiss obtained during this study agrees with this convention. However, the conclusion that an intrusive relationship exists between the greenstone belt and granitoid as exposed on the south bank of the Sebakwe River, was reached as a result of considerable deliberation in the field and independently of the same conclusion reached by Harrison (1970). At the time convincing evidence supporting this conclusion was considered apparent and as such, it would be wrong to now dismiss or ignore this interpretation. Therefore, until further fieldwork is conducted to satisfy the data one way or the other, permeation of quartz-rich fluids or intrusion of a small, late granitoid phase is postulated for the contact with a note that the sample on which geochronology was conducted was collected 2.6km into the granitoid mass away from the granite-greenstone contact.

6.2.2 Implications for the geochronological composition of the Zimbabwe Craton

The most significant regional implication of the geochronological data obtained during this study, is that there is direct evidence that the oldest rocks in the Zimbabwe Craton are not confined to the Tokwe Segment as defined by Wilson (1990). Indeed, the *oldest* rock so far dated from the craton is the 3565Ma Sebakwe River Gneiss from this study. This date was obtained on a melt phase which is clearly a partial melt of another amphibolitic component. The precursor phase is therefore older still and probably equates with the Sebakwian remnants present in the Tokwe Segment. The age for the Sebakwe River Gneiss is supported by a 3456Ma age obtained for the Kwekwe Gneiss, indicating that Tokwean age rocks are most definitely present in the middle of the craton. In conjunction with 3-3.2Ga Sm-Nd T_{DM} model ages & Pb-Pb zircon ages obtained from granitoid clasts from Shamvaian conglomerates in the Harare Greenstone Belt (Jelsma, 1993 & Dougherty-Page, 1994, respectively), the Tokwean ages obtained from the Midlands provide direct evidence for the existence of an ancient proto-continental core which probably underlies the whole craton with

continuous extent from the Tokwe Segment in the south, through the Midlands, into the Harare Greenstone Belt in the north of the craton (see Fig. 6.2). Kusky (1998), based on reinterpretation of existing geochronometric and model age data, hypothesised the existence of a 3.6-2.95Ga 'Tokwe Terrane' acting as a coherent unit by the end of this time. The data reported in this study would appear to indicate a more regionally extensive ancient origin to this unit but basically confirms this hypothesis. However, the palaeotectonic interpretation suggested by Kusky (1998) and indeed implied in the spelling of the nomenclature used (terrane *vs* terrain), is not followed. As such the term Tokwe Proto-craton is preferred in order to avoid any genetic implications to the nomenclature and will be used from here-on. This terminology is coincident with Stowe (1971) who described a central protocratonic unit of pre-3.4Ga crust, composed of 3 granitoid nuclei, which stabilised and formed the nucleus for craton growth. With the possible identification of *c.*3.2Ga crust in the north of the craton, it is suggested that the Tokwe Proto-craton as defined here, extends this far. This proto-craton may have existed as a number of smaller nuclei as suggested by Stowe (1971) or as a single large nuclei, forming the foundation for formation of the rest of the craton. On the basis of the synchronous formation of the Tokwe River Gneisses and the Rhodesdale Granitoid samples reported in this study, a single large nuclei is favoured. As such it is probably untenable that the craton could have grown by accretion in a north and north-westward direction as suggested by Wilson (1979). Instead, the 3.2-3.6Ga Early-Archaean proto-craton already extended to the north of the presently delineated craton and the rest of its growth was dominated by intrusive and extrusive addition with possibly some marginal accretion. This does not preclude some of the growth from being diachronous as is often suggested for the *c.*2.6Ga Chilimanzi suite.

The first precise age for the Tokwe Segment is reported in this study at 3455 ± 2Ma. Whilst other dates are available for these rocks (see compilation in Taylor *et al.*, 1991) these are imprecise. The amazing precision of this result confirms beyond doubt the time-frame for these stratigraphically important proto-cratonic rocks.

The leucosome component dated (Zimb.95/09), correlates with other granitoid phases and intrusions in the south of the craton such as the Mont d'Or Granodiorite and Mushandike Granite, as well as providing a source for the detrital zircon peak reported by Dodson *et al.*, (1988) at 3350Ma. This sample would therefore appear to be a remnant component of a granitic melt probably sourced from the Tokwe Gneiss, and producing these *c.*3.3Ga

Figure 6.2

Regional extent of the Tokwe Proto-craton

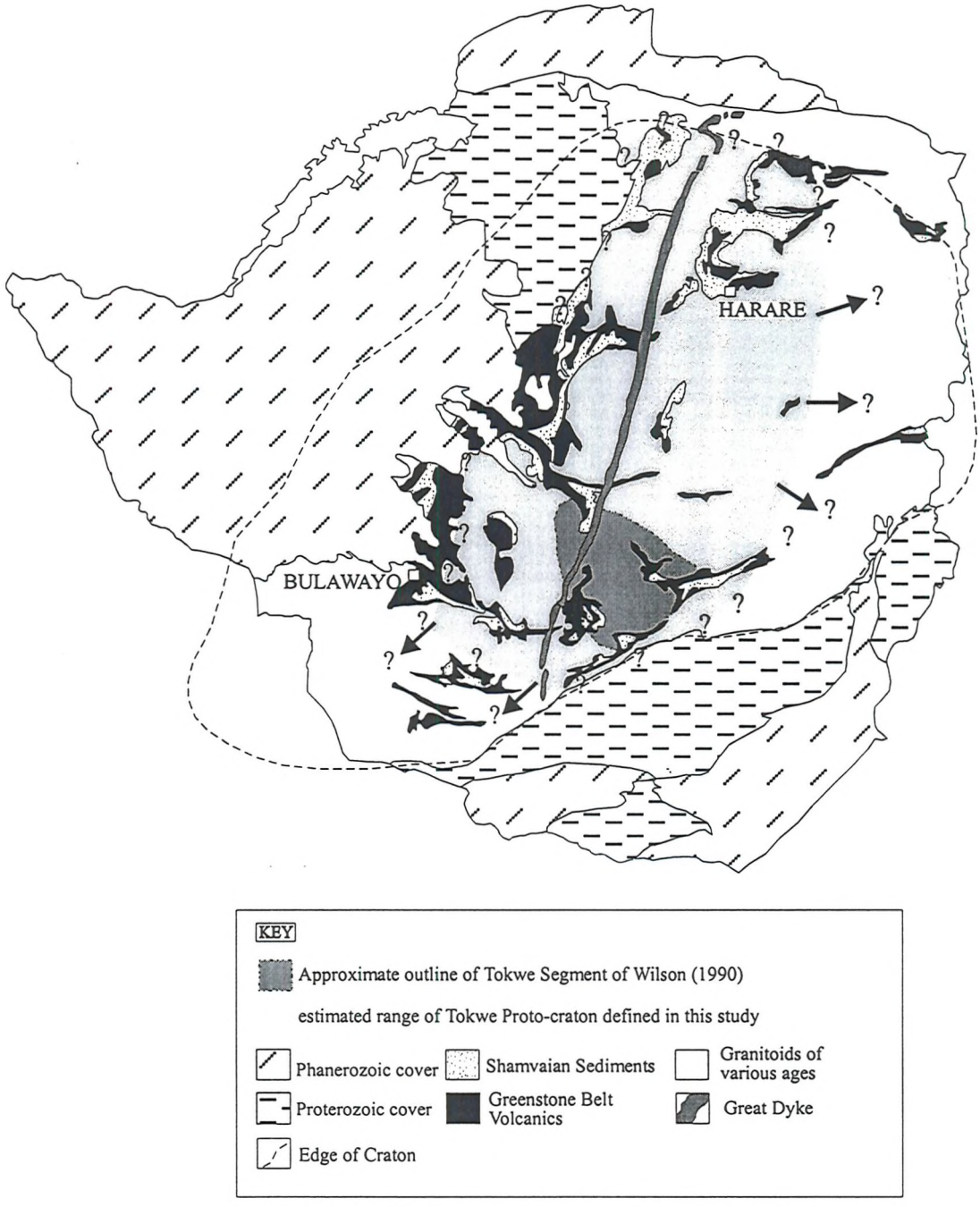

granitoids. This is not a widely recognised time of magma production within the Zimbabwe Craton and more geochronology conducted on the granites and gneisses therein may well increase the profile of this period in Early Archaean time.

Two other regional samples were dated in order that a regional geochronological framework could be constructed. The sample dated as an example of the *c.*2.9Ga Chingezi suite, recorded a 2672 ± 14Ma crystallisation age with a *c.*2850Ma inheritance. Such an age is more reminiscent of that obtained for the Sesombi Suite (2673 ± 5Ma, Dougherty-Page, 1994; 2668 ± 17Ma, this study). It is suggested that this sample represents a case of 'mistaken identity' and clearly indicates the problems in assigning granitoid intrusives to particular regional suites purely dependent on field-based characteristics. Unless unequivocal field relationships are apparent (i.e. good cross-cutting relationships with rocks of known age), such correlations are probably best avoided.

The sample selected as an example of the Chilimanzi suite produced a complex data array indicating crystallisation around 2.64Ga ago. In comparison to a 2601 ± 14Ma age determined by Jelsma (1993) on the Murehwa batholith adjacent to the Harare Greenstone Belt, a craton wide diachroneity in this event may be apparent as hypothesised by Wilson (1979). An increase in the age of this intrusive suite may be seen from north to south in the craton, indicating a *c.*40Ma diachronism in this crustal anatectic event.

6.3 GEOCHEMISTRY

6.3.1 Implications for the Generation and Evolution of the Midlands Greenstone Belt.

The geochemical data produced in this study strongly suggest a separate origin for the basalts and andesite-rhyodacites. The basalts can be derived as a partial melt of lherzolitic mantle whilst the andesites require melting of a previously existing basaltic source. One can be envisioned as derived from the other especially in light of the new U-Pb zircon ages determined in this study which show that the Mafic Formation basalts are *c.*200Ma older than the Maliyami Formation andesites and rhyodacites. Other possible origins for the andesite-rhyodacite suite are production of the initial basalt melt, followed by interaction with crustal material adding water, oxidising the magma and driving it onto an ilmenite-amphibole fractionation trend. Such models, along with depleted mantle (T_{DM}) model ages for both the basalts and andesite-rhyodacites which are older than the crystallisation age of the rocks, indicate possible crustal assimilation. Trace element and Nd-isotope variations indicate that

this is a possibility but requires probably less than 0.5% assimilation of crustal material. Total homogenisation of this assimilant, into the relevant magmas, is not required as indicated by the variable $\varepsilon_{Nd(t)}$ and $Nd_{(i)}$ ratios.

An alternative hypothesis to continental crustal contamination of the magmas, is that each lithology was generated from a different source. The basalts possess 3.2-3.4Ga T_{DM} model ages and the andesite-rhyodacites one of *c.*2.85Ga. This latter model age is suspiciously similar to the crystallisation age of the Mafic Formation lithologies and since the andesites and rhyodacites are most easily modelled by partial melting of basalts converted to amphibolite and/or garnet-amphibolite, an origin by melting of these 2880Ma rocks would seem credible. This further implies that the 3.2-3.4Ga model age of the Mafic Formation rocks is the signature of a real component. Nägler *et al.* (1997) produced Re-Os isotope data to show that the sub-continental lithospheric mantle (SCLM) beneath the Tokwe Segment was substantially depleted and began formation before 3.8Ga. Since Tokwean age rocks have now been directly recorded in the Midlands, with identical and older ages to those in the Tokwe Segment, the presence of a similar depleted SCLM component beneath the Midlands portion and possibly the whole craton, may be argued. Indeed, the data of Nägler *et al.* (1997) records model ages from *c.*3.0-3.9Ga with the oldest dates at the northern limit of the Tokwe Segment as defined. It is therefore suggested that the 3.2-3.4Ga T_{DM} model ages recorded in the Midlands represent sampling of the SCLM below this greenstone belt and that this depleted mantle component possibly represents the residue after large scale crustal separation events (Boyd, 1989; Walker *et al.*, 1989) or storage of mafic crust (Chase & Patchett, 1988) between 3.2 and 3.4Ga ago with a possible history back to *c.*3.8Ga ago (Nägler *et al.*, 1997). This indicates that at 2880Ma the Mafic Formation rocks were conceived by melting of the SCLM and preserved the 3.2-3.4Ga mantle separation age of this depleted mantle component. At 2.7Ga a new thermal pulse caused melting of the SCLM, resulting in basalts also recording a 3.2-3.4Ga T_{DM} model age, but also caused melting of *c.*2.9Ga basalts from the previous magmatic episode suggesting that some of this material had remained as an underplate to the SCLM. This underplate *must* represent CHUR-derived material in order to retain its 2.9Ga T_{DM} whose signature was then passed on when melting of these basalts generated the andesites which evolved to the rhyodacites. Rhyodacites may also have been generated directly from the 2.9Ga basaltic underplate through small scale partial melting.

Figure 4.16b would appear to suggest that there are two distinctly different components being sampled by the basalts and andesite-rhyodacites. Thus, although it is recognised that mixing of different proportions of crustal and mantle components results in different T_{DM} model ages (Arndt & Goldstein, 1987), this is not a relevant argument in distinguishing the two lithological suites. For assimilation alone to be the cause of the isotopic variation seen in the Midlands Greenstone Belt rocks, an argument for compositionally selective sampling of different crustal components at any point in time (i.e. contamination of the basalts by 3.2-3.4Ga crust and of the andesite-rhyodacites by *c.*2.85Ga crust) would have to be believed. Some samples (Zimb.150 & 189) do show significantly disturbed isotopic characteristics indicative of assimilation of ancient crustal material but this only serves to support the model of SCLM and basaltic underplating since it illustrates that assimilation at either 2.9 or 2.7Ga results in a significantly increased T_{DM}.

The conclusion therefore, illustrated in Figure 6.3, is that the T_{DM} results as displayed in Table 4.2 reflect the Nd isotope composition of an ancient mantle component beneath the Midlands portion of the Zimbabwe Craton. This ancient component separated from the chondritic mantle reservoir approximately 3.2 to 3.4Ga ago and was sampled by basaltic volcanics 2.9Ga ago. The 2.9Ga event (Mafic Formation) provided heat for melting of the older mantle component and produced new primary (basalt) material which remained at depth, probably underplating the *c.*3.4Ga SCLM. After transformation to (garnet-) amphibolite, this 2.9Ga underplate was then remelted to produce the 2.7Ga andesites and rhyodacites of the Maliyami and Felsic Formations, the basalts of which again represent melts from the SCLM. A minor variation on this is that instead of forming an underplate, the 2.9Ga basalts may have formed a thick volcanic pile whose base was then melted with the next thermal pulse. This may indeed be a more favourable scenario and allows for recognition of 2.9Ga basalts within the Midlands Greenstone Belt which possess a 2.9Ga T_{DM}. Either way, the model allows for the close spatial and temporal relationship necessitated by the mingled magma textures seen in the field and thin section.

Projection of the $\varepsilon_{Nd(t)}$ calculations through to present day, result in an increase of only 0.5 epsilon units. This indicates very little in-growth over 2.7Ga and illustrates the CHUR-

Figure 6.3

Diagram to illustrate the suggested model for the source of the volcanic lithologies of the Midlands Greenstone Belt

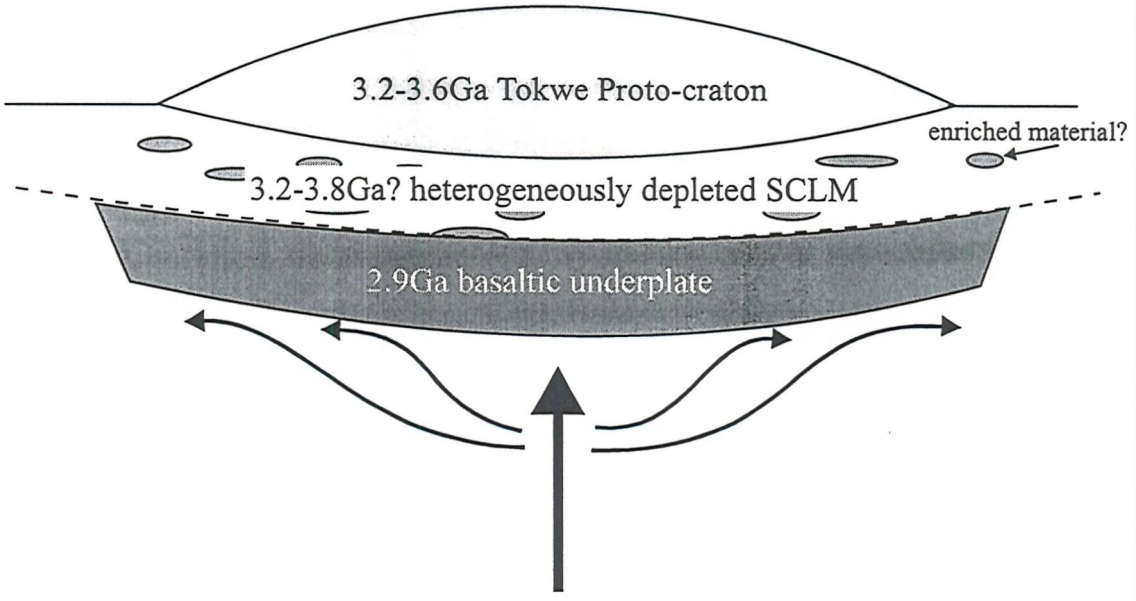

1) Generation of proto-craton or large volume melts in the Early Archaean forms heterogeneously depleted sub-continental lithospheric mantle (SCLM) component.

2) 2.9Ga basaltic melt provides thermal anomaly to melt SCLM and leaves basaltic underplate.

3) Second thermal pulse at 2.7Ga generates more basalts from the SCLM and melts basaltic underplate left by 2.9Ga event resulting in andesites and rhyodacites.

like flat REE pattern and Sm/Nd ratio of the samples. Since back-projection of $\varepsilon_{Nd(t)}$ cannot therefore result in an age for separation from CHUR, this also suggests that the depleted mantle source must have possessed a significant LREE depletion to generate an $\varepsilon_{Nd(t)}$ value of *c.*+3 from the time of its formation (*c.*3.4Ga) to 2.7Ga ago. Conclusions from this are that the basalts must represent a relatively small melt fraction of the depleted mantle component such that the very high Sm/Nd ratio (heavily LREE depleted) of this component is decreased to a lower sub-CHUR Sm/Nd ratio (slightly LREE depleted) which therefore only grows through time-integration by 0.5 epsilon units. Figure 6.4 although diagrammatic, may help understanding of this concept.

6.3.2 Implications for the palaeotectonics of the Midlands Greenstone Belt.

6.3.2.1 Kusky model

Two models for greenstone belt generation and evolution in Zimbabwe have recently been forwarded and will now be considered. Since the majority of recognised greenstone belts in Zimbabwe are recognised as Upper Bulawayan (*c.*2.7Ga) in age, this discussion will primarily deal with the Late Archaean evolution of the craton.

The consensus which has held sway for a number of years now, is that the greenstone belts of Zimbabwe have all been formed in an environment similar to an intra-continental rift setting (Wilson, 1979; Bickle & Nisbet, 1993 and references therein; Wilson *et al.*, 1995; see Chapter 2 for review). Kusky (1998) considered the Zimbabwean greenstone belts to be of two principal types. Those forming the 'southern magmatic belt' (those with the U4E succession as delineated by Wilson *et al.* 1995) were considered to represent passive margin sedimentation and oceanic crustal sequences erupted in the Sea of Umtali, formed as a result of rifting of the early cratonic block (see section 2.3.2). This interpretation was based largely on the work of Fedo & Eriksson (1996) on the sediments of the Buhwa Greenstone Belt and the recognition of the Mberengwa (Belingwe) Greenstone Belt as an allochthonous oceanic plateau (Kusky & Kidd, 1992; Kusky & Winsky, 1995). The greenstones of the 'northern magmatic belt' were considered by Kusky (1998) to be the result of subduction of an oceanic slab (i.e. arc related) from the NW beneath the edge of the 'Tokwe Terrane' (see section 2.3.2 for definition).

Figure 6.4 Origin and evolution of the Nd-isotope signature of Midlands Greenstone Belt magmas.

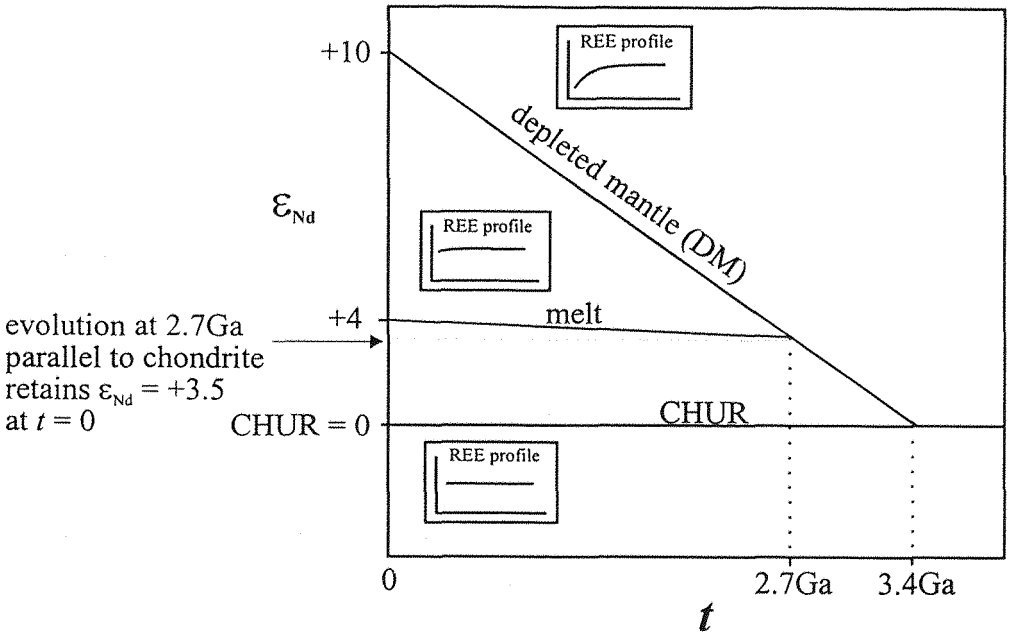

This subduction model for the formation of the Midlands Greenstone Belt raises a number of questions which must be addressed in the light of the current study. The subduction model implies direct melting of the subducting slab to generate the andesitic and rhyodacitic volcanics (after Martin, 1993). Based on the U-Pb zircon and Sm-Nd results of this study, such a slab would have to be *c.*200Ma old. Whilst oceanic crust of this age is apparent today, such old cold portions of oceanic crust could not have survived in the high temperature, convective recycling conditions of the Archaean (Davies, 1995). Bickle *et al.* (1994) calculate that the average age of subducting crust in the Archaean would have been *c.*20Ma. Also the subducting slab would have to reach sufficient temperature and pressure conditions to allow conversion to garnet-amphibolite. Whether Archaean oceanic crust could subduct in a way similar to today, thereby generating the pressures required to form garnet in the slab, remains controversial (see section 6.4). Pressures generated in a volcanic pile may therefore be a better solution. The Kusky (1998) model would also require the SCLM component recognised in this study, to be present in the mantle wedge and the basalt melts to be generated from it by passage of the andesitic melt. This is considered unlikely since the temperature of the andesite melt would be too low to cause melting of the depleted SCLM.

6.3.2.2 Dirks & Jelsma model

Whilst Kusky (1998) invokes major crustal shortening along strike-slip faults, allowing fluid to infiltrate the crust and cause major crustal anatexis, Dirks & Jelsma (1998) invoke thrust stacking of the 2.7Ga volcanic stratigraphy to generate this same Chilimanzi event. The latter authors recognise Fe-rich, siliceous, mylonitic deformation fabrics within horizons conventionally considered to be BIF's and suggest that the greenstone belt stratigraphy of the Zimbabwe Craton was thrust stacked along these zones, thereby disturbing the equilibrium geotherm and causing major anatexis.

Although direct structural evidence is not available, the geochronological results from this study imply major structural kinematics within the Midlands Greenstone Belt around 2.68-2.69Ga ago to juxtapose the 2.9Ga Mafic Formation succession in its present position along-side the 2.7Ga Maliyami and Felsic Formations. This may be considered support for the interpretation of Dirks & Jelsma (1998) but it is stressed that no study conducted on the Midlands Greenstone Belt (Macgregor, 1932; Stowe, 1971; Harrison, 1970; Campbell & Pitfield, 1994; Herrington, 1995; McKeagney, 1998;) has recognised any of the features

indicative of their layer-parallel mylonite zones and this explanation, at least for the Midlands region, would appear at best unlikely.

6.4 MODELS OF GREENSTONE BELT PALAEOTECTONICS AND GENERATION

The literature on the origin and evolution of continents and greenstone belts is vast and has recently been the subject of a significant compilation of papers (de Wit & Ashwal, 1997). The discussion given here in no way attempts to summarise this literature base but instead provides a few examples to illustrate the models proposed for Zimbabwe in a world-wide context.

Condie & Harrison (1976) and Kusky (1998) have inferred modern-day plate tectonic subduction environments for the generation of the Midlands Greenstone Belt. Whilst it is recognised that the lithologies present can be generated in such an environment, other palaeotectonic situations can be envisioned and modelled to produce andesitic and rhyodacitic magmas. The presence of these lithologies does not automatically indicate a subduction zone setting just because this is the environment which most commonly produces such magmas today. Since the thermal regime was very different in the Archaean, it is not unreasonable to suspect that the tectonic regimes and their characteristic lithostratigraphies were also different and that direct extrapolation of uniformitarianism back to the Archaean may not be realistic. The model proposed in this study, remelting of depleted sub-continental lithospheric mantle (SCLM) and basaltic underplate, is preferred to a subduction model for the reasons stated in section 6.3.2.1. Also, studies on the Mberengwa (Belingwe) (Scholey, 1992; Nisbet *et al.*, 1993; Brake, 1996 and Silva, 1998) and Harare-Shamva greenstone belts (Jelsma, 1993; Jelsma *et al.*, 1996) all agree that the presence of komatiitic volcanics and the volcano-sedimentary stratigraphy, indicate plume-generated magmatism in an intracontinental or marginal setting. Although no komatiites (*sensu stricto*) are recognised in the Midlands Greenstone Belt, the heat source for the melting required may well be plume related. Melting as a result of entrainment of mantle in the plume or of the ambient surrounding mantle may be envisioned (Campbell *et al.*, 1989). A dissenting voice was provided by McDonough & Ireland (1993) who concluded from ion-probe work on glass inclusions in olivines from komatiites, that these high temperature volcanics represented oceanic plateau, intraplate magmatism. It is argued that the presence of siliciclastic sediments, including the Sebakwe

River Conglomerate, within the volcanic succession, precludes this scenario for the Midlands Greenstone Belt.

Cattell *et al.* (1984) recognise the existence of a heterogeneous depleted mantle component beneath the Abitibi Greenstone Belt. This is the same conclusion as derived in this study for the Midlands Greenstone Belt since on a large scale, contamination effects are small if present at all. Chase & Patchett (1988) suggest that production and storage of oceanic crust could be the cause of the depleted mantle often recognised in Archaean studies. They conclude that extraction of continental crust is an implausible model for the generation of the depletion since very little pre-3.0Ga continental crust is preserved which might be the result of this. To argue that the early continental crust was rapidly destroyed and recycled into the upper mantle does not allow enough time for time-integrated evolution of the $^{143}Nd/^{144}Nd$ ratio. The significant volumes of oceanic crust generated in the Archaean are therefore a more likely candidate for this depletion but must be 'stored' in order to maintain the depletion whilst gradual melting and release from the stored component allows buffering of the depletion, preventing an excessively high ε_{Nd} value developing. Takahahshi *et al.* (1998) suggest that apparent heterogeneity of the source could result from melting of ambient mantle material entrained in a rising plume. Melts erupted from the plume then either sample an enriched, CHUR-like material or the depleted komatiitic material. Storage of the enriched material (Chase & Patchett, 1988) satisfies the need indicated by Galer & Goldstein (1991) for a complementary enriched component to the depleted Archaean upper mantle. They concluded that gradual depletion over time could not have occurred but that extensive depletion before 3.8Ga with no crustal recycling, was a better model. Other studies (McCulloch & Bennett, 1993; 1994) suggested a progressive depletion of the upper mantle, increasing the thickness of the depleted layer with time. However, this requires sampling of the same thin layer of mantle through-out time which may be unreasonable.

Magmatic underplating is recognised as occurring in the Archaean and Proterozoic by Sun *et al.* (1995) who also consider it the thermal anomaly causing intracrustal melting. Hill (1993) incorporated a subduction model to this interpretation, suggesting that the basaltic slab would have been more buoyant in the Archaean due to increased temperature and decreased viscosity of the upper mantle, causing it to subduct at a shallow angle, possibly resulting in underplating of the continent. Another suggestion by Hill (1993), uses an analogy with the present Ontong-Java Plateau. Increased volcanism in the Archaean would most probably have

generated a thicker oceanic crust such as is produced during periods of intense magmatism at mid-ocean ridges today. These plateaux are less conducive to subduction when they abut an overriding plate at subduction zones. Three scenarios are then hypothesised as possible results, not necessarily mutually exclusive. The plateau may be obducted forming a greenstone belt in the way suggested by Kusky & Kidd (1992); the zone of subduction may step back to the rear of the plateau and create a new subduction zone; and/or the direction of subduction may reverse its polarity. If the thickened crust (plateau) is isolated in this way, it then provides a site for remelting of its base and generation of a continental block (de Wit *et al.*, 1992).

These few comments have been provided as a small example of some of the current theories regarding the formation of continents and their associated greenstone belts. The aim is to highlight the extensive range of ideas, and to indicate that the hypothesis proposed in this study for the origin and evolution of the Midlands Greenstone Belt, is by no means isolated. To review all the models and possibilities for the generation of the Midlands Greenstone Belt and cratonic environments around the world, is far beyond the scope of this study but provides an interesting focus from which to take the research forward. Particularly, it is stressed that no single model may work for the generation of all greenstone belts but that individual situations may require specific solutions. As far as the Zimbabwe Craton is concerned however, it does appear that from study of its greenstone belts to date (Mberengwa (Belingwe), Harare-Shamva, and Midlands), that all have a similar volcano-stratigraphic, geochemical, geochronological and tectonic history which strongly suggests a similar and maybe singular model for their generation.

CHAPTER 7 - CONCLUSIONS

7.1) MAIN CONCLUSIONS

Fieldwork, geochemistry and zircon geochronology conducted on the volcanic and intrusive stratigraphy of the Midlands Greenstone Belt has resulted in conclusions which deviate significantly from those conventionally perceived for this large, gold-rich terrain in the Zimbabwe Craton.

Fieldwork has confirmed the existence of a gabbroic to granitic gneissic enclave, here termed the Sebakwe River Gneiss, within the Mafic Formation volcanics west of Kwekwe. The volcanics themselves are recognised as bimodal with epiclastic felsic conglomerates and dacitic pyroclastics indicating this nature. Intimately associated bimodal volcanics observed in the Maliyami Formation east of the Shamvaian outcrop, are recognised as distinct magmatic compositions intermingled as a result of eruption through the same conduit. This is probably the outcome of a pulse of mafic magmatism disturbing a fractionating andesitic magma residing in an upper crustal magma chamber. Within this same stratigraphy an oolitic limestone is revealed, with significant implications for interpretation of the environment of deposition and possibly the atmospheric conditions 2.7Ga ago. As a result, a continental-shelf marginal-sea environment of deposition is interpreted for the Mafic Formation lithologies expanding to a warm, shallow (wave-base), agitated oxygen-rich epicontinental sea during the deposition of the Maliyami and Felsic Formations.

Zircon geochronology has indicated that the Mafic Formation stratigraphy of Harrison (1970) exposed to the west of Kwekwe is 2880 ± 8Ma old. This was previously considered to belong to the 2.7Ga Upper Bulawayan along with the Maliyami and Felsic Formations dated at 2701 ± 6Ma (U-Pb zircon) by Wilson *et al.* (1995) and 2739 ± 33Ma (Sm-Nd isochron) in this study. The Mafic Formation is therefore probably more representative of the Lower Belingwean (L1-L2) succession of Wilson *et al.* (1995). Other results have shown that the marginal granitoid which forms the basement to the greenstone belt is 3456 ± 6Ma old, virtually identical to an age of 3455 ± 2Ma obtained for the Tokwe River Gneisses. This clearly indicates rocks of Tokwean age in the centre of the craton, with the temporal relationship of the results indicating synchronous formation. A multi-phase gabbroic to granitic gneissic enclave within the 2880Ma volcanics is the oldest rock so far dated from the Zimbabwe Craton at 3565 ± 21Ma. This reflects the antiquity of the craton as a whole but

particularly the Midlands region. The Sesombi Tonalite records two events at 2668 ± 17Ma and 2626 ± 8Ma, the former of which probably represents its crystallisation age and the latter whose interpretation is unsure. This intrusive is slightly preceded by a concordant age of 2677Ma obtained for the Giraffe Porphyry, a sub-volcanic intrusive constraining the end of the 2.7Ga Upper Bulawayan volcanism.

Other regional samples dated include a 3368 ± 9Ma leucosome of the Tokwe River Gneisses probably reflecting a granite generation event at this time resulting in intrusive bodies such as the Mushandike and Mont d'Or granites. A sample thought to represent the *c.*2.9Ga Chingezi Suite revealed a 2672 ± 14Ma Sesombi-like age with *c.*2.85Ga inheritance, probably reflecting the lack of unambiguous field constraints on this sample. Another sample dated as a representative of the *c.*2.6Ga Chilimanzi Suite revealed a complex array of sub-concordant analyses interpreted as a crystallisation age of *c.*2640Ma. Compared to an age of 2601Ma obtained for a member of the suite from the north of the craton (Jelsma, 1993) this possibly indicates a south to north diachroneity in the Chilimanzi event as suggested by Wilson (1979).

As a result of the zircon geochronology, major structural kinematics are inferred to have juxtaposed the different volcanic chronostratigraphies by 2.67Ga, the age of a belt-wide mineralisation event (Darbyshire *et al.*, 1996). This predicts a 10-15Ma time-frame within which the rocks were juxtaposed and tilted through *c.*90°. Also on the basis of results from zircon geochronology, a possible regional unconformity similar to that seen in the National Monument section in the Mberengwa (Belingwe) Greenstone Belt is hypothesised between the 2.9Ga volcanic succession of the Mafic Formation and the *c.*3.5Ga basement.

Major, trace and REE geochemistry indicates that the basalts from both the 2.9Ga & 2.7Ga chronostratigraphies have a LREE depleted source and have undergone the same evolution of approximately 65% fractionation of a 70% plagioclase 30% clinopyroxene assemblage. The andesites and rhyodacites are most likely sourced from melting of a previously existing basaltic component transformed to amphibolite possibly containing garnet, and have evolved by fractionating ilmenite, amphibole and plagioclase. Some rhyodacites and porphyries including the Late Porphyries and Sesombi Tonalite, must have had garnet in the source from which they were derived to generate the very low Y and HREE concentrations. Some mixing between magmas is seen to be occurring in the field and in thin section, but is hard to identify in the geochemistry. End-members with significantly opposing

compositions (e.g. basalt and rhyodacite) are not considered to have been able to mix due to the extreme differences in their eruption temperature and viscosity (Philpotts, 1990). This has resulted in the spectacular mingled-magma features displayed in the field.

Sm-Nd isotope geochemistry results in variable $\varepsilon_{Nd(t)}$ values from +3.49 to +1.53. This could indicate <0.5% contamination by continental crust but is considered more indicative of sampling of a heterogeneous mantle component. Depleted mantle (T_{DM}) model ages determined for the basalts, indicates that they were derived from a depleted sub-continental lithospheric mantle which has a mantle separation age of 3.2-3.4Ga. This is considered similar to that identified by Nägler *et al.* (1997) beneath the Tokwe Segment, and in the light of the Tokwean ages determined for the Midlands region in this study, a sub-continental lithospheric mantle (SCLM) component is hypothesised to extend this far. Andesites and rhyodacites record a *c.*2.85Ga depleted mantle model age and are thought to be derived by melting of a basaltic underplate of this age.

As a result of these investigations, an extensive, ancient protocratonic core is directly recognised and considered to underlie a large proportion of the Zimbabwe Craton as seen today, forming a stable continental block about and through which greenstone belt volcanism was extruded. The term Tokwe Proto-craton is suggested for this terrain whose existence precludes the northwest-ward directed growth and accretion model suggested for the craton by Wilson (1979). The formation of the greenstone belt is envisioned to result from the arrival of a mantle plume or other thermal anomaly at *c.*2.9Ga depositing a basaltic layer beneath the Tokwe Proto-craton. This caused melting in the *c.*3.4Ga SCLM and left an underplate of basalt which, suffered partial melting to form melts of andesite to rhyodacite compositions, during a subsequent thermal event at *c.*2.7Ga. This event also generated more basaltic melt from the SCLM. It is however stressed, that based on the data presented in this study a model for the generation of the Midlands Greenstone Belt volcanics through melting and heat supply by subduction, cannot be totally ruled out but at this present point in time, a source for the heat by impingement of a mantle plume or other thermal anomaly directly beneath a stable cratonic block is preferred.

7.2) SUGGESTIONS FOR FUTURE RESEARCH

7.2.1) Structure and Sedimentology

A detailed ground based structural investigation of the Midlands Greenstone Belt is now considered essential. Little is understood regarding the nature of the three major shear zones in the belt (Munyati, Sherwood and Taba-Mali) and study of them would help understanding of the juxtaposition of the 2.9Ga Mafic Formation succession and the 2.7Ga Maliyami and Felsic Formation sequence. Recent preliminary investigations indicate that the Tabi-Mali shear zone as currently defined does not possess the major kinematics this model suggests. However, if the Shamvaian outcrop resides in a structurally defined basin such as a flower structure, the main kinematic indicators may well be buried from view. For these reasons a sedimentological investigation of the Shamvaian outcrop is also strongly suggested to determine the depositional facies indicated by these sediments.

Structural studies are also important in the Mafic Formation section for interpretation of the gold mineralisation and would help ascertain the likelihood of the suggested Lower Belingwean regional unconformity with the Sebakwe River Gneiss.

7.2.2) Geochronology

More precise dating of Sebakwe River Gneiss should be conducted to confirm the *c.*3.5Ga age determined in this study. More detailed grain selection through extremely careful picking and imaging prior to analysis would help increase the precision and concordancy, and decrease the MSWD.

More dating of the granitoids comprising the Zimbabwe Craton would help better delineate the Tokwe Proto-craton. This is considered especially important for the eastern and central regions of the craton where little geological and geochronological constraint is recognised. Delineation of these older terrains could have significant implications for mineral exploration.

Single grain zircon geochronology conducted for this study has highlighted the necessity to image a representative subset, or possibly even the actual grains, before analysis. Recognition of complex crystallisation and recrystallisation features within zircon crystals now renders even ID-TIMS dissolution results open to interpretation. Imaging and microscale analysis through in-situ laser ablation or ion-probe techniques is considered the way forward for this geochronological technique.

7.2.3) Isotope Geochemistry

Detailed isotope work is recommended to confirm or refute the SCLM and basaltic underplate model suggested in this study. A combined Sm-Nd, Pb-Pb and Re-Os study, although laborious, would help to accomplish this since no single isotope system would remain closed to magmatic, alteration and structural influences across the craton.

7.2.4) Palaeotectonic Interpretation

The implementation and combination of the suggested studies would significantly increase the understanding of the Zimbabwe Craton which is currently undergoing somewhat of a revolution in interpretation (Dirks & Jelsma, 1998; Kusky, 1998). It may then be possible to decipher the palaeotectonic environment(s) which constructed the craton. This could have significant academic and economic ramifications.

REFERENCES

Arndt, N.T. & Goldstein, S.L., 1987. Use and abuse of crust-formation ages. *Geology*, **15**, 893-895.

Arth, J.G. & Barker, F., 1976. Rare-earth partitioning between hornblende and dacitic liquid and implications for the genesis of trondhjemitic-tonalitic magmas. *Geology*, **4**, 534-536.

Bacon, C.R., 1989. Crystallisation of accessory phases in magmas by local saturation adjacent to phenocrysts. *Geochimica et Cosmochimica Acta*, **53**, 1055-1066.

Baldock, J.W. & Evans, J.A. 1988. Constraints on the age of the Bulawayan Group metavolcanic sequence, Harare Greenstone Belt, Zimbabwe. *Journal of African Earth Sciences*, 7, 795-804.

Barker, F. & Arth, J.G. 1976. Generation of trondhjemitic-tonalitic liquids and Archaean bimodal trondhjemite-basalt suites. *Geology*, **4**, 596-600.

Bea, F. 1996. Controls on the trace element composition of crustal melts. *Transactions of the Royal Society of Edinburgh: Earth Sciences*, **87**, 33-41.

Benisek, A. & Finger, F. 1993. Factors controlling the development of prism faces in granite zircons: a microprobe study. *Contrib. Mineral. Petrol.* **114**, 441-451.

Beukes, N.J., 1977. Transition from siliciclastic to carbonate sedimentation near the base of the Transvaal Supergroup, Northern Cape Province, South Africa. *Sedimentary Geology*, **18**, 201-221.

Bickle, M.J., Martin, A. & Nisbet, E.G. 1975. Basaltic and peridotitic komatiites and stromatolites above a basal unconformity in the Belingwe greenstone belt, Rhodesia. *Earth and Planetary Science Letters*, **27**, 155-162.

Bickle, M.J. & Nisbet, E.G. 1993. *The geology of the Belingwe Greenstone Belt, Zimbabwe.* (eds) Geological Society of Zimbabwe Special Publications, **No.2**, 167-174.

Bickle, M.J., Arndt, N.T., Nisbet, E.G., Orpen, J.L., Martin, A., Keays, R.R. & Renner, R. 1993. Geochemistry of the igneous rocks of the Belingwe Greenstone Belt: Alteration, contamination and petrogenesis. *In*: Bickle, M.J., & Nisbet, E.G. (eds) *The geology of the Belingwe Greenstone Belt, Zimbabwe.* Geological Society of Zimbabwe Special Publications, **No.2**, 167-174.

Bickle, M.J., Nisbet, E.G. & Martin, A. 1994. Archaean Greenstone Belts are not Oceanic Crust. *Journal of Geology*, **102**, 121-138.

Blenkinsop, T.G., Fedo, C.M., Bickle, M.J., Eriksson, K.A., Martin, A., Nisbet, E.G. & Wilson, J.F. 1993. Ensialic origin for the Ngezi Group, Belingwe greenstone belt, Zimbabwe. *Geology*, **21**, 1135-1138.

Blenkinsop, T.G., Fedo, C.M., Bickle, M.J., Eriksson, K.A., Martin, A., Nisbet, E.G., Wilson, J.F. & Orpen, J.L. 1994. Ensialic origin for the Ngezi Group, Belingwe greenstone belt, Zimbabwe - reply. *Geology*, **22**, 767-768.

Bliss, N.W. 1970. *The geology of the country around Gatooma.* Rhodesia Geological Survey Bulletin **No.64**, 240pp

Boyd, F.R., 1989. Compositional distinction between oceanic and continental lithosphere. *Earth and Planetary Science Letters*, **96**, 15-26.

Brake, C. 1996. *Tholeiitic magmatism in the Belingwe Greenstone Belt, Zimbabwe.* Unpublished PhD thesis, University of Edinburgh.

Campbell, I.H., Griffiths, R.W. & Hill, R.I., 1989. Melting in an Archaean mantle plume: heads it's basalts, tails it's komatiites. *Nature*, **339**, 697-699.

Campbell, S.D.G. & Pitfield, P.E.J. 1994. *Structural controls of gold mineralisation in the Zimbabwe Craton - exploration guidelines.* Zimbabwe Geological Survey Bulletin, **No.101**, 270pp.

Cattell, A., Krogh, T.E. & Arndt, N.T., 1984. Conflicting Sm-Nd whole rock and U-Pb zircon ages for Archean lavas from Newton Township, Abitibi Belt, Ontario. *Earth and Planetary Sc. Letters*, **70**, 280-290.

Chapman, H.J. & Roddick, J.C. 1994. Kinetics of Pb release during the zircon evaporation technique. *Earth and Planetary Science Letters,* **121**, 601-611.

Chase, C.G. & Patchett, P.J., 1988. Stored mafic/ultramafic crust and early Archaean mantle depletion. *Earth and Planetary Sc. Letters*, **91**, 66-72.

Chauvel, C., Dupre, B. & Arndt, N.T. 1993. Pb and Nd isotopic correlation in Belingwe komatiites and basalts. *In*: Bickle, M.J., & Nisbet, E.G. (eds) *The geology of the Belingwe Greenstone Belt, Zimbabwe*. Geological Society of Zimbabwe Special Publications, **No.2**, 167-174.

Cheburkin, A.K., Frei, R. & Shotyk, W. 1997. An energy-dispersive miniprobe multielement analyzer (EMMA) for direct analysis of trace elements and chemical age dating of single mineral grains. *Chemical Geology,* **135**, 75-87.

Cherniak, D.J., Hanchar, J.M. & Watson, E.B. 1997a. Rare-earth diffusion in zircon. *Chemical Geology,* **134**, 289-301.

Cherniak, D.J., Hanchar, J.M. & Watson, E.B. 1997b. Diffusion of tetravalent cations in zircon. *Contrib. Mineral. Petrol.*, **127**, 383-390.

Cheshire, P.E., Leach, A., & Milner, S.A., 1980. *The Geology of the Country between Gwelo and Redcliff.* Zimbabwe Geological Survey Bulletin **No.86**

Claoue-Long, J.C., Compston, W. & Cowden, A. 1988. The age of the Kambalda greenstones resolved by ion-microprobe: implications for Archaean dating methods. *Earth and Planetary Science Letters*, **89**, 239-259.

Compston, W., Kinny, P.D., Williams, I.S. & Foster, J. 1986. The age and Pb-loss behaviour of zircons from the Isua supercrustal belt as determined by ion-microprobe. *Earth and Planetary Science Letters*, **80**, 71-81.

Condie, K.C., & Harrison, N.M., 1976. Geochemistry of the Archaean Bulawayan Group, Midlands Greenstone Belt, Rhodesia. *Precambrian Research*, **3**, 253-271

Coward, M.P. 1976. Archaean deformation patterns in Southern Africa. *Philosophical Transactions of the Royal Society, London,* **A283**, 313-331.

Coward, M.P., James, P.R. & Wright, L. 1976. Northern margin of the Limpopo mobile belt, southern Africa. *Bulletin of the Geological Society of America*, **87**, 601-611.

Darbyshire, D.P.F., Pitfield, P.E.J. & Campbell, S.D.G., 1996. Late Archean and Early Proterozoic gold-tungsten mineralisation in the Zimbabwe Archean Craton: Rb-Sr and Sm-Nd isotope constraints. *Geology*, **24**, no.1, 19-22.

Davies, G.F., 1995. Punctuated tectonic evolution of the Earth. *Earth and Planetary Sc. Letters*, **136**, 363-379.

de Wit, M.J., Roering, C., Hart, R.J., Armstrong, R.A., de Ronde, C.E.J., Green, R.W.E., Tredoux, M., Peberdy, E. & Hart, R., 1992. Formation of an Archaean continent. *Nature*, **357**, 553-562.

de Wit, M. & Ashwal, L., 1997. *Greenstone Belts.* Oxford Monographs on Geology and Geophysics, No.35, 809pp. Clarendon Press, Oxford.

Deer, W.A., Howie, R.A. & Zussman, J. 1966. *An Introduction to the Rock-forming Minerals*, 1st edition. Longman, London.

Deer, W.A., Howie, R.A., & Zussman, J., 1982. *Rock Forming Minerals, Volume 1A - Orthosilicates (2nd edition).* Longman, London. 919pp

Dirks, P.H.G.M. & Jelsma, H.A., 1998. Horizontal accretion and stabilisation of the Archaean Zimbabwe Craton. *Geology*, **26**, no.1, 11-14.

Dodson, M.H., Compston, W., Williams, I.S. & Wilson, J.F. 1988. A search for ancient detrital zircons in Zimbabwean sediments. *Journal of the Geological Society, London,* **145**, 977-983.

Dougherty-Page, J.S. 1994. *The Evolution of the Archaean Continental Crust of Northern Zimbabwe.* Unpublished PhD thesis, Open University, Milton Keynes.

Dougherty-Page, J.S. & Foden, J. 1996. Pb-Pb zircon evaporation date for the Charleston Granite, South Australia: comparisons with other zircon geochronology techniques. *Australian Journal of Earth Sciences,* **43**, 133-137.

Dowty, E. 1976. Crystal structure and growth: II. Sector zoning in minerals. *American Mineralogist,* **61**, 460-469.

Eriksson, K.A., Krapez, B. & Fralick, P.W., 1994. Sedimentology of Archaean greenstone belts: signatures of tectonic evolution. *Earth-Science Reviews*, **37**, 1-88.

Eriksson, K.A. 1995. *Crustal growth, surface processes and atmospheric evolution of the early Earth.* In Coward, M.P. & Ries, A.C. (eds), *Early Precambrian Processes,* Geol. Soc. Spec. Publ. No.**95**, p.109-126.

Faure, G. 1986. *Principles of Isotope Geology* (2nd edition) 589 pp., London, Wiley.

Fedo, C.M. & Eriksson, K.A. 1996. Stratigraphic framework of the ~3.0Ga Buhwa greenstone belt: A unique stable shelf succession in the Zimbabwe Archaean craton. *Precambrian Research*, **77**, 161-178.

Foster, R.P., Mann, A.G., Stowe, C.W. & Wilson, J.F. 1986. Archaean gold mineralisation in Zimbabwe, *in* Anhaeusser, C.R., and Maske, S. (eds.), Mineral deposits of southern Africa. *Geological Society of South Africa*, **1**, 43-112.

Frei, R. & Kamber, B.S. 1995. Single mineral Pb-Pb dating. *Earth and Planetary Science Letters,* **129**, 261-268.

Galer, S.J.G. & Goldstein, S.L., 1991. Early mantle differentiation and its thermal consequences. *Geochim. Cosmochim. Acta.*, **55**, 227-239.

Govindaraju, K., 1994. 1994 compilation of working values and sample description for 383 geostandards. *Geostandards Newsletter*, **18** (Special Isuue), 158pp.

Hamilton, P.J. 1977. Sr isotope and trace element studies of the Great Dyke and Bushveld Mafic Phase and their relation to early Proterozoic magma genesis in southern Africa. *Journal of Petrology*, **18**, 24-52.

Hanchar, J.M. & Miller, C.F. 1993. Zircon zonation patterns as revealed by cathodoluminescence and back-scattered electron images: Implications for interpretation of complex crustal histories. *Chemical Geology,* **110**, 1-13.

Harrison, N.M. 1968. A reassessment of the stratigraphy of the Precambrian basement complex around Que Que, Gwelo district, Rhodesia. *Annex. Trans. Geol. Soc. S.Africa*, **71**, 113-123.

Harrison, N.M. 1970. *The Geology of the Country around Que Que.* Rhodesia Geological Survey Bulletin **No.67.**

Hawkesworth, C.J., Moorbath, S., O'Nions, R.K. & Wilson, J.F. 1975. Age relationship between greenstone belts and granites in the Rhodesian Archaean craton. *Earth and Planetary Science Letters*, **25**, 251-262.

Hawkesworth, C.J. & O'Nions, R.K. 1977. The petrogenesis of some Archaean volcanic rocks from Southern Africa. *Journal of Petrology*, **18**, part 3, 487-520.

Hawkesworth, C.J., Bickle, M.J., Gledhill, A.R., Wilson, J.F. & Orpen, J.L. 1979. A 2.9 b.y. event in the Rhodesian Archaean. *Earth and Planetary Science Letters*, **43**, 285-297.

Helmsteadt, H.W.A., Padgham, A. & Brophy, J.A. 1986. Multiple dykes in the Lower Cam Group, Yellowknife Greenstone Belt: evidence for Archaean seafloor spreading? *Geology*, **14**, 562-566.

Henson, B.J. & Green, D.H. 1973. Experimental study of the stability of cordierite and garnet in pelitic compositions at high pressures and temperatures. III. Synthesis of experimental data and geological applications. *Contrib. Mineral. Petrol.*, **38**, 151-166.

Herrington, R.J., 1995. *Late Archaean structure and gold mineralisation in the Kadoma region of the Midlands Greenstone Belt, Zimbabwe.* In Coward, M.P. & Ries, A.C. (eds), *Early Precambrian Processes,* Geol. Soc. Spec. Publ. **No.95**, 295pp.

Hickman, M.H. 1978. Isotopic evidence for crustal reworking in the Rhodesian Archaean craton, southern Africa, *Geology*, **6**, 214-216.

Hill, R.I., 1993. Mantle plumes and continental tectonics. *Lithos*, **30**, 193-206.

Hirata, T. & Nesbitt, R.W. 1995. U-Pb isotope geochronology of zircon: evaluation of the laser probe-inductively coupled plasma mass spectrometry technique. *Geochimica et Cosmochimica Acta,* **59**, 2491-2500.

Horwitz, R.C. & Pidgeon, R.T. 1993. 3.1Ga tuff from the Sholl belt in the west Pilbara: further evidence for diachronous volcanism in the Pilbara craton of Western Australia. *Precambrian Research*, **60**, 175-183.

Jelsma, H.A., 1993. *Granites and Greenstones in Northern Zimbabwe: tectono-thermal evolution and source regions.* Unpublished PhD thesis, Free University, Amsterdam, Netherlands.

Jelsma, H.A., Vinju, M.L., Valbracht, P.J., Davies, G.R., Wijbrans, J.R. & Verdurmen, E.A.T., 1996. Constraints on Archaean crustal evolution or the Zimbabwe Craton: a U-Pb zircon, Sm-Nd and Pb-Pb whole rock isotope study. *Contrib. Mineral. Petrol.*, **124**, 55-70.

Kalsbeek, F. 1992. The statistical distribution of the mean squared weighted deviation - Comment: Isochrons, errorchrons, and the use of MSWD-values. *Chemical Geology (Isotope Geoscience Section)*, **94**, 241-242.

Keesman, I., Matthes, S., Schreyer, W. & Seifert, F., 1971. Stability of almandine in the system FeO-(Fe_2O_3)-Al_2O_3-SiO_2-(H_2O) at elevated temperatures. *Contrib. Mineral. Petrol.*, **31**, 132-144.

Kober, B. 1986. Whole-grain evaporation $^{207}Pb/^{206}Pb$ age investigations on single zircons using a double-filament thermal ion source. *Contrib. Mineral. Petrol.*, **93**, 63-71.

Krogh, T.E. 1973. A low contamination method for the hydrothermal decomposition of zircon and extraction of U and Pb for isotopic age determinations. *Geochimica et Cosmochimica Acta,* **37**, 485-494.

Krogh, T.E. 1982a. Improved accuracy of U-Pb dating by selection of more concordant fractions using a high gradient magnetic separation technique. *Geochimica et Cosmochimica Acta,* **46**, 631-636.

Krogh, T.E. 1982b. Improved accuracy of U-Pb zircon dating by creation of more concordant systems using an air abrasion technique. *Geochimica et Cosmochimica Acta,* **46**, 637-649.

Kusky, T.M. & Kidd, W.S.F. 1992. Remnants of an Archean oceanic plateau, Belingwe greenstone belt, Zimbabwe. *Geology*, **20**, 43-46.

Kusky, T.M., Winsky, P.A. & Kidd, W.S.F. 1994. Ensialic origin for the Ngezi Group, Belingwe greenstone belt, Zimbabwe - comment. *Geology*, **22**, 766-767.

Kusky, T.M. & Winsky, P.A. 1995. Structural relationships along a greenstone/shallow water shelf contact, Belingwe greenstone belt, Zimbabwe. *Tectonics*, **14**, no.2, 448-471.

Kusky, T.M. 1998. Tectonic setting and terrain accretion of the Archaean Zimbabwe Craton. *Geology*, **26**, no.2, 163-166.

Le Maitre, R.W., Bateman, P., Dudek, A., Keller, J., Le Bas, M.J., Sabine, P.J., Schmid, R., Sorensen, H., Streckeisen, A., Woolley, A.R. & Zanettin, B. 1989. *A classification of igneous rocks and glossary of terms.* Blackwell, Oxford.

Lee, J.K.W. & Tromp, J. 1995. Self-induced fracture generation in zircon. *Journal of Geophysical Research,* **100**, No.B9, 17,753-17,770.

Lee, J.K.W., Williams, I.S. & Ellis, D.J. 1997. Pb, U and Th diffusion in natural zircon. *Nature,* **390**, 159-161.

Loth, G. & Höll, R. 1996. Cathodoluminescence Invcstigation of the Evolution of Zircon Crystal Shapes Applied to Supplement Geochemical Studies. *Journal of Conference Abstracts,* **1**(1), 370.

Ludwig, K.R. 1980. Calculation of uncertainties of U-Pb isotope data. *Earth and Planetary Science Letters*, **46**, p. 212-20.

Macgregor, A.M. 1932. *The Geology of the Country around Que Que, Gwelo District.* Bull. Geol. Surv. Rhod., **No.20.**

Macgregor, A.M. 1951. Some milestones in the Precambrian of Southern Rhodesia. *Transactions of the Geological Society of South Africa*, **54**, xxvii-lxxi.

Martin, A. 1978. *The Geology of the Belingwe - Shabani Schist Belt.* Rhodesia Geological Survey, Bulletin No. 83, 220 pp.

Martin, A., Nisbet, E.G., Bickle, M.J. & Orpen, J.L. 1993. Rock units and stratigraphy of the Belingwe Greenstone Belt: The complexity of the tectonic setting. *In*: Bickle, M.J., & Nisbet, E.G. (eds) *The geology of the Belingwe Greenstone Belt, Zimbabwe.* Geological Society of Zimbabwe Special Publications, **No.2**, 13-37.

Martin, H. 1993. The mechanisms of petrogenesis of the Archaean continental crust - comparison with modern processes. *Lithos,* **30**, 373-388.

McCulloch, M.T. & Bennett, V.C., 1993. Evolution of the early Earth: constraints from 143Nd-142Nd isotopic systematics. *Lithos*, **30**, 237-255.

McCulloch, M.T. & Bennett, V.C., 1994. Progressive growth of the Earths continental crust and depleted mantle: geochemical constraints. *Geochim. Cosmochim. Acta.* **58**, no.21, 4717-4738.

McDonough, W.F. & Ireland, T.R., 1993. Intraplate origin of komatiites inferred from trace elements in glass inclusions. *Nature*, **365**, 432-434.

McKeagney, C.J., 1998. Structural and alteration characteristics of the Indarama lode gold deposits, Zimbabwe; implications for craton-wide tectonism and mineralisation. *Unpublished PhD thesis, Southampton University.*

Mezger, K. & Krogstad, E.J. 1997. Interpretation of discordant U-Pb zircon ages: An evaluation. *Journal of Metamorphic Geology,* **15**, 127-140.

Moorbath, S.M., Wilson, J.F., Goodwin, R. & Humm, M. 1977. Further Rb-Sr age and isotope data on early and late Archaean rocks from the Rhodesian craton. *Precambrian Research*, **5**, 229-239.

Moorbath, S.M., Whitehouse, M.J. & Kamber, B.S., 1997. Extreme Nd-isotope heterogeneity in the early Archaean - fact or fiction? Case histories from Northern Canada and West Greenland. *Chemical Geology*, **135**, 213-231.

Nägler, Th.F., Kramers, J.D., Kamber, B.S., Frei, R. & Prendergast, M.D.A. 1997. Growth of the subcontinental lithospheric mantle beneath Zimbabwe started at or before 3.8Ga: Re-Os study on chromites. *Geology*, **25**, no.11, 983-986.

Nasdala, L., Pidgeon, R.T. & Wolf, D. 1996. Heterogeneous metamictisation of zircon on a microscale. *Geochimica et Cosmochimica Acta,* **60**, No.6, 1091-1097.

Nisbet, E.G., Bickle, M.J. & Martin, A. 1977. The mafic and ultramafic lavas of the Belingwe Greenstone Belt, Rhodesia. *Journal of Petrology*, **18**, part 4, 521-566.

Nisbet, E.G., Bickle, M.J., Martin, A., Orpen, J.L. & Wilson, J.F. 1982. Komatiites in Zimbabwe. *In: Komatiites*. Arndt, N.T. & Nisbet, E.G. (eds). George Allen & Unwin, London. 526pp.

Nisbet, E.G., Arndt, N.T., Bickle, M.J., Cameron, W.E., Chauvel, C., Cheadle, M., Hegner, E., Kyser, T.K., Martin, A., Renner, R. & Roedder, E. 1987. Uniquely fresh 2.7 Ga komatiites from the Belingwe greenstone belt, Zimbabwe. *Geology*, **15**, 1147-1150.

Nisbet, E.G., Bickle, M.J., Orpen, J.L. & Martin, A., 1993. Controls on the formation of the Belingwe Greenstone Belt, Zimbabwe. *In*: Bickle, M.J., & Nisbet, E.G. (eds) *The geology of the Belingwe Greenstone Belt, Zimbabwe*. Geological Society of Zimbabwe Special Publications, **No.2**, 234pp.

Noble, S.R., Tucker, R.D., and Pharaoh, T.C., 1993. Lower Palaeozoic and Precambrian igneous rocks from eastern England, and their bearing on late Ordovician closure of the Tornquist Sea: constraints from U-Pb and Nd isotopes: *Geological Magazine*, **130**, p. 835-846.

O'Hara, M.J. & Matthews, R.E. 1981. Geochemical evolution in an advancing, periodically replenished, periodically tapped, continuously fractionated magma chamber. *Jour. Geol. Soc. Lond.*, **138**, 237-277.

Orpen, J.L. 1978. *The geology of the southwestern part of the Belingwe greenstone belt and the adjacent country - the Belingwe Peak area.* Unpublished D.Phil. thesis, University of Rhodesia.

Orpen, J.L. & Wilson, J.F. 1981. Stromatolites at c.3500 Myr and a granite-greenstone unconformity in the Zimbabwean Archaean. *Nature*, **291**, 218-220.

Parrish, R.R., 1987. An improved micro-capsule for zircon dissolution in U-Pb geochronology. *Chemical Geology (Isotope Geoscience Section),* **66**, p. 99-102.

Peucat, J.J., Vidal, P., Bernard-Griffiths, J. & Condie, K.C., 1989. Sr, Nd and Pb isotopic systematics in the Archaean low to high-grade transition zone of southern India: syn-accretion vs. post-accretion granulites. *J.Geol.*, **97**, 537-550.

Philpotts, A.R. 1990. *Principles of Igneous and Metamorphic Petrology.* Prentice Hall, New Jersey. 498pp.

Pidgeon, R.T. 1992. Recrystallisation of oscillatory zoned zircon: some geochronological and petrological implications. *Contrib. Mineral. Petrol.* **110**, 463-472.

Pupin, J.P. 1980. Zircon and Granite Petrology. *Contrib. Mineral. Petrol.* **73,** 207-220.

Ramakrishnan, S.S, Gokhale, K.V.G.K. & Subbarao, E.C. 1969. Solid solubility in the system zircon-hafnon. *Mat. Res. Bull.*, **4**, 323-328.

Rapp, R.P., Watson, E.B. & Miller, C.F. 1991. Partial melting of amphibolite/eclogite and the origin of Archaean trondhjemites and tonalites. *Precambrian Research,* **51**, 1-25.

Robertson, I.D.M. 1976. *The Geology of the country around Battlefields, Gatooma District.* Rhodesia Geological Survey Bulletin **No.76.**

Rollinson, H.R., 1993. *Using geochemical data: evaluation, presentation, interpretation.* Longman, London. 352pp.

Schärer, U. & Allègre, C.J. 1982. Uranium-lead system in fragments of a single zircon grain. *Nature,* **295**, 585-587.

Scholey, S.P. 1992. The geology and geochemistry of the Ngezi Group volcanics, Belingwe greenstone belt, Zimbabwe. *Unpublished PhD thesis, Southampton University.*

Sergeev, S.A., Meier, M. & Steiger, R.H., 1995. Improving the resolution of single-grain U/Pb dating by use of zircon extracted from feldspar: Application to the Variscan magmatic cycle in the central Alps. *Earth and Planetary Science Letters*, **134**, 37-51.

Shannon, R.D. 1976. Revised effective ionic radii and systematic studies of interatomic distances in halides and chalcogenides. *Acta Crystallogr.* **A32**, 751-767.

Silva, K.E. 1998. Komatiites from the Belingwe Greenstone Belt, Zimbabwe: constraints on the development of Archaean Greenstone Belts. *Unpublished PhD thesis, Royal Holloway College, University of London.*

Speer, J.A. 1980. *Zircon.* In: Ribbe, P.H. (ed) Orthosilicates. Reviews in Mineralogy, **5**, Mineralogical Society of America, 67-103.

Stacey, J.S. & Kramers, J.D. 1975. Approximation of terrestrial lead isotope evolution by a two-stage model. *Earth and Planetary Science Letters*, **26**, 207-221.

Steiger, R.H. & Wasserburg, G.J. 1969. Comparative U-Th-Pb systematics in $2.7x10^9$yr plutons of different geologic histories. *Geochimica et Cosmochimica Acta,* 33, 1213-1232.

Stern, T.W., Goldich, S.S. & Newell, M.F. 1966. Effects of weathering on the U-Pb ages of zircon from the Morton Gneiss, Minnesota. *Earth and Planetary Science Letters,* **1**, 369-371.

Stowe, C.W. 1971. Summary of the Tectonic Development of the Rhodesian Archaean Craton. *Spec. Publ. Geol. Soc. Aust., 3, p.377-383.*

Stowe, C.W. 1979. A sequence of plutons in the central portion of the Rhodesdale Granitic terrane. *Rhodesia. Trans. Geol. Soc. S. Africa, 82, p.277-285.*

Sun, S-S. & Nesbitt, R.W. 1978. Petrogenesis of Archaean ultrabasic and basic volcanics: evidence from rare earth elements. *Contrib. Mineral. Petrol.*, **65**, 301-325.

Sun, S-S., Warren, R.G. & Shaw, R.D., 1995. Nd isotope study of granites from the Arunta Inlier, central Australia: constraints on geological models and limitation of the method. *Precambrian Research*, **71**, 301-314.

Takahahshi, E., Nakajima, K. & Wright, T.L., 1998. Origin of the Columbia River Basalts: melting model of a heterogeneous plume head. *Earth and Planetary Sc. Letters* (*in press*).

Taylor, P.N., Kramers, J.D., Moorbath, S., Wilson, J.F., Orpen, J.L. & Martin, A. 1991. Pb/Pb, Nd-Sm and Rb-Sr geochronology in the Archean craton of Zimbabwe. *Chemical Geology (Isotope Geosciences Section)*, **86**, 175-196.

Taylor, S.R. & Gorton, M.P., 1977. Geochemical application of Spark source mass spectrography-III. Element sensitivity, precision and accuracy. *Geochim. Cosmochim. Acta.*, **41**, 1375-1380.

Taylor, S.R. & McLennan, S.M. 1985. *The Continental Crust: its composition and Evolution.* Blackwell, Oxford. 312pp.

Taylor, S.R. & McLennan, S.M. 1995. The geochemical evolution of the continental crust. *Reviews of Geophysics,* **33**, 2, 241-265.

Tilton, G.R. 1960. Volume diffusion as a mechanism for discordant lead ages. *Jour. Geophys. Res.*, **65**, No.9, 2933-2945.

Treloar, P.J., Coward, M.P. & Harris, N.B.W. 1992. Himalayan-Tibetan analogies for the evolution of the Zimbabwe Craton and Limpopo Belt. *Precambrian Research*, **55**, 571-587.

Treloar, P.J. & Blenkinsop, T.G. 1995. Archaean deformation patterns in Zimbabwe: true indicators of Tibetan-style crustal extrusion or not? *In*: Coward, M.P., & Ries, A.C. (eds) *Early Precambrian Processes*. Geological Society of London Special Publication, **95**, 109-126.

Tsomondo, J.M., Wilson, J.F. & Blenkinsop, T.G. 1992. Reassessment of the structure and stratigraphy of the early Archaean Selukwe Nappe, Zimbabwe. *In*: Glover, J.E., & Ho,

S.E. (eds) *The Archaean: Terrains, Processes and Metallogeny*. Geology Department (Key Centre) & University Extension, The University of Western Australia, **22**, 123-135.

Vavra, G. 1990. On the kinematics of zircon growth and its petrogenetic significance: a cathodoluminescence study. *Contrib. Mineral. Petrol.* **106**, 90-99.

Walker, R.J., Carlson, R.W., Shirey, S.B. & Boyd, F.R., 1989. Os, Sr, Nd and Pb isotope systematics of southern African xenoliths: Implications for the chemical evolution of subcontinental mantle. *Geochim. Cosmochim. Acta.*, **53**, 1583-1595.

Watson, E.B. & Yan Liang 1995. A simple model for sector zoning in slowly grown crystals: Implications for growth rate and lattice diffusion, with emphasis on accessory mineral in crustal rocks. *Am. Mineral.*, **80**, 1179-1187.

Watson, E.B. 1996. Dissolution, growth and survival of zircons during crustal fusion: kinetic principles, geological models and implications for isotopic inheritance. *Trans. Roy. Soc. Edin.: Earth Sc.*, **87**, 43-56.

Watson, E.B., Cherniak, D.J., Hanchar, J.M., Harrison, T.M. & Wark, D.A. 1997. The incorporation of Pb into zircon. *Chemical Geology*, **141**, 19-31.

Wendt, I. & Carl, C. 1991. The statistical distribution of the mean squared weighted deviation. *Chemical Geology (Isotope Geoscience Section)*, **86**, 275-285.

Wendt, I. 1992. The statistical distribution of the mean squared weighted deviation - reply. *Chemical Geology (Isotope Geoscience Section)*, **94**, 242-243.

Wetherill, G.W. 1956a. Discordant uranium-lead ages, 1. *Trans. Am. Geophys. Union*, **37**, 320-326.

Wetherill, G.W. 1956b. Discordant uranium-lead ages, 2. *Jour. Geophys. Res.*, **68**, No.10, 2957-2965.

Williams, I.S., Compston, W., Black, L.P., Ireland, T.R. & Foster, J.J. 1984. Unsupported radiogenic Pb in zircon: a cause of anomalously high Pb-Pb, U-Pb and Th-Pb ages. *Contrib. Mineral. Petrol.*, **88**, 322-327.

Wilson, J.F., Bickle, M.J., Hawkesworth, C.J., Martin, A., Nisbet, E.G. & Orpen, J.L. 1978. Granite - greenstone terrains of the Rhodesian Archaean craton. *Nature*, **271**, 23-27.

Wilson, J.F. 1979. A preliminary appraisal of the Rhodesian Basement Complex. *Special Publication of the Geological Society of South Africa*, **5**, 1-23.

Wilson, J.F. 1990. A craton and its cracks: some of the behaviour of the Zimbabwe block from the Late Archaean to the Mesozoic in response to horizontal movements, and the significance of its mafic dyke fracture patterns. *Journal of African Earth Sciences*, **10**, 483-501.

Wilson, J.F., Nesbitt, R.W. & Fanning, C.M. 1995. *Zircon geochronology of Archaean felsic sequences in the Zimbabwe Craton: a revision of greenstone stratigraphy and a model for crustal growth.* In Coward, M.P. & Ries, A.C. (eds), *Early Precambrian Processes,* Geol. Soc. Spec. Publ. **No.95**, 295pp.

Wolf, M.B. & Wyllie, P.J., 1994. Dehydration melting of amphibolite at 10kb: effects of temperature and time. *Contrib. Mineral. Petrol.*, **115**, 369-383.

Wyllie, P.J., Wolf, M.B. & van der Laan, S.R., 1997. Conditions for formation of tonalites and trondhjemites: magmatic sources and products. *In:* de Wit, M. & Ashwal, L. *Greenstone Belts* Oxford Monographs on Geology and Geophysics, No.35, 809pp. Clarendon Press, Oxford.

APPENDIX

METHODOLOGY OF ANALYTICAL TECHNIQUES

No data are given here since it has all been reproduced in the text during the course of discussion.

Appendix A - Zircon Geochronology

In order to keep this information brief, concise and of practical use, the description of the procedures used in zircon extraction and analysis will be in bullet point form.

A-1 Zircon separation & preparation for analysis

Note: Cleanliness is of extreme importance at each stage. Prior to each step the work area and equipment must be cleaned thoroughly.

1) Rock crushing

- (A crusher accessible from all sides and inside is preferable for ease of cleaning).
- Pass the sample through at decreasing size settings, rather than a single pass at the finest setting, to avoid metal contamination.
- Clean the crusher ready for the next sample - a good vacuum followed by a wipe-down with wet paper towel is preferable.

2) Disc Milling

- Set plate separation to just less than 1mm.
- Feed in sample slowly with adequate dust extraction system in operation.
- Clean mill thoroughly including removal of mill plates - wipe down.

3) Sieving

- Sieve sample into three size fractions - >250μm; 250-125μm; <125μm. (Sieve time approx. 30mins)
- Disposable sieve cloths are preferable for ease of cleaning.

4) Rogers/Wilfley Table

- Clean table thoroughly before use - vacuum and wipe-down table surface and taps; rinse collecting vessels for 'lights'; wash collecting vessels for 'heavies'; replace 'heavies' pipes.
- Run table without sample for a period of time until satisfied any material possibly present has run off.
- Slowly spoon on the desired size fraction in a thixotropic to saturated form (It may be necessary to wash the sample first to remove most of the clay size fraction, thereby avoiding possible adherence of the heavier minerals to the sticky clays; generally, the slower the sample is fed onto the table the better the process of heavy mineral separation and concentration).
- Pass the collected 'heavies' over the table again.
- Wash 'heavies' into suitable receptacle, add acetone and dry under heat lamp (A rapid drying process is necessary to avoid attraction and sticking of any zircons to any oxidising grains/particles).
- Wash 'lights' into suitable receptacle and dry in drying oven.

5) Frantz Magnetic Separator

- *Clean the Frantz thoroughly* - dismantle and wash all parts; vacuum Frantz (N.B. possibility for cross-contamination of samples high at this stage if cleaning ineffective).
- Remove metallic particles (bits of disc plate) from sample using a hand-magnet (failure to do a thorough job will cause blockage and entrapment of sought minerals during first pass).
- Fill hopper and run sample at 0.1A at appropriate feed rate (The slower the feed rate the less the entrainment and the better the separation).
- Repeat at 0.2A, 0.5A, 1.0A, 1.5a and maximum amperage (usually around 1.7A), thereby progressively extracting less magnetic material.
- If sample permits (i.e. if you have enough left at this stage) run sample at diamagnetic settings..... The final non-magnetic fraction should prove to contain the least metamict, least included and most transparent zircons.

6) Heavy liquids - Di-Iodomethane (Methylene Iodide - MI)

- *N.B. This procedure must be conducted in a fume cupboard*
- Wash all apparatus with acetone and/or soapy water before use, checking each piece under a microscope for any contaminant material.
- Arrange apparatus and label separate beakers for collection of neat MI and MI-washings.
- Add MI to funnel making sure the tap is closed.
- Add appropriate amount of sample (addition of too much sample will lead to a poor separation).
- Stir gently with a glass rod to ensure all dense grains have had a chance to fall but avoid contact between the bottom of the resulting vortex and the settled grains.
- Allow to settle for a few minutes
- Receiving the MI through a filter paper into a clean beaker, drain off the settled material with a decisive action of the tap.
- Replace filter paper and drain off 'MI float'.
- Pour clean MI back into bottle through a filter paper.
- Wash sample, 'float' and apparatus thoroughly with acetone and pour 'MI washings' into a bottle for disposal or recovery.
- Wash sample and 'float' from respective filter papers into separate receptacles using acetone and dry under a heat lamp.
- Clean up, placing all contaminated material (tissues, etc.) into a sealing plastic bag for disposal.

The sample should now be ready for hand picking.

N.B. A more recent development to the procedure has seen the sieved sample passed over the Superpanner and the heavy minerals pipetted off, followed by heavy liquid separation and then magnetic separation on the Frantz as described in the procedure above. This has the advantage of decreasing processing time and increasing separation efficiency.

7) Hand picking

- place the separated grains into a small sample dish and add alcohol

- using a pair of needle-point tweezers (checked for cleanliness under the microscope) choose the best grains. Transparent grains with a lack of inclusions, cracks and metamict material are preferable.

8) Air abrasion

- pipette the chosen grains into an abrader and remove the excess alcohol
- add a small amount of clean pyrite (as Pb-free as possible) and close the abrader
- abrade for as long as necessary to remove any rim material and ensure a single phase of zircon is constituting the remnant grain (3hrs @ 4psi is a good start). N.B. different zircons abrade differently and at different speeds. Check regularly if uncertain.

9) Washing

- pre-wash - using alcohol, pipette the grains with as little pyrite as possible, into a Pyrex petri-dish containing 4M reagent grade HNO_3. Heat in a fume cupboard at a low temperature on a hotplate for approximately 30mins.
- allow to cool
- using a microscope and an acid washed pipette, remove the HNO_3 and rinse twice with Milli-Q water.
- check the grains again whilst in the laboratory and select the very best grains for dissolution.
- main wash - using an acid washed Teflon pipette, transfer the grains individually into separate, acid washed 10ml Pyrex beakers previously half-filled with distilled 4M HNO_3.
- heat in a fume cupboard at a low temperature on a hotplate for approximately 30mins.
- allow to cool and then briefly ultrasonic each beaker to ensure the grains are at the bottom
- decant off the acid and rinse twice with Milli-Q water
- rinse with a small amount of distilled acetone and decant
- add a small amount of distilled acetone and place on a hotplate in a fume cupboard at low heat to dry

- make sure the grain remains 'free' by tapping the sides of the beaker with a pair of tweezers. If the grain sticks, repeat the acetone washes.

The grain is now ready for weighing

A-2 ID-TIMS (Conventional technique) - Mineral Dissolution and Analysis

A-2.1 MINERAL DISSOLUTION & CHEMISTRY

1) Weighing - N.B. CLEAN THE WORK AREA AND LAY DOWN PAPER!!!!

- calibrate the Cahn microbalance with the 20mg weight
- construct a foil boat from aluminium foil previously washed in distilled acetone and dried in the oven.
- transfer the grain from the Pyrex beaker to the boat by tipping the beaker and tapping the sides with a pair of tweezers.
- place the boat on the microbalance for weighing
- tip the grain from the boat into a dissolution capsule

N.B. for sub-microgram samples, pipetting directly into the dissolution capsule after estimating the size proportions, using an acid-washed pipette and acetone may be preferable, then remove the excess acetone.

2) Adding the dissolution acids and spike

- add 25 drops of distilled 29M HF and 2 drops of distilled 8M HNO_3
- spike - dispense the required amount of spike onto a clean piece of parafilm
  - add appropriate amount of $^{205}Pb/^{235}U$ mixed spike (~1.1mg) using a calibrated micro-pipette
  - tap the capsule on working surface to ensure the spike has mixed with the acid

3) Dissolution (using Parr bomb and Parrish (1987) capsules)

- place the capsules in their dissolution sleeve
- pour 6.5ml of distilled 29M HF and 0.5ml of distilled 8M HNO3 into the sleeve
- close sleeve, place in metal jacket and close bomb

- place in the oven at 240°C for 3 nights
- remove bomb and allow to cool
- extract sleeve and transfer to clean lab
- carefully remove capsules, washing each individually in Milli-Q water
- open each capsule and place on a hotplate to dry down
- allow to cool
- add 27 drops of distilled 3.1M HCl to each capsule and return to sleeve
- pour 7ml of distilled 3.1M HCl into the sleeve
- reconstruct bomb and place in the oven at 180°C overnight
- remove bomb and allow to cool

4) Chemistry

- preparation of columns
    - remove columns from acid using tongs and rinse with Milli-Q water
    - place columns on cleaning carousel
    - fill columns with Milli-Q and fill column stem with resin so that it is seen in the base of the bowl (~30 drops).
    - cleaning - fill the column bowls with 4 repetitions of Teflon distilled water and distilled 6M HCl, ending with a water stage.
- conditioning - 20 drops 3.1M HCl
- load sample from dissolution capsules
- wash on load - 3 x 2 drops 3.1M HCl
- elute - 13 drops 3.1M HCl
- collect Pb - in acid washed PMP beaker
    - 22 drops 6.2M HCl
- collect U - in the same beaker as the Pb
    - 26 drops Teflon distilled water
- add one drop 1M H_3PO_4 and dry down to a small drop
- cover PMP beaker with parafilm and store

5) Preparation and Clean-up Practices

- Pyrex washing beakers - store/clean in 50:50 mixture of 6M HCl:8M HNO_3

- remove from acid using tongs
- rinse twice with Milli-Q water
- check for contaminant grains under a microscope
- half fill with distilled 4M HNO_3
- the beaker is now ready to accept the grain

- after use - rinse well to ensure no grains remain in the beaker
- submerge and invert beaker in an ultrasonic bath ensuring no air bubbles are trapped in the beaker. Ultrasonic for 5 mins
- wipe around the inside of each beaker vigorously with a paper towel
- rinse twice with Milli-Q water and return to the acid bath

- PMP beakers for chemistry - use new beakers every time
- rinse twice with Milli-Q water both inside and out
- submerge and invert in acid bath containing reagent grade 6M HCl, ensuring no air bubbles are trapped inside
- covering with a watch glass, warm the acid bath on a low heat on a hotplate for 1 hour
- remove beakers from acid bath using tongs and rinse twice with Milli-Q water
- fill with Milli-Q water and transfer to clean air hood
- rinse again and add 6-7ml distilled 6M HCl
- heat on a hotplate at low heat for 1 hour
- remove to cool; rinse well with Milli-Q water, dry and cover with parafilm

- Dissolution capsules - when clean, store wrapped in parafilm
- rinse capsule and lid 3 times with Milli-Q water
- add 30 drops 29M HF and 5 drops 8M HNO_3
- place in dissolution sleeve and add 6ml 29M HF and 1ml 8M HNO_3 to the sleeve
- place sleeve in metal jacket, close bomb and place in oven at 240°C for 3 nights

- remove to cool
- empty contents of capsules, rinse well with Milli-Q water and add 30 drops 6M HCl
- replace capsules in sleeve and add 7ml 6M HCl to sleeve
- place in oven at 180°C for 1 night
- remove to cool and repeat acid steps twice more for a total of 3 acid cleans
- finally, rinse well with Milli-Q water and store wrapped in parafilm. If capsule is to be used, ensure that it is dry before attempting to place a mineral grain inside.

A-2.2 ANALYSIS

6) Degassing Filaments

- strip filament posts of remnant Re - **N.B. use gloves for all stages after this!**
- boil posts in Milli-Q water for ~15mins
- boil posts in 10% reagent grade H_2O_2 for ~15mins to remove grease and Re which has plated out on the insulators
- rinse filaments in Milli-Q water and dry in a vacuum oven for 1-2 hours
- spot weld Re filaments onto posts
- place filaments in degasser and pump down to $1x10^{-7}$ mbars
- increase amperage through the filaments until they have spent 20mins at 4.5A. **Do not allow pressure to degrade to more than $5x10^{-6}$ mbars**
- flash filaments at ~3.5A to remove any residue settled on them from degassing of adjacent filament banks
- allow to cool before venting unit and removing filaments

7) Loading Filaments

- lay down Kimwipes and parafilm
- fit clean pipette tip to pipette
- apply parafilm safety-strips to filament if required (thin stripes of parafilm applied at ~2.2A as barriers in precaution to overbanking of sample)
- remove parafilm from top of sample beaker

- lay beaker on its side with sample at the top
- place a drop of ultra-pure water inside the beaker and rinse pipette tip 3 times
- place a drop of silica gel inside the beaker **N.B. ensure silica gel is shaken before dispensing to ensure homogenisation**
- pipette a small amount of the silica gel onto the sample and mix
- pipette the mixture onto the filament at ~2.2A, in small aliquots to avoid overbanking (spreading of the load during evaporation)
- allow melting of silica gel and phosphoric acid in sample until a drop of clear liquid is present
- turn up the filament current - the parafilm will burn off at ~3-3.5A and then the phosphoric acid at ~5-5.5A.
- dry down the load until the sample is a grey-white colour. **N.B. Do not dry down too hard as the sample may easily come away from the filament**
- store in a suitable holder ready for adding to turret assembly

8) Analysis

Samples were run on a VG 354 thermal ionisation mass spectrometer (TIMS) using single filaments with Re ribbon. Pb was analysed first at temperatures up to 1350°C, followed by U at around 1450°C.

All data were obtained by single collector peak jumping (**Noble *et al.*, 1993**) on a VG 354 mass spectrometer fitted with a Wide Aperture Retarding Potential filter (abundance sensitivity of 54ppb) and a Philips ion-counting Daly detector. Samples were run for approximately 100 ratios until the internal precision on the $^{207}Pb/^{206}Pb$, $^{208}Pb/^{206}Pb$ and $^{205}Pb/^{206}Pb$ analyses was <0.05% and that on the $^{204}Pb/^{206}Pb$ was as small as possible at the measured ratio. Generally, it was not possible to achieve the preferred precision on the $^{206}Pb/^{204}Pb$ ratio since they were generally very low (<500) as a result of the variable fall-in blanks obtained at the time (see below).

Standards used were NBS 982 & 983 with ratios of 0.46707 & 0.071201 $^{207}Pb/^{206}Pb$, 1.00016 & 0.013619 $^{208}Pb/^{206}Pb$ and 36.739 & 2695 $^{206}Pb/^{204}Pb$ respectively. NBS 982 is contaminated. External reproducibility was <0.1% (2 S.D.) at the time of analysis.

9) Data reduction and calculation

All data reduction and age calculation was conducted using the Pbdat and Isoplot programs of Ludwig (1980) and all common Pb was removed, assuming zero Pb content of the zircons, using a common Pb composition of $^{206}Pb/^{204}Pb = 18.19 \pm 1.6\%$, $^{207}Pb/^{204}Pb = 15.58 \pm 1\%$ and $^{208}Pb/^{204}Pb = 38.5 \pm 1.6\%$ measured at the time of analysis.

Procedural blanks for Pb were highly variable for each sample due to a reduction in the extraction efficiency of the fume hood and degeneration of the hotplate coating during the time of chemical preparation. The U blank remained constant at <0.1pg for each sample whilst the Pb blank values for each sample were - Zimb.95/09 2.5-9.1pg (62.5pg exception); Zimb.95/14 2.7-10.7pg (22.2pg exception); Zimb.141 7.8-20.4pg (155.5pg exception) and Zimb.226 14.1-88.3pg (110.8pg exception).

Appendix B - Sm/Nd TIMS and ICP-MS techniques

Sm/Nd and Nd-isotope analyses were carried out on 31 samples using TIMS for determination of the $^{143}Nd/^{144}Nd$ isotope ratio and solution ICP-MS for the Sm/Nd ratio, and additionally on 12 of these samples by isotope dilution (ID-)TIMS. A comparison between the two data sets for these 12 samples as determined by the two techniques is given in Table 4.2/2.

Nd isotope ratios determined by TIMS were measured on a seven-collector VG Sector 54 mass spectrometer with a separable-filament source. The REE were initially separated from major elements and Ba by cation exchange, before isolation of Nd on Teflon powder columns coated with HDEHP. Isotope ratios were determined as the average of >100 ratios by measuring ion intensities in multi-dynamic collection mode and were normalised to $^{146}Nd/^{144}Nd = 0.7219$. Measured values for JMC321 were $^{143}Nd/^{144}Nd = 0.511121 \pm 8$ (2 S.D., n=54) during the run period. This is equivalent to $^{143}Nd/^{144}Nd = 0.511858$ for the La Jolla standard, often quoted as an international standard. Total blanks were <<200pg for Nd which represents <0.05% of the concentration of both elements in the measured fraction. Sm determinations were measured in the same way after initial preparation by isotope dilution using a $^{145}Nd/^{149}Sm$ mixed spike.

Table 4.2/2 - Comparison of Sm/Nd data obtained by ID-TIMS and TIMS/ICP-MS combination

SUMMARY OF DATA FOR 143/144Nd(i) using ID-TIMS
(External reproducibility = 0.1% 2.S.D.)

Sample no.	Lithology	143/144m		Sm/Nd		Nd ppm	147/144		Nd(i) @ relevant age			εNd(t)		T(CHUR)	error range in Ma		T(DM)	error range in Ma		Sm/Nd
			± 2 S.E.		± 2 S.D.			± 2 S.D.	age	143/144(i)	± 2 S.D.		± 2 S.D.		+ 2 S.D.	- 2 S.D.		+ 2 S.D.	- 2 S.D.	% 2 S.D.
Zimb.170	dacite	**0.511251**	5	**0.184244**	0.000184	7.5	**0.111398**	0.000111	2.7Ga	**0.509266**	12	**2.60**	0.24	**2.47E+09**	3	3	**2.81E+09**	3	3	0.1
Zimb.226	KKG	**0.510439**	6	**0.160207**	0.000160	16.7	**0.096847**	0.000097	3.456Ga	**0.508225**	12	**1.64**	0.24	**3.33E+09**	3	3	**3.51E+09**	3	3	0.1
Zimb.061	basalt	**0.512828**	6	**0.330242**	0.000330	6.6	**0.199747**	0.000200	2.7Ga	**0.509270**	14	**2.66**	0.27	**9.25E+09**			**3.49E+09**	50	49	0.1
Zimb.141	P2 SRG	**0.511884**	5	**0.274520**	0.000275	39.4	**0.166006**	0.000166	3.565Ga	**0.507968**	14	**-0.59**	0.27	**3.71E+09**	20	20	**4.01E+09**	14	14	0.1
Zimb.209	dacite	**0.511398**	5	**0.201982**	0.000202	8.0	**0.122127**	0.000122	2.7Ga	**0.509222**	12	**1.73**	0.24	**2.52E+09**	4	4	**2.90E+09**	4	4	0.1
Zimb.150	dacite	**0.511078**	5	**0.191595**	0.000192	12.7	**0.115838**	0.000116	2.88Ga	**0.508875**	12	**-0.44**	0.24	**2.92E+09**	4	4	**3.20E+09**	4	4	0.1
Zimb.135	basalt	**0.512484**	5	**0.305075**	0.000305	10.3	**0.18451**	0.000185	2.88Ga	**0.508976**	14	**1.53**	0.27	**1.92E+09**	29	28	**3.45E+09**	22	21	0.1
Zimb.028	basalt	**0.512694**	5	**0.322019**	0.000322	7.2	**0.194767**	0.000195	2.7Ga	**0.509224**	13	**1.77**	0.26	**-4.49E+09**			**3.64E+09**	37	37	0.1
Zimb.189	rhyodacite	**0.511625**	4	**0.257907**	0.000258	5.6	**0.155951**	0.000156	2.7Ga	**0.508847**	13	**-5.64**	0.25	**3.75E+09**	14	14	**3.99E+09**	11	11	0.1
Zimb.151	basalt	**0.512892**	5	**0.338396**	0.000338	5.2	**0.204682**	0.000205	2.88Ga	**0.509000**	14	**2.01**	0.27	**4.79E+09**			**4.31E+09**	99	94	0.1
Zimb.184	basalt	**0.512826**	4	**0.329706**	0.000330	7.3	**0.199423**	0.000199	2.7Ga	**0.509273**	14	**2.74**	0.27	**1.02E+10**			**3.43E+09**	48	47	0.1
Zimb.072	basalt	**0.512728**	5	**0.321010**	0.000321	16.7	**0.194158**	0.000194	2.7Ga	**0.509269**	13	**2.65**	0.26	**-5.51E+09**			**3.27E+09**	32	32	0.1

SUMMARY OF DATA FOR ICP-MS and TIMS derived 143/144Nd(i) after normalisation to BHVO-1 = 0.2467
(External reproducibility = 2% 2.S.D.)

Sample no.	Lithology	143/144m		Sm/Nd		Nd ppm	147/144		Nd(i) @ relevant age			εNd(t)		T(CHUR)	error range in Ma		T(DM)	error range in Ma		Sm/Nd
			± 2 S.E.		± 2 S.D.			± 2 S.D.	age	143/144(i)	± 2 S.D.		± 2 S.D.		+ 2 S.D.	- 2 S.D.		+ 2 S.D.	- 2 S.D.	% 2 S.D.
Zimb.170	dacite	**0.511251**	5	**0.179860**	0.003597	7.2	**0.108748**	0.002175	2.7Ga	**0.509314**	49	**3.53**	0.96	**2.39E+09**	60	57	**2.74E+09**	57	55	2.0
Zimb.226	KKG	**0.510439**	6	**0.161855**	0.003237	18.0	**0.097843**	0.001957	3.456Ga	**0.508202**	55	**1.19**	1.08	**3.36E+09**	67	65	**3.54E+09**	60	58	2.0
Zimb.061	basalt	**0.512828**	6	**0.326873**	0.006537	5.9	**0.197709**	0.003954	2.7Ga	**0.509306**	80	**3.38**	1.58	**2.64E+10**			**3.05E+09**	988	600	2.0
Zimb.141	P2 SRG	**0.511884**	5	**0.275379**	0.005508	38.2	**0.166526**	0.003331	3.565Ga	**0.507956**	89	**-0.83**	1.74	**3.77E+09**	462	371	**4.05E+09**	303	264	2.0
Zimb.209	dacite	**0.511398**	5	**0.200036**	0.004001	7.3	**0.120951**	0.002419	2.7Ga	**0.509243**	53	**2.15**	1.04	**2.48E+09**	81	76	**2.86E+09**	76	72	2.0
Zimb.150	dacite	**0.511078**	5	**0.194443**	0.003889	12.8	**0.117560**	0.002351	2.88Ga	**0.508843**	55	**-1.09**	1.07	**2.98E+09**	90	85	**3.26E+09**	81	77	2.0
Zimb.135	basalt	**0.512484**	5	**0.299220**	0.005984	10.3	**0.180968**	0.003619	2.88Ga	**0.509043**	79	**2.85**	1.55	**1.49E+09**	442	278	**3.08E+09**	379	304	2.0
Zimb.028	basalt	**0.512694**	5	**0.314553**	0.006291	6.7	**0.190251**	0.003805	2.7Ga	**0.509305**	78	**3.35**	1.53	**-1.33E+09**			**2.94E+09**	564	408	2.0
Zimb.189	rhyodacite	**0.511625**	4	**0.256400**	0.005128	5.7	**0.155040**	0.003101	2.7Ga	**0.508863**	65	**-5.32**	1.28	**3.67E+09**	292	252	**3.92E+09**	216	195	2.0
Zimb.151	basalt	**0.512892**	5	**0.327677**	0.006554	5.1	**0.198198**	0.003964	2.88Ga	**0.509124**	85	**4.43**	1.68	**2.39E+10**			**2.52E+09**	858	511	2.0
Zimb.184	basalt	**0.512826**	4	**0.322603**	0.006452	6.7	**0.195126**	0.003903	2.7Ga	**0.509350**	80	**4.24**	1.56	**-1.94E+10**			**2.64E+09**	696	456	2.0
Zimb.072	basalt	**0.512728**	5	**0.324581**	0.006492	15.6	**0.196318**	0.003926	2.7Ga	**0.509231**	80	**1.90**	1.57	**-4.11E+10**			**3.67E+09**	1054	669	2.0

Sm/Nd ratios derived by ICP-MS were calculated from the concentrations determined during analysis of the whole rock solution for REE and selected trace elements (see Appendix C below). The 2σ external error is generally ~2% for ICP-MS in comparison to ~0.1% by ID-TIMS. This translates to larger errors on the calculated ε_{Nd} value and significant expansion of this error during calculation of model ages. Model age values used for these calculations were $^{147}Nd/^{144}Nd = 0.1967$ & $^{144}Nd/^{143}Nd = 0.512638$ CHUR and $^{147}Nd/^{144}Nd = 0.2137$ & $^{144}Nd/^{143}Nd = 0.51315$ depleted mantle (T_{DM}; Peucat *et al.*, 1989). As a result, for two samples with the same Sm/Nd error the sample with the older model age possesses the larger age error since it is calculated as a percentage of the age. The reason for the high T_{DM} model age for sample Zimb.151 as determined by ID-TIMS is largely unknown but may have cause in the less-than-smooth nature of its REE pattern (see Figure 4.8) if this is an accurate reflection of the pattern for the sample. Minor variations in the Sm/Nd ratio caused by later events significantly affect the Nd isotope data derived from such rocks (Moorbath *et al.*, 1997). However, calibration error is a more likely cause of the non-smooth REE pattern for Zimb.151 and is a major factor which limits the model age precision attainable using ICP-MS derived Sm/Nd ratios, causing much larger errors than those obtained from ID-TIMS derived data (see Appendix C below). As such, all the Nd isotope determinations determined by ID-TIMS are accepted in preference to those determined by ICP-MS/TIMS although it is noted that the data obtained by this latter method is surprisingly, good enough to generate a reasonable isochron for these rocks. Extra vigilance during the ICP-MS determination of the Sm/Nd ratio of the sample, for example by including only these elements in the determination, may significantly improve the accuracy of the ratio.

Appendix C - ICP-MS analysis for REE and selected trace elements

REE and trace element analyses were performed on a VG Elemental PlasmaQuad PQ2+ ICP-MS. Sample introduction was in a 2% HNO_3 solution using a Meinhard nebuliser and Gilson peristaltic pump after preparation of calcined sample by normal acid dissolution techniques using an $HF/HClO_4$ mix and 6M HCl storage solution.

Data acquisition used a Galileo Channeltron detector in peak jumping mode with 3 points per peak, 10.24msec dwell time and 10msec quad settle time. Acquisition consisted of 5 repetitions of 30sec runs per sample resulting in a typical within run precision of <1%RSD.

Calibration of the trace element data was achieved using a suite of selected international rock standards that were run at the same time as the unknown daughter solutions. They comprise BHVO-1, JB-2, JB-3, JA-1, JR-1, JG-2, BE-N, and BRR-1 (an in-house standard). BHVO-1 was also used as a drift monitor to which all the samples were drift corrected (at a Sm/Nd ratio = 0.2467). This was especially important for the use of the Sm/Nd ratio in Nd-isotope studies. Calibration was also crucial for this since a smooth REE pattern is a pre-requisite in order to calculate Sm/Nd data like that shown in Table 4.2. This is because any slight variation in the Sm/Nd ratio resulting from calibration factors, has a huge influence on the resultant model age and ε_{Nd} values.

Recommended concentrations for the standards (with the exception of BRR-1) can be found in Govindaraju (1994) and other sources. Using these standards and recommended values for calibration each time, an unknown sample typically displays an external reproducibility of <5% (2 S.D.).

An off-line custom written computer program, the ICP-MS Data Manipulation Program, was used for data processing. This program applies a drift and blank correction to the raw data and produces a multi-standard calibration based on the recommended values of the rock standards.

Appendix D - X-Ray Fluorescence techniques

Major and trace element concentrations were determined by XRF analysis using fused glass discs and pressed powder pellets respectively. Sample powders were prepared using a hydraulic rock-splitter, jaw-crusher and case-hardened purified steel pot in a TEMA® mill.

Fused glass discs were made using sample calcined overnight in porcelain crucibles at temperatures around 970°C. An accurately weighed portion of this was then mixed with flux

in a 5:1 ratio for making the bead. Spectroflux® 100 or 100B flux containing lithium tetraborate and a 1:4 mix of lithium tetraborate and lithium metaborate respectively was used, the choice of flux depended on the nature of the sample. Great effort was made to ensure homogeneity of mixing. Pressed power pellets were made using non-calcined sample and polyvinyl aldehyde (PVA) binder with 12 tonnes applied pressure.

Samples were run on a Philips® PW1400 automatic sequential wavelength dispersive X-ray Fluorescence spectrometer with count times for trace elements of 100 or 200 seconds depending on the required level of detection for each element. Detection limits for each element are given in Table D-1.

Problems with the calibration of Y and Nb at low concentrations are apparent (see Fig. 4.2) due to a non-zero intercept of the calibration line at zero intensity of the standards. This is a result of inappropriate standard selection to represent these lower concentrations. As a result of this, Nb concentrations as determined by ICP-MS have been used in consideration of the data as has Y data for those samples with concentrations <4ppm as determined by XRF.

Appendix E - Scanning Electron Microscopy

Zircon images were acquired using a JEOL 6400 SEM in back-scattered electron (BSE) mode at 20kV with a current of $3x10^{-9}$A and a working distance of 15mm. Sample stubs were coated with a conductive layer of carbon.

Appendix F - Locality details for samples used for zircon geochronology

(see Table F-1)

Table D-1

Element	X-ray	Detection limit (ppm)
Ba	Lβ	10
Ce	Lβ	10
Cr	Kα	4
La	Kα	6
Ni	Kα	1.5
Nb	Kα	1.06
Rb	Kα	1.06
Sr	Kα	1.06
V	Kα	4
Y	Kα	1.06
Zn	Kα	1.5
Zr	Kα	1.06

Table F-1

Sample	Locality details
Zimb.150 - Dacitic volcanic from the Mafic Formation near Kwekwe	G.R. Kwekwe 1829 D4 QK90601300; *west of the ford across the Sebakwe River south of Indarama Mine*
Zimb.164 - Giraffe Porphyry	G.R. Sebakwe Poort 1829 D3 QK79300795
Zimb.226 - Rhodesdale Granitoid/Kwekwe Gneiss	G.R. Kwekwe 1829 D4 QK97601300; *2.6km east of the greenstone-granitoid contact*
Zimb.141 - Phase 2, Sebakwe River Gneiss	G.R. Kwekwe 1829 D4 QK92601250
Zimb.95/02 - Sesombi Tonalite	G.R. Just north of area displayed on Sebakwe Poort 1829 D3
Zimb.95/06 - Chilimanzi Granite	G.R. 1930 D2 647249; *Southdale Farm, 43km north of Masvingo in layby on east side of main road.*
Zimb.95/09 - Leucosome in the Tokwe Gneiss	G.R. 1930 D3 TN602044; *In tributary of Shashi River 150m north of northern boundary fence of Redman Farm*
Zimb.95/14 - Tokwe River Gneiss	G.R. Mashaba 2030 A2 TN317798; *In bed of Tokwe River below old Masvingo to Bulawayo road*
Zimb.95/29 - Chingezi Suite Granitoid	G.R. Mberengwa 2029 D4 QH962447; *~80m south of Mtshingwe dolerite and 1km north of Rh81/10 collected by Taylor et al. (1991)*

STRATIGRAPHY OF THE MIDLANDS GREENSTONE BELT, ZIMBABWE (SEBAKWE RIVER SECTION)